SANDIA REPORT

SAND99–0979
Unlimited Release
Printed April 1999

Lithium/Manganese Dioxide (Li/MnO_2) Battery Performance Evaluation: Final Report

David Ingersoll and Nancy H. Clark

Prepared by
Sandia National Laboratories
Albuquerque, New Mexico 87185 and Livermore, California 94550

Sandia is a multiprogram laboratory operated by Sandia Corporation, a Lockheed Martin Company, for the United States Department of Energy under Contract DE-AC04-94AL85000.

Sandia National Laboratories

Issued by Sandia National Laboratories, operated for the United States Depart-ment of Energy by Sandia Corporation.

Available to DOE and DOE contractors from
Office of Scientific and Technical Information
P.O. Box 62
Oak Ridge, TN 37831

Prices available from (703) 605-6000
Web site: http://www.ntis.gov/ordering.htm

Available to the public from
National Technical Information Service
U.S. Department of Commerce
5285 Port Royal Rd
Springfield, VA 22161

NTIS price codes
Printed copy: A07
Microfiche copy: A01

SAND99-0979
Unlimited Release
Printed April 1999

Lithium/Manganese Dioxide (Li/MnO_2) Battery Performance Evaluation: Final Report

David Ingersoll
Lithium Battery Research and
Development Department

Nancy H. Clark
Energy Storage Systems Analysis and
Development Department

Sandia National Laboratories
P.O. Box 5800
Albuquerque, NM 87185-0613

Abstract

In February 1997, under the auspices of the Product Realization Program, an initiative to develop performance models for lithium/manganese dioxide-based batteries began. As a part of this initiative, the performance characteristics of the cells under a variety of conditions were determined, both for model development and for model validation. As a direct result of this work, it became apparent that possible Defense Program (DP) uses for batteries based on this cell chemistry existed. A larger effort aimed at mapping the performance envelope of this chemistry was initiated in order to assess the practicality of this cell chemistry, not only for DP applications, but also for other uses. The work performed included an evaluation of the cell performance as a function of a number of variables, including cell size, manufacturer, current, pulse loads, constant current loads, safety, etc. In addition, the development of new evaluation techniques that would apply to any battery system, such as those related to reliability assessments began. This report describes the results of these evaluations.

Acknowledgments

The authors would like to acknowledge David Weigand for contributing the aged cells for this project. We would also like to thank the following individuals for their contribution to this project:

Imelda Francis, Technical Editor, ASAP
Merrillee A. Dolan and Mindy Mae, Technical Editors, Tech Reps, Inc.
Jackie Ripple, Word Processing, Tech Reps, Inc.
Lina Castillo, Administrative Assistance, Sandia National Laboratories
Rosemary Dunivan, Administrative Assistance, Sandia National Laboratories
Gwen Pullen, Administrative Assistance, Sandia National Laboratories

Intentionally Left Blank

Contents

Figures

Tables

Intentionally Left Blank

Acronyms and Abbreviations

ACR	alternating current resistance
ANN	artificial neural network
COTS	commercial off-the-shelf
DOD	depth of discharge
DOE	Department Of Energy
DP	defense programs
ESR	equivalent series resistance
FID	flame ionization detectors
GC/MS	gas chromatography/mass spectrometry
H	high rate
ID	identification
iR	ohmic polarization
Li/MnO_2	lithium/manganese dioxide
$Li/SOCl_2$	lithium/thionyl chloride
MSDS	material safety data sheet
NSWC	Naval Service Warfare Center
NSWC	Naval Surface Warfare Center
OCV	open circuit voltage
PTC	positive temperature coefficient (thermal expansion switch)
RT	room temperature
SEM	scanning electron microscopy
TIC	total ion chromatogram
VH	very high rate
XRD	x-ray diffraction

Intentionally Left Blank

1. Introduction

David Ingersoll and Nancy H. Clark

1.1 Introduction

In February 1997, under the auspices of the Product Realization Program, a small initiative to develop performance models for lithium/manganese dioxide (Li/MnO_2)-based batteries began. As a part of this initiative, the performance characteristics of the cells under a variety of conditions were determined both for model development and for model validation. As a direct result of this work, it became apparent that these were possible Defense Program (DP) uses for batteries based on this cell chemistry. Consequently, in late October 1997, a larger effort to map the performance envelope of this chemistry began to examine more fully the practicality of this cell chemistry for DP applications. This work included evaluating the cell performance as a function of a number of factors, such as cell size, manufacturer, environment, discharge rate, pulse versus constant current discharge, safety, and reliability, etc. This report describes the results of these initial evaluations, which were completed by August 1998. As will be evident, because of the short duration of this activity, many questions remain unanswered regarding a variety of issues.

One objective was to develop information that would allow design engineers to evaluate the practical utility of Li/MnO_2-based chemistry for their power needs. To this end, characterization focused on collection and presentation of information and data that would allow for this initial evaluation. Characterizations were made not only within the operating range specified by the manufacturer, but also well outside of that range to more fully characterize the performance envelope. In addition, much of the initial work presented here focused on the cell level, although some battery information is included. Finally, the information is presented in such a way that the design engineer can begin to compare and make tradeoffs between performance and design considerations. This work provides enough information that a sense of the performance characteristics of cells based on this chemistry can be obtained.

1.2 Li/MnO_2 Cells

The lithium/manganese dioxide (Li/MnO_2) cell chemistries are based on a negative electrode composed of metallic lithium and a solid cathode of manganese dioxide, which exhibits a nominal cell voltage of 3 V. Liquid solutions composed of an anhydrous aprotic solvent and a lithium salt are employed as the electrolyte. Typical solvents used include propylene carbonate, tetrahydrofuran, dimethoxyethane, ethylene carbonate, and others. To improve performance characteristics over a wide operational range, mixtures of two or more solvents are typically employed. The salts most commonly used are either lithium triflate or lithium perchlorate. The gravimetric energy density and volumetric energy of these systems fall typically in the range of 230 Wh/kg and 580 Wh/l, respectively.

Cells and batteries employing this chemistry have widespread use in consumer and military applications, including watches, computer memory backup power, cameras, photoflash units, medical equipment, and many others. Among the many reasons for their widespread use are high-rate capability, wide operational temperature range (–40°C to +70°C), low self-discharge (<1% per year), high voltage, flat voltage profile, and high-energy density. An example of a low-temperature application is the Swiss

military emergency radio communication system, which must operate in a pulse mode at –40°C and which utilizes a "squashed" D cell.

Because of the rate requirements of the application, only spiral-wrapped configurations were evaluated. In addition, because of cost and schedule considerations only commercial off-the-shelf (COTS) cells were studied. This study evaluates only cylindrical cells because of their widespread availability.

1.3 Availability

Several sizes of cells are commercially available; however, only the 2/3A, C, 5/4C, and D sizes are included in this initial work. Table 1-1 summarizes the various cell sizes as well as the sources of the cells included in this study.

Table 1-1. Li/MnO_2 Cell Sources Studied

Vendor	2/3A	C	5/4C	D
Sanyo	+			
Sony	+			
Panasonic	+			
Varta	+			
Kodak	+			
Duracell	+			
Eveready	+			
Ultralife standard version	+	+	+	+
Ultralife high-rate version				+
Bluestar				+
Silberkraft low-temperature version		M52TT	M56TT	+M20TT
Silberkraft standard version		M52	BlankTT	+M20

+Cells on test at SNL

The 2/3A cells are readily available from a number of vendors at virtually any required level of production. Availability of larger cells is limited to a smaller number of vendors, including Ultralife, Bluestar, and Silberkraft. Ultralife C and 5/4C, which were cells built by hand, were evaluated for this study. Ultralife standard version D cells were used in this study. Production at Bluestar is currently limited, and the delivery of cells requires long lead times. Bluestar is attempting to resume full production at this time. Silberkraft routinely produces cells in all of the larger sizes studied here as well as cells in other large and nonstandard sizes, such as the DD cell.

At least two of the vendors provide two versions of the larger cells. Silberkraft has available both the standard cell and a special low-temperature version of the cell. The low-temperature version was specifically developed for military use in cold environments. This version of the cell presumably differs from its standard counterpart only in the formulation of the electrolyte.

Similarly, Ultralife has available two versions of various cells. One is its standard cell and the other is designated as a very high-rate version of the product. The differences in cell design between these two versions have not yet been identified because of limited availability of the cells. One of the differences in these two cells is in the type of manganese dioxide used. Ultralife is in the process of phasing out the very high-rate version.

1.4 Overview of Report

Sections 2 through 5 report the results of testing cells of a given size and, in some cases, batteries made up of cells of that size. Results of testing of cells at both constant current and various pulse profiles will be reported. Section 6 reports on the performance of aged 2/3A and D cells. Section 7 reports on internal characteristics of 2/3A and D cells. Section 8 reports on testing protocols and limitations of the testing used to generate the data reported in Sections 2 through 6. Section 9 reports on an initial study to predict reliability of Li/MnO_2 cells. Section 10 reports results of safety tests done on D cells/batteries and some design considerations to increase the safety. Section 11 shows how PSpice models can be used to model performance. Section 12 reports the summary and conclusions from the report.

This page intentionally left blank.

2. 2/3A Cell Behavior

David Ingersoll, Nancy H. Clark, Jill L. Langendorf, and Lorie E. Davis

2.1 Introduction

The 2/3A-size cell is widely used in several consumer applications, including cameras and photoflash units for cameras. The cells are also often used as backup power for personal computers. The camera and photoflash applications typically require high-rate capability, and this necessitates a spiral-wound configuration. The backup power application typically employs a bobbin design; however, a spiral configuration has been used. The spiral-wound cells are currently available from several manufacturers including Duracell, Eveready, Kodak, Ultralife, Panasonic, Sony, Sanyo, and Varta. In addition, some of the manufacturers build two or more versions of the cells that differ not only in physical appearance but also in their performance and market. For example, Panasonic markets at least three versions of its 2/3A cells. One cell is a bobbin design. The other two cells are a spiral-wrap design; one is marketed primarily in Asia (the white version) and the other is marketed in the U.S. (the black version). Table 2-1 summarizes performance characteristics of these cells. In reviewing the list of vendors, it should be noted that not all of them manufacture cells. Rather, they place their own label on products manufactured by others and market them as their own.

For the most part, the cells are cathode-limited. However, the discharge characteristics of some of the cells provide evidence of an anode limitation, as will be seen in the next section where the constant-current discharge characteristics of the cells are discussed.

Table 2-1. Summary Listing of Energy Density and Specific Energy of 2/3A Cells. The energy was determined using a nominal cell voltage of 2.9 V. Discharge rate was 10 million PS at RT

Vendor	Capacity At 2.0 V (Ah)	Gravimetric Energy Density (Wh/kg)	Volumetric Energy Density (Wh/l)
Duracell	1.5	263	611
Eveready	1.2	210	491
Kodak	1.1	202	449
Panasonic Black	1.1	203	455
Panasonic White	1.2	207	462
Sanyo	1.4	253	541
Sony	1.2	214	472
Ultralife	1.6	270	632
Varta	1.6	274	643

2.2 Constant Current Discharge – Cells

Nominal capacities of all the cells were determined by discharging the cells at the relatively low rate of 10 mA, and the discharge curves for the cells evaluated are shown in Figure 2-1. The nominal capacity of these cells using a 2-V cutoff is shown in Table 2-2. As seen, the nominal capacity varies between about 1 and 1.6 Ah, depending on the vendor. Other characteristics worth noting include the relatively flat and stable voltage plateau at 3 V. The cathode versus anode limitation differences between the cells obtained from different vendors can be seen from the shape of discharge curves. Those with sharp drop-offs like the lithium half cell are anode-limited. Those with more gentle drop-offs like Li/MnO_2 are cathode-limited.

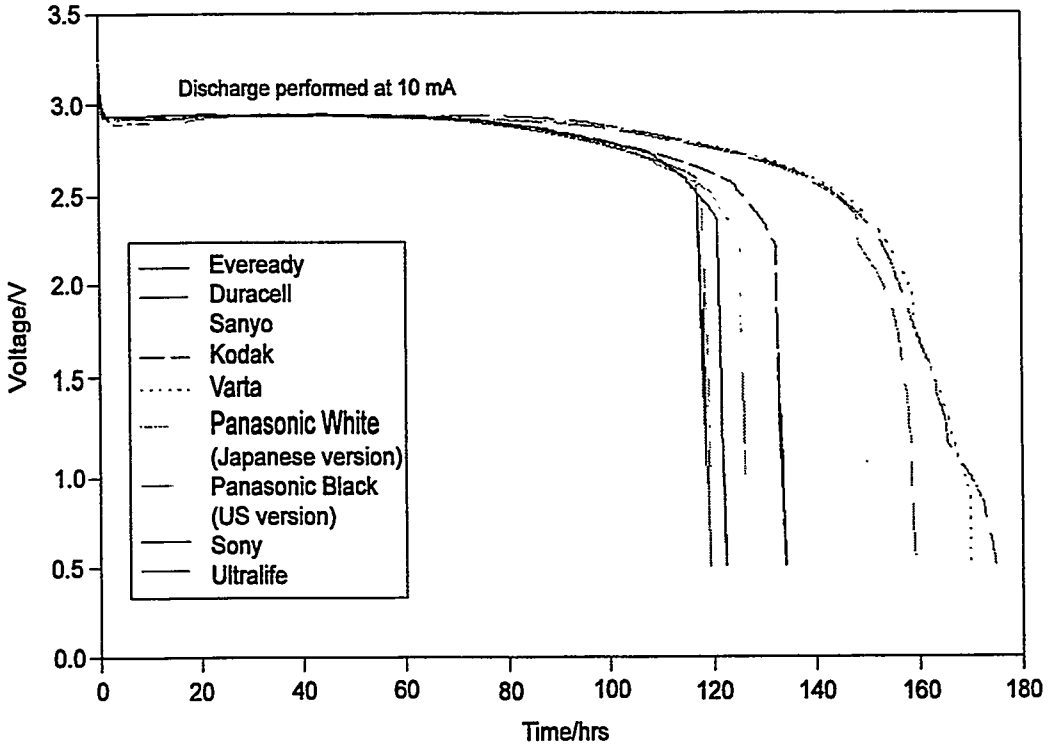

Figure 2-1. Voltage profiles of 2/3A cells discharged at 10 mA and room temperature.

The effect of the discharge rate on both capacity and voltage was also determined for all of the 2/3A cells for rates between 10 mA and 2 A. In every case, the cell voltage and capacity decreased with increasing current. Neither of these effects is surprising, and the lower voltage plateaus arise principally from the equivalent series resistances (ESRs) of the cells, which are on the order of 0.5 Ω. This behavior is illustrated in Figure 2-2 for the Sanyo cell. As should be evident upon examination of the data, these small cells are capable of supporting a 2 A continuous load, albeit at lower voltages and capacities than those observed at less demanding conditions, for example, lower current. Another interesting characteristic of these cells' behavior is the relationship between voltage and discharge rate, which is plotted in Figure 2-3. As can be seen, although not linear, it is well behaved. In general, all of the 2/3A cells behave similarly, as shown by the data in Table 2-2, which summarizes the performance characteristics of all the cells under a variety of constant-current discharge rates.

Table 2-2. Nominal Capacities as a Function of Constant Current Discharge Rate for Commercial 2/3A Cells

VENDOR	APPLIED CURRENT								
	10 mA	40 mA	100 mA	250 mA	500 mA	750 mA	1 A	1.5 A	2 A
KODAK									
Capacity at Cutoff, mAh	1319	1257	1218	1192	1019	865	725	437	513
Cutoff Voltage	2.25	2.25	2	1.75	1.75	1.5	1.5	1.5	1
EVEREADY									
Capacity at Cutoff, mAh	1171	1324	1238	1157	1058	801	743	588	499
Cutoff Voltage	2.25	2	2	2	1.75	1.75	1.75	1.5	1.25
DURACELL									
Capacity at Cutoff, mAh	1485	1491	1377	1277	1236	1228	1149	993	830
Cutoff Voltage	2.25	2	2	2	2	1.75	1.5	1.5	1.25
SANYO									
Capacity at Cutoff, mAh	1362	1349	1282	1233	1128	1015	985	779	523
Cutoff Voltage	2	2	2	1.75	1.75	1.5	1.5	1.5	1.5
VARTA									
Capacity at Cutoff, mAh	1582	1447	1352	1347	1258	1261	1143	1001	871
Cutoff Voltage	2	2	2	2	2	1.75	1.75	1.5	1.25
PANASONIC BLACK (U.S. version)									
Capacity at Cutoff, mAh	1221	1256	1198	1140	1047	805	800	566	556
Cutoff Voltage	2.5	2	2	2	1.75	1.75	1.5	1.5	1
PANASONIC WHITE (Japanese version)									
Capacity at Cutoff, mAh	1413	1286	1244	1161	1069	804	567	494	539
Cutoff Voltage	2	2	2	1.75	1.5	1.5	1.5	1.5	1
ULTRALIFE									
Capacity at Cutoff, mAh	1564	-	1399	1298	1332	1317	1226	1055	1008
Cutoff Voltage	2	-	2	2	1.5	1.5	1.5	1.5	1
SONY									
Capacity at Cutoff, mAh	1213	-	1244	-	1053	893	753	431	387
Cutoff Voltage	2	-	2	-	1.5	1.5	1.5	1.5	1.25

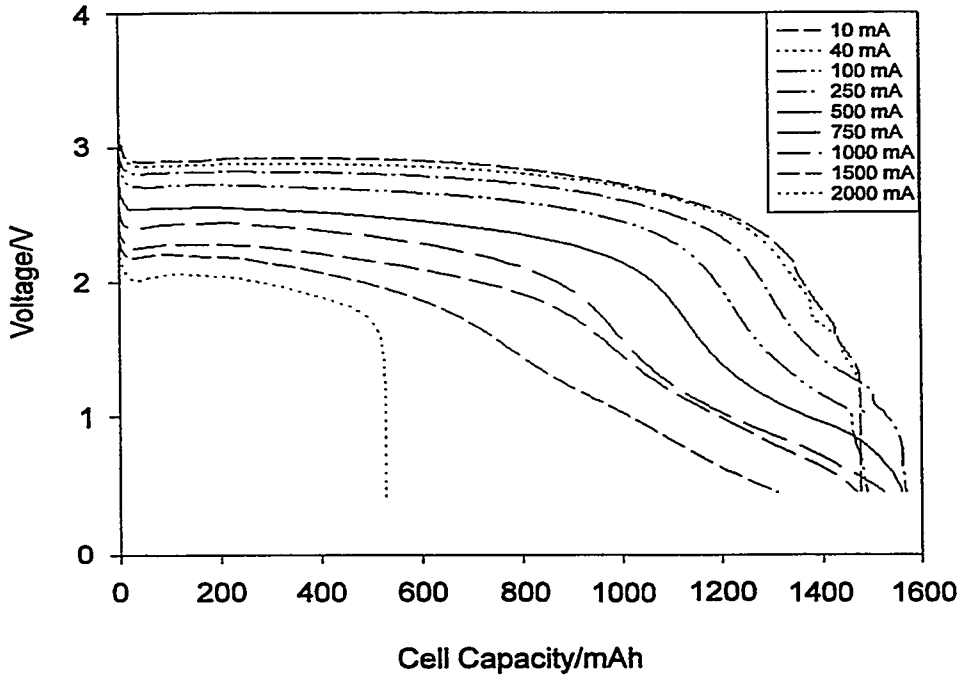

Figure 2-2. Discharge profiles of 2/3A Sanyo cells at room temperature at various rates of discharge.

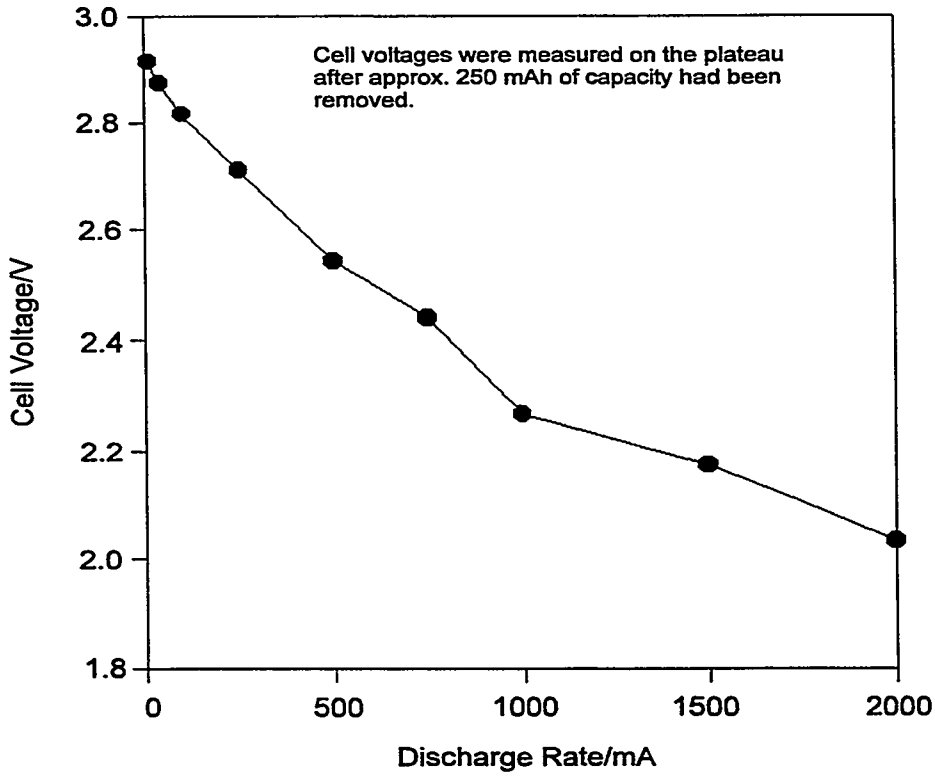

Figure 2-3. Cell voltage as a function of discharge rate for Sanyo 2/3A cells at room temperature.

The last issue to be considered for constant current discharge relates to the effect of temperature on the cell voltage and current. In general, as the temperature is decreased, the equivalent series resistance of the cell increases. This is not particularly surprising when one considers the processes occurring in the cell. For example, the solution conductivity is a function of temperature and changes by about an order of magnitude between room temperature and low subambient temperatures. Consequently, the equivalent series resistance of the cell is expected to increase as the temperature decreases, which will then lead to a lower cell voltage at low temperatures. This process, as well as others, ultimately leads to a decrease in both the voltage and usable capacity. This behavior is illustrated in Figure 2-4 for the Kodak 2/3A cell.

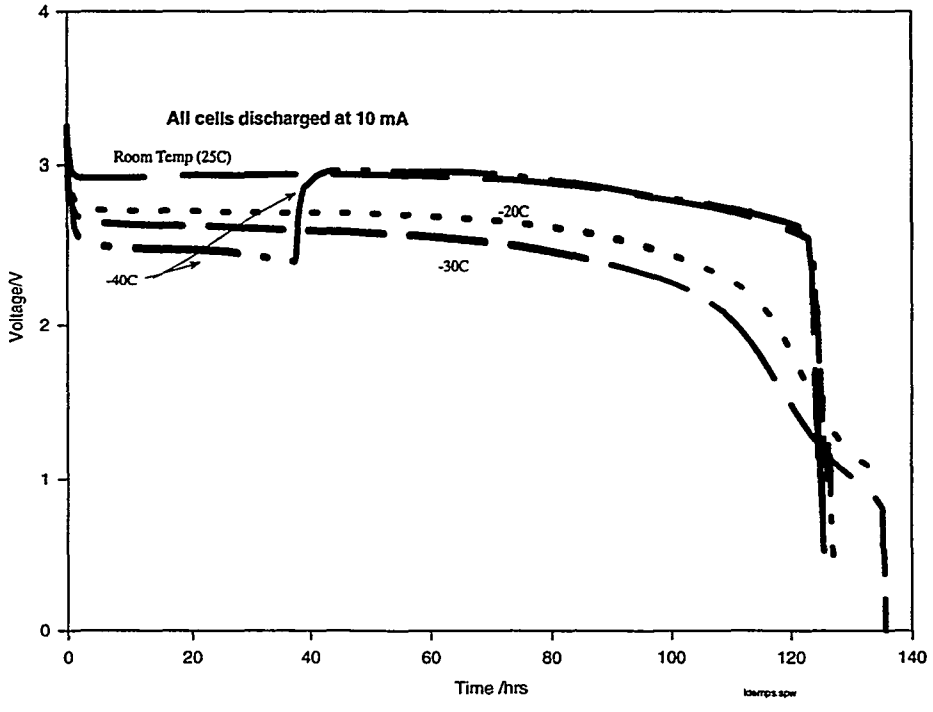

Figure 2-4. Effect of temperature on discharge behavior of Kodak 2/3A cells when discharged at a constant current of 10 mA.

Another interesting feature of this chemistry exhibited by many of the cells studied and illustrated by the data shown here, during the discharge of the cell at –40°C, the cell voltage is approximately 2.5 V, during which time the compressor of the temperature chamber failed, and the cell temperature increased to room temperature. As this occurred, the voltage of the cell returned to that observed for the discharge conducted entirely at room temperature. In fact, the remainder of the discharge curve essentially overlays the room-temperature discharge. That is, the temperature effects appear entirely reversible and well behaved for this chemistry. Furthermore, the total capacity removed is comparable to that obtained when the entire discharge is performed at room temperature. The ability to remove all of the useful energy stored in these cells by discharging the cell at room temperature subsequent to discharge at lower temperatures is characteristic for this chemistry, as will be seen in subsequent chapters. We have also evaluated the cells under conditions of pulsed loads, and these results are described in the next section.

The relative behavior of the cells changes, depending on conditions. Although one might select the Duracell product over most of the others because of its superior performance at room temperature, under other conditions, such as low temperatures, a different product might be preferable.

2.3 Pulse Load Behavior – Cells

An example of an evaluation of this chemistry under conditions of pulsed load at room temperature is shown by the data of Figure 2-5. This figure shows the voltage versus time characteristics of a Varta 2/3A cell under a repetitive pulse train of 714 mA for 3 sec, followed by open circuit stand for 17 sec. This pulsed train was repeated until the cell voltage reached 1.0 V during any part of the pulse profile. Because of the nature of the pulse train applied, the amount of data collected during the experiment and the limitations imposed by the physical size of the paper, these data appear as a single solid performance envelope, although they do consist of discrete pulses. This discrete behavior is illustrated in the insert in Figure 2-5, which shows this discrete behavior using an expanded scale of a small portion of data collected. In this plot, the room temperature discharge behavior of the Varta 2/3A cell is shown under a pulse load regime consisting of 3 sec at 714 mA followed by a rest at open circuit for 17 sec. The 714 mA pulse in a 2/3A cell is the approximate equivalent of a 5 A pulse in a D cell. Furthermore, the combination of a high-duty cycle and a large magnitude pulse is a harsh condition for any battery system and constitutes worst-case conditions for the system. Nevertheless, as shown by the data, the cell is capable of providing significant capacity under these conditions.

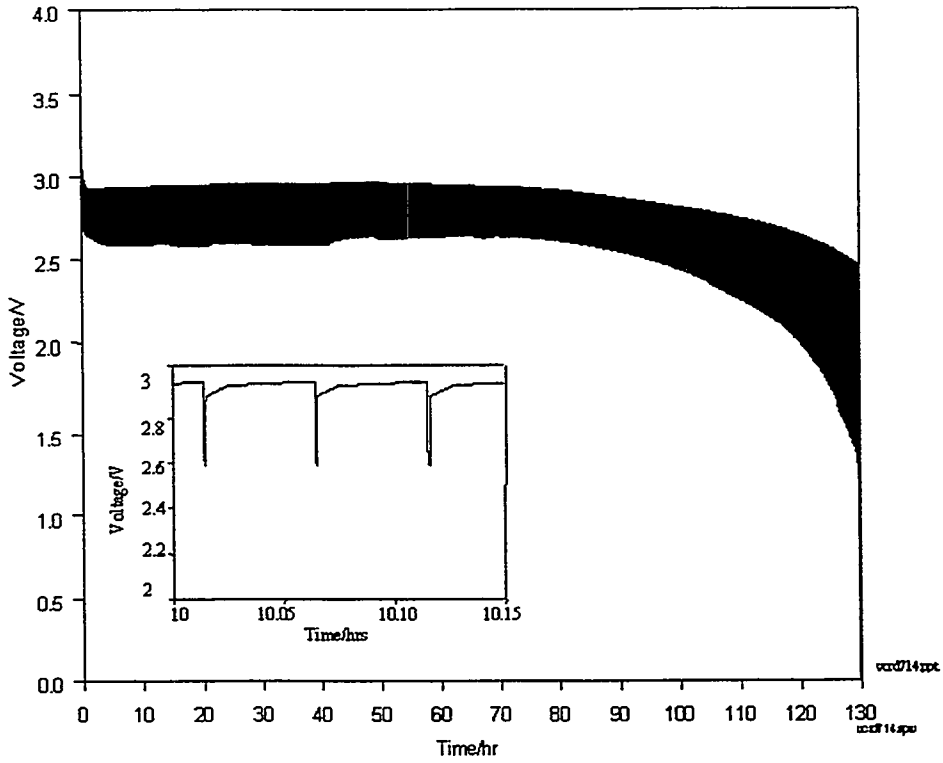

Figure 2-5. Pulse load response of Varta 2/3A cell at room temperature to pulse train consisting of 714 mA for 3 sec followed by 17 sec at open circuit. Shown in the inset is an expanded view of the battery behavior, illustrating the voltage drop of the cell during this pulse.

These data also illustrate that this change in voltage (ΔV) resulting from the change in current is a direct measure of the equivalent series resistance of the cell. The ΔV is relatively constant during the initial portion of the discharge, indicating that the effective equivalent series resistance is relatively constant. As the depth of discharge increases, however, the ΔV increases, signifying an increase in the equivalent series resistance. Although it does increase during the course of discharge, the increase is relatively small.

This pulse test was also performed at elevated temperature, and an example of 2/3A cell behavior is shown in Figure 2-6. In this case, however, the cell response shown for the Varta cell is basically the same as that shown in the preceding figure. As is seen, the cell is capable of providing the requisite currents. In this case, the voltage drop is somewhat less than that observed at room temperature; that is, the cell performs better. This is because the equivalent-series resistance of the cell, which is composed of a number of factors in the cell (for example, the reaction kinetics and mobility of solution species), is enhanced at elevated temperature. This leads to a lower effective equivalent series resistance and hence improved performance.

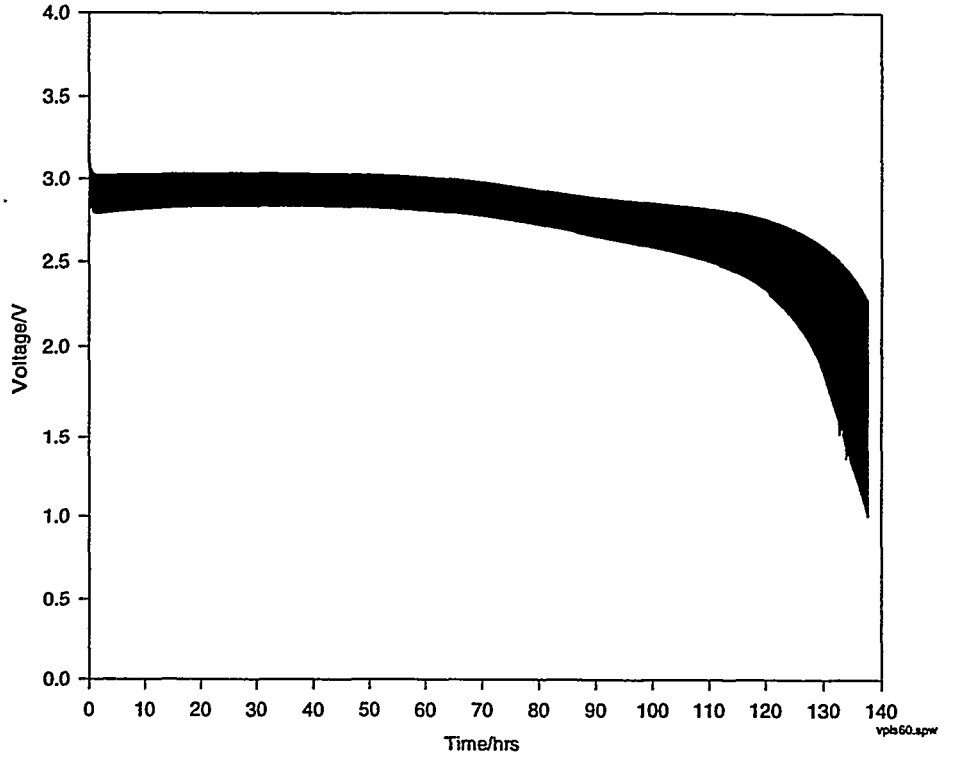

Figure 2-6. Pulse load response of Varta 2/3A cell at 60°C to pulse train consisting of 714 mA for 3 sec followed by 17 sec at open circuit.

Finally, the pulse response of the cell at low temperature, in this case a Sony cell, is shown by the data in Figure 2-7. As seen, the cell is capable of supplying the requisite currents at these low temperatures, albeit at lower voltages and lowered capacities than those observed at room temperature. Also, the voltage drop is larger under these conditions because at lower temperatures, the effective equivalent series resistance is significantly higher than that observed at room temperature.

As in the case of the constant-current discharge at low temperature, if the temperature of the cell is allowed to increase after performing the discharge at low temperature, additional capacity can be obtained. This is shown in Figure 2-8, which shows the continued discharge of the Sony cell shown in Figure 2-7 after it had been allowed to equilibrate at room temperature.

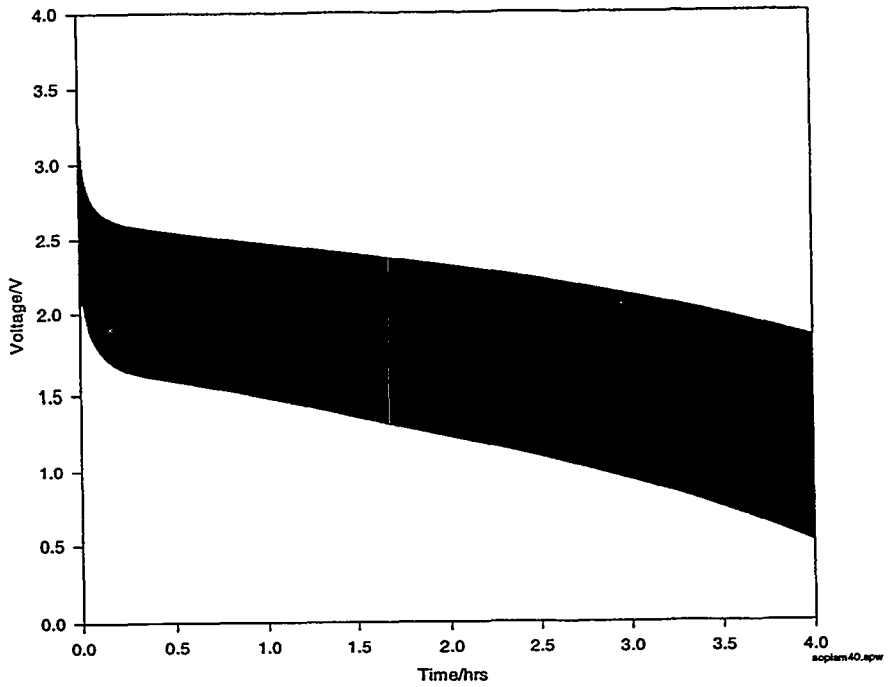

Figure 2-7. Pulse-load response of Sony 2/3A cell at –40°C to pulse train consisting of 714 mA for 3 sec followed by 17 sec at open circuit.

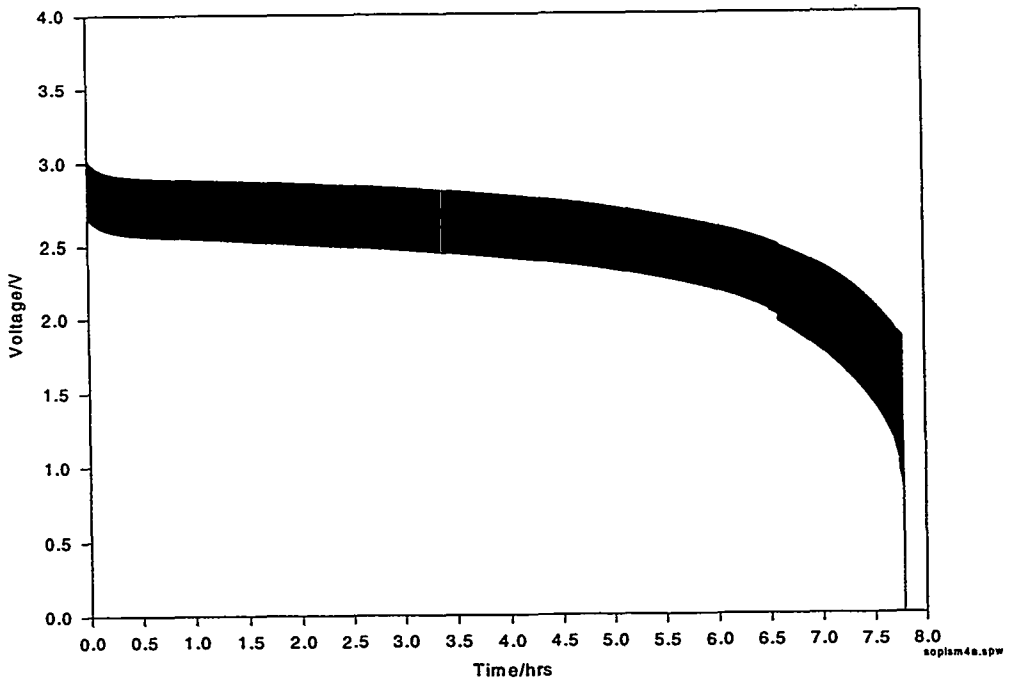

Figure 2-8. Continued pulse-load response Sony 2/3A cell shown in Figure 2-7 after allowing the cell temperature to equilibrate to room temperature. The pulse train used consisted of 714 mA for 3 sec followed by 17 sec at open circuit.

2.4 Pulse Load Behavior – Batteries

Although there are applications suitable for single cells, it is often the case that multiple cells in series/parallel configurations (that is, batteries) would be used. We have evaluated the cells in battery configurations, and some examples of these are described below. We focused on a D-cell equivalent configuration consisting of seven 2/3A cells in parallel. (In this context, the term equivalent is strictly on a volumetric basis only.) These studies were performed at both ambient and subambient temperature conditions. Cells from several vendors were studied in this configuration, but only the results obtained for the Sanyo 2/3A cells are included here.

The pulse train used in these studies consists of a 3-sec 5-A pulse followed by a rest at open circuit for 17 sec, for a total cycle time of 20 sec. (Recall that the 714-mA pulse used for the single cell studies is comparable to the 5-A pulse in a D cell.)

As seen in Figures 2-9 and 2-10, the seven-cell string is capable of supporting this load while maintaining a nominal loaded voltage at about 2.25 V at room temperature. (Recall that in this seven-parallel string configuration, the nominal current through any cell is on the order of 714 mA.) The voltage drop of 0.75 V across the battery stack is primarily associated with the effective equivalent series resistance of the cells making up the string. For the 2/3A cells studied, this value is on the order of about 0.5 Ω per cell. A significant feature of the 2/3A cells that contributes to the equivalent series resistance is the positive temperature coefficient (PTC) of the thermal expansion safety device employed in the cells. This device is present in the commercial cells to prevent, or at least minimize, the possibility of a cell overheating because of cell shorting. PTCs increase cell equivalent series resistance by as much as 90%. Therefore, the possibility exists of reducing the voltage drop at higher pulse loads as well as at low temperatures simply by removal of this design feature.

These cells are also capable of supporting this pulse load at subambient temperatures, as seen in Figures 2-11 and 2-12, which show the pulse behavior at –20°C and at –40°C. As seen, the seven-cell configuration is capable of supporting the 5 A load; however, the voltage drop is larger in this case than in the case of the D cell, as will be seen. This may result from differences in electrode surface area between the D cell and the seven cells in parallel, but may also arise from the fact that the 2/3A cells have PTC devices, while the D cells do not. In fact, a significant fraction of the total equivalent series resistance of the 2/3A cells arises from this device as previously mentioned.

2.5 Conclusions

The cells are capable of supporting a wide range of loads over a large temperature range. In addition, their performance in a battery configuration is seen to be consistent with their behavior at the cell level. Consequently, a first approximation of their behavior in a battery configuration can be obtained by examination of the cell behavior.

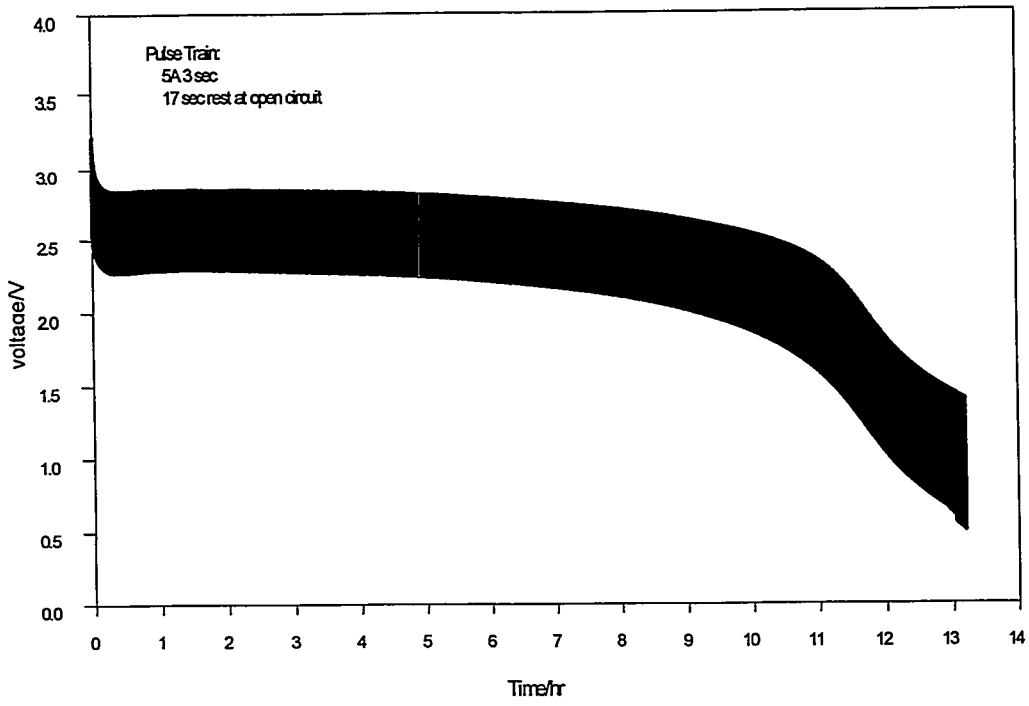

Figure 2-9. Sanyo 2/3A seven-parallel string pulse behavior at room temperature.

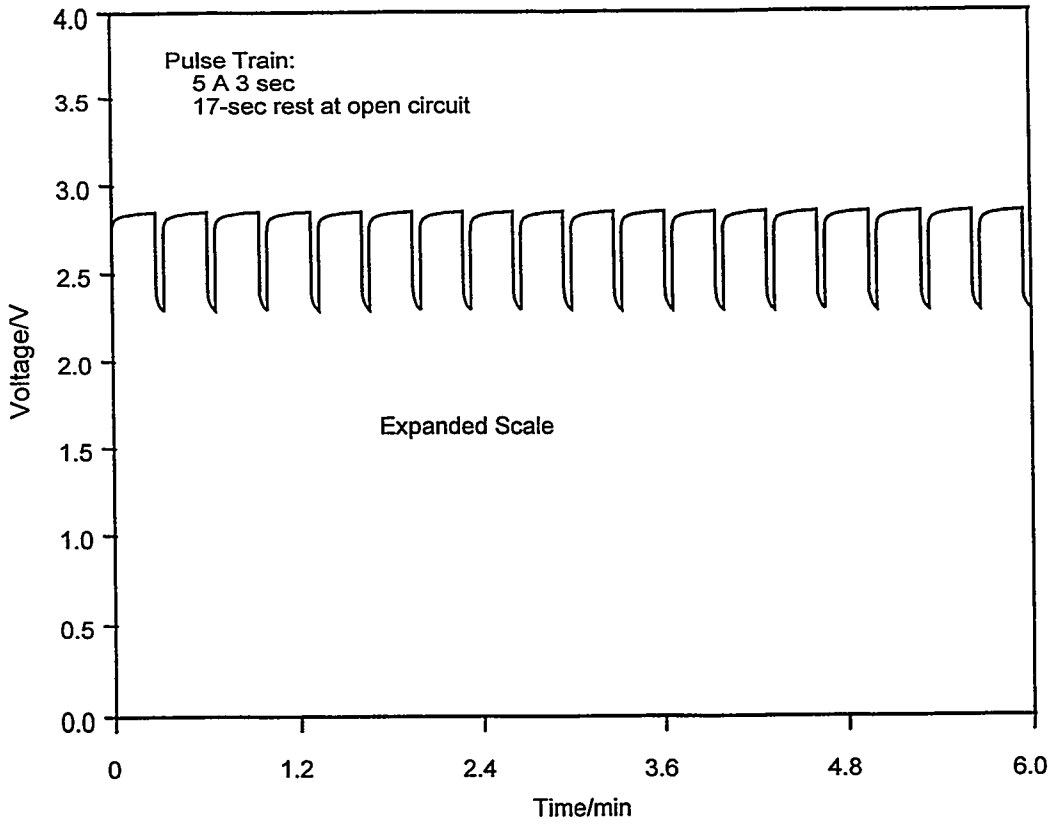

Figure 2-10. Sanyo 2/3A seven-parallel string pulse behavior at room temperature.

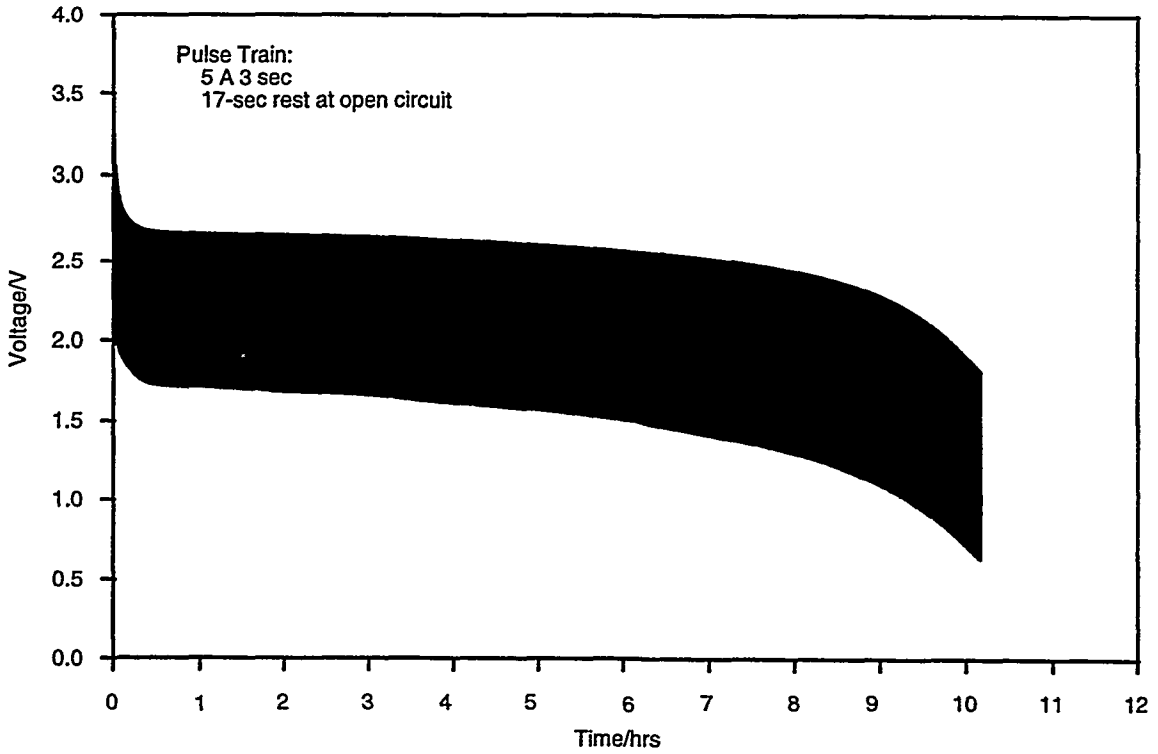

Figure 2-11. Sanyo 2/3A seven-parallel string pulse behavior at –20°C.

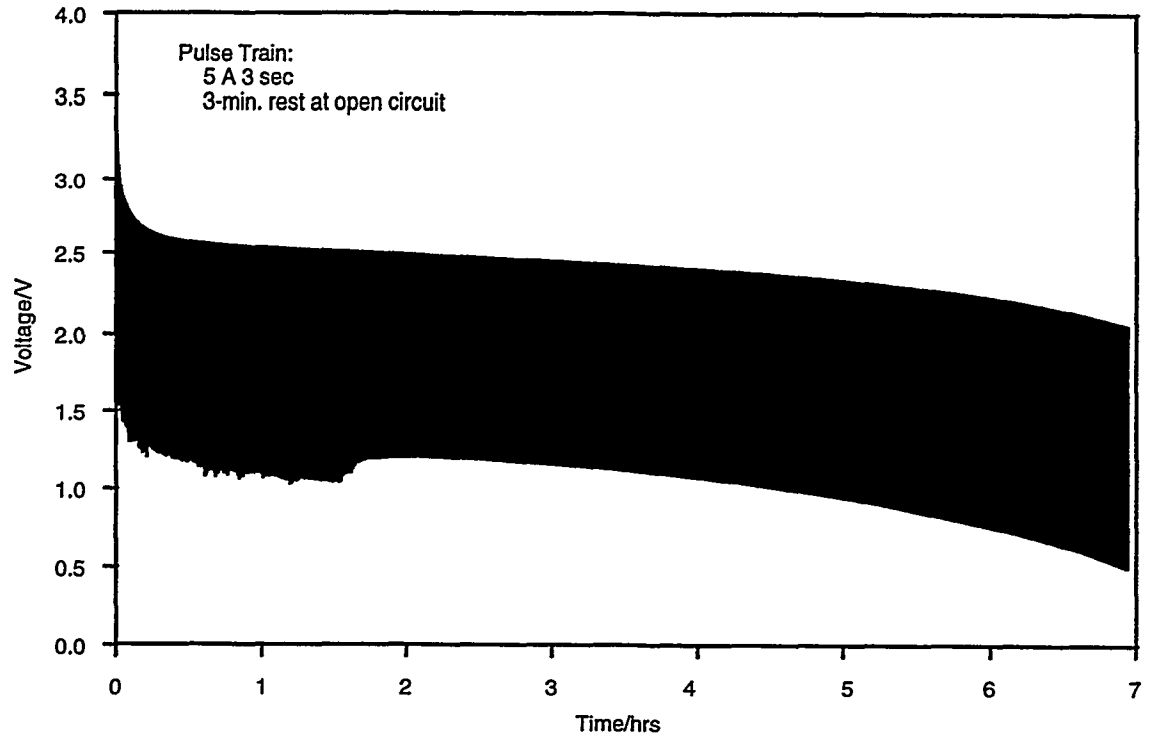

Figure 2-12. Sanyo 2/3A seven-parallel string pulse behavior at –40°C.

This page intentionally left blank

3. C Cell Behavior

Nancy H. Clark, David Ingersoll, Jill L. Langendorf, and Lorie E. Davis

3.1 Introduction

For the most part, the data shown in this section correspond to the worst-case conditions likely to be encountered, such as low temperatures, but moderate conditions were also evaluated. Furthermore, in reviewing the data contained here, it should be recalled some variability in the cell performance exists, and that the degree of variability increases as one operates cells closer to the edge of their performance envelope (for example, at very low temperatures). The two commercial sources for lithium/manganese dioxide C-size cells are Ultralife, and Silberkraft. The cell model currently available from Ultralife is U2550VH-T2-UF and Silberkraft is M52. Table 3-1 summarizes some of the performance characteristics of the cells at room temperature. In deriving these energy numbers, nominal voltages of 2.9 V were used.

Table 3-1. Summary Characteristics of C Cells Evaluated at Room Temperature and Constant Current Discharge of 50 mA Using a Nominal Voltage of 2.9 V

Vendor	Capacity (Ah) (0.5-V cutoff)	Gravimetric Energy Density (Wh/kg)	Volumetric Energy Density (Wh/l)
Silberkraft M52 (low temperature)	5.7	225	470
Ultralife U2550VH-T2-UF	5.2	225	495

3.2 Constant Current Behavior

Figures 3-1 and 3-2 show the constant current discharge behavior of the Ultralife and Silberkraft C cells at room temperature. When the total capacity is calculated from this data, it remains about the same over the range of currents studied. The nominal plateau voltage is lower at higher currents. At room temperature, the cells exhibit a nominal plateau voltage of 3 V, while at –40°C, the nominal plateau voltage is approximately 2.0 V because of the increased equivalent series resistance of the cell at low temperature. The nominal capacities of the cells at room temperature are 5.2 Ah for the Ultralife cell and 5.5 Ah for the Silberkraft cells, while at lower temperatures, the capacities are lower. The spikes seen in the discharge curve at low temperature result from the cell being placed on open circuit for a short time. When this occurred, the cell voltage went to an open circuit no-load condition.

Based on these data, it is clear that some additional capacity should remain in the cell after complete discharge at –40°C, although the amount should be relatively small. Nevertheless, this additional capacity can be obtained by allowing the temperature of the cell to increase and then continuing the discharge at room temperature. Besides being able to obtain this additional capacity, the voltage of the cell also increases in direct response to the decrease of the equivalent series resistance of the cell as the temperature is raised. This behavior was measured by discharging an Ultralife cell at 50 mA constant current at –40°C. A capacity of 4.1 Ah was measured. After discharge, the cell is allowed to warm to room temperature over a period of six hours, during which time the cell voltage is monitored. After equilibration of the cell temperature, the discharge is continued at 50 mA. An additional 1.3 Ah was removed. Thus, the total measured capacity at –40°C and room temperature was 5.4 Ah.

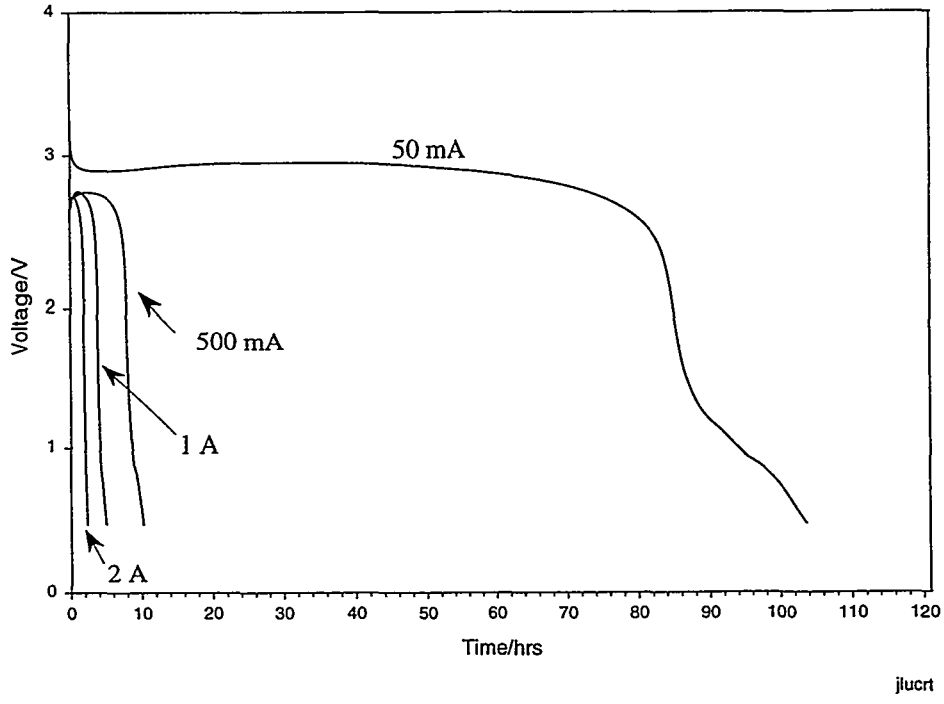

Figure 3-1. Comparison of discharge profiles for Ultralife C cell discharged at various rates at room temperature.

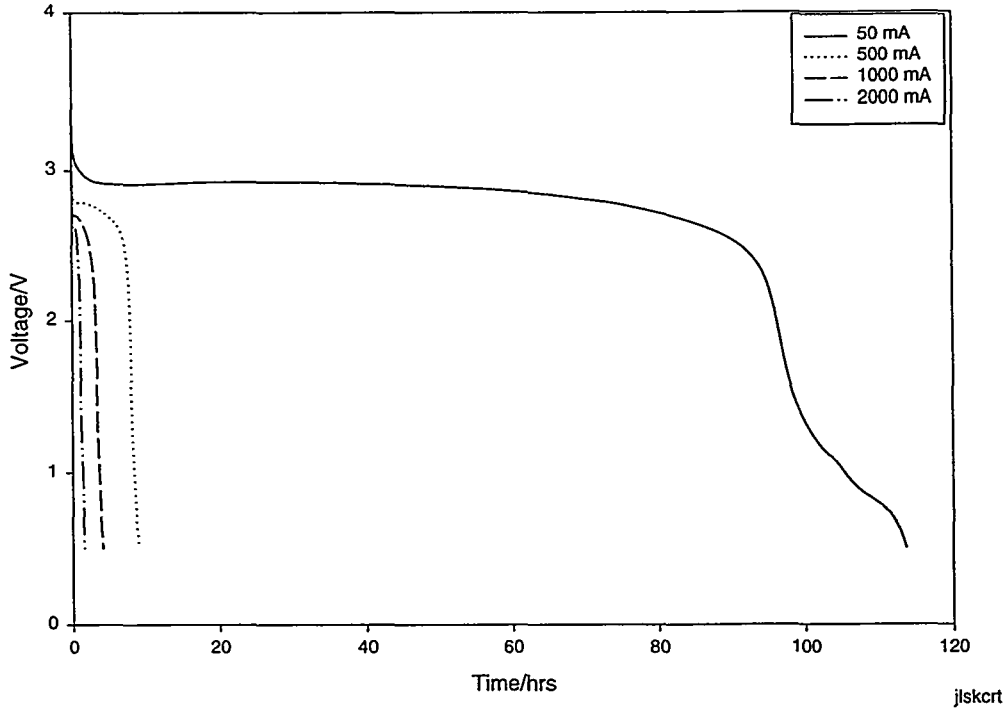

Figure 3-2. Comparison of discharge profiles for Silberkraft C cells discharged at various rates at room temperature.

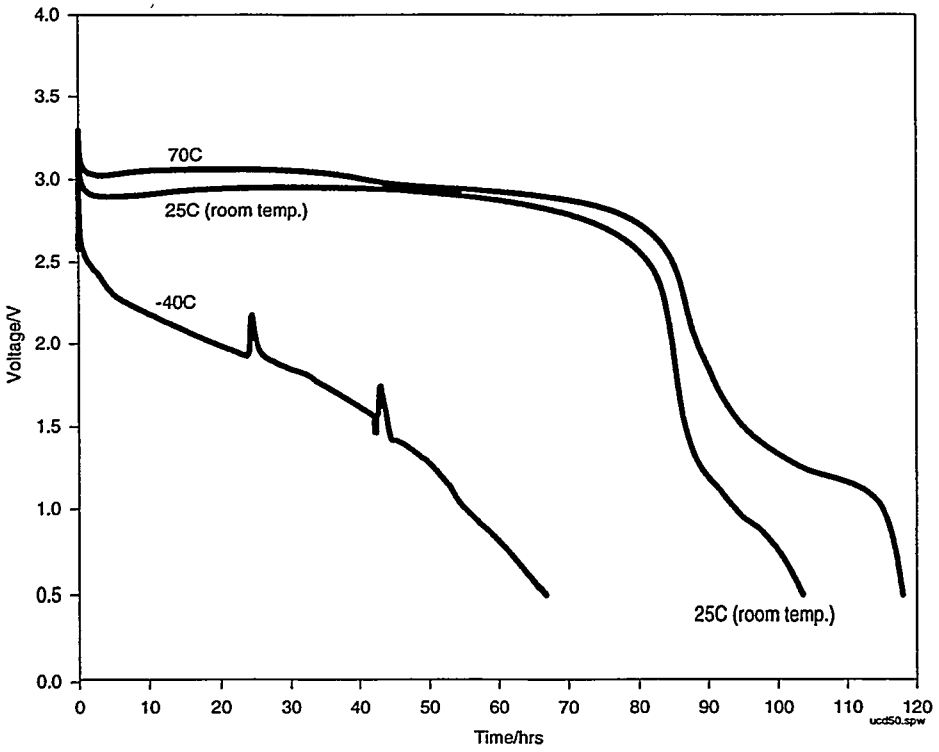

Figure 3-3. **Comparison of discharge profiles for Ultralife C cells discharged at 50 mA at various temperatures. The spikes seen in the –40°C discharge curve result from a momentary open-circuit condition on the cell.**

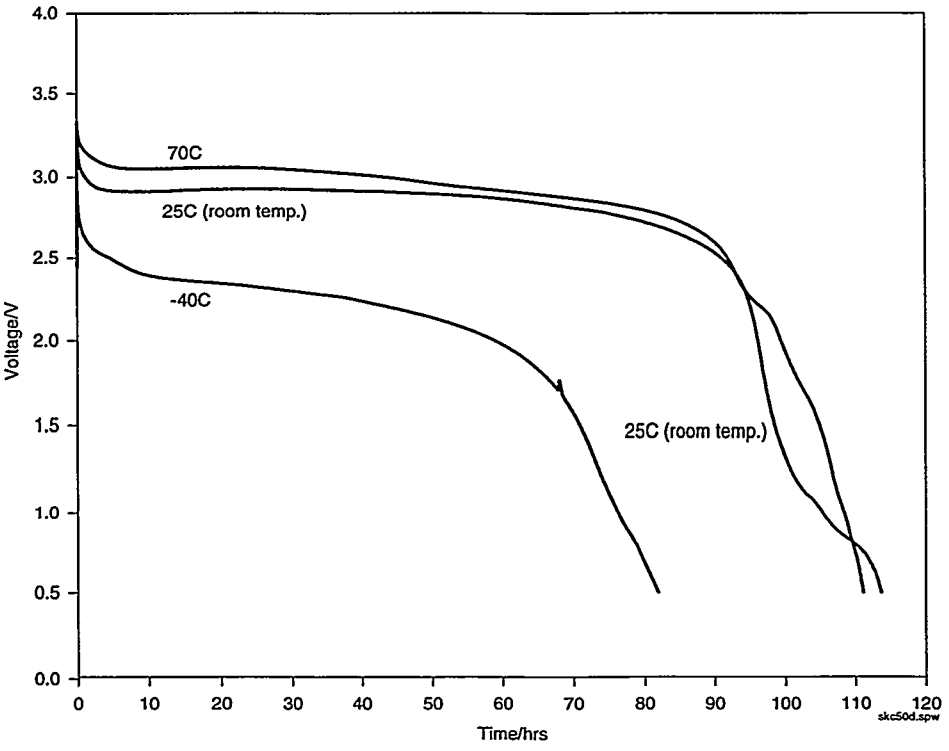

Figure 3-4. **Comparison of discharge profiles for Silberkraft C cells discharged at 50 mA at various temperatures.**

3.3 Pulse Discharge Behavior

Ultralife and Silberkraft C cells were tested using three pulse trains. One pulse train was 2 A for 3 sec, followed by rest at open circuit for 17 sec. Another was 2 A for 3 sec, followed by rest at open circuit for 27 sec. The last was 3 A for 3 sec, followed by rest at open circuit for 27 sec. The data show that the number of pulses a C cell can perform are about the same at room temperature and 70°C, producing the same effective capacity. The plots reflect a difference in run time because there are longer rest periods at 70°C. The run time is significantly shorter at –40°C, which reduces the effective capacity. Figure 3-5 through 3-7 also show that for Ultralife C cells, the nominal operating voltage increases as temperature increases.

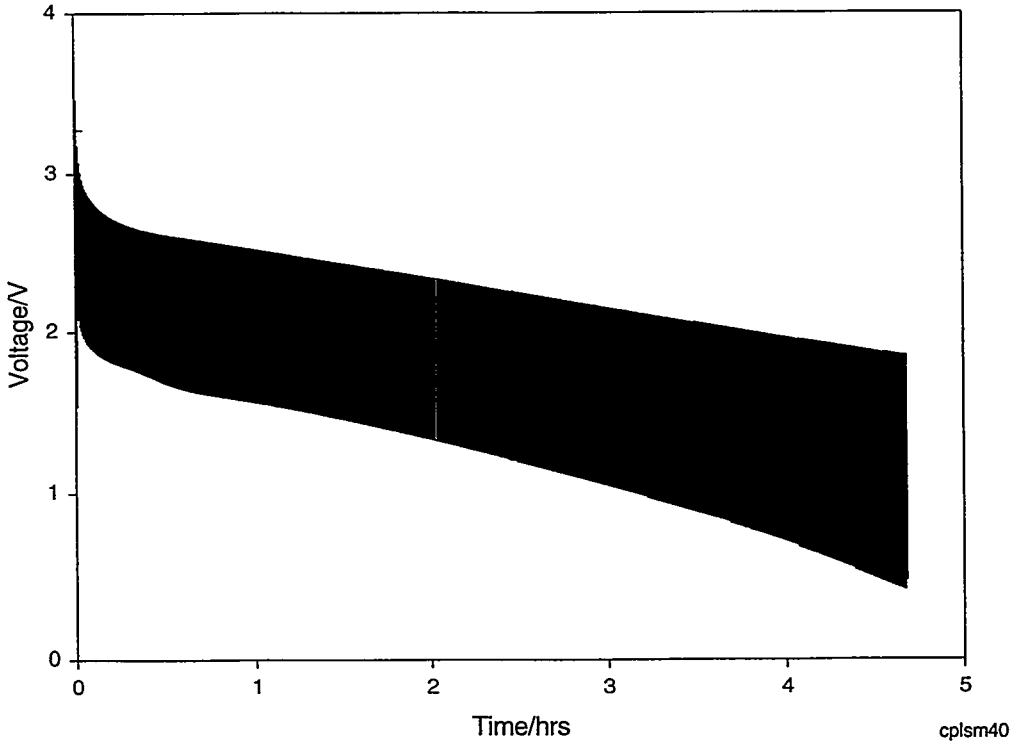

Figure 3-5. Pulse discharge behavior of Ultralife C cells at –40°C. The pulse profile consisted of a 3-sec pulse at 2 A, followed by a rest at open circuit for 17 sec.

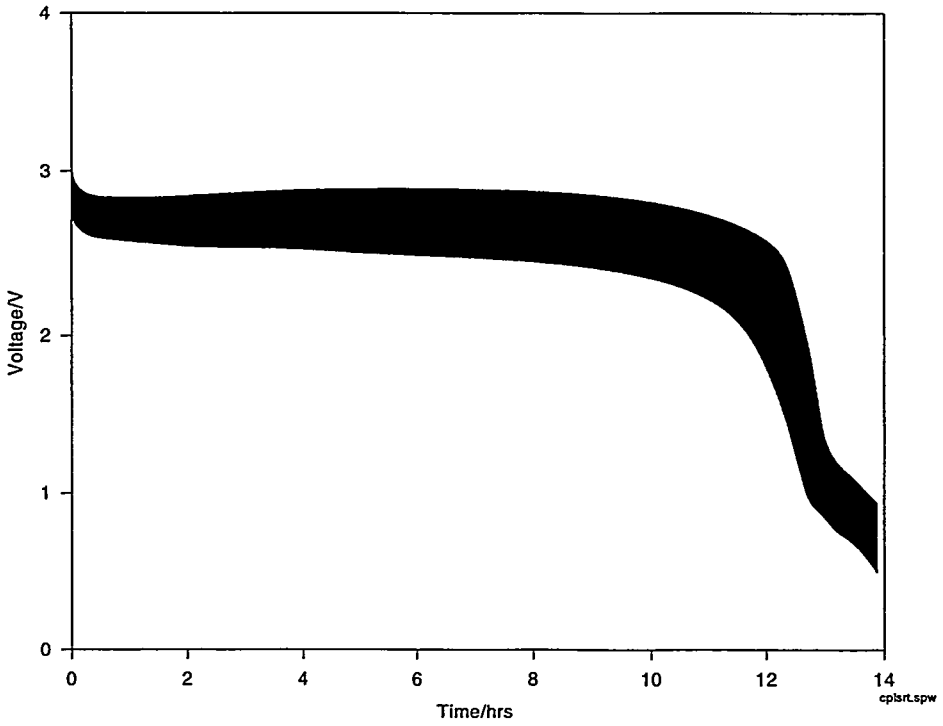

Figure 3-6. **Pulse discharge behavior of Ultralife C cell at room temperature. The pulse profile consisted of a 3-sec pulse at 2 A, followed by a rest at open circuit for 17 sec.**

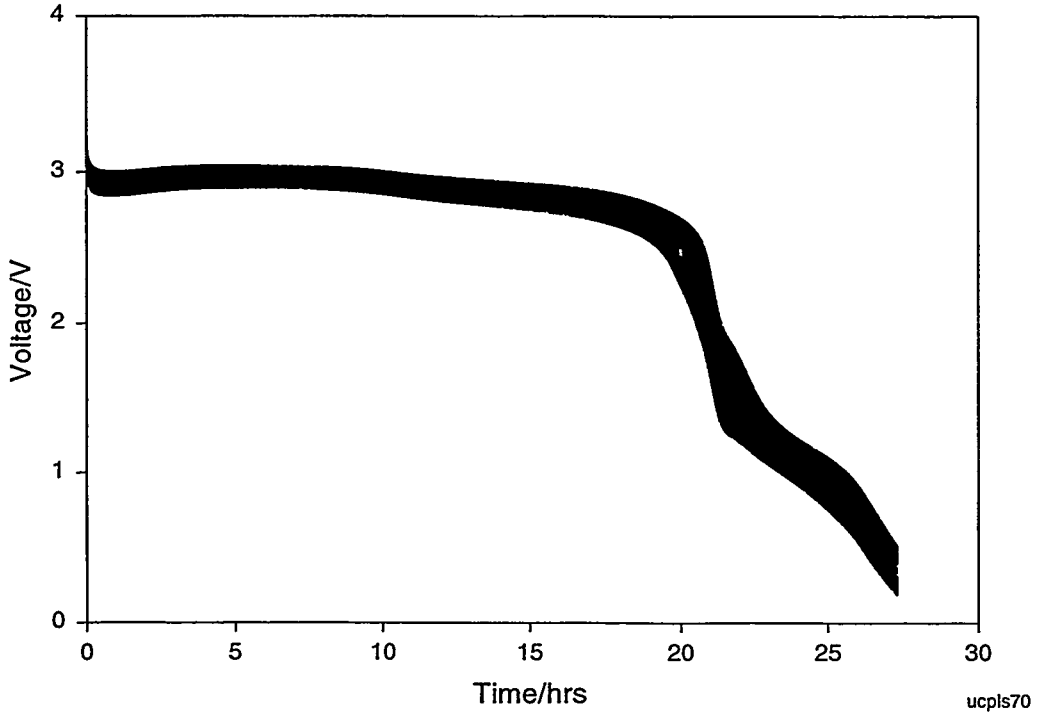

Figure 3-7. **Pulse discharge behavior of Ultralife C cell at 70°C. The pulse profile consisted of a 3-sec pulse at 2 A, followed by a rest at open circuit for 27 sec.**

Figures 3-8 through 3-11 show similar behavior for the Silberkraft cells under the same conditions. The Silberkraft cells were also tested at higher currents because they have higher capacity. Using higher currents did result in expected shorter run times and nominal voltage decreases.

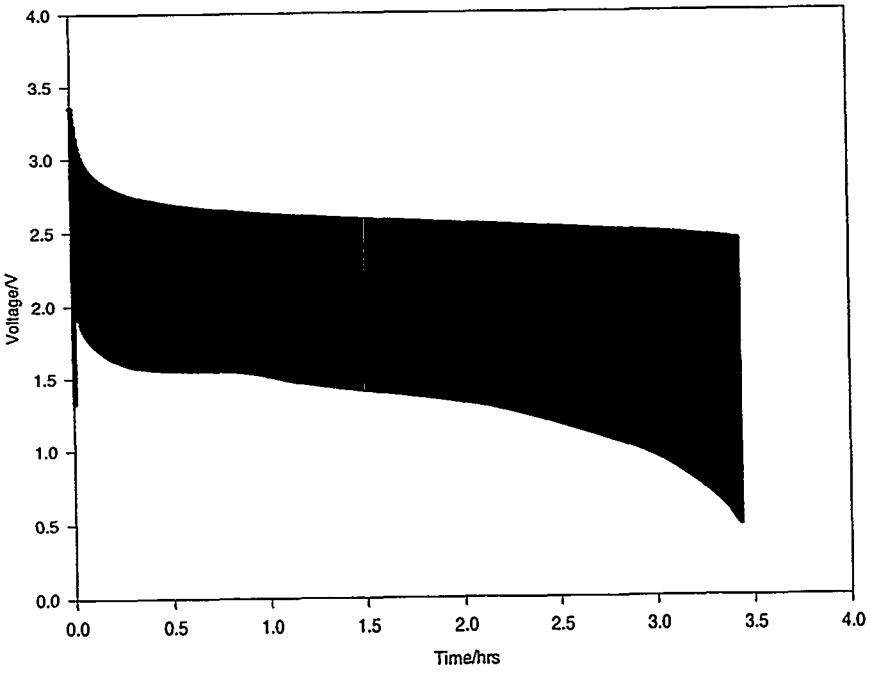

Figure 3-8. Pulse discharge behavior of Silberkraft C cell at –40°C. The pulse profile consisted of a 3-sec pulse at 3 A, followed by a rest at open circuit for 27 sec.

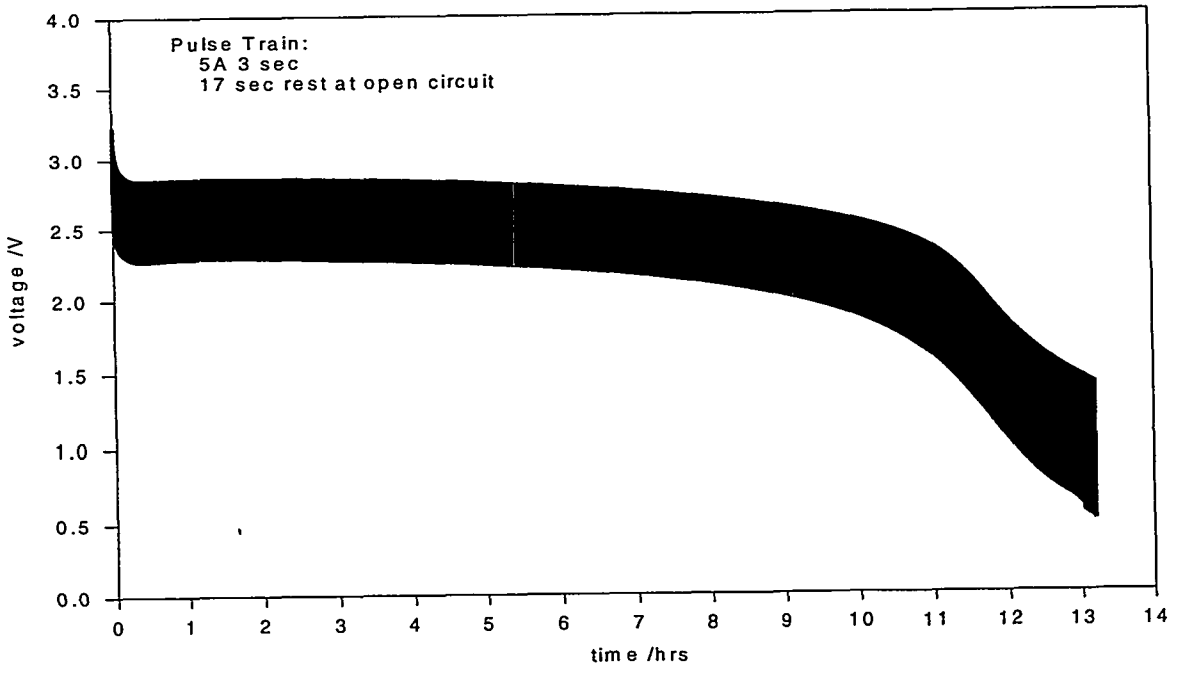

Figure 3-9. Sanyo 2/3A seven-parallel string pulse behavior at room temperature.

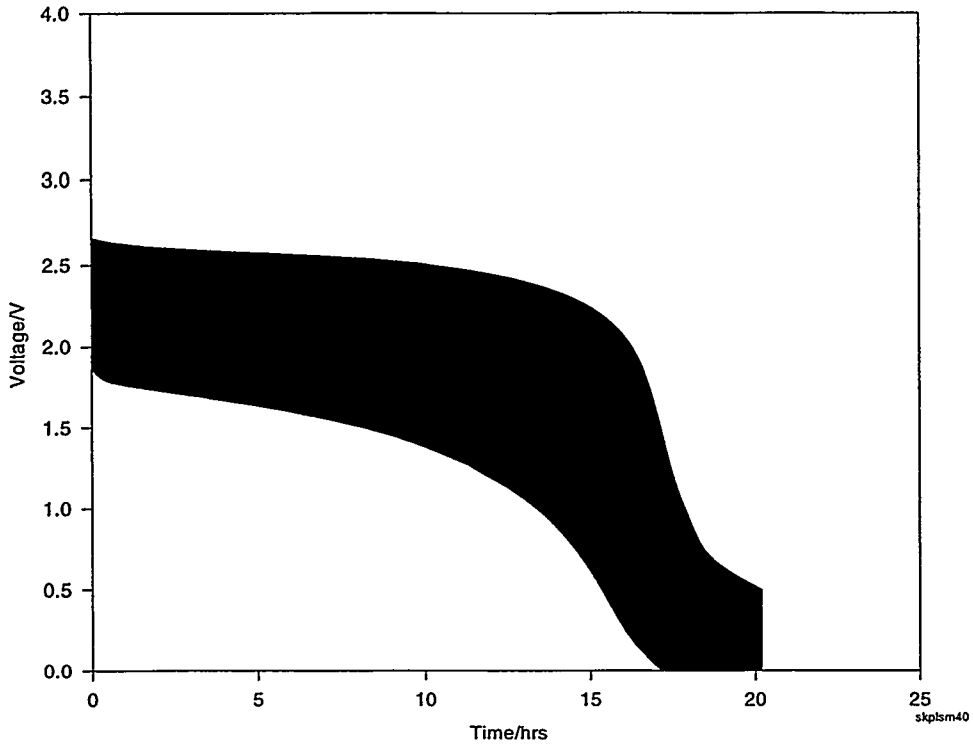

Figure 3-10. **Pulse discharge behavior of Silberkraft C cell at –40°C. The pulse profile consisted of a 3-sec pulse at 2 A, followed by a rest at open circuit for 27 sec.**

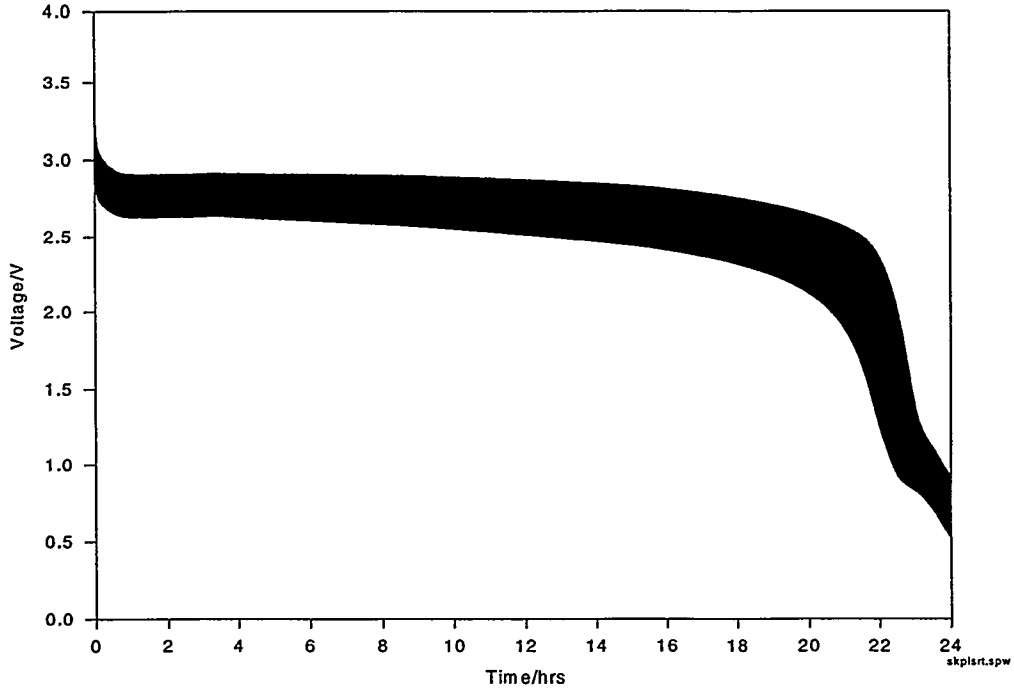

Figure 3-11. **Pulse discharge behavior of Silberkraft C cell at room temperature. The pulse profile consisted of a 3-sec pulse at 2 A, followed by a rest at open circuit for 27 sec.**

3.4 A Summary of Results From C Cell Tests

The previous sections show samples of the test data gathered on C cells. Tables 3-2 and 3-3 show a summary of all the data collected on C cells plus the capacity extracted after the cell was warmed to room temperature. No nominal voltages are given in these cases because they are a combination of discharges at two temperatures. The data are shown as a function of the type of test, that is, constant current and pulse discharge at 2 A and 3 A, with a 17- and 27-sec rest period. The data provided at a given temperature are capacity and the nominal voltage. For pulse discharges, the voltage range is provided for the cell with no current applied, and then the loaded voltage is provided with current applied. The data show that the total effective capacity for C cells is about 5 Ah ± 10% for all tests, although Silberkraft does have consistently higher capacities. The data show that if the cells run at low temperatures, less effective capacity is available and the nominal voltage is lower.

Table 3-2. Summary of Capacity and Voltage at 50% DOD Measured for C Cells of Various Vendors as a Function of Temperature for Constant Current Discharge of 50 Milliamps

Temperature	Ultralife	Silberkraft
RT	5.7 Ah	5.2 Ah
	2.88 V	2.92 V
–40°C	4.1 Ah	3.3 Ah
	2.27 V	1.90 V
–40°C + RT	5.4 Ah	5.5 Ah
+70°C	5.6 Ah	5.9 Ah
	2.96 V	2.94 V

Table 3-3. Summary of Capacity and Open Circuit and Loaded Voltage at 50% DOD Measured for C Cells of Various Vendors as a Function of Temperature for Pulse Discharges

Test Profile 2 A Pulse Discharge 17-sec rest	Silberkraft	Test Profile 3 A Pulse Discharge 17-sec rest	Silberkraft	Test Profile 2 A Pulse Discharge 27-sec rest	Ultralife
RT	4.8 Ah	RT	4.3 Ah	RT	4.2 Ah
	2.9-2.5 V		2.9-2.0 V		2.9-2.5 V
–20°C	3.8 Ah	–20°C	4.1 Ah	–20°C	4.0 Ah
	2.7-2.0 V		2.7-1.8 V		2.5-1.9 V
–20°C + RT	4.7 Ah	–20°C + RT	5.0 Ah	–20°C + RT	5.0 Ah
					2.0-1.3 V

Table 3-3. Summary of Capacity and Open Circuit and Loaded Voltage at 50% DOD Measured for C Cells of Various Vendors as a Function of Temperature for Pulse Discharges (continued)

Test Profile 2 A Pulse Discharge 17-sec rest	Silberkraft	Test Profile 3 A Pulse Discharge 17-sec rest	Silberkraft	Test Profile 2 A Pulse Discharge 27-sec rest	Ultralife
–40°C	4.2 Ah 2.6-1.7 V	–40°C	1.0 Ah 2.6-1.4 V	–40°C	1.7 Ah 2.0-1.0 V
–40°C + RT	5.1 Ah	–40°C + RT	4.6 Ah	–40°C + RT	4.9 Ah 2.8-2.4 V
+70°C	5.0 Ah 3.0-2.7 V	0	4.3 Ah 2.8-2.1 V	+70°C	5.5 Ah 2.9-2.8 V
		0 + RT	4.7 Ah		

Intentionally Left Blank

4. 5/4C Cell Behavior

Nancy H. Clark, David Ingersoll, Jill L. Langendorf, and Lorie E. Davis

4.1 Introduction

Currently, the only commercial sources for lithium/manganese dioxide 5/4C-size cells are Ultralife and Silberkraft. Cells for this study were available from Ultralife. For the most part, the data shown correspond to the worst-case conditions likely to be encountered, such as low temperatures, but moderate conditions were also evaluated.

4.2 Constant Current Behavior

The cell currently available from Ultralife is U2560VH. Table 4-1 summarizes some of the performance characteristics of the cells at room temperature under constant-current discharge at relatively low rates. In deriving these energy numbers, nominal voltages of 2.9 V were used.

Figures 4-1 and 4-2 show the behavior of the Ultralife cells at room temperature and at –40°C. As calculated from these figures, the total capacity remains about the same over a range of currents. As shown, at room temperature, the cells exhibit a nominal plateau voltage of 3 V, while at –40°C, the nominal plateau voltage used is approximately 2.0 V because of the increased equivalent series resistance of the cell at low temperatures. The nominal capacities at room temperature of the Ultralife cell is 7.1 Ah and 5.0 Ah at –40°C. The "spikes" seen in the discharge curves at low temperature result from the cell being placed on open circuit for a short time. When this occurs, the cell voltage reflects a no-load condition.

Based on this, it is clear that some additional capacity should remain in the cell after complete discharge at –40°C, although the amount should be relatively small. Nevertheless, this additional capacity can be obtained by allowing the temperature of the cell to increase and then continuing the discharge at room temperature. After discharge, the cell is allowed to warm to room temperature over a period of six hours, during which time the cell voltage is monitored. After equilibration of the cell temperature, the discharge is continued at 50 mA. The total measured capacity at –40°C and room temperature was 7.2 Ah. Besides being able to obtain this additional capacity, the voltage of the cell also increases in direct response to the decrease of the equivalent series resistance of the cell as the temperature is raised.

Table 4-1. Summary of Characteristics of 5/4C Cells Evaluated at Room Temperature and Constant Current Discharge of 50 mA Using a Nominal Voltage of 2.9 V

Vendor	Capacity (Ah) (0.5-V cutoff)	Gravimetric Energy Density (Wh/kg)	Volumetric Energy Density (Wh/l)
Ultralife U2560VH	7.1	294	654

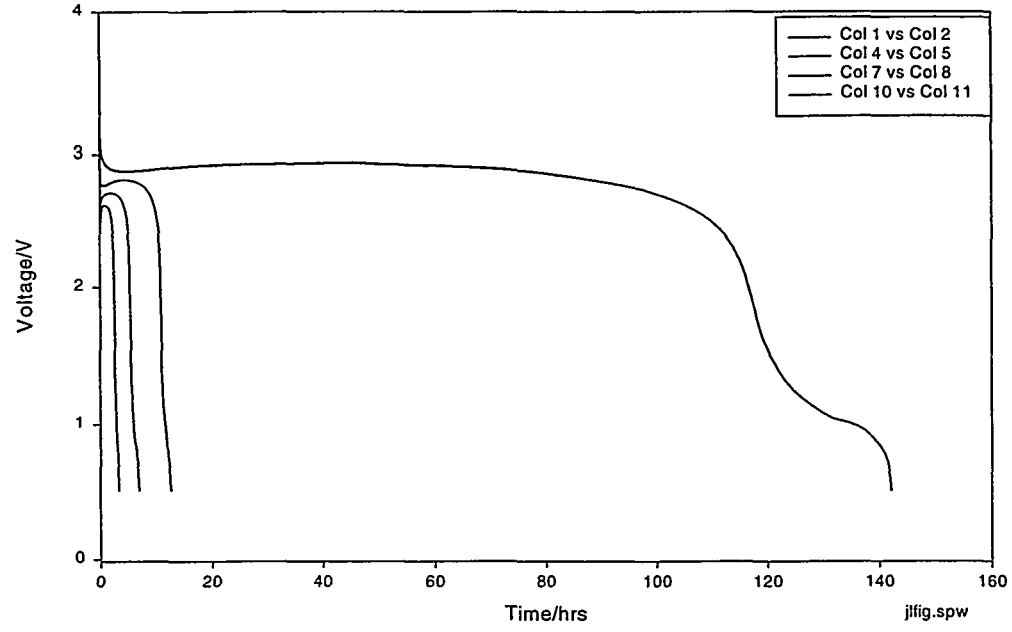

Figure 4-1. **Comparative discharge curves for 5/4C cells discharged at constant current rates of 50 mA, 500 mA, 1000 mA, and 2000 mA, with the 50mA curve lasting the longest and the 2000 mA curve being the shortest. All the cells were discharged at room temperature.**

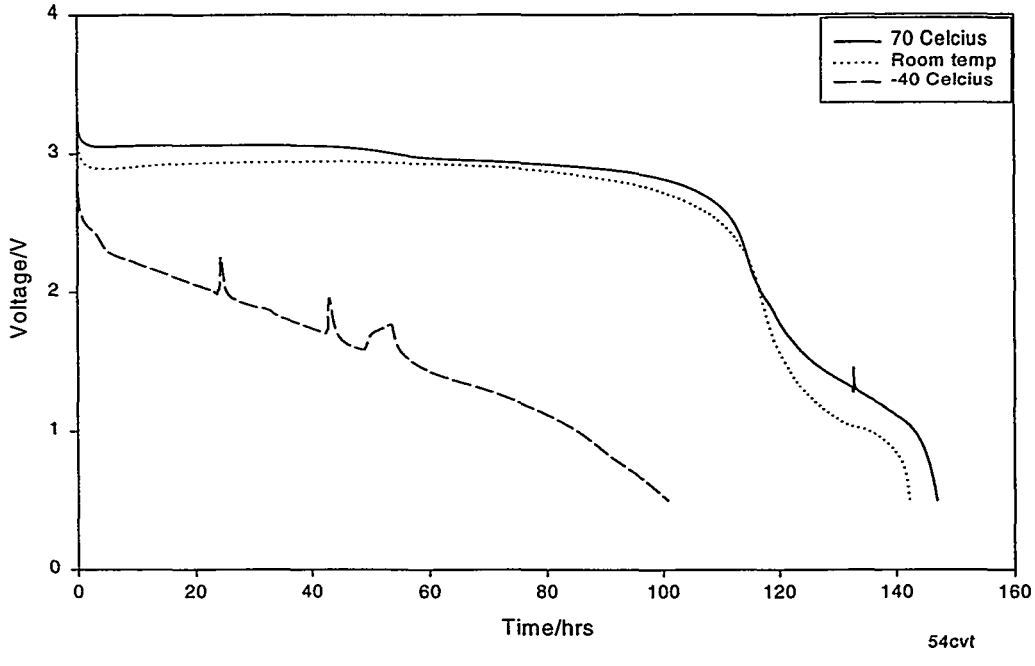

Figure 4-2. **Comparative discharge curves for 5/4C cells discharged at a constant current of 50 mA at various temperatures. The spikes shown in the discharge curve at –40°C arise from a momentary open-circuit condition on the cell.**

4.3 Pulse Discharge Behavior

Ultralife cells were also tested using a pulse train of 3 sec at 2 A followed by a rest at open circuit for 27 sec at ambient and at low temperatures. The data show that the number of pulses a cell can provide is related to the temperature. Figure 4-3 shows the room temperature behavior of the 5/4C cell, which can serve as the basis for comparison against. At –40°C, Figure 4-4, very few operations are performed compared to –20°C. Figures 4-4 through 4-6 show that for Ultralife cells, the nominal operating voltage increases as temperature increases. Figure 4-6 does show however that if the cell is allowed to return to room temperature and pulsing is continued, the total number of pulses increases significantly.

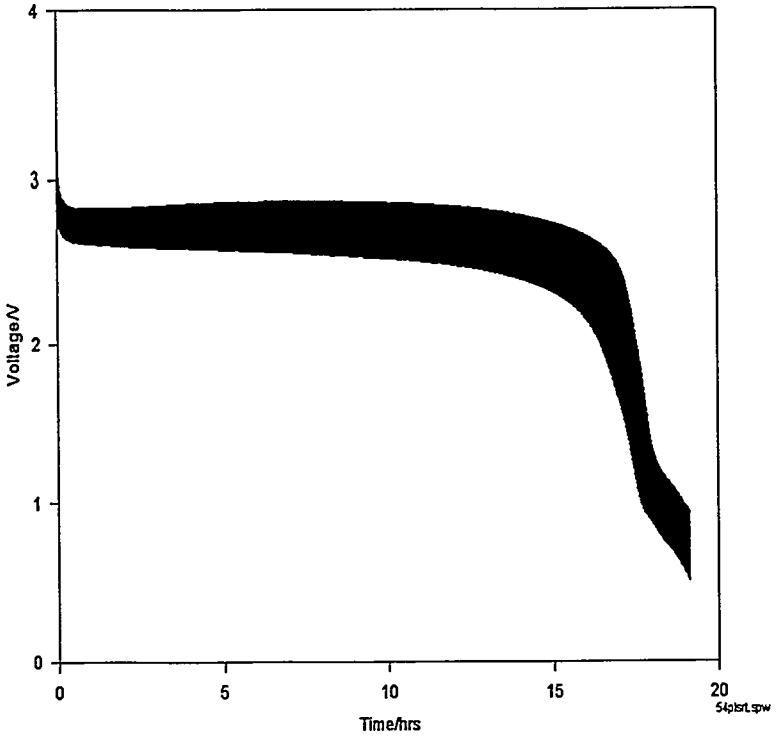

Figure 4-3. **Pulse discharge behavior for Ultralife 5/4C cell at room temperature. The pulse discharge profile was composed of a 3-sec pulse at 2 A, followed by an open circuit stand for 27 sec.**

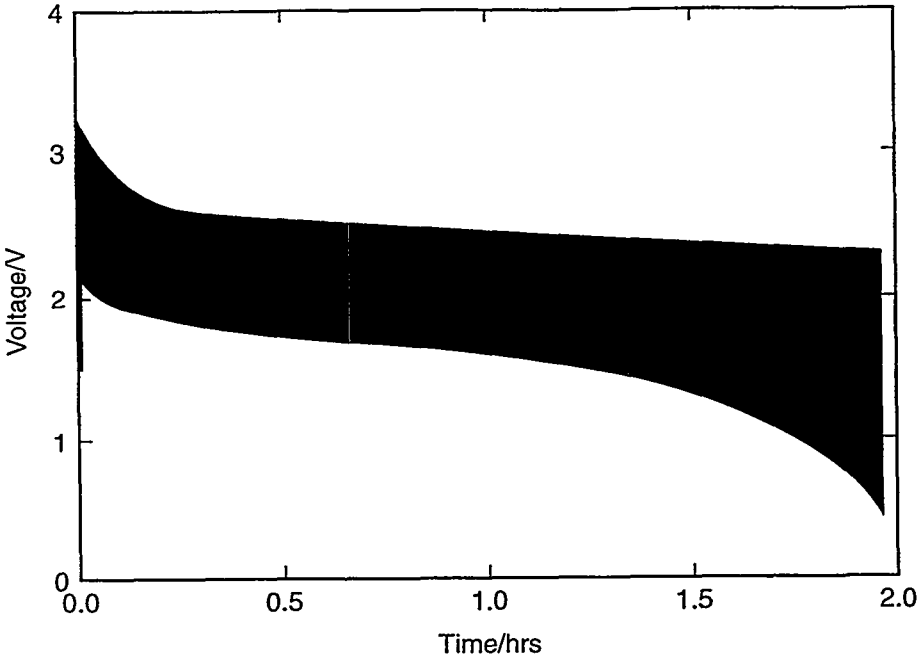

Figure 4-4. **Pulse discharge behavior for Ultralife 5/4C cell at –40°C. The pulse discharge profile was composed of a 3-sec pulse at 2 A, followed by an open circuit stand for 27 sec.**

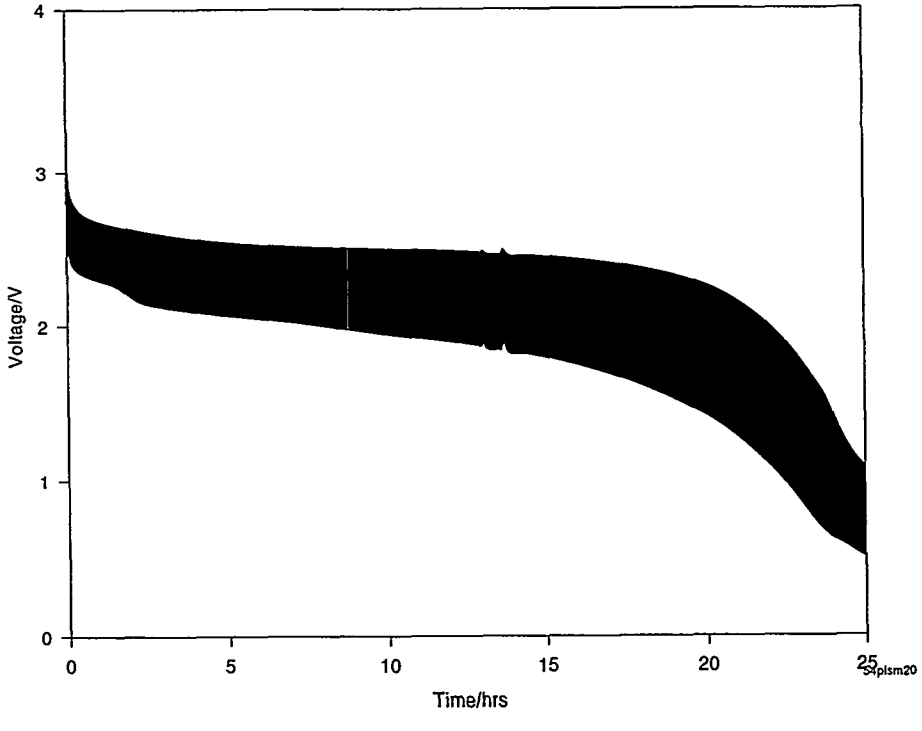

Figure 4-5. **Pulse discharge behavior for Ultralife 5/4C cell at –20°C. The pulse discharge profile was composed of a 3-sec pulse at 2 A, followed by an open circuit stand for 27 sec.**

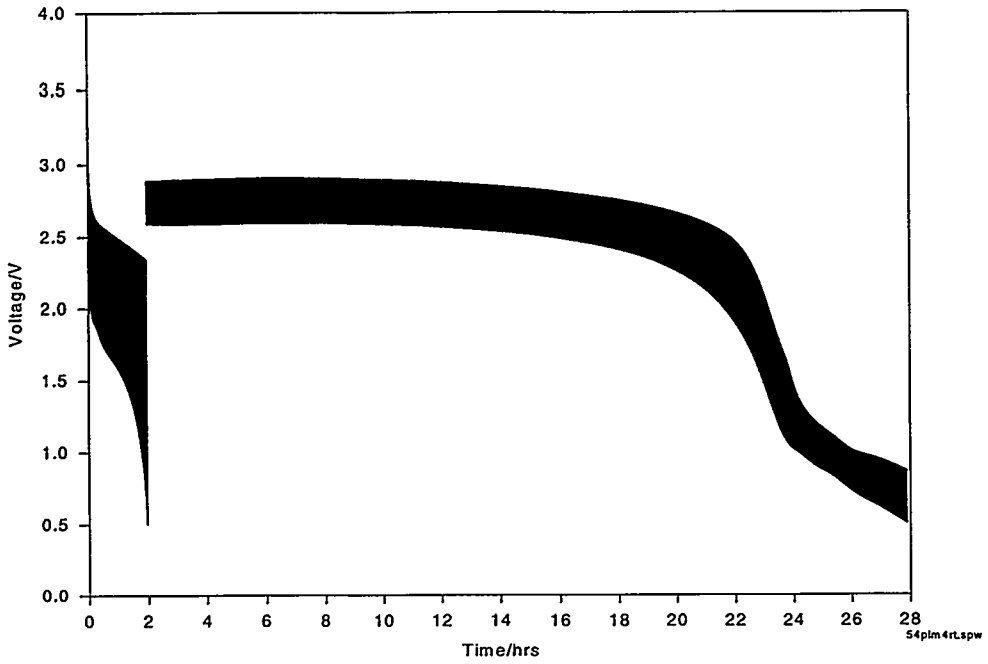

Figure 4-6. Pulse discharge behavior for Ultralife 5/4C cell at –40°C followed by continuation of the pulse discharge after allowing the cell to warm to room temperature. The pulse discharge profile was composed of a 3-sec pulse at 2 A, followed by an open circuit stand for 27 sec.

4.4 Summary

Tables 4-2 and 4-3 show a summary of the data collected on 5/4C cells plus the capacity extracted after the cell was warmed to room temperature. There are no nominal voltages given in these cases because they are a combination of discharges at two temperatures. The data are shown as a function of the type of test, that is, constant current or pulse discharge. The data provided at a given temperature are capacity and the nominal voltage. For pulse discharges, the voltages given represent the OCV cell voltage loaded at 50% DOD. The low temperature plus room temperature data are equal the total capacity extracted at the low temperature. The data show that the total effective capacity for 5/4C cells is about 7 Ah ± 10% for all tests. The data also show that if the cells run at low temperatures, less effective capacity is available. Nominal voltage also decreases as a function of temperature.

Table 4-2. Summary of Capacity and OCV at 50% DOD Measured for 5/4C Cells as a Function of Temperature for Constant Current of 50 mA Discharges

Temperature	Vendor
	Ultralife
RT	7.1 Ah
	2.91 V
–40°C	5.0 Ah
	1.70 V
–40°C + RT	7.3 Ah
	1.67 V
+70°C	7.3 Ah
	2.94 V

Table 4-3. Summary of Capacity and OCV and Load Voltage Measured for 5/4 C Cells as a Function of Temperature for Pulse Discharges of 2 A Pulse Discharge with 27-sec Rest

Temperature	Vendor
2 A Pulse Discharge with 27-sec rest	Ultralife
RT	5.7 Ah
	2.89 – 2.53 V
–20°C	5.0 Ah
	2.49 – 1.88 V
–20°C + RT	6.1Ah
–40°C	0.8 Ah
	2.41 – 1.43 V
–40°C + RT	5.6 Ah

5. D-Cell Performance Behavior

David Ingersoll, Nancy H. Clark, Jill L. Langendorf, and Lorie E. Davis

5.1 Introduction

Three commercial sources for lithium/manganese dioxide D-size cells exist: Ultralife, Bluestar, and Silberkraft. Ultralife is a U.S. corporation with production facilities in the United Kingdom where the D cells are produced. Bluestar is a Canadian corporation with production facilities in Canada. Silberkraft is a German corporation with production facilities for their lithium/manganese dioxide line in Germany. Currently, Silberkraft manufactures two versions of their D cells, and Ultralife manufactures only one although two others have been available in the past. The two Silberkraft versions are the M20 and M20TT; the primary difference is that the M20TT is a low-temperature version of the standard M20 cell. This performance difference is achieved by using a different solvent system. The cell currently available from Ultralife is the U3360H, and the other two cells that were available were designated U3360 and U3360VH. The primary difference between these versions of Ultralife cells is the relative rate capabilities, corresponding to standard rate, high rate (H), and very high rate (VH). The difference in rate capability is achieved through both engineering (e.g., electrode surface areas) and materials differences (e.g., different manganese dioxides). The cells included in this evaluation are those that were readily available, namely: (1) Ultralife very high rate and high rate; (2) Bluestar; and (3) Silberkraft standard cell M20 and low-temperature cell M20TT. Both the Ultralife and Bluestar cells were available in very limited quantity, while the Silberkraft cells were more readily available. This section, which discusses the D-cell performance, is organized according to their availability. Ultralife and Bluestar cell characteristics are discussed together followed by the discussion of Silberkraft cells.

5.2 Constant-Current Behavior

The constant-current discharge characteristics of the D cells are similar to those observed for the cells of other sizes discussed thus far. Figure 5-1 shows the behavior of the Bluestar and Ultralife D cells at room temperature and at –40°C. As shown, at room temperature the cells exhibit a nominal plateau voltage of 3 V, while at –40°C the nominal plateau voltage is approximately 2.5 V. The increased equivalent series resistance of the cell at low temperatures causes this lower voltage. The nominal capacities at room temperature of both the Ultralife and Bluestar cells are in the range of 10 Ah, while at lower temperatures the capacities are lower by less than 10%. The spikes seen in the discharge curves at –40°C result from an open circuit condition of the cells for a short time. This is caused by a human or machine error.

Table 5-1 summarizes some of the constant-current discharge characteristics of the cells at room temperature. In deriving the energy numbers, nominal voltages of 2.9 V were used.

Table 5-1. Summary of Characteristics of D Cells Evaluated at Room Temperature and Constant-Current Discharge of 50 mA Using a Nominal Voltage of 2.9 V

Vendor	Capacity (Ah) (2 V cutoff)	Gravimetric Energy Density (Wh/kg)	Volumetric Energy Density (Wh/l)
Silberkraft M20TT (low temperature)	10.5	265	563
Silberkraft M20 (standard)	10.7	279	575
Ultralife U3360VH (very high rate)	9.6	239	516
Ultralife U3360H (standard)	11.1	274	594
Bluestar	10.6	282	615

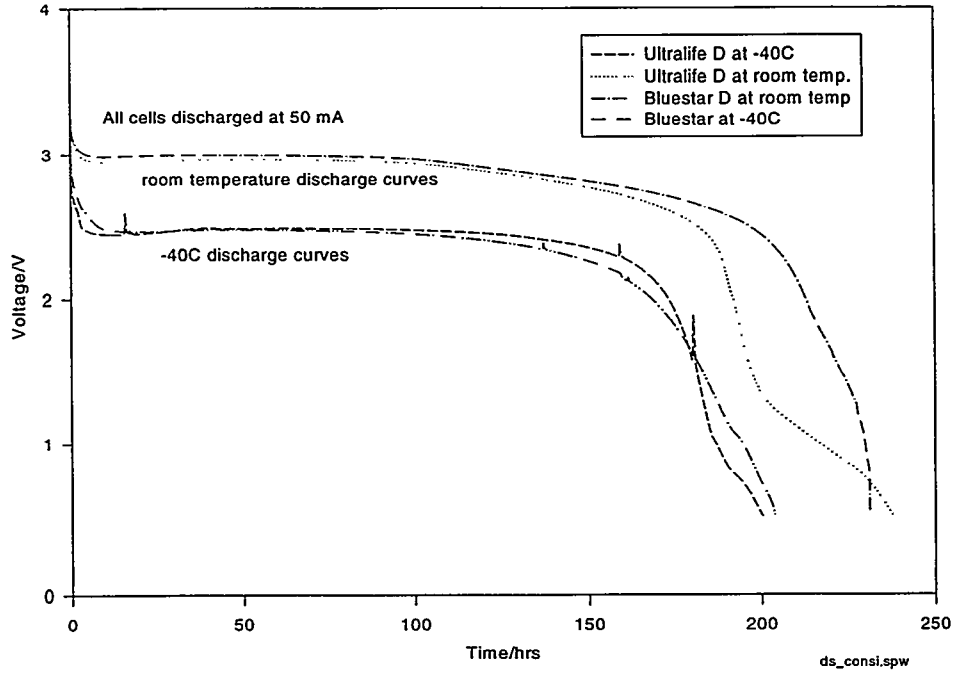

Figure 5-1. Discharge profiles of Ultralife U3360VH and Bluestar D cells at a constant-current rate of 50 mA at room temperature and –40°C.

The data show that some additional capacity should remain in the cell after complete discharge at –40°C, although the amount should be relatively small. This additional capacity can be obtained by allowing the temperature of the cell to increase and then continuing the discharge at this higher temperature. Besides being able to obtain this additional capacity, the voltage of the cell should also increase in direct response to the decrease of the equivalent series resistance of the cell as the temperature is raised. The data in Figure 5-2 demonstrate this behavior. After discharge, the cell is allowed to warm to room temperature for six hours, during which time the cell voltage is monitored. After equilibration of the cell temperature, the discharge is continued at 50 mA. As seen, an additional amount of capacity can be obtained at a higher voltage. Also, a significant increase in cell voltage occurs immediately after discontinuation of the first discharge at –40°C. The magnitude of the change in voltage is a reflection of the equivalent series resistance of the cell at the end of discharge at –40°C.

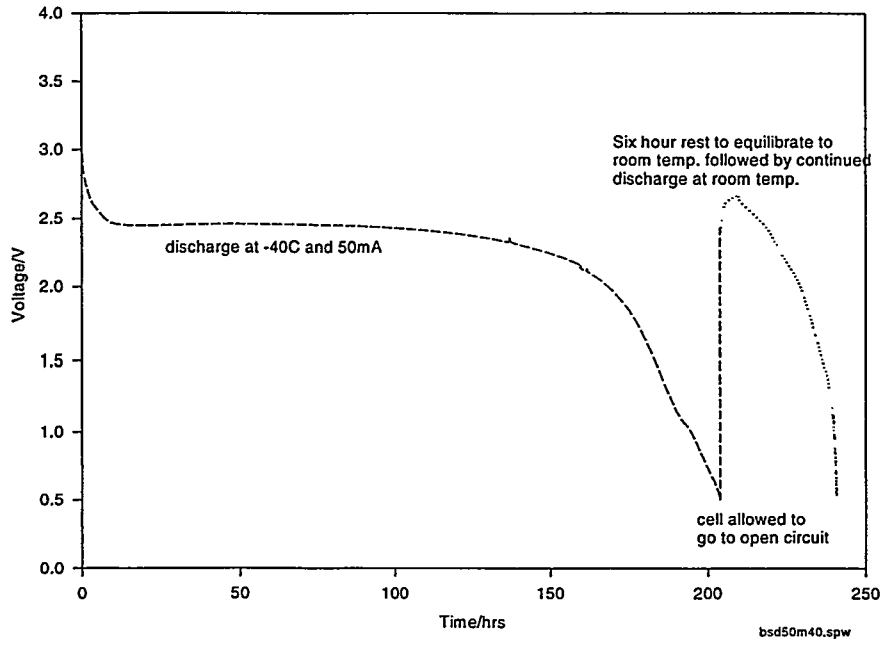

Figure 5-2. Discharge curves for a Bluestar cell at –40°C followed by the continued discharge of the cell after warming to room temperature. The cell voltage is monitored during the entire process. Both discharges were carried out at a constant current of 50 mA.

The behavior of the Silberkraft cells is similar in many respects to that of the Bluestar and Ultralife cells. Figure 5-3 shows the constant-current discharge profiles of the Silberkraft M20 standard cell for temperatures ranging from –55°C to as high as 70°C. As shown, as the temperature decreases, the cell voltage decreases.

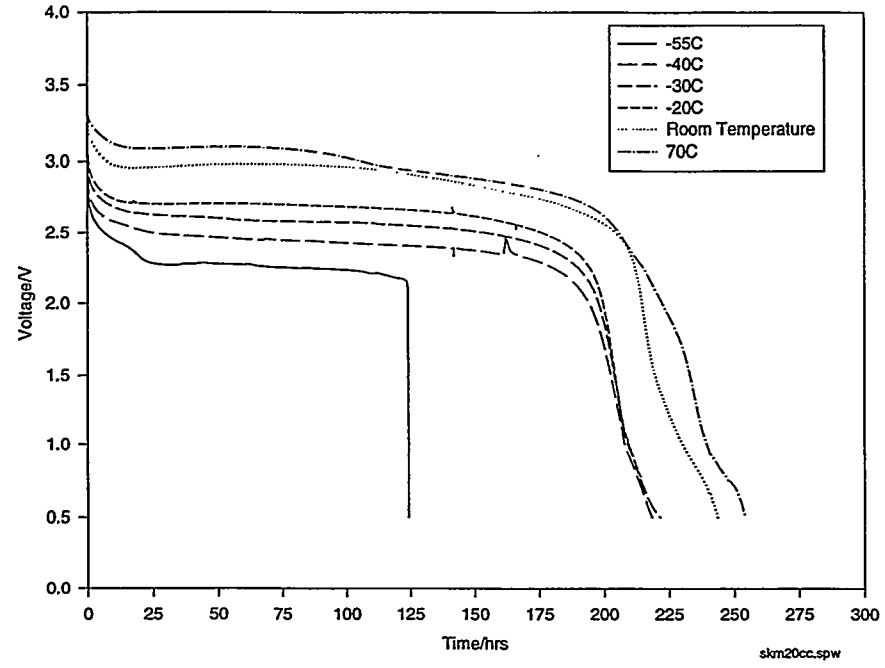

Figure 5-3. Constant-current discharge profiles for Silberkraft M20 standard D cell performed at various temperatures. All cells were discharged at 50 mA.

As in the case the other D cells, additional capacity remains in the cell after discharge at low temperature that can be recovered once the cell temperature increases. This is illustrated in Figure 5-4, which shows the discharge curve for the M20 cell at –55°C, followed by continued discharge at room temperature. For these data, the cell was discharged at a constant rate of 30 mA. In this case, the capacity removed at –55°C is approximately 0.6 Ah, and at room temperature, the capacity obtained is approximately 9.6 Ah. This clearly demonstrates that the capacity is not irreversibly lost at subambient temperature conditions but is only inaccessible. These data also illustrate the somewhat variable nature of cells in general when operated under extreme conditions, such as very low temperature. As shown, only about 0.6 Ah is removed at –55°C and 30 mA for the cell measured in Figure 5-4, compared to 6.2 Ah for a different cell used in the preceding figure at –55°C and 50 mA. (See Chapter 9 for a more complete treatment of these issues.)

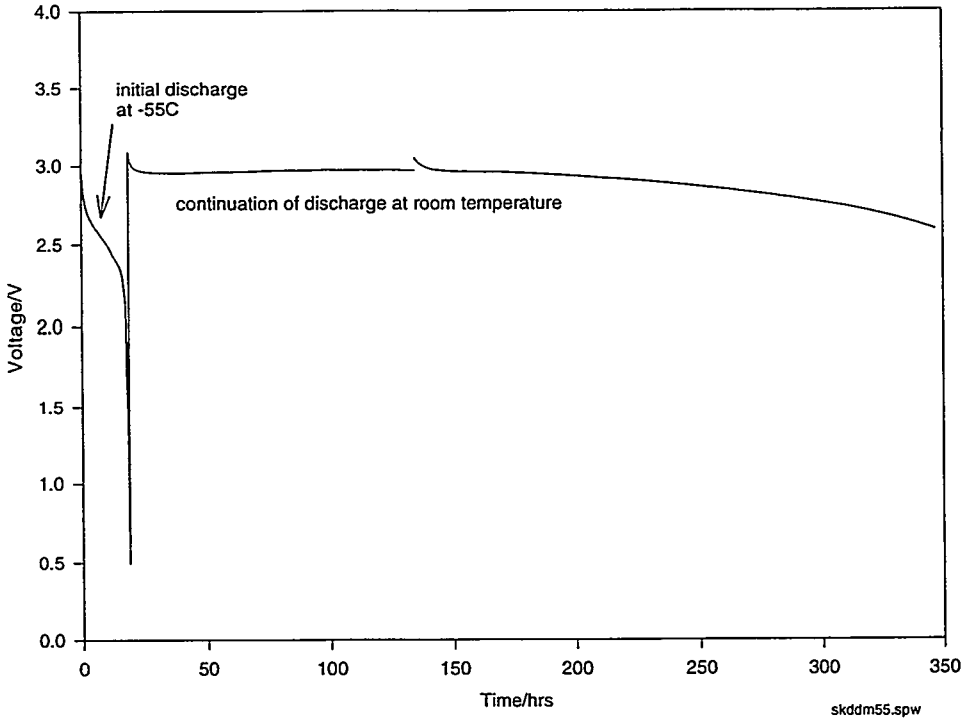

Figure 5-4. Discharge curves for a Silberkraft M20 cell at –55°C followed by the continued discharge of the cell after warming to room temperature. The cell voltage is monitored during the entire process. Both discharges were carried out at a constant current of 30 mA. Discontinuity at about 130 hr corresponds to a temporary open circuit cell state for 15 min.

Similar data were obtained for the Silberkraft M20TT cell, which is specifically designed to operate at low temperatures. Comparative discharge curves for this cell at different temperatures and 50 mA constant current are shown in Figure 5-5. The cell seems to perform better than the standard version at –55°C. Although at room temperature, both cells provide comparable capacity. It is generally assumed that the difference between the low-temperature version and the standard cell is the use of a different electrolyte; therefore, these results are not surprising.

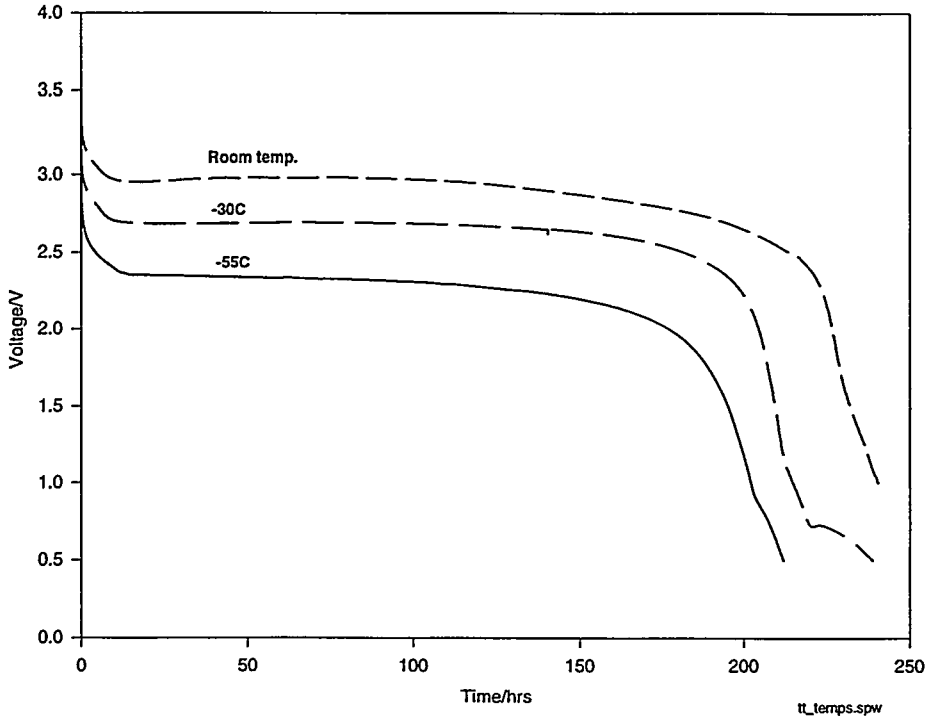

Figure 5-5. Constant-current discharge profiles for Silberkraft M20TT D cell performed at various temperatures. All cells were discharged at 50 mA.

5.3 Pulse Discharge Behavior

An initial series of tests to evaluate the ability of the Bluestar and Ultralife cells to deliver 5 A and 10 A, 5-sec pulses at room temperature and as a function of state of charge were performed. In this case, the cells were pulsed at 5 A and 10 A for 5 sec each with a 5-min rest at open circuit between pulses. After applying this pulse train, 0.5 Ah of capacity was removed from the cells at a rate of 0.1 A. This process was continued until the voltage of the cell during the 0.1 A discharge dropped to below 2 V.

As shown in Figures 5-6 through 5-9, the Bluestar and Ultralife cells are able to support both the 5 A and 10 A pulsed loads over a wide capacity range at room temperature. In comparing these data, it should be noted that the change in voltage with applied current is less for the Bluestar cell at room temperature, indicating a lower equivalent series resistance in the Bluestar cell than in the Ultralife cell.

Preliminary testing at subambient conditions was performed for both types of cells. The pulse test protocol used for this evaluation is similar to that just described and consists of a 5-sec, 5-A pulse followed by a 5-sec, 10-A pulse. If cell voltage dropped below 0.05 V during a pulse, that pulse was terminated. Before and after the pulses the cell was allowed to stand at open circuit for 5 min. Between pulse trains, 0.23 Ah (as opposed to 0.5 Ah as in the previous test) was removed from the cell at a rate of 0.1 A. The total amount of capacity removed for one cycle, that is one complete pulse train and one 0.1 A discharge between pulse trains, is approximately 0.25 Ah. The test was terminated when the cell voltage dropped below 2 V during the 0.1 A discharge portion of the test. These tests were performed on just one cell each.

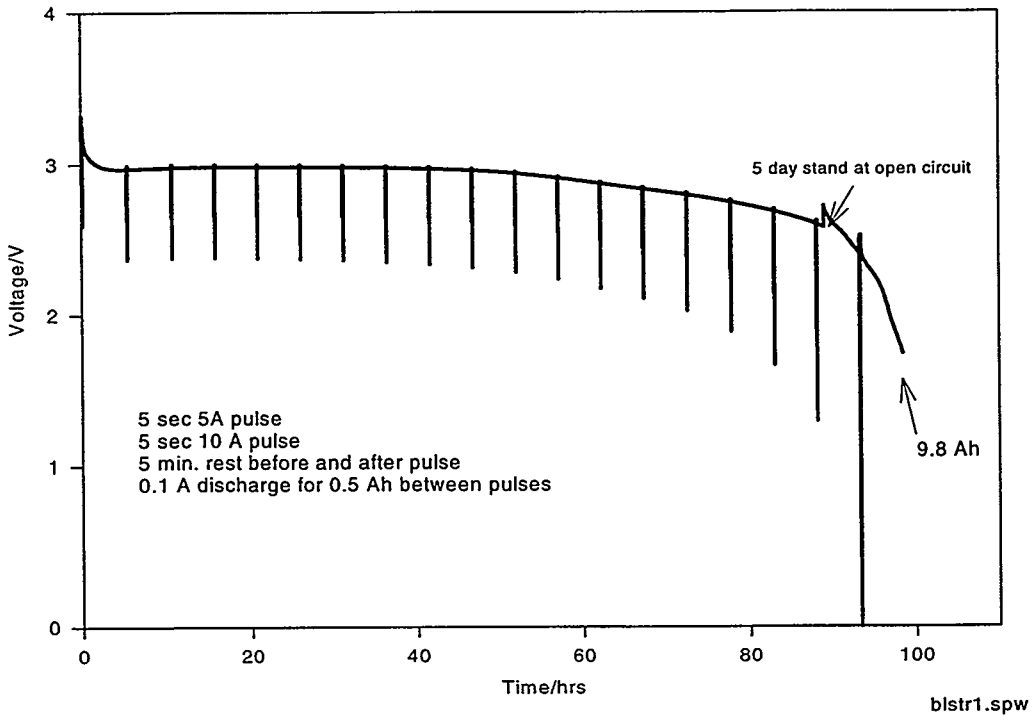

Figure 5-6. Discharge behavior of Bluestar D cell. Pulsing of 5 A and 10 A was periodically applied during the discharge. The discharge was carried out at room temperature.

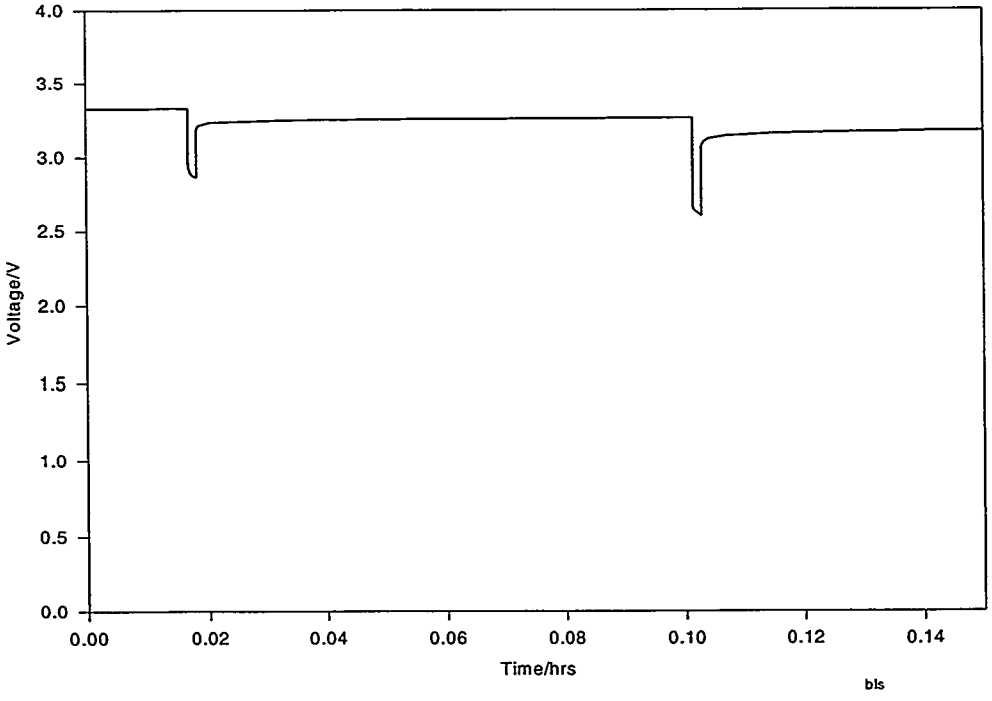

Figure 5-7. Expanded view of that portion of the discharge curve of the previous figure showing the detailed response behavior of the Bluestar D cell to the first pulse train applied, that is, first 5 A and 10 A pulses.

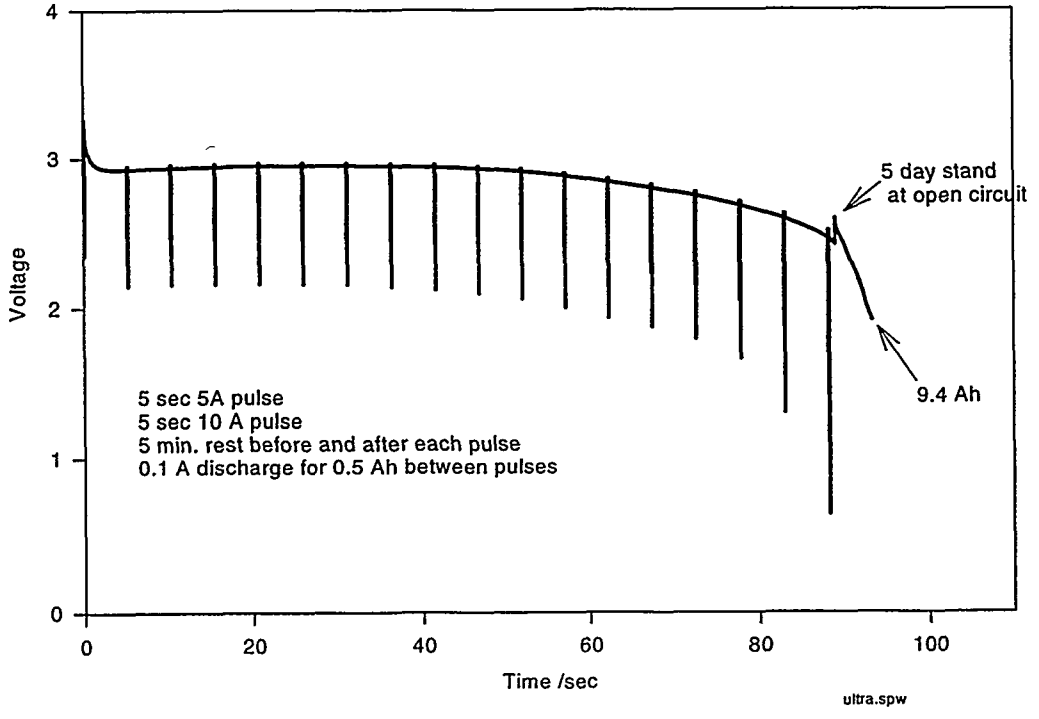

Figure 5-8. Room temperature discharge behavior of Ultralife U3360VH D cell. Periodic pulses of 5 A and 10 A were applied to the cell during the discharge.

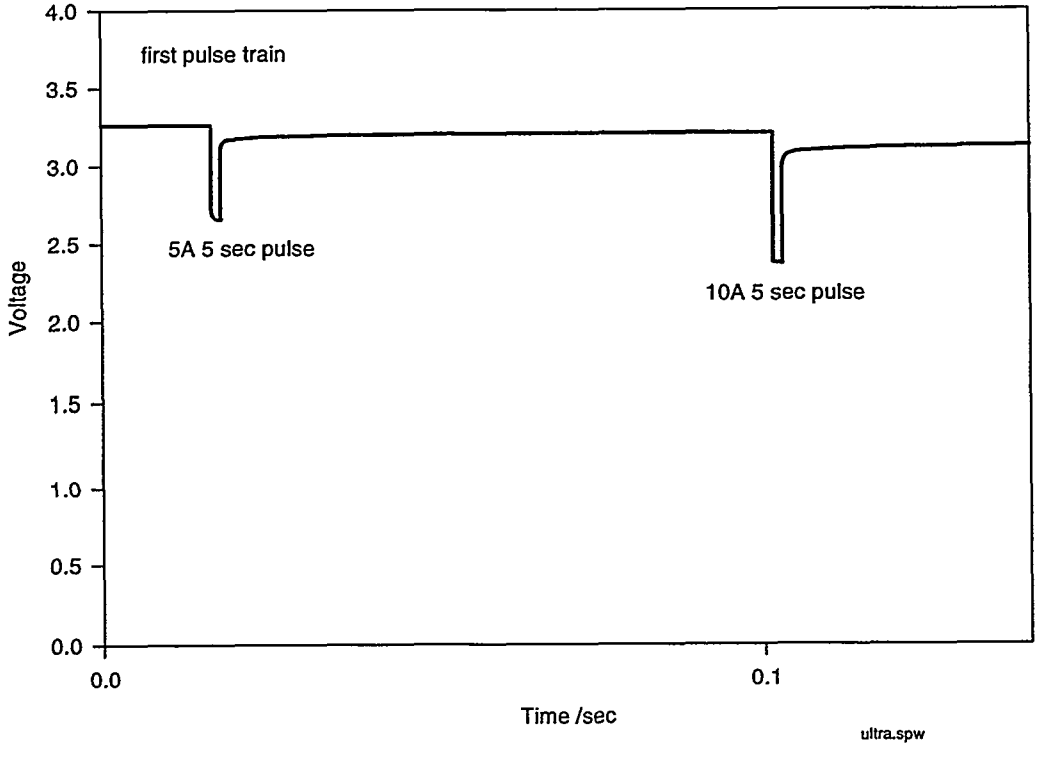

Figure 5-9. Expanded view of the first pulse profile applied to the Ultralife U3360VH D cell shown in Figure 5-8 illustrates the cell response to 5 A and 10 A pulses at room temperature.

As Figures 5-10 through 5-13 show, both cell types are capable of supporting the 5 A and 10 A loads at –40°C. However, here the Ultralife cell outperforms the Bluestar cell. That is, the voltage drop observed in the case of the Bluestar cell is significantly greater than for the Ultralife cell, and more capacity can be removed from the Ultralife cell.

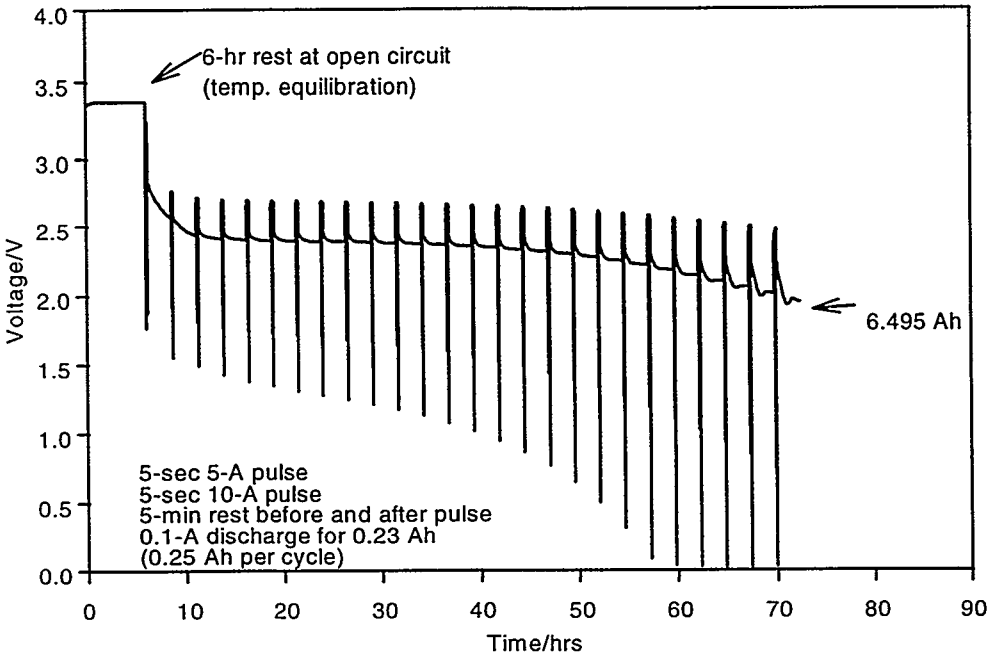

Figure 5-10. Discharge of fresh Bluestar D cell at –40°C. The pulse behavior of the cell was evaluated at currents of 5 A and 10 A at periodic intervals during the discharge.

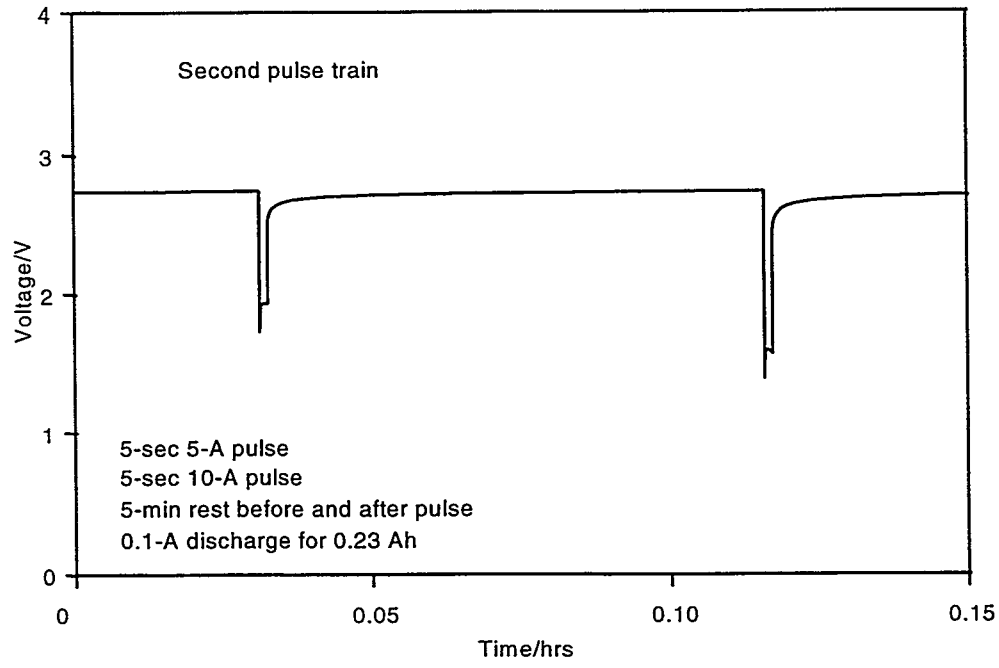

Figure 5-11. Expanded view of a portion of the data from Figure 5-10 sec pulse train applied to the Bluestar D cell.

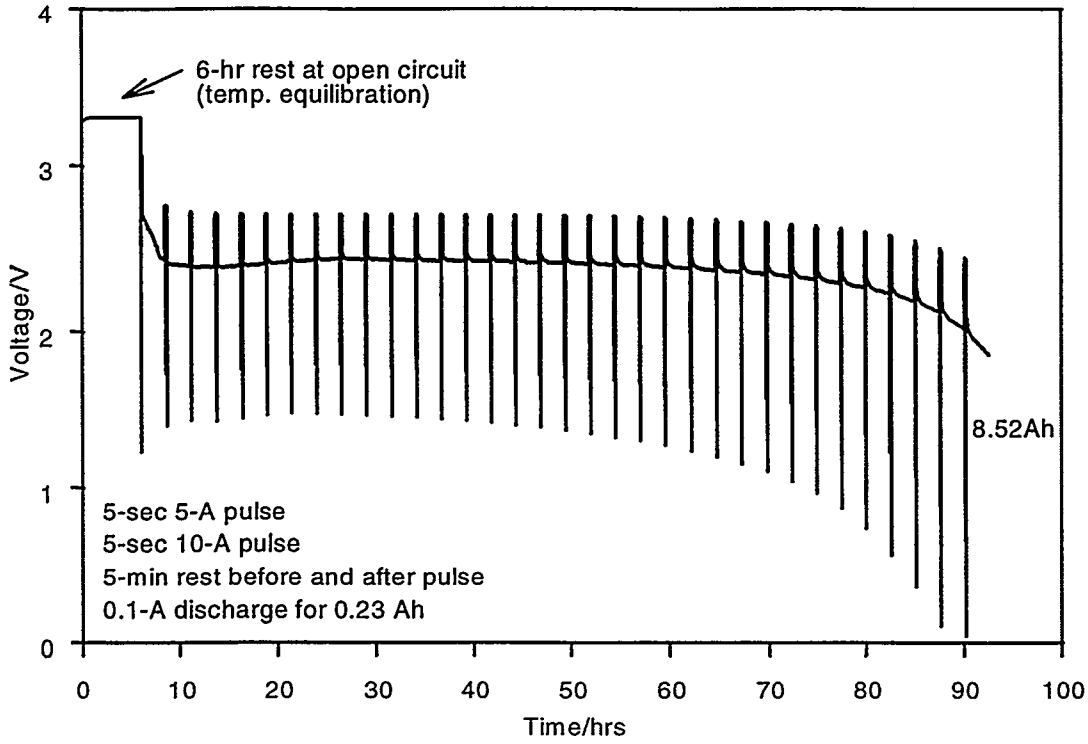

Figure 5-12. Pulse-discharge behavior of fresh Ultralife U3360VH D cell at –40°C. Pulse behavior was evaluated at 5 A and 10 A currents.

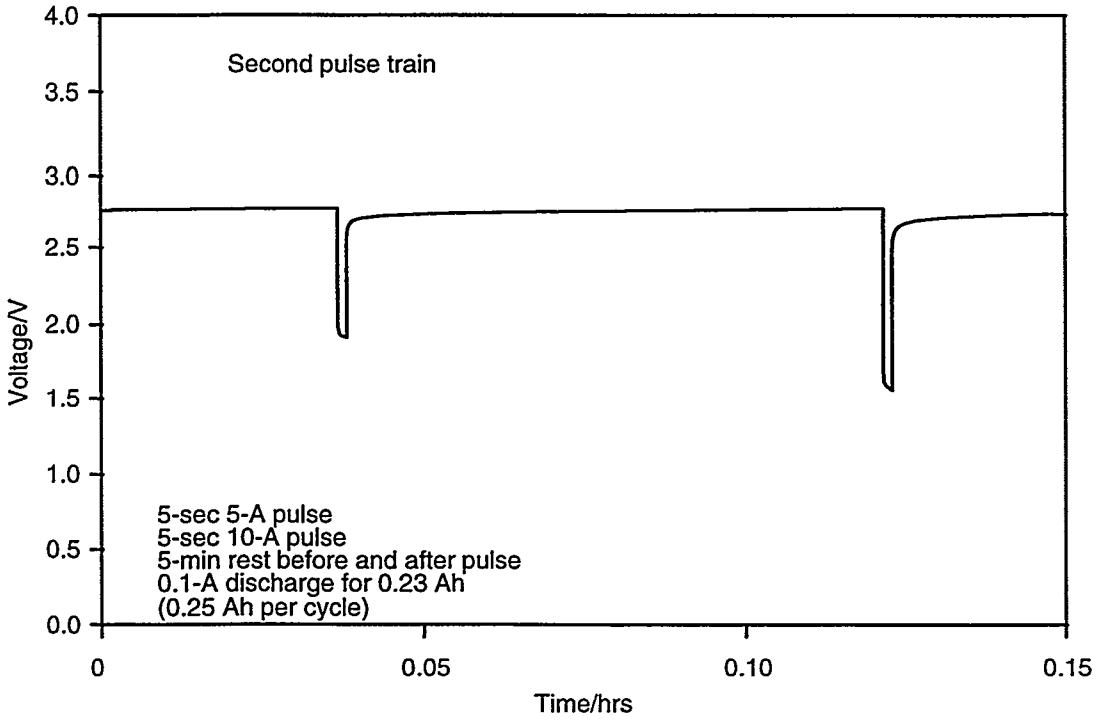

Figure 5-13. Expanded view of a portion of the data from Figure 5-12 sec pulse train applied to the Ultralife U3360VH cell shown in Figure 5-12 at –40°C.

Data were also collected under subambient conditions at a higher duty cycle for both the Ultralife and Bluestar cells. In this case, a 3-sec, 5-A pulse was applied to the cell followed by a 17-sec rest at open circuit. The behavior for both the Bluestar and Ultralife cells at –40°C is shown in Figures 5-14 through 5-17. As is evident, both cells are capable of providing the requisite current under these extreme conditions.

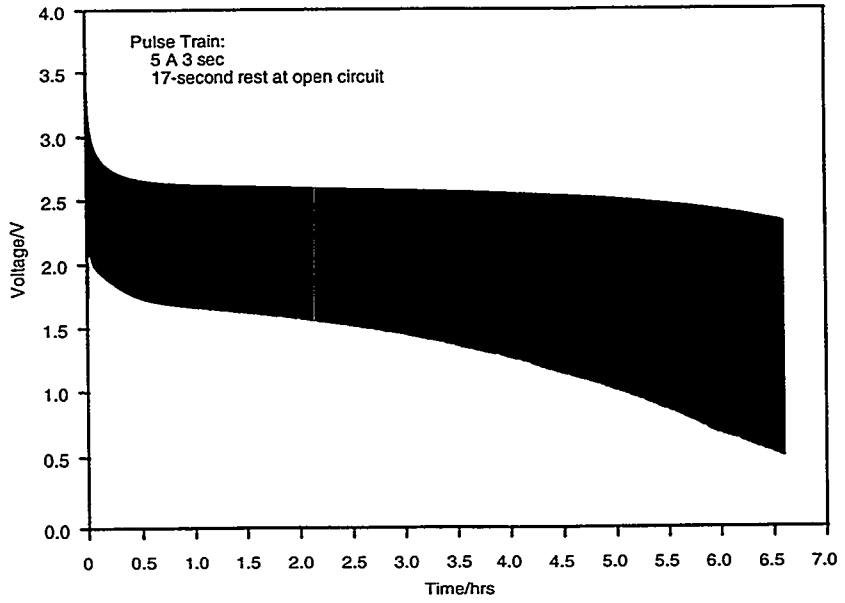

Figure 5-14. Pulsed-discharge behavior of a Bluestar D cell at –40°C. The cell was equilibrated for 6 hr at –40°C before testing. The pulse profile consisted of 3 sec at 5 A followed by 17 sec at open circuit.

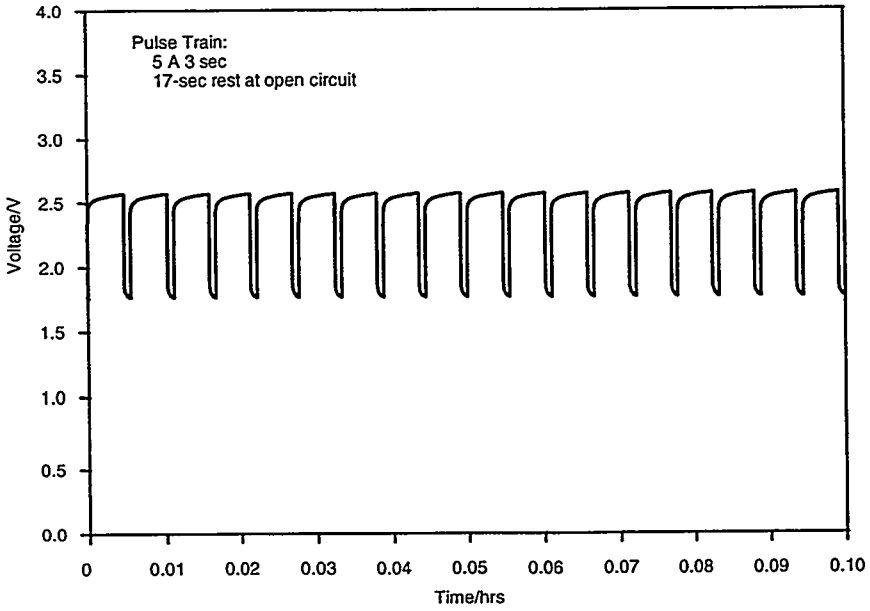

Figure 5-15. Expanded view of a portion of the data from Figure 5-14 showing the pulsed discharge behavior of a Bluestar D cell at –40°C. The cell was equilibrated for 6 hr at –40°C before testing. This view shows the initial pulse behavior of the cell to the 3-sec at 5 A pulse followed by 17 sec at open circuit.

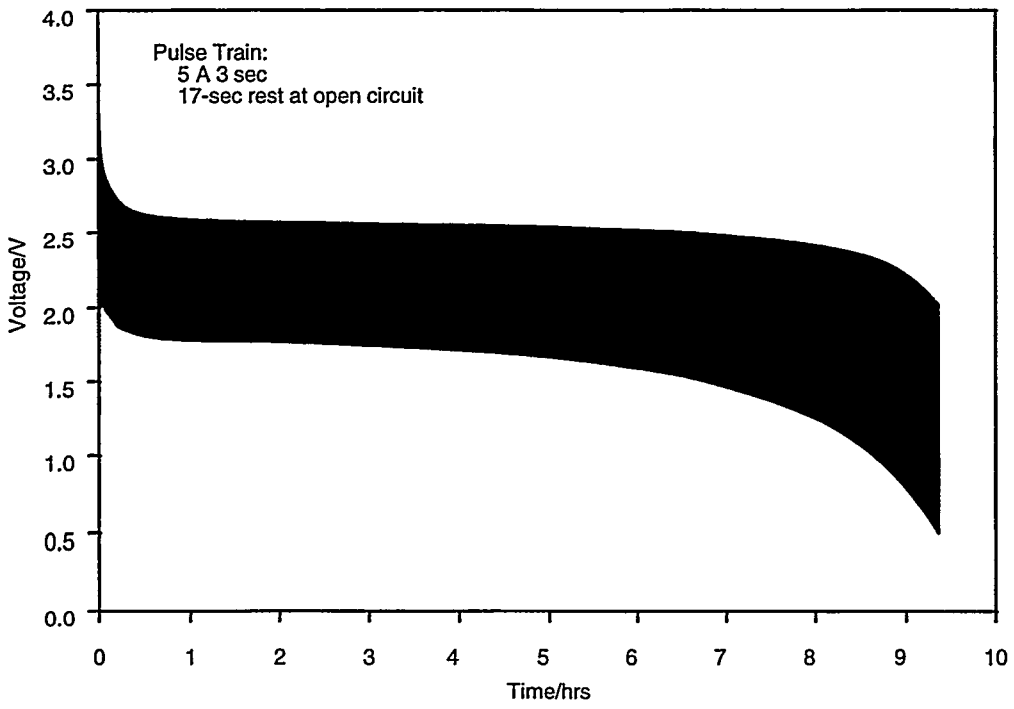

Figure 5-16. Pulse-discharge behavior of Ultralife U3360VH D cell at –40°C. The cell was equilibrated for 6 hr at –40°C before testing. The pulse profile consisted of 3 sec at 5 A followed by 17 sec at open circuit.

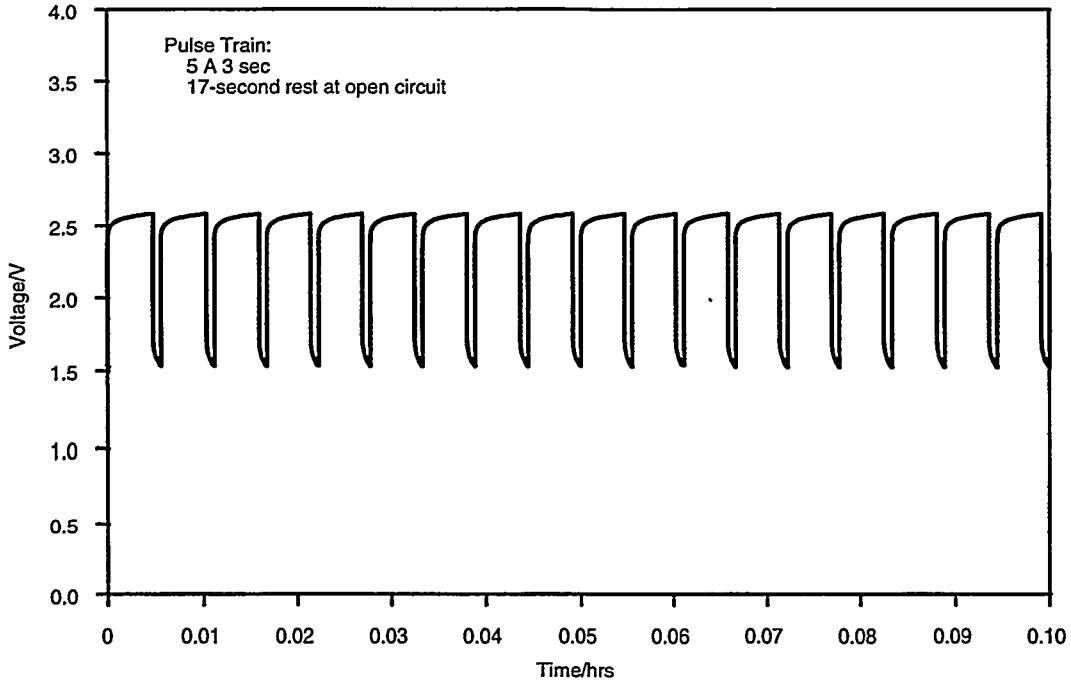

Figure 5-17. Expanded view of the pulse-discharge behavior of Ultralife U3360VH D cell at –40°C shown in Figure 5-16. The cell was equilibrated for 6 hr at –40°C before testing. The view shown is the initial behavior of the cell to the pulse profile of 3 sec at 5 A followed by 17 sec at open circuit.

After reaching end of discharge at –40°C, additional unreacted material remains in the cell. This remaining material, which represents unused capacity, can be recovered once the temperature of the cell increases, as is graphically depicted in Figures 5-18 and 5-19. It shows a continuation of the pulse discharge once the temperature of the cells is allowed to increase to room temperature (the pulse train employed is the same as that used at –40°C). In this case, however, the Ultralife cell does not run as long as the Bluestar cell because more usable capacity was removed from the Ultralife cell at –40°C than from the Bluestar cell.

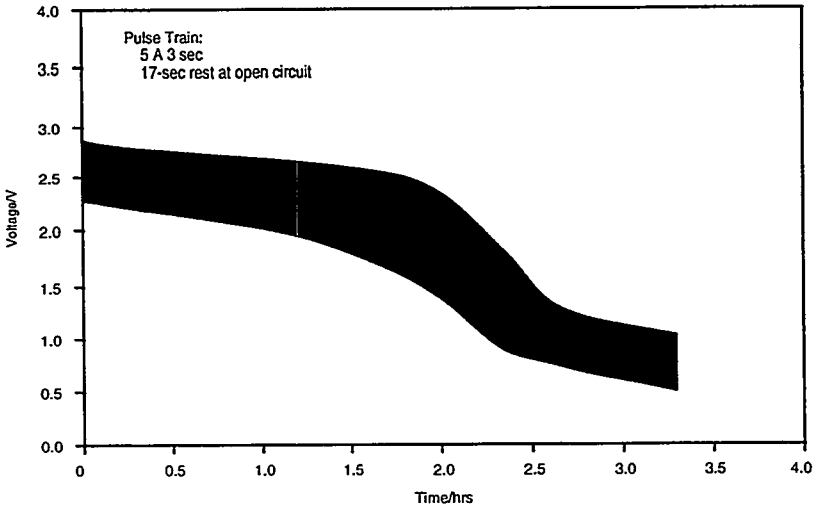

Figure 5-18. Continuation of pulse discharge of Ultralife U3360VH D cell at room temperature after completing discharge at –40°C shown in Figures 5-16 and 5-17. The pulse train used is the same as that used previously, namely, 3 sec at 5 A followed by 17 sec at open circuit.

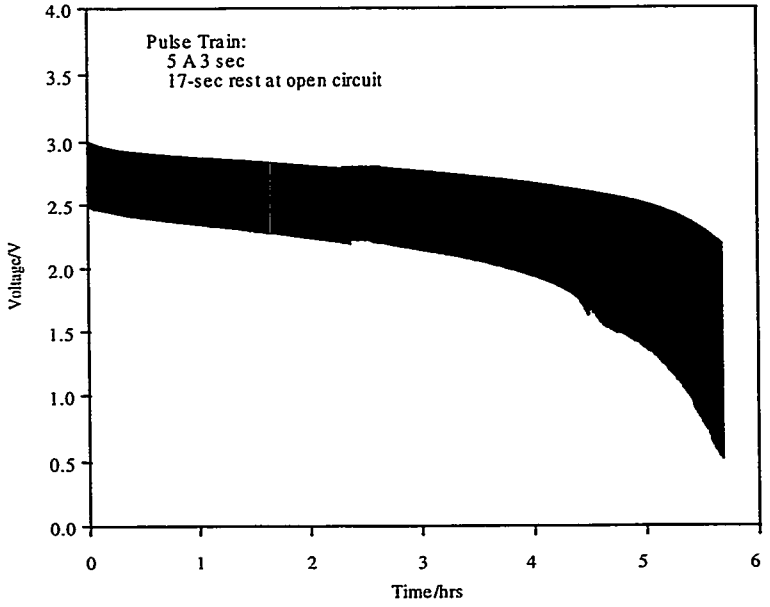

Figure 5-19. Continuation of pulse discharge of Bluestar D cell at room temperature after completing discharge at –40°C shown in Figures 5-14 and 5-15. The pulse train used is the same as that used previously, namely, 3 sec at 5 A followed by 17 sec at open circuit.

Data were also collected at –20°C for both cells. The pulse train employed was the higher-duty cycle consisting of 3-sec, 5 A pulses followed by a 17-sec stand at open circuit. These data are shown in Figures 5-20 and 5-21 below. Again, both cells can support the load at these lower temperatures, and the performance observed from the Ultralife cell is still superior to that seen from the Bluestar cell, both in terms of the voltage drop and capacity delivered.

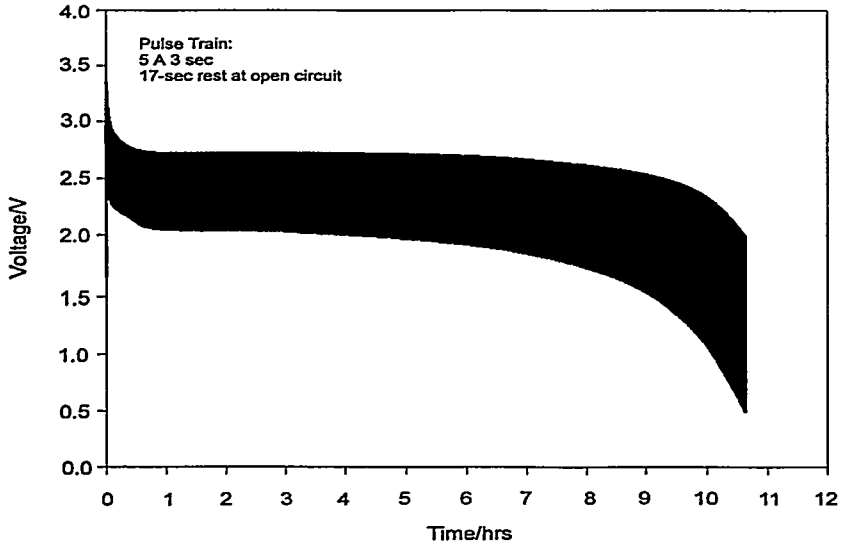

Figure 5-20. Pulsed discharge behavior of the Bluestar D cell at –20°C. The cell was equilibrated for 6 hr at –20°C before testing. The pulse profile consisted of 3 sec at 5 A followed by 17 sec at open circuit.

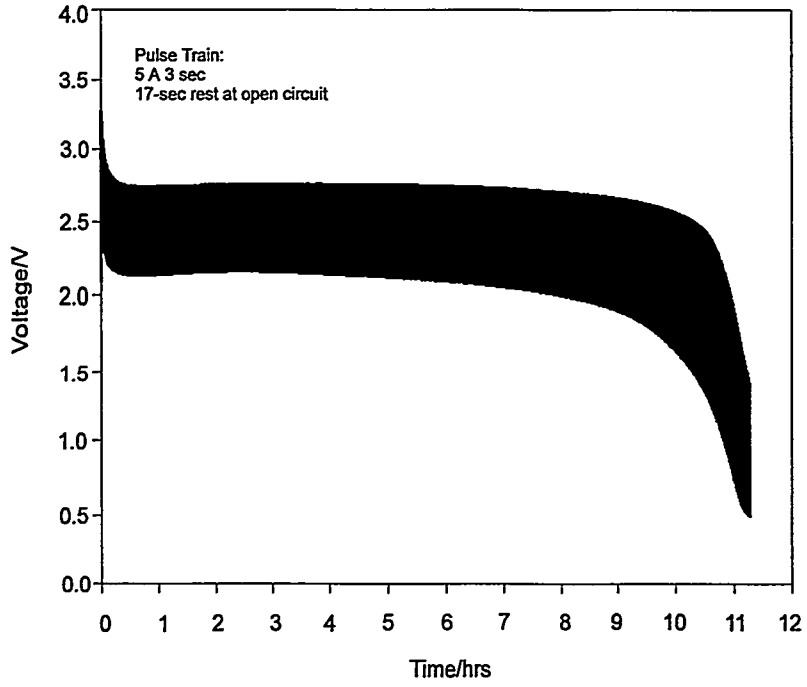

Figure 5-21. Pulsed discharge behavior of Ultralife U3360VH D cell at –40°C. The cell was equilibrated for 6 hr at –40°C before testing. The pulse profile consisted of 3 sec at 5 A followed by 17 sec at open circuit.

Both versions of the Silberkraft cells perform comparably to the Ultralife and Bluestar cells under pulsed-load conditions. Under the relatively benign conditions of room temperature, the cells are able to provide capacities in line with constant-current discharge behavior, as shown in Figures 5-22 and 5-23, where the pulse envelope is observed under a 3-sec, 5 A pulse followed by 17 sec at open circuit for both the standard and room temperature versions of the cells. As expected, the low-temperature version (M20TT) performs at least as well as, if not better than, the standard version at room temperature because of its different electrolyte composition. This ultimately manifests as a lower voltage drop during the pulse train, and this is observed experimentally. For comparative purposes, Figure 5-24 shows the performance of the same cell type at –20°C.

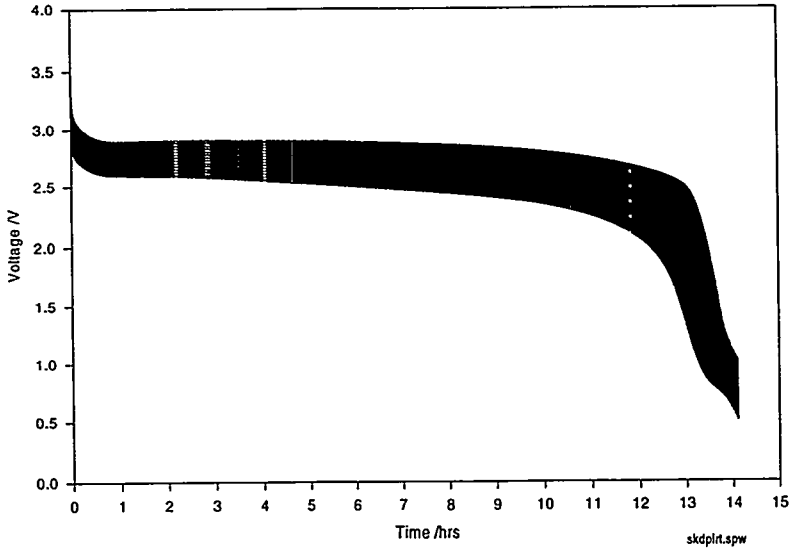

Figure 5-22. Pulsed discharge behavior of Silberkraft M20 at room temperature. The cell was discharged using a pulse train of 3 sec at 5 A followed by 17 sec at open circuit.

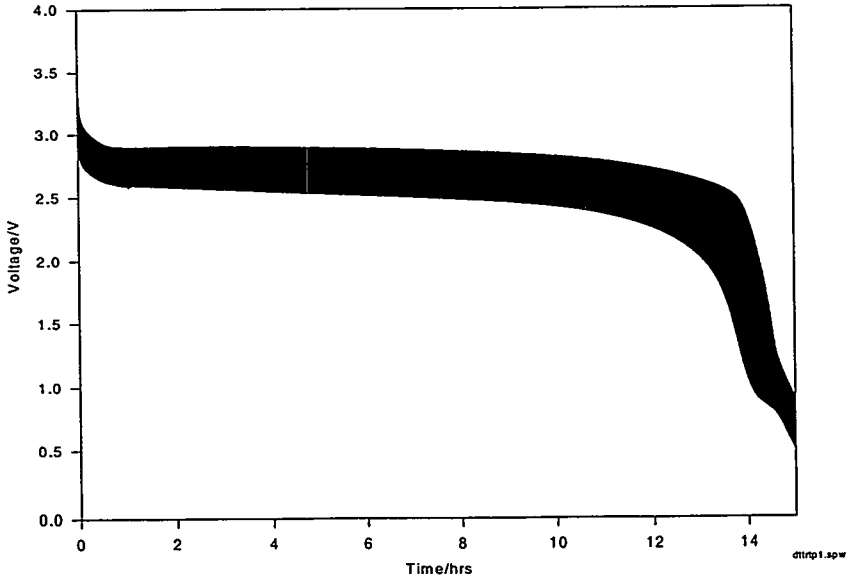

Figure 5-23. Pulsed discharge behavior of Silberkraft M20TT at room temperature. The cell was discharged using a pulse train of 3 sec at 5 A followed by 17 sec at open circuit.

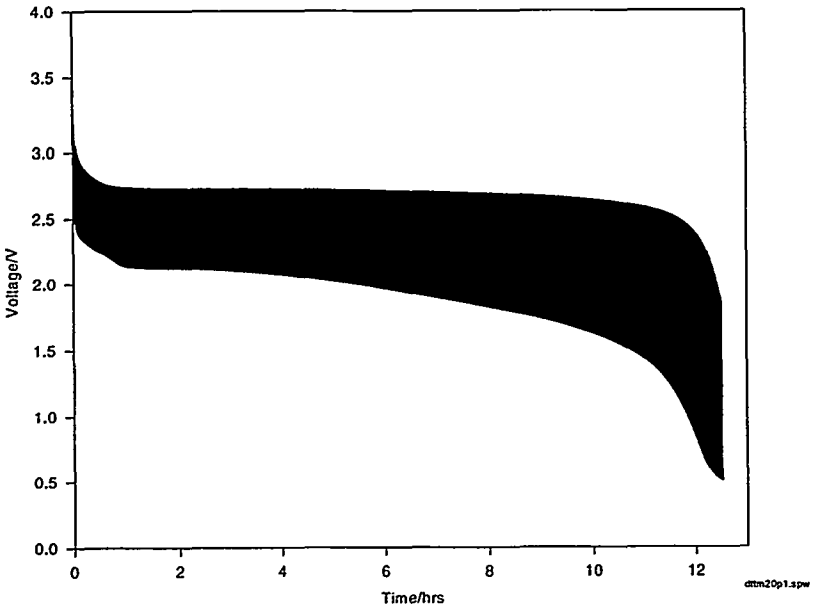

Figure 5-24. Pulse discharge behavior of Silberkraft M20TT at –20°C. The cell was discharged using a pulse train of 3 sec at 5 A followed by 17 sec at open circuit.

Figures 5-25 and 5-26 show that the low-temperature version performs significantly better at low temperature and should be used if –40°C performance is required. In order to display the performance of more than one cell on a single graph, a trace of the external envelope was made of the plot shown in Figure 5-26. Figure 5-27 is traced from four different tests of M20TT cells. These data show that even for the low-temperature version of Silberkraft M20TT cells, the variability in performance that exists at –40°C can be significant. The capacity removed at –40°C under the pulse profile is significantly less than that obtained at room temperature, but by continuing the discharge at a higher temperature additional capacity can be obtained (as seen in Figures 5-28 and 5-29).

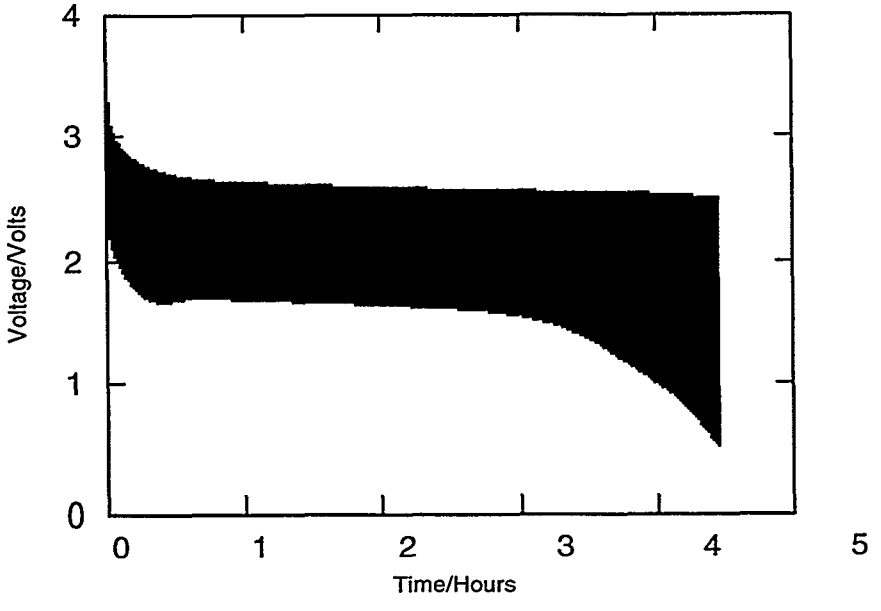

Figure 5-25. Pulse discharge behavior of Silberkraft M20 at –40°C. The cell was discharged using a pulse train of 3 sec at 5 A followed by 17 sec at open circuit.

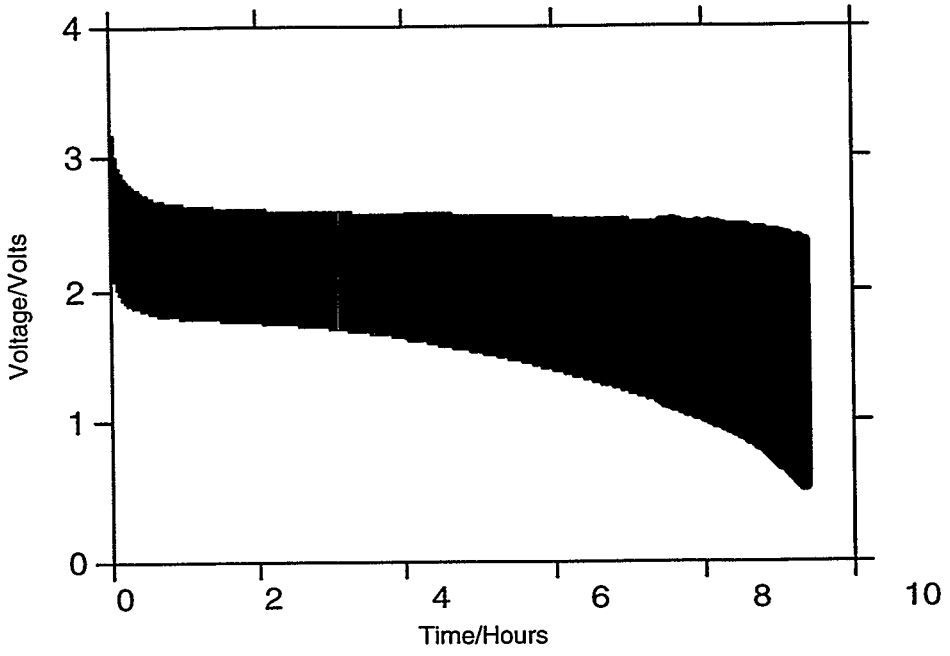

Figure 5-26. Pulse discharge behavior of Silberkraft M20TT at –40°C. The cell was discharged using a pulse train of 3 sec at 5 A followed by 17 sec at open circuit.

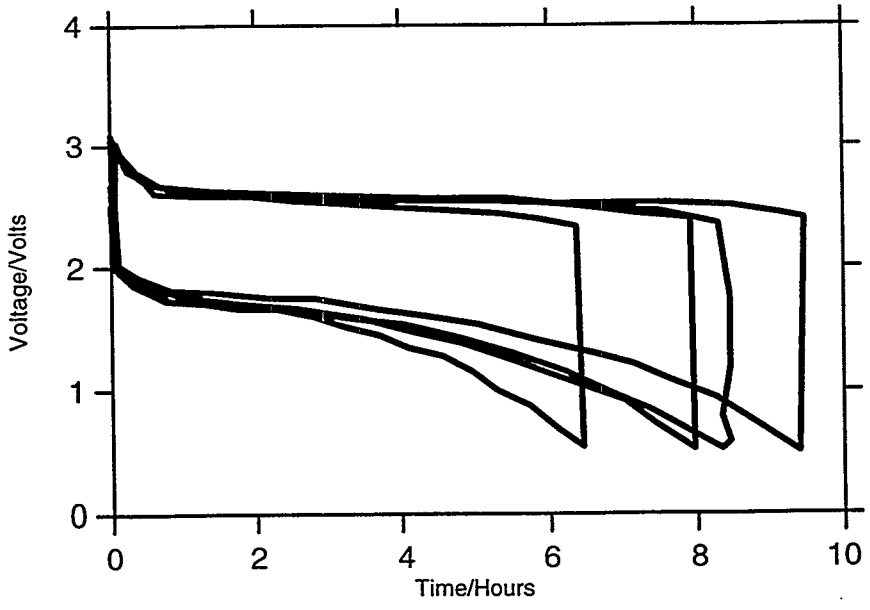

Figure 5-27. Envelope of four different cells pulse discharges of Silberkraft M20TT at –40°C. The cell was discharged using a pulse train of 3 sec at 5 A followed by 17 sec at open circuit.

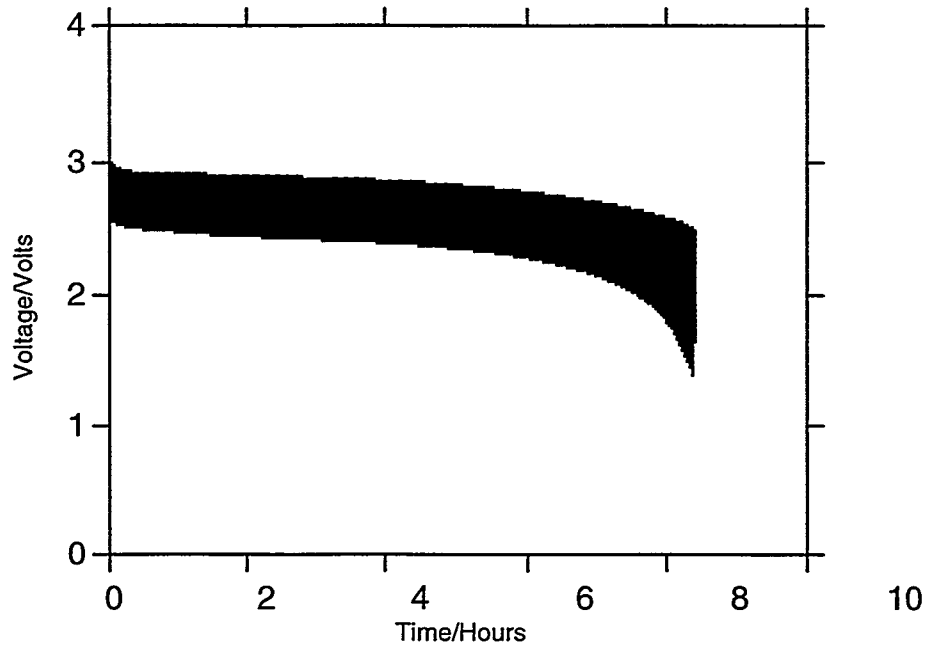

Figure 5-28. Continuation of pulse discharge of Silberkraft D M20 cell at room temperature after completing discharge at –40°C as shown in Figure 5-25. The pulse train is the same as was previously used, namely, 3 sec at 5 A followed by 17 sec at open circuit.

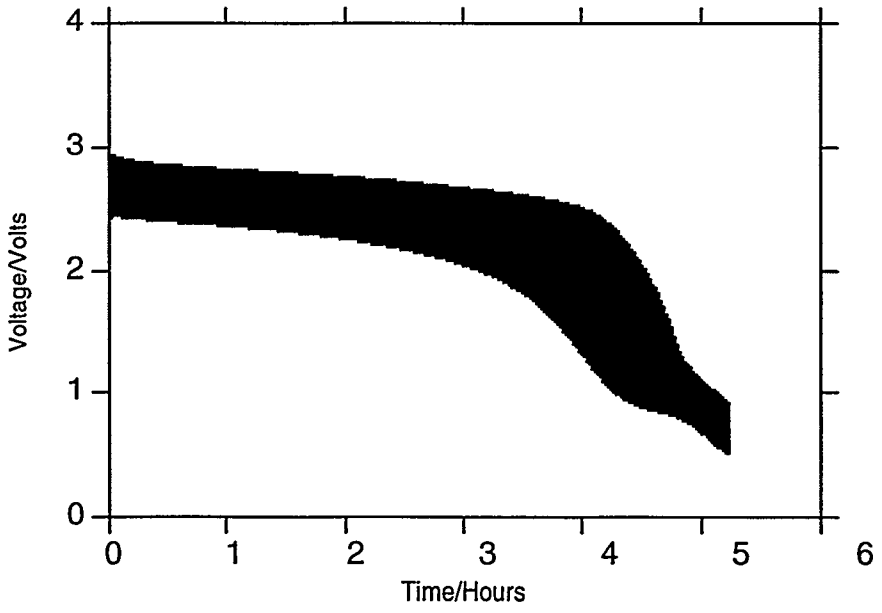

Figure 5-29. Continuation of pulse discharge of Silberkraft D M20TT cell at room temperature after completing discharge at –40°C as shown in Figure 5-26. The pulse train is the same as was previously used, namely, 3 sec at 5 A followed by 17 sec at open circuit.

In addition to evaluating the cells at various temperatures, we also evaluated the cells at different currents. Figures 5-30 and 5-31 show the discharge curves for the Silberkraft M20TT cell discharged at –40°C using both a 4 A and 3 A pulse.

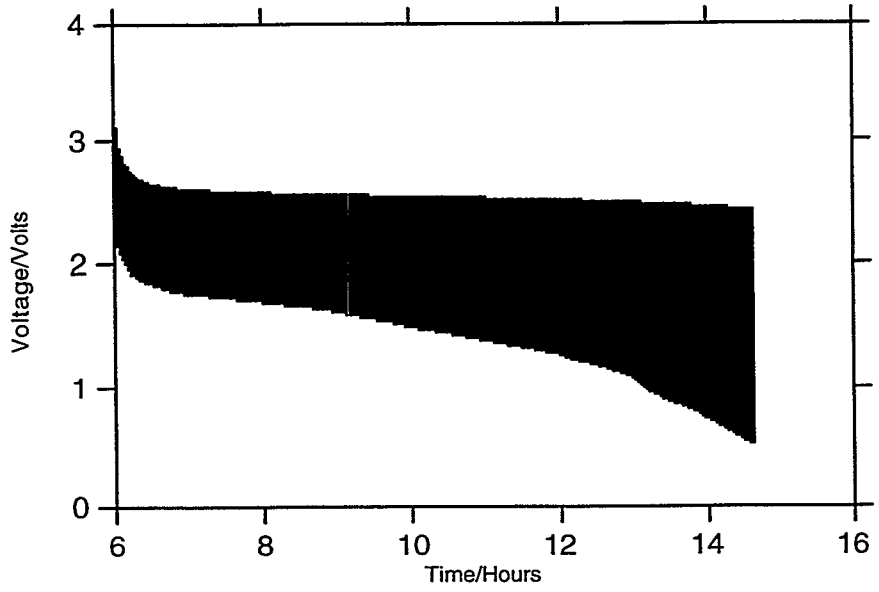

Figure 5-30. Pulse-discharge behavior of Silberkraft M20TT at –40°C. The cell was discharged using a pulse train of 3 sec at 4 A followed by 17 sec at open circuit.

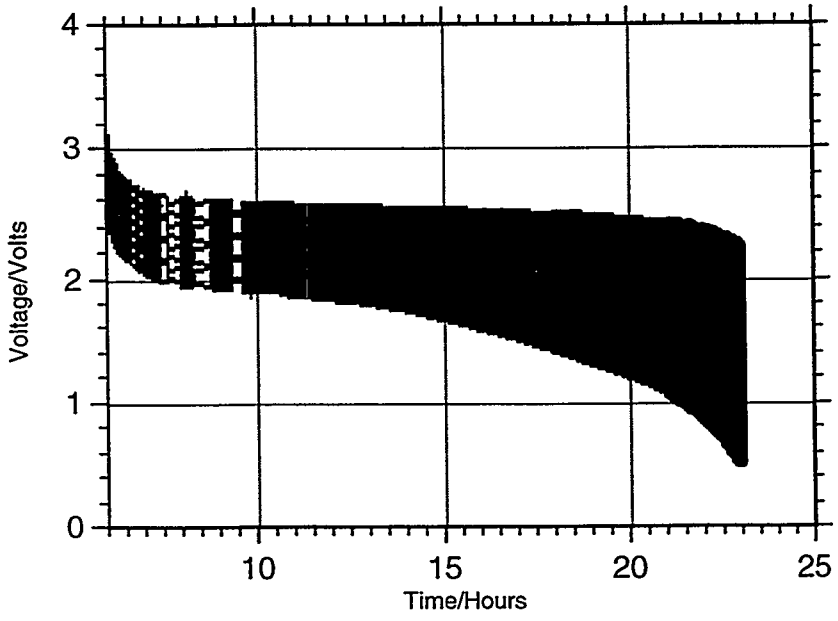

Figure 5-31. Pulse-discharge behavior of Silberkraft M20TT at –40°C. The cell was discharged using a pulse train of 3 sec at 3 A followed by 17 sec at open circuit.

Finally, the pulse profile used to obtain Figures 5-30 and 5-31, employing a 17-sec rest at open circuit, is relatively severe. In fact, a large amplitude pulse train having a high-duty cycle presents severe conditions for any battery system. Furthermore, low temperatures exacerbate this condition. Consequently, if the duty cycle of the pulse train can be decreased, thereby allowing the battery to recover, additional capacity might be obtained. (This situation does not hold for all battery chemistries, such as lithium/thionyl chloride. The morphology of the lithium chloride deposit formed under conditions of high pulse rates affects future performance and morphology of the deposit and is not expected to change significantly on standing.) This characteristic is in fact observed in both the M20 and M20TT cells discharged at –40°C, as seen in Figures 5-32 and 5-33, which show the discharge behavior for the cells under a lower duty pulse. Under these conditions, the capacity removed in one day equals the capacity removed under severe profile conditions.

5.4 Battery Behavior

Single-cell behavior provides useful information that can, in some circumstances, provide predictive information regarding the behavior of a battery. A determination of this possibility was made by comparing single-cell behavior to the performance characteristics of a battery consisting of 12 cells connected in series, and these results are described below.

The Silberkraft cells were evaluated in a battery configuration consisting of 12 cells in series, at both room temperature and –40°C under a pulsed load. The pulsed load discussed here consists of a single 2.4-sec, 5-A pulse followed by four 0.8-sec, 5-A pulses with a 3-min rest at open circuit between each pulse. This pulse train was repeated until the voltage under load was equal to or less than some predefined value, which is evident on examination of the data.

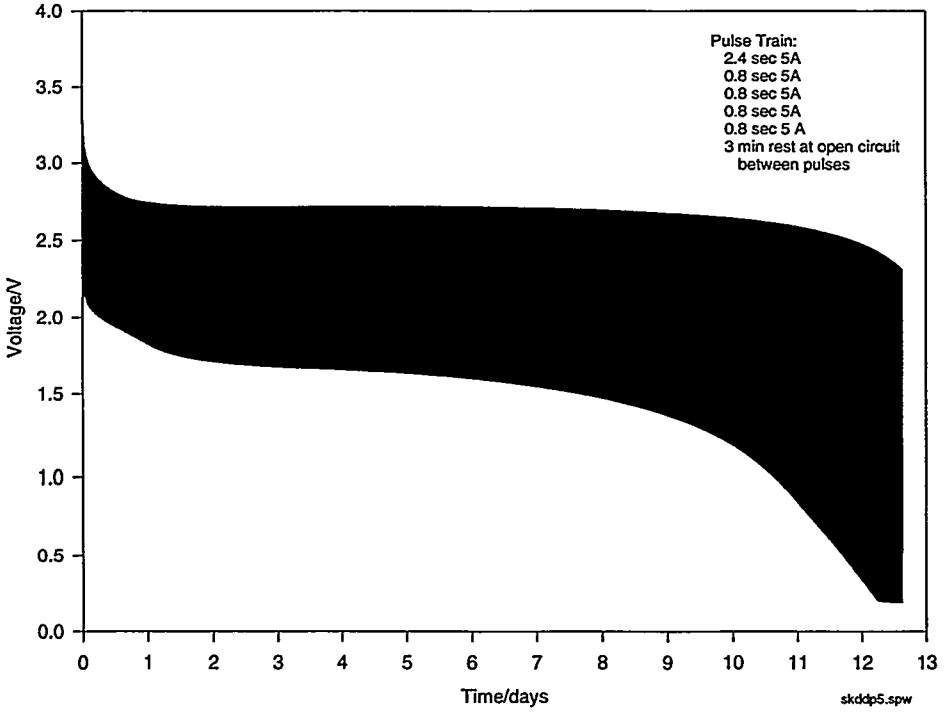

Figure 5-32. Pulse-discharge behavior of Silberkraft M20 standard D cell at –40°C. The pulse train applied consisted of 2.4 sec at 5 A followed by four 0.8-sec 5 A pulses with 3-min rests at open circuit between pulses.

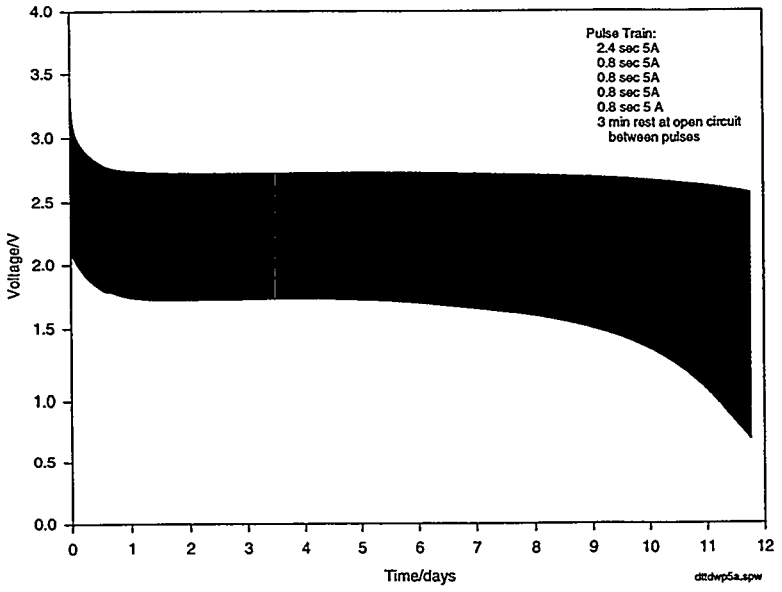

Figure 5-33. Pulse-discharge behavior of Silberkraft M20TT low-temperature D cell at –40°C. The pulse train applied consisted of 2.4 sec at 5 A followed by four 0.8-sec 5 A pulses with 3-min rests at open circuit between pulses.

Figure 5-34 shows the behavior of the M20 cell when this pulse load was performed at room temperature. The capacity removed from this cell during this test was 10.6 Ah, very close to the capacity obtained from this type of cell under a constant-current discharge regime. In this test the cells were connected to one another by welding a 0.003-inch-thick, 0.116-inch-wide nickel ribbon between the tabs. At least three spot-weld connections were made at each tab. All of the cells had the same orientation with respect to one another, and as such the length of the nickel ribbon from one cell to the next was at least as long as the cell, which amounts to a length of about 2.66 inches. Because 12 cells were in series, there were 12 pieces of nickel ribbon in the entire battery stack, one of which was used to connect the battery stack to the test equipment. The other connection to the test equipment was made directly to the tab on the last cell in the battery.

Even though it is a metallic conductor, the overall dimensions of the nickel ribbon in the entire battery stack in combination with the currents applied during the pulse train (5 A) will result in a significant voltage drop across the cell interconnects during the pulse. This is most easily seen when the voltage profile of the battery behavior just described is compared with that observed when the individual cells are directly welded to one another at their tabs using at least eight spot welds (see Figure 5-35). As shown, an additional 2- to 3-V voltage drop is associated with the use of the nickel ribbon to make cell-to-cell connections.

The battery behavior for both versions of the Silberkraft cell was evaluated at –40°C. Cell interconnects were made using the nickel ribbon previously described. Consequently, a portion of the voltage drop observed during pulse application can be attributed to the cell interconnects. Based on the data previously shown, this amounts to about 2 to 3 V for the battery stack. Figures 5-36 and 5-37 show the data obtained for the M20 and M20TT cells. In both cases, the batteries were allowed to equilibrate at –40°C for six hours prior to application of the pulse. At periodic intervals during the application of the pulse train, the test procedure was suspended because of tester limitations. During this time, the cells were allowed to rest for longer than the 2-min rests of the procedure. After this occurred, the cells recovered and displayed an increase in the voltage and a decrease in the voltage drop upon application of the subsequent pulses. Evidence of this behavior is seen in both figures.

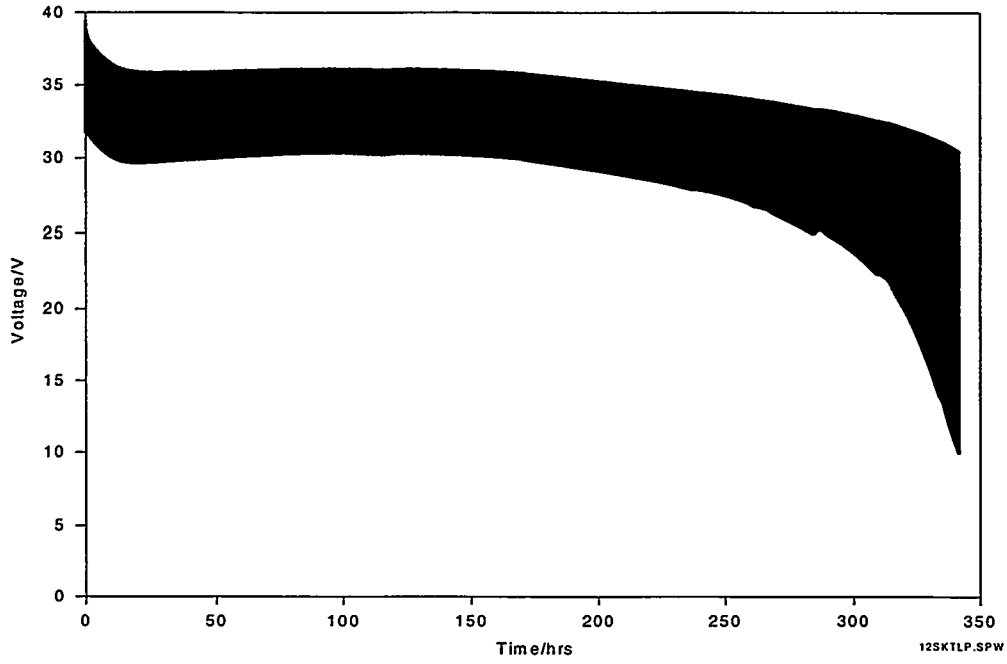

Figure 5-34. Voltage profile of a Silberkraft battery consisting of 12 M20 cells in series connected with nickel ribbon to a pulse load at room temperature.

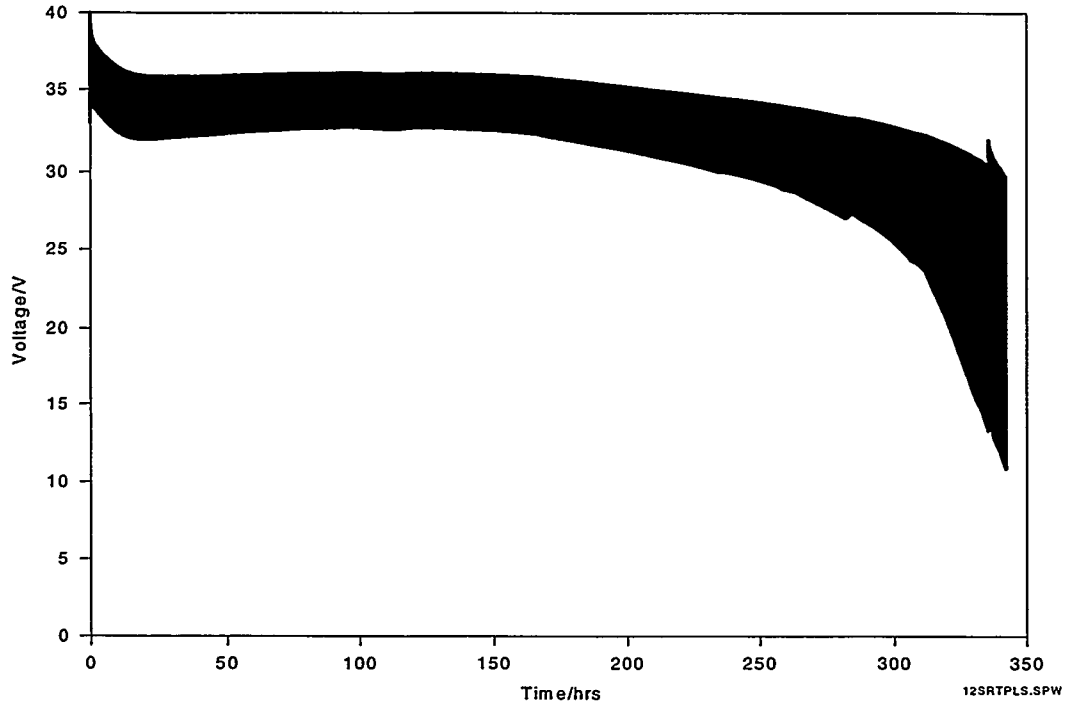

Figure 5-35. Voltage profile of a Silberkraft battery consisting of 12 M20 cells in series connected directly at the tabs at room temperature.

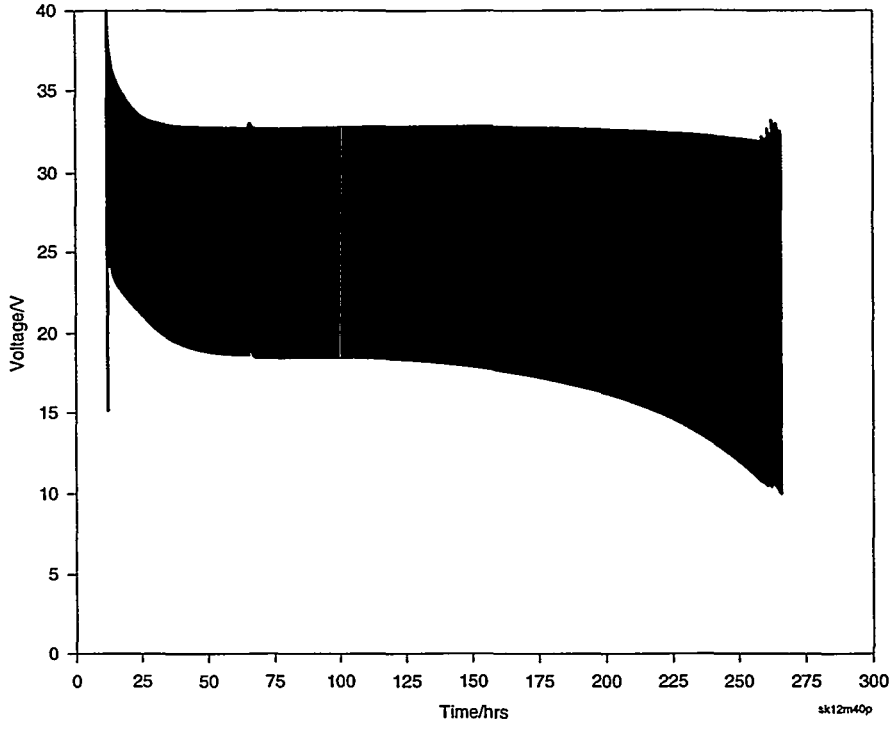

Figure 5-36. Voltage profile of battery composed of 12 Silberkraft M20 cells in a series configuration at –40°C.

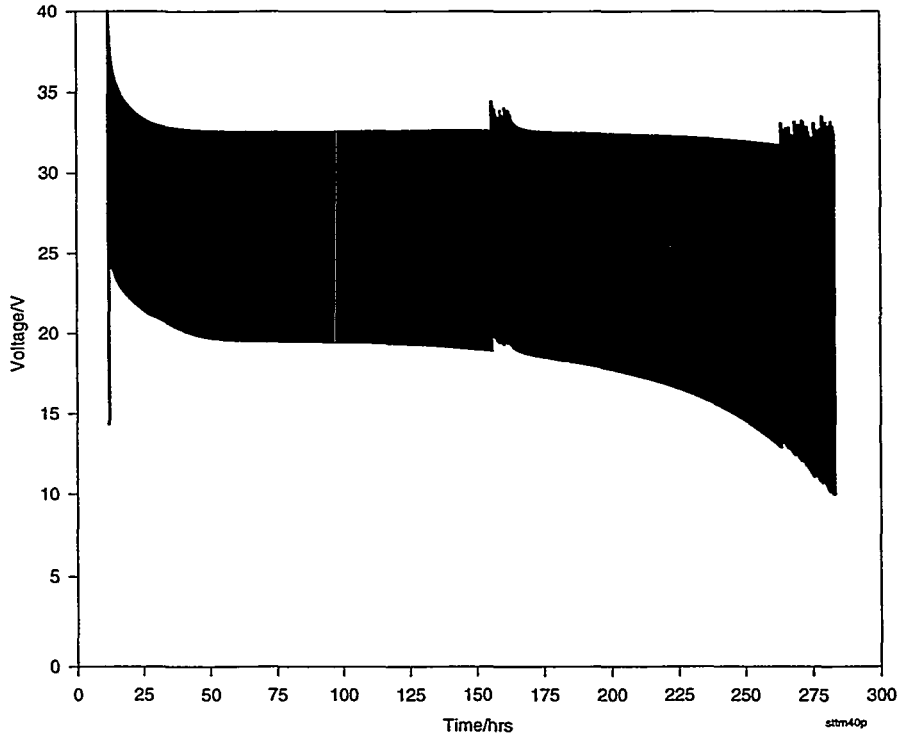

Figure 5-37. Voltage profile of battery composed of 12 Silberkraft M20TT cells in a series configuration at –40°C.

5.5 Summary

Summary data for the constant-current discharge tests and the pulse tests are presented in Tables 5-2 through 5-4 for both individual cells and battery configurations. When enough data were available, averages and standard deviations are shown. In constant-current discharge tests of individual cells, the end of test occurs when the cell voltage reaches 0.5 V. The loaded voltage data shown in the tables correspond to the loaded voltage of the cell when the cell reaches 50% depth of discharge of the full measured capacity. These data clearly illustrate that the capacity is a function of temperature. Further, these data demonstrate (1) if cells tested at low temperature are warmed to room temperature, additional capacity can be removed, and (2) total capacity obtained over all of the temperatures employed is equal to the total nominal room temperature capacity. The constant-current discharge of the Silberkraft M20 cells at –55°C showed significant variability in performance. In general, we observed two populations, one of which provides relatively low capacity (the data shown in the table) and the other providing much more capacity (>6 Ah). The reason for this disparate behavior is not known, although we suspect that it could be because we are operating the cell under conditions close to their operational limits. This behavior also accounts for the higher loaded voltage of the M20 cell at –55°C versus the loaded voltages measured at higher temperatures. In this case, because very little capacity was removed, the cell was still in its early stages of discharge and had not reached the 3-V plateau. Note the small standard deviation in the replicate cell data, indicating good cell-to-cell reproducibility.

Table 5-2. Summary of Constant Current 50 mA Discharge Behavior of D Cells

	Silberkraft M20	Silberkraft M20TT	Bluestar	Ultralife U3660H
Average capacity Ah/std dev/n (cell temp: –55°C)	0.3/0.1/4(5.7/0.3/5)**	9.8/0.4/8	-	0.1
Loaded voltage at 50% DOD (cell temp: –55°C)	2.5 V (2.3 V)**	2.3 V	-	2.4 V
Average capacity Ah/std dev/n (cell temp: –55°C + RT*)	13.0/0.7/4(12.7/0.3/5)**	12.3/(0.4)/8	-	11.1
Average capacity Ah/std dev/n (cell temp: –40°C)	10.8/0.3/9	11.4/0.2/8	10.2	9.8/0.3/10
Loaded voltage at 50% DOD (cell temp: –40°C)	2.4 V	2.6 V	2.5 V	2.5 V
Average capacity Ah/std dev/n (cell temp: –40°C + RT*)	13.1/0.4/9	12.7/0.4/8	11.8	10.6/0.4/10
Capacity Ah (cell temp: –20°C)	10.7	11.8		10.9
Loaded voltage at 50% DOD (cell temp: –20°C)	2.7 V	2.8 V	-	2.7 V
Capacity Ah (cell temp: –20°C + RT*)	-	12.8	-	11.3
Loaded voltage at 50% DOD (cell temp: –20°C + RT*)	-	-		-

Table 5-2. Summary of Constant Current 50 mA Discharge Behavior of D Cells (continued)

	Silberkraft M20	Silberkraft M20TT	Bluestar	Ultralife U3660H
Average capacity (Ah)/std dev/n (cell temp: RT)	12.6/0.3/16	12.5/0.3/15	10.8	11.0/0.2/14
Loaded voltage at 50% DOD (cell temp: RT)	2.98 V	2.99 V	3.01 V	2.97 V
Capacity Ah (cell temp: +70°C)	12.7	-	-	11.3
Loaded voltage at 50% DOD (cell temp: +70°C)	3.1 V	-	-	3.0 V

* Indicates discharge at nominal temperature until voltage reaches 0.5 V followed by continued discharge at room temperature to 0.5 V
** Indicates data for the second population, as described in text.

Table 5-3. Summary of Pulse Discharge Behavior

	Silberkraft M20	Silberkraft M20TT	Bluestar	Ultralife U3660H
Average capacity Ah/std dev/n (cell temp: −40°C)	1.7/1.0/5	6.1/0.8/4	5.0	7.0
Open circuit voltage at 50% DOD (cell temp: −40°C)	2.6 V	2.6 V	2.5 V	2.5 V
Loaded voltage at 50% DOD (cell temp: −40°C)	1.6 V	1.7 V	1.7 V	1.6 V
Average capacity Ah/std dev/n (cell temp: −40°C + RT*)	11.1/0.3/3	11.1/0.1/2	9.1	9.5
Capacity Ah (cell temp: −20°C)	8.7	9.4	8.0	8.5
Open circuit voltage at 50% DOD (cell temp: −20°C)	2.7 V	2.7 V	2.7 V	2.8 V
Loaded voltage at 50% DOD (cell temp: −20°C)	1.9 V	2.0 V	2.0 V	2.1 V
Capacity Ah (cell temp: −20°C + RT*)	10.8	-	9.0	10.0
Capacity Ah (cell temp: RT)	10.6	11.3	9.1	-
Open circuit voltage at 50% DOD (cell temp: RT)	2.9 V	2.9 V	2.9 V	-
Loaded voltage at 50% DOD (cell temp: RT)	2.5 V	2.5 V	2.1 V	-

* Indicates discharge at nominal temperature until voltage reaches 0.5 V followed by continued discharge at room temperature to 0.5 V.

Table 5-4. Summary of Battery Behavior

	BATTERY CONFIGURATION				
		4 in series		12 in series	
	Bluestar	Silberkraft M20	Silberkraft M20TT	Silberkraft M20	Silberkraft M20TT
Capacity Ah (cell temp: –40°C)	5.3	8.0	5.4	7.9**	8.4**
Open circuit voltage at 50% DOD (cell temp: –40°C)	10.2 V	10.2 V	10.1 V	32.8 V	32.6 V
Loaded voltage at 50% DOD (cell temp: –40°C)	5.4 V	3.3 V	5.0 V	18.3 V	19.2 V
Capacity Ah (cell temp: –40°C + RT*)	9.1	11.8	11.0	-	-
Capacity Ah (cell temp: –20°C)	-	10.5	-	-	-
Open circuit voltage at 50% DOD (cell temp: –20°C)	-	10.9 V	-	-	-
Loaded voltage at 50% DOD (cell temp: –20°C)	-	7.8 V	-	-	-
Capacity Ah (cell temp: –20°C + RT*)		11.6			
Capacity Ah (cell temp: RT)	9.3	11.5	-	9.8	10.0
Open circuit voltage at 50% DOD (cell temp: RT)	11.7 V	11.5 V	-	35.5 V	35.5 V
Loaded voltage at 50% DOD (cell temp: RT)	10.1 V	9.8 V	-	29.7 V	28.6 V

* Indicates discharge at nominal temperature until voltage reaches 0.5 V followed by continued discharge at room temperature to 0.5 V

** Indicates tests using the realistic pulse train with voltages given for the 2.4-sec pulse

Pulse data were acquired on the various cells and battery configurations using two different pulse trains. The accelerated pulse train that was used employed a current of 5 A for 3 sec. This was followed by a rest period of 17 sec at open circuit for both the individual cells and the four-in-series battery configuration, while the 12-in-series battery configuration used a 3-min rest period at open circuit voltage. This was repeated until the cell voltage was less than 0.5 V in the case of the individual cells and the four-in-series configuration. The end-of-test condition used for the 12-cell series configuration was 18.0 V. The second, more realistic pulse train consisted of a 2.4-sec pulse at 5 A followed by four successive 0.8-sec 5 A pulses. In this case, all pulses were separated by a rest period of 3 min at open circuit voltage. The pulse train was repeated until the voltage dropped below 10.0 V for the 12-cell series batteries. The two different pulse trains were designed such that the amount of energy consumed in one hour of the accelerated pulse train equals that consumed in one day of the realistic pulse train. It was generally assumed that the accelerated pulse train was a worst-case scenario, but it also allowed us to collect data rapidly for a variety of cells.

In reviewing these data, it is interesting to note that the total measured capacity in a pulse application is within approximately 20% and is often the same as the capacity measured in a constant current discharge mode. This behavior results from a number of factors, including the fact that in the realistic pulse train, the 3-min rest between pulses allows sufficient time for the cells to recover.

Intentionally Left Blank

6. Aged Cell Characteristics

David Ingersoll, Nancy H. Clark, Jill L. Langendorf, and Lorie E. Davis

6.1 Introduction

Worst-case conditions for most battery systems can be summarized by the phrase "old and cold." For lithium-based battery systems, this term has three distinct meanings, one of which is somewhat unique to lithium-based systems. Generally, because of its extremely high reactivity, lithium metal will react with virtually anything with which it comes into contact. In a cell configuration, this is typically either air or the electrolyte solution system. When this reaction occurs, a film forms on the surface of the lithium metal, thereby increasing the effective cell resistance. Depending on the fundamental characteristics of this film, such as thickness, this resistance can become quite large. In addition, at low temperature not only does the film impedance generally increase, but the contribution to the resistance from other sources, such as the reaction kinetics, also increases. The confluence of these factors can result in an effective cell resistance of such magnitude that the cell will not support a load. If current can be passed, the film can be disrupted to such an extent that the effective resistance will drop, allowing passage of current, and there will be a voltage delay in the cell response. These effects are most notable in lithium/liquid catholyte systems, such as those using lithium/thionyl chloride and lithium/sulfur dioxide. An initial evaluation of a lithium/solid cathode system has begun under conditions that are known to result in significant voltage delay effects in lithium/liquid catholyte systems as described in this work.

In addition, in active battery systems (as opposed to reserve systems), aging of the cell typically leads to irreversible capacity loss primarily as a result of self-discharge. Currently, the rate of self-discharge in cells based on the lithium/manganese dioxide chemistry is reported by most manufacturers to be less than 1% per year under normal storage conditions of up to 60°C. In fact, some of the manufacturers of the 2/3A even guarantee 10-year shelf lives of their batteries with no loss of capacity.

To address these issues in the lithium/manganese dioxide chemistry, an initial evaluation was performed on the effect of both short- and long-term storage at elevated temperature on capacity and pulse behavior. These studies were performed using 2/3A cells as well as some short-term tests with D cells. For comparative purposes, some short-term aging tests using lithium/sulfur dioxide D cells, a common liquid catholyte system, were performed under aging conditions identical to those used for the lithium/manganese dioxide cells. The results of these investigations are described in this chapter.

6.2 2/3A Cell Aging Behavior

The long-term aging studies were performed using 2/3A cells that were obtained from Sanyo and Duracell. The storage temperatures included 30°C, 40°C, 50°C, and 60°C. These cells were stored at the indicated temperatures for 1.38 years and 1.83 years. After storage, the cells were visually inspected (no abnormalities were detected) and discharged using the protocol described below.

The cells aged for 72 weeks were discharged at room temperature at a constant current of 10 mA, and the resulting data were compared with the discharge curves obtained from fresh cells of the same lot discharged shortly after initial receipt. As shown by the data in Figure 6-1, the discharge behavior of the

Sanyo cells is the same as that observed for the fresh cell. For the Duracell cells (Figure 6-2), there is some variability; however, some of this can be attributed to cell-to-cell variability.

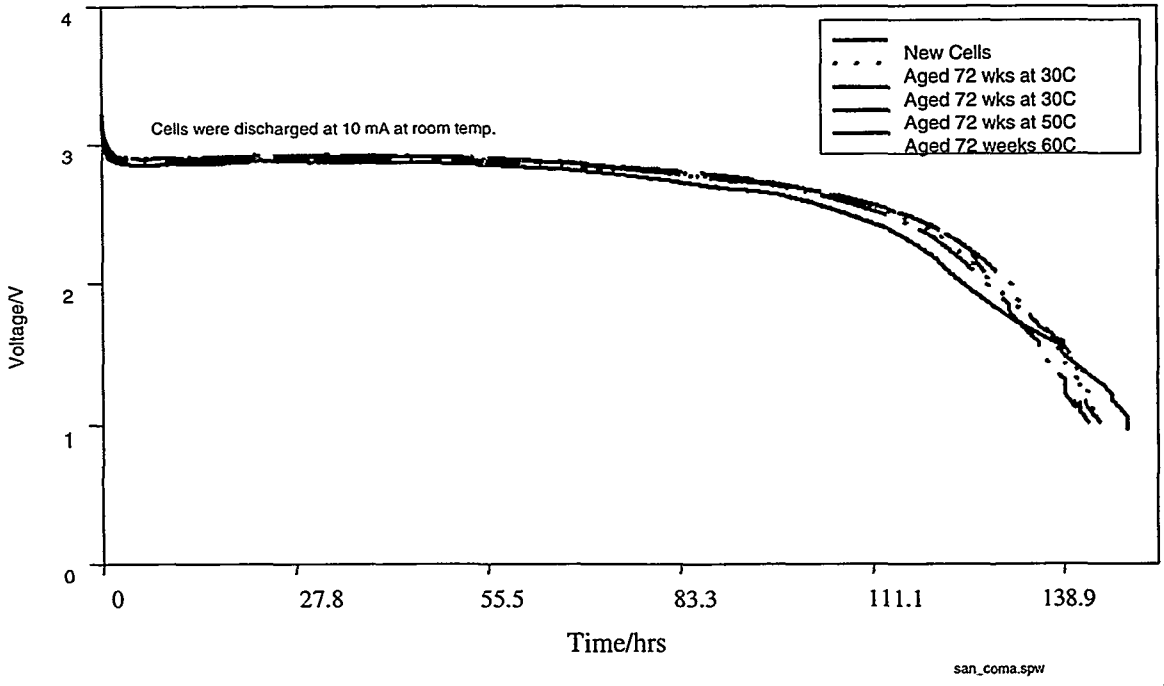

Figure 6-1. Comparison of discharge behavior of new and aged Sanyo 2/3A cells. The cells were discharged at room temperature at a constant current of 10 mA.

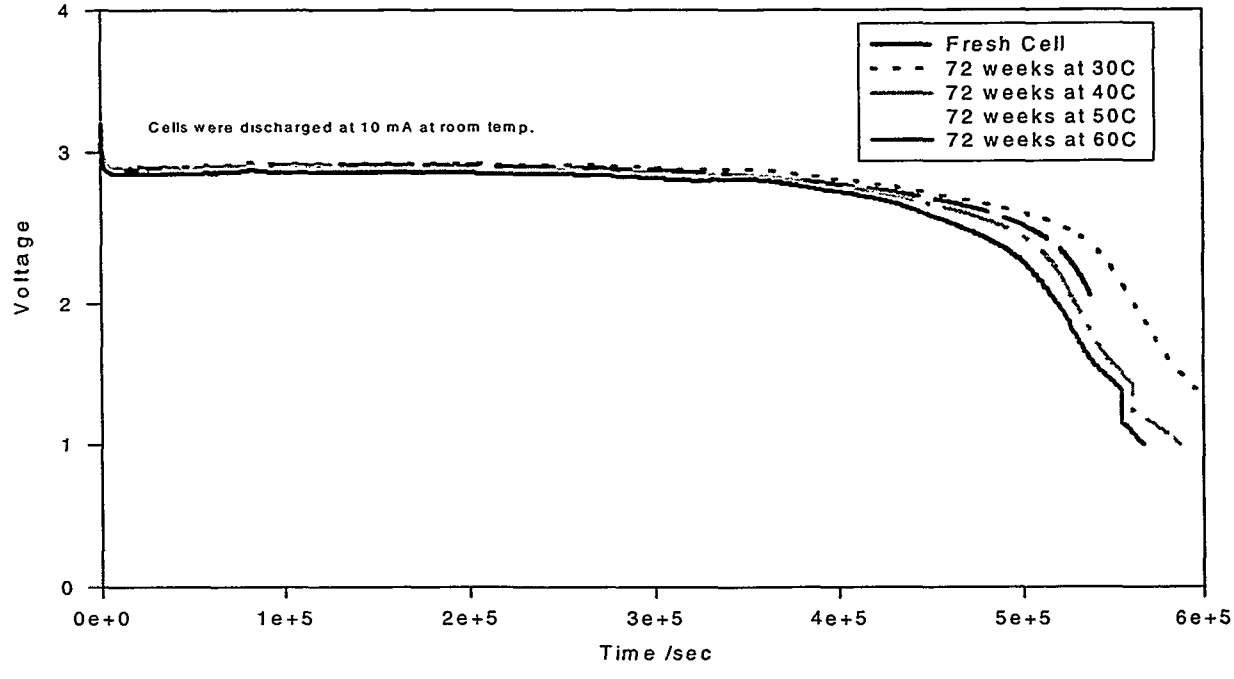

Figure 6-2. Comparison of discharge curves of new and aged Duracell 2/3A cells. The cells were discharged at room temperature at a constant current of 10 mA.

Some pulse testing was also performed at –40°C on Duracell and Sanyo 2/3A cells that had been aged 72 weeks (1.38 years) in ovens at temperatures of 30°C, 40°C, 50°C, and 60°C. These data are shown in Figures 6-3 through 6-8. In general, the cells can support the loads and exhibit little voltage delay even after long storage times under conditions in which lithium/liquid catholyte systems would have difficulty performing.

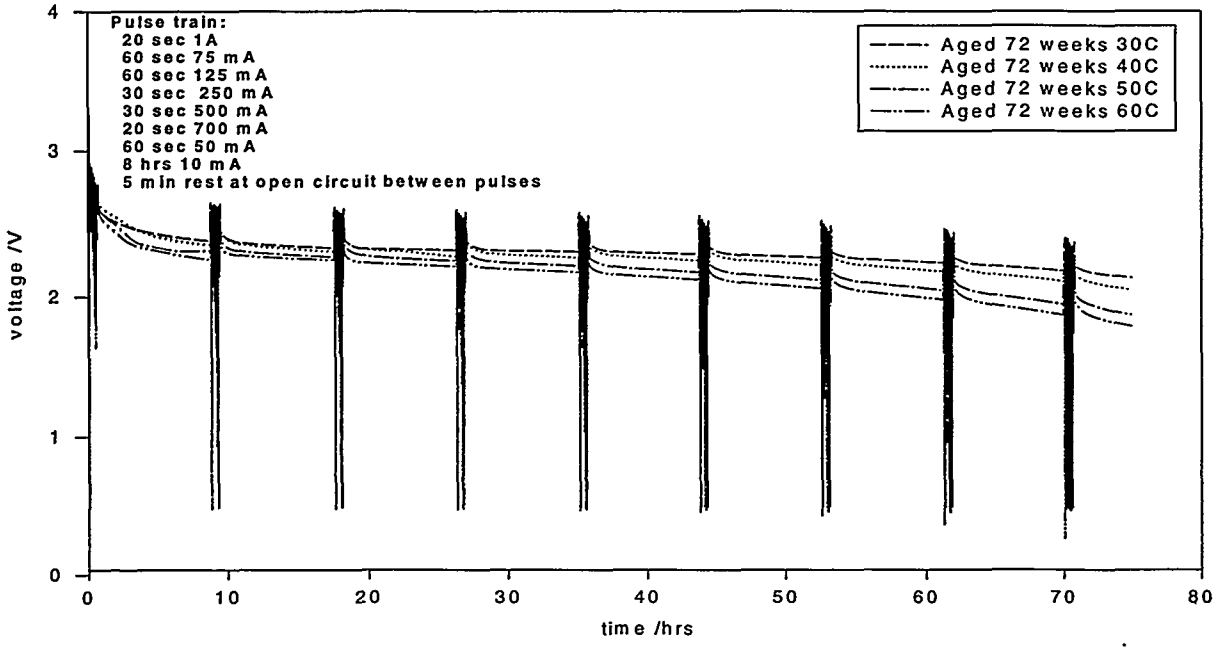

Figure 6-3. Pulse test behavior of aged Sanyo 2/3A Li/MnO_2 cells. The cells were discharged at –40°C.

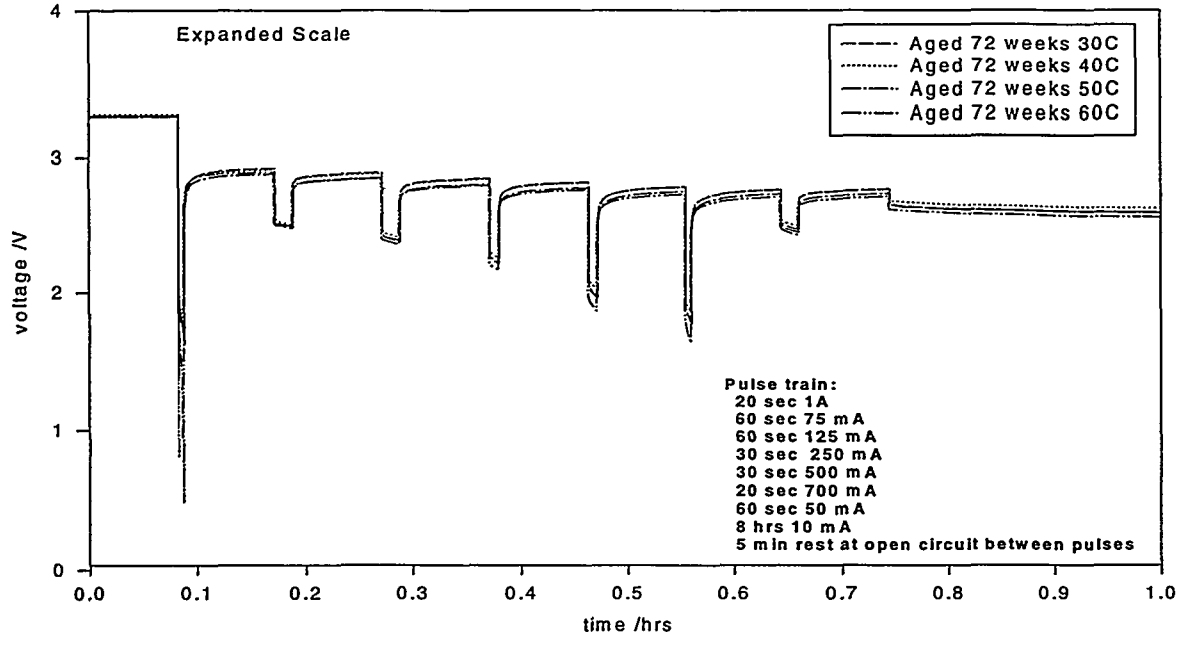

Figure 6-4. Expanded view of the pulse test behavior of aged Sanyo 2/3A Li/MnO_2 cells shown in Figure 6-3 showing the first pulse train. The discharge was performed at –40°C.

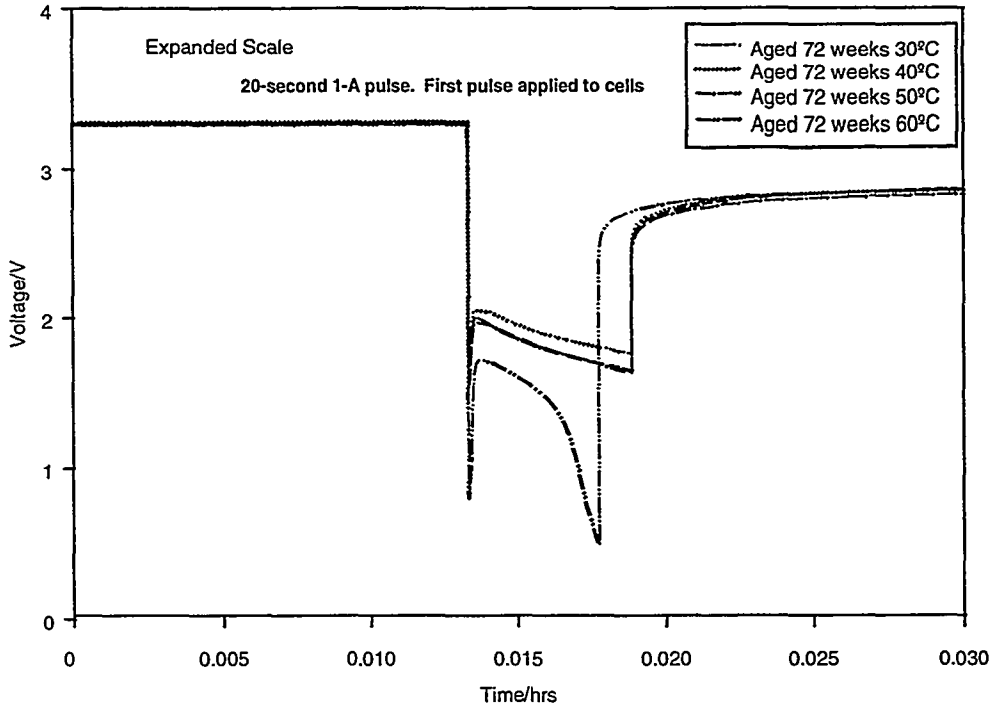

Figure 6-5. **Expanded view of the pulse test behavior of aged Sanyo 2/3A Li/MnO_2 cells shown in Figure 6-3 showing the first pulse applied to the cell. The discharge was performed at –40°C.**

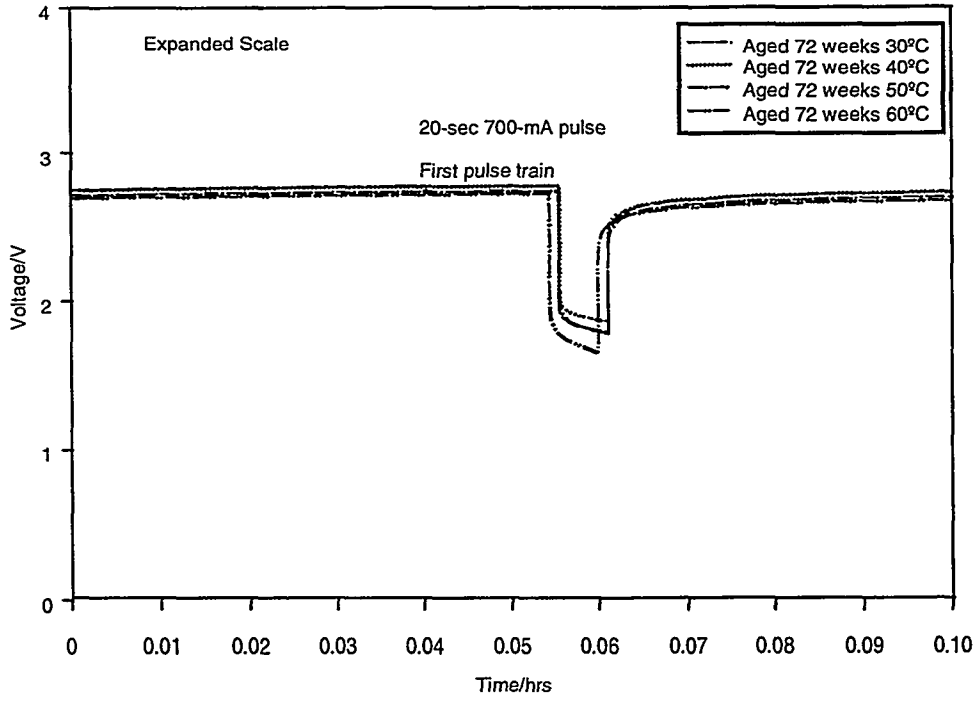

Figure 6-6. **Expanded view of the pulse test behavior of aged Sanyo 2/3A Li/MnO_2 cells shown in Figure 6-3 showing the first 700 mA pulse (5 A D-cell equivalent) applied in the first pulse train to the cell. The discharge was performed at –40°C.**

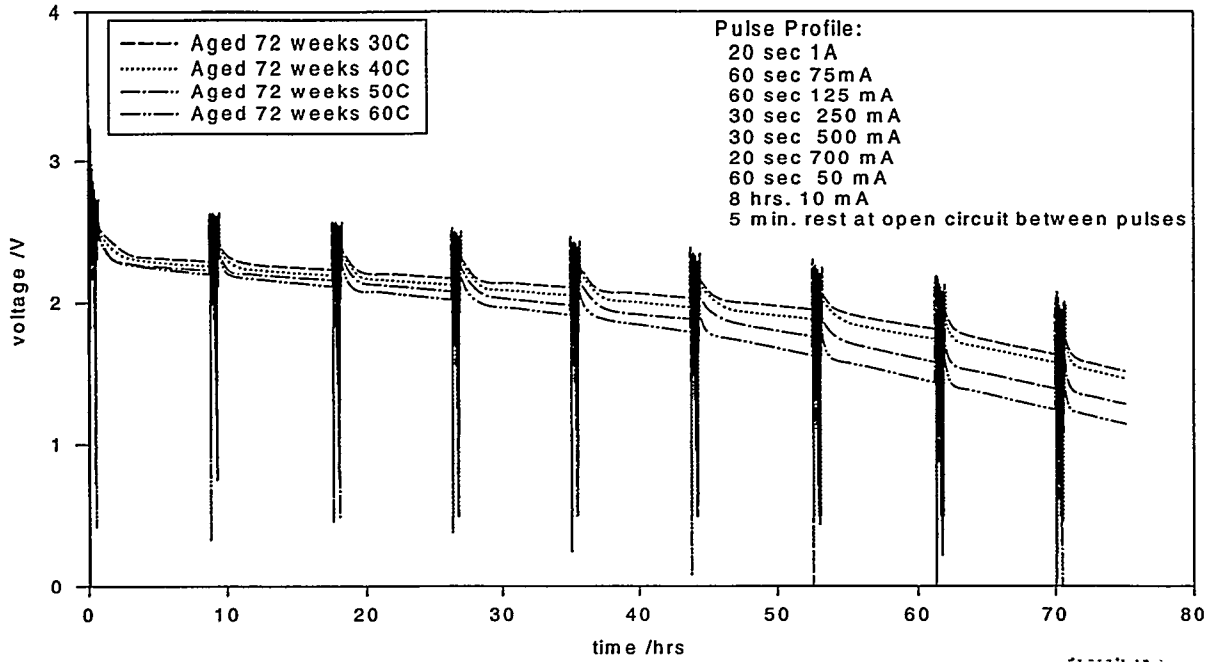

Figure 6-7. Pulse test behavior of aged Duracell 2/3A Li/MnO_2 cells. The cells were discharged at –40°C.

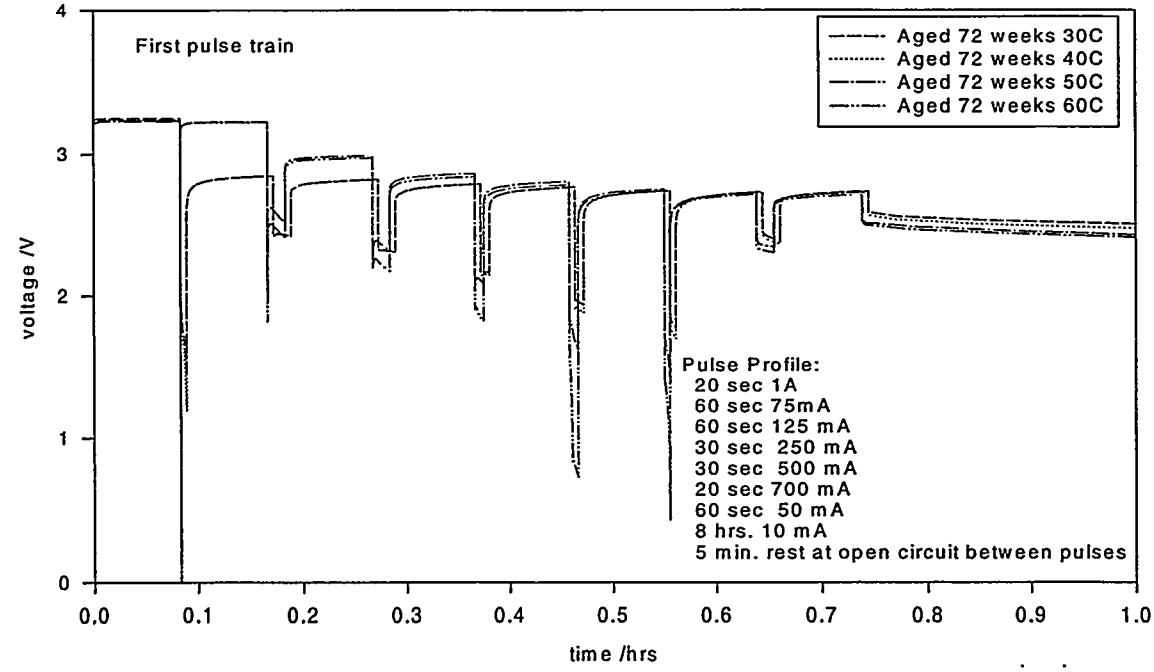

Figure 6-8. Expanded view of the pulse test behavior of aged Duracell 2/3A Li/MnO_2 cells shown in Figure 6-7 showing the first pulse train. The discharge was performed at –40°C.

While the Duracell cells behave similarly to the Sanyo cells, their performance under these conditions is inferior to that of the Sanyo cells, as shown in the preceding figures. This is consistent with the Duracell cell performance that was previously observed under conditions of low temperature and is not solely a reflection of the aging characteristics of the cell. At least some of this behavior is because of the cell construction, in particular, the reliance on a compression connection between the positive current collector and the tab rather than use of a welded attachment (see Chapter 7).

Sony and Duracell 2/3A cells were also aged for 1.83 years at 30°C, 40°C, 50°C, and 60°C, and their subambient temperature performance was evaluated under pulsed-load conditions. The temperature used for the pulse testing was –40°C, and the cells were allowed to equilibrate at this temperature for 6 hr before application of loads. The first pulse applied to the cells was a 5-sec, 714-mA pulse, which is approximately equivalent to a 5-A pulse in a D cell. A 5-sec pulse width was used for the first pulse to more fully characterize any voltage delay and to determine the time needed to stabilize the cell voltage.

After the first pulse, the cells were allowed to rest at open circuit for 17 sec before pulsing again at 714 mA for 3 sec. Thereafter, pulsing continued at 714 mA for 3 sec followed by a rest at open circuit for 17 sec. This pulse train continued until the cell voltage dropped below 0.5 V.

Figures 6-9 and 6-10 below show the first pulse applied to the Sanyo and Duracell cells, respectively. As shown, all of the aged cells from both vendors are able to support the pulse load at these low temperatures. However, a slight delay is evident in the first pulse, which stabilizes within the first 2 sec in every case. The term "delay" is somewhat of a misnomer because the magnitude of the voltage drop and its duration are significantly less than that typically observed in cells employing other chemistries, such as lithium/thionyl chloride, for which the term was initially intended. However, its source is presumably the same and probably arises because of higher initial interfacial impedance resulting from the aging process. For the Duracell cell aged at 60°C for 1.83 years, a low voltage of 0 V was reached during the initial transient, which is not shown in the figure. Those cells aged at the higher temperatures exhibit lower voltages throughout the pulse train.

Figures 6-11 and 6-12 show some of the subsequent 3-sec, 714 mA pulses applied to the aged Sanyo and Duracell cells, respectively. As can be seen, all of the aged cells from the two manufacturers are capable of supporting these subsequent pulses under subambient temperature conditions.

Short-term aging studies also were performed using conditions that can lead to significant voltage delay in liquid catholyte systems. The initial series of tests was performed using the test protocol outlined below.

Step 1 Hold cell at 55°C for two weeks in an oven.
Step 2 Allow to cool to room temperature.
Step 3 Cool to –40°C and allow to equilibrate over 6 hr.
Step 4 Pulse battery, 5 sec at 5 A and 5 sec at 10 A, 5-min rest at open circuit between pulses.
Step 5 Warm to room temperature.
Step 6 Remove 2 Ah capacity at 0.2 A.
Step 7 Repeat process beginning with Step 1.

These experiments were performed on Kodak 2/3A cells arranged in a seven-cell parallel string. In this series of studies, the cells were allowed to age for 2 weeks at 55°C before pulse testing at –40°C. Aging for a longer time would lead to more significant voltage delays in the case of the liquid catholyte systems. Once again, 5 A and 10 A pulses were applied to the cells.

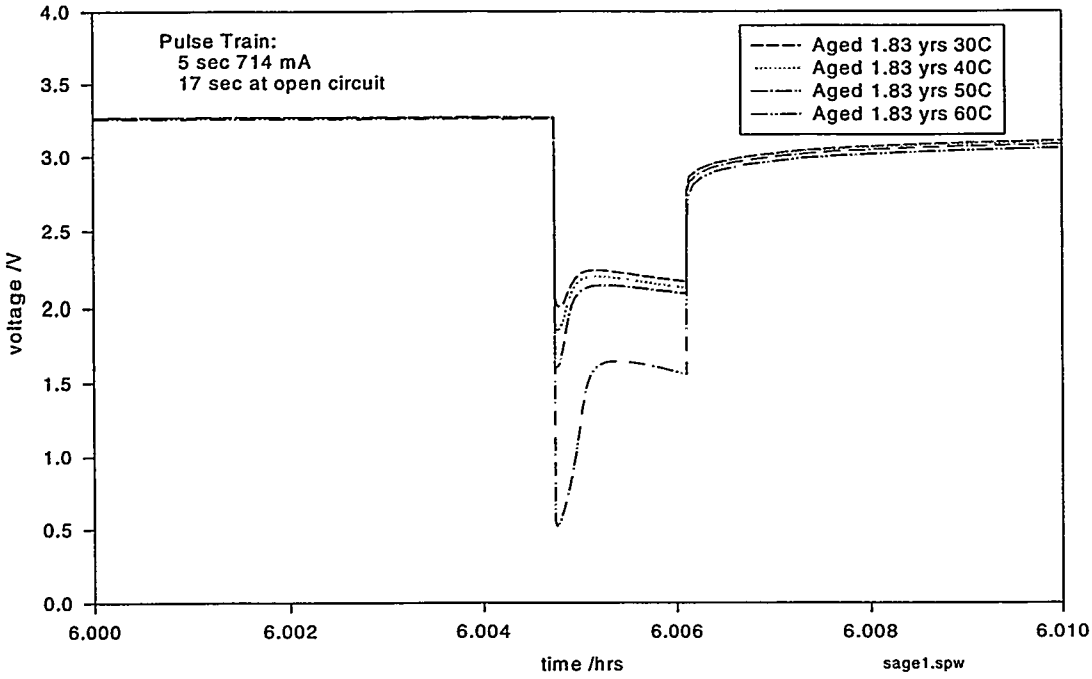

Figure 6-9. Voltage behavior of aged Sanyo 2/3A cells at –40°C to the first pulse applied to the cell.

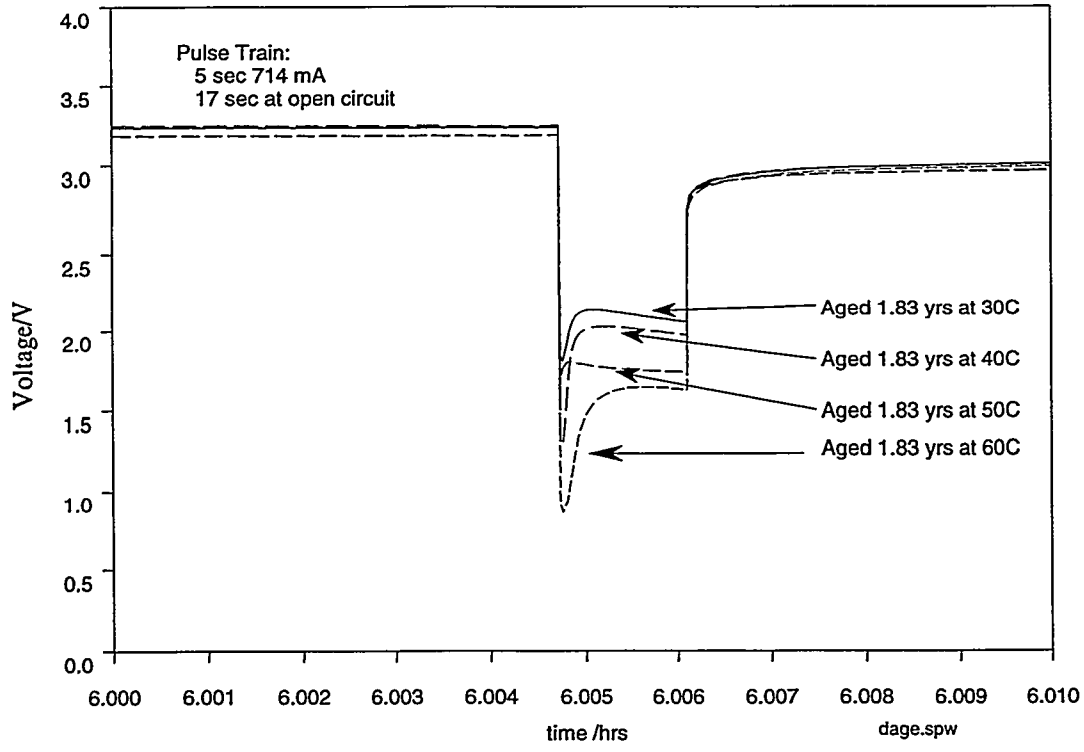

Figure 6-10. Voltage behavior of aged Duracell 2/3A cells at –40°C to the first pulse applied to the cell.

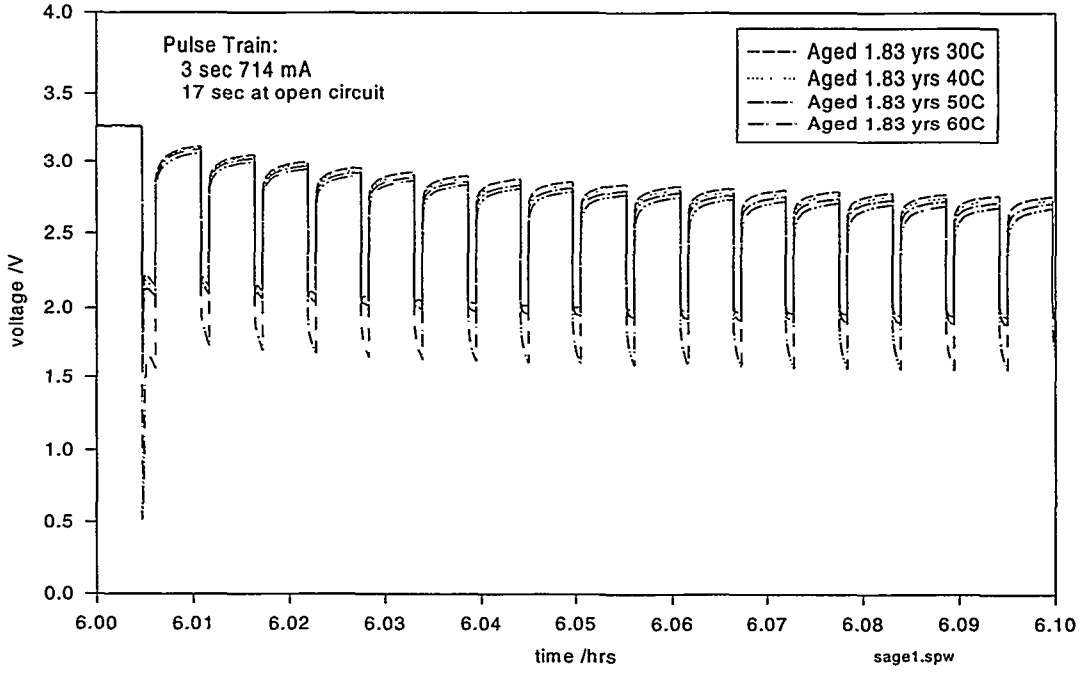

Figure 6-11. Pulse behavior of aged Sanyo 2/3A cells at –40°C. The cells were aged 1.83 years at the temperatures indicated.

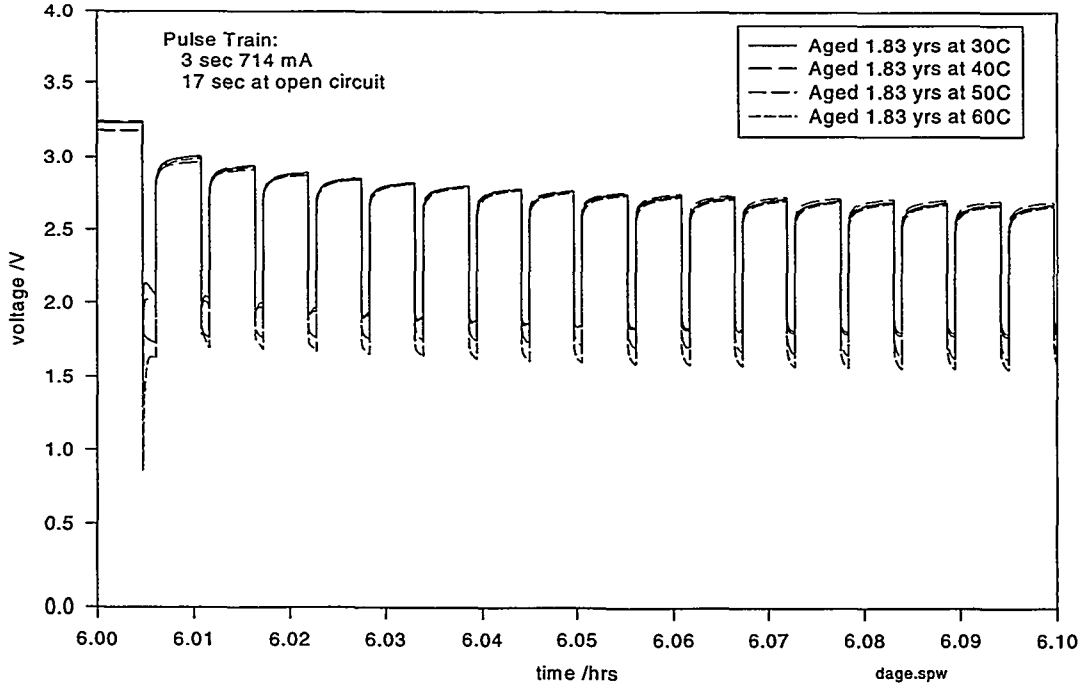

Figure 6-12. Initial pulse behavior of aged Duracell 2/3A cells at –40°C for cells aged 1.83 years at the indicated temperatures.

Figure 6-13 shows the pulse behavior response for this battery after 0 Ah, 2 Ah, 4 Ah, and 6 Ah were removed, corresponding to four cycles of the above procedure. The 5-A pulse data are shown on the right, and the 10-A pulse data are shown on the left. The first pulse (on both right and left) corresponds to 0 Ah, second to 2 Ah, third to 4 Ah, and fourth to 6 Ah. These data reveal that the cells can support the loads under these conditions and that there is some delay in the voltage response, typically on the order of 2 sec as calculated from the first spike on 5-A pulse. However, after this initial 2-sec delay, the voltage increases to a stable level. Finally, the cells can support this pulse protocol when up to at least 6 Ah has been removed. The data show that there is a small voltage delay, and the cells can support both loads.

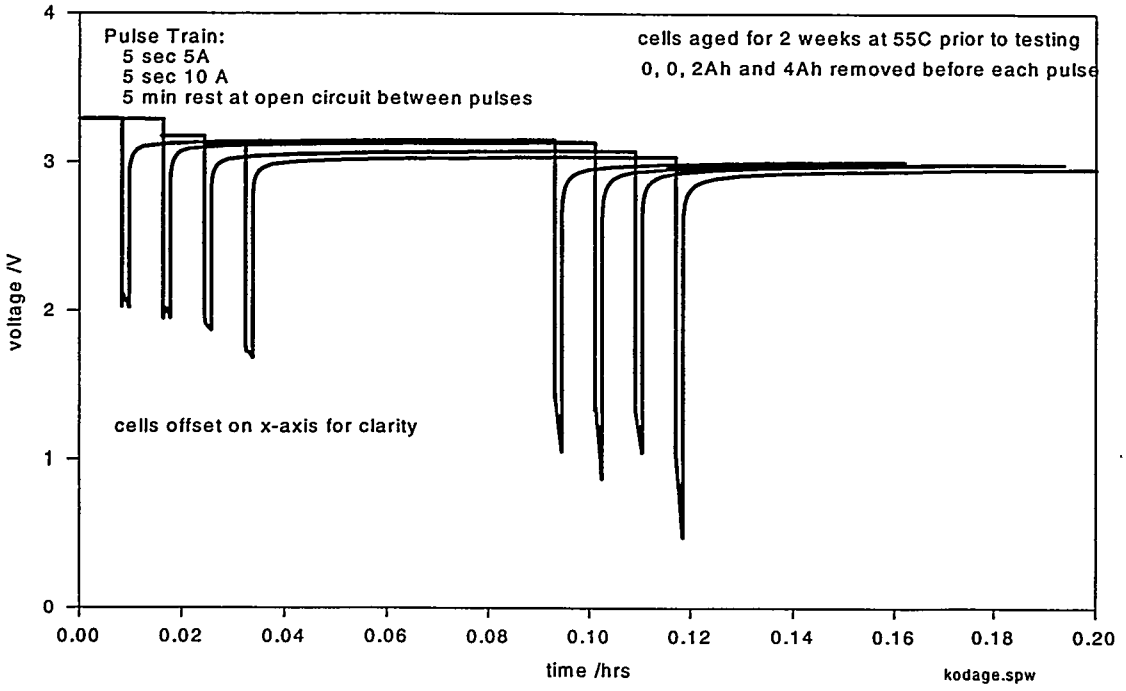

Figure 6-13. Pulse behavior of Kodak 2/3A cells arranged in a 7-cell parallel string at –40°C.

6.3 D Cell Aging Behavior

A series of short-term aging studies was also performed on D cells using conditions that can lead to significant voltage delay in liquid catholyte systems. The initial series of tests was performed using the test protocol outlined below.

Step 1 Hold cell at 55°C for one week in an oven.
Step 2 Allow to cool to room temperature.
Step 3 Cool to –40°C and allow to equilibrate over 6 hr.
Step 4 Pulse battery, 5 sec at 5 A and 5 sec at 10 A, 5-min rest at open circuit between pulses.
Step 5 Warm to room temperature.
Step 6 Remove 2 Ah capacity at 0.2 A.
Step 7 Repeat process beginning with Step 1.

Figures 6-14 and 6-15 show the pulse behavior response for one of these cells at 0-Ah, 2-Ah, 4-Ah, and 6-Ah removed, corresponding to four cycles of the above procedure. (Data from only one cell are shown because both of the cell tests behave similarly to this point.) These data reveal that the cells can support the loads under these conditions and that there is some delay in the voltage response, typically on the order of 2 sec. However, after this initial 2-sec delay, the voltage increases to a stable level. The cells can support this pulse protocol when up to at least 6 Ah has been removed. When one additional cycle of this procedure was repeated, that is, after 8 Ah had been removed and the cells were again aged in the oven at 55°C, the burst disc in one of the cells failed in a nonviolent manner for an unknown reason. When cooled to –40°C and pulsed, the other cell was not able to support the load. This is not surprising in view of its behavior under isothermal conditions at –40°C (see Chapter 5).

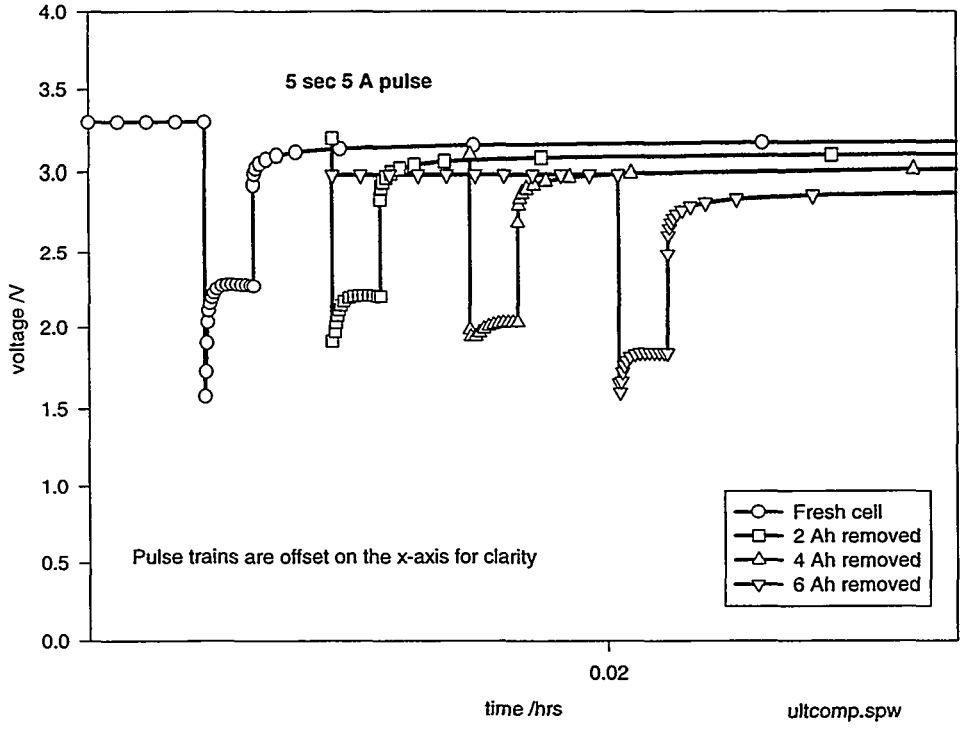

Figure 6-14. Pulse behavior of aged Ultralife U3360VH Li/MnO_2 D cell at –40°C. The cell was aged one week at 55°C after every pulse train.

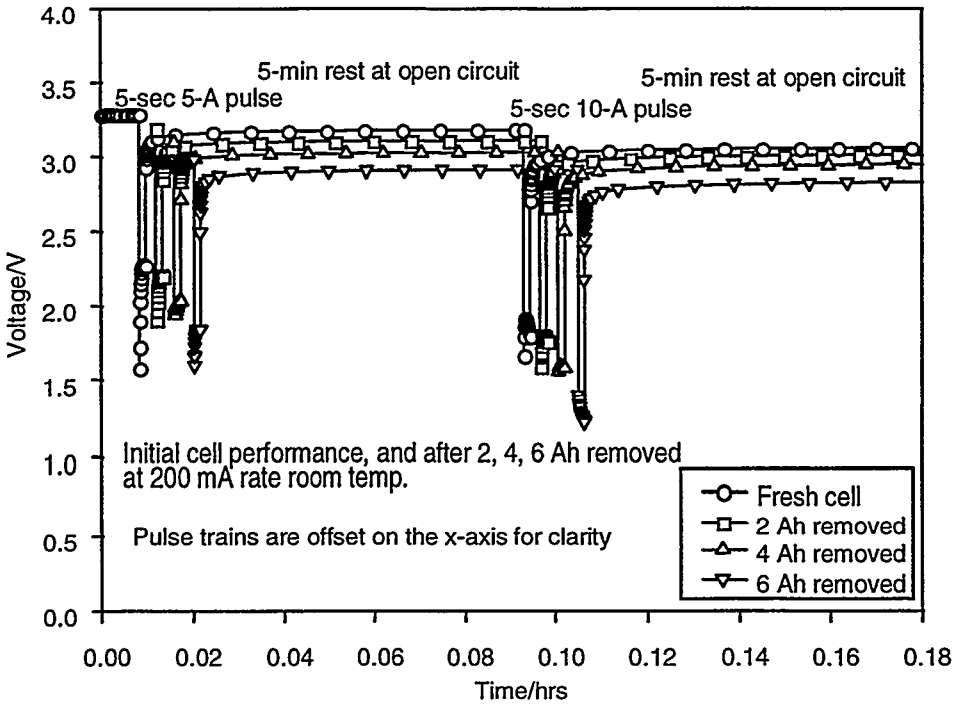

Figure 6-15. Pulse behavior of aged Ultralife U3360VH Li/MnO_2 D cell at –40°C. The cell was aged one week at 55°C after every pulse train.

Experiments under more severe conditions were initiated on Bluestar and Ultralife D cells. In this series of studies, the cells were aged for 2 weeks at 55°C before pulse testing at –40°C. Aging for a longer time may cause more significant voltage delays. Once again, 5 A and 10 A pulses were applied to the cells. As shown in Figures 6-16 and 6-17, there is no significant voltage delay, and the cells can support both loads.

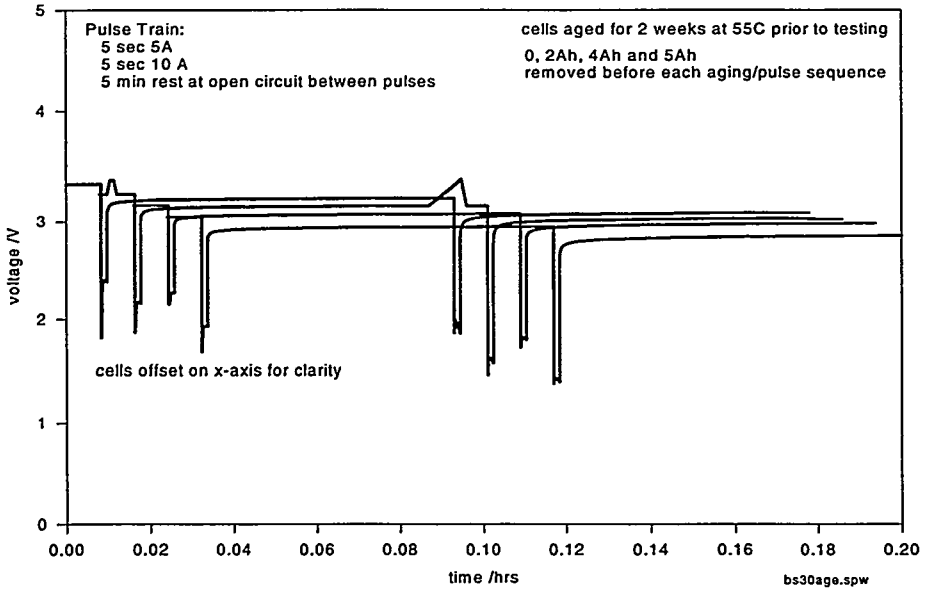

Figure 6-16. Pulse behavior of Bluestar D cells at –40°C. The cell was aged for two weeks at 55°C before application of the pulse train.

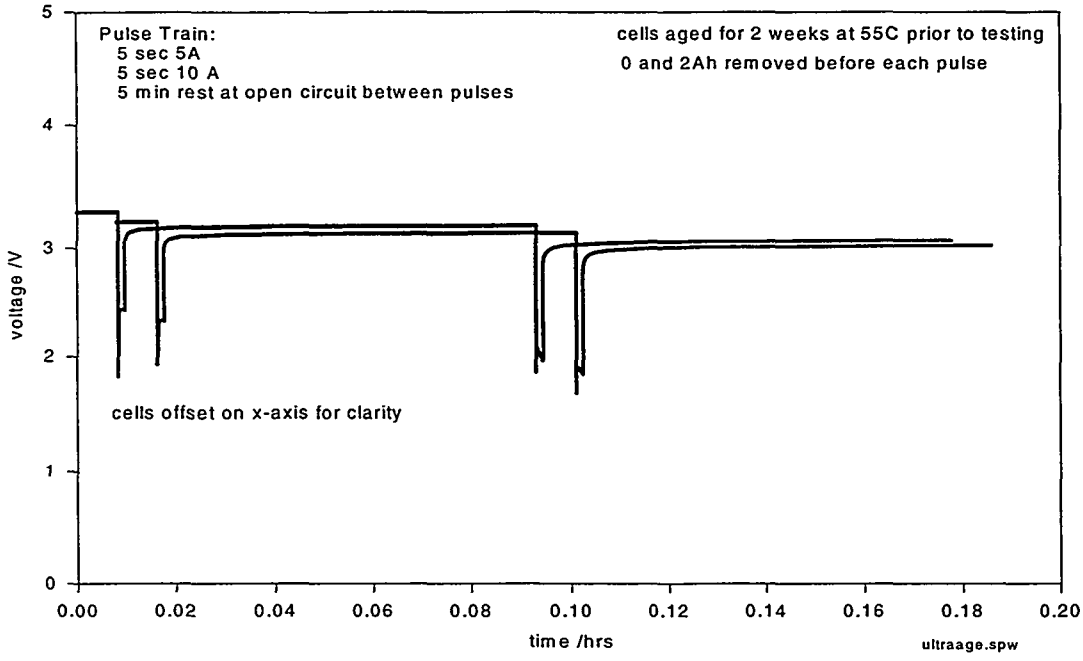

Figure 6-17. Pulse behavior of Ultralife U3360VH D cells at –40°C. The cell was aged two weeks at 55°C before application of the pulse train.

A series of more conventional aging studies began on the D-cells, which were placed into ovens with regulated temperature of 50°C. The cells remained in the oven for either three weeks or eight weeks (two populations of cells were used). At the end of this time period the cells were removed from the oven and placed into an environmental chamber with a constant temperature of –40°C. After reaching thermal equilibrium, the cells were discharged under pulse load conditions.

The first pulse applied to a cell was a 5-A pulse for 5 sec. This was the only time that a cell was pulsed for 5 sec. The next five pulses make up a pulse train that was repeatedly applied to complete the discharge. The first pulse in this group was a 5 A 3-sec pulse. The remaining four pulses were 5 A 0.8-sec pulses. After every pulse, the cells were allowed to rest at open circuit for 3 min. The pulse discharge protocol was continued on the cells until the voltage was equal to or less than 0.5 V during the pulse train.

This test protocol allowed evaluation of cell performance under "worst case" conditions for lithium cells, namely "old and cold." In addition, the use of a 5-sec pulse as the first pulse applied to the cells allows us to determine how much time is required for the cells to achieve a steady state voltage when the cells are first used after having been aged.

Figures 6-18 through 6-20 shows the discharge curves for the three types of D cells (Silberkraft M20 and M20TT and the Ultralife U3360H) after having been aged for three weeks. As is seen, both Silberkraft cells are able to support the load for extended periods of time without significant loss of capacity. In fact, the total capacity obtained from these cells is similar to that observed in an unaged cell (see Chapter 5). The performance of the Ultralife cell is significantly worse than the Silberkraft cells and is also inferior to the very high rate U3360VH version of the Ultralife D cell.

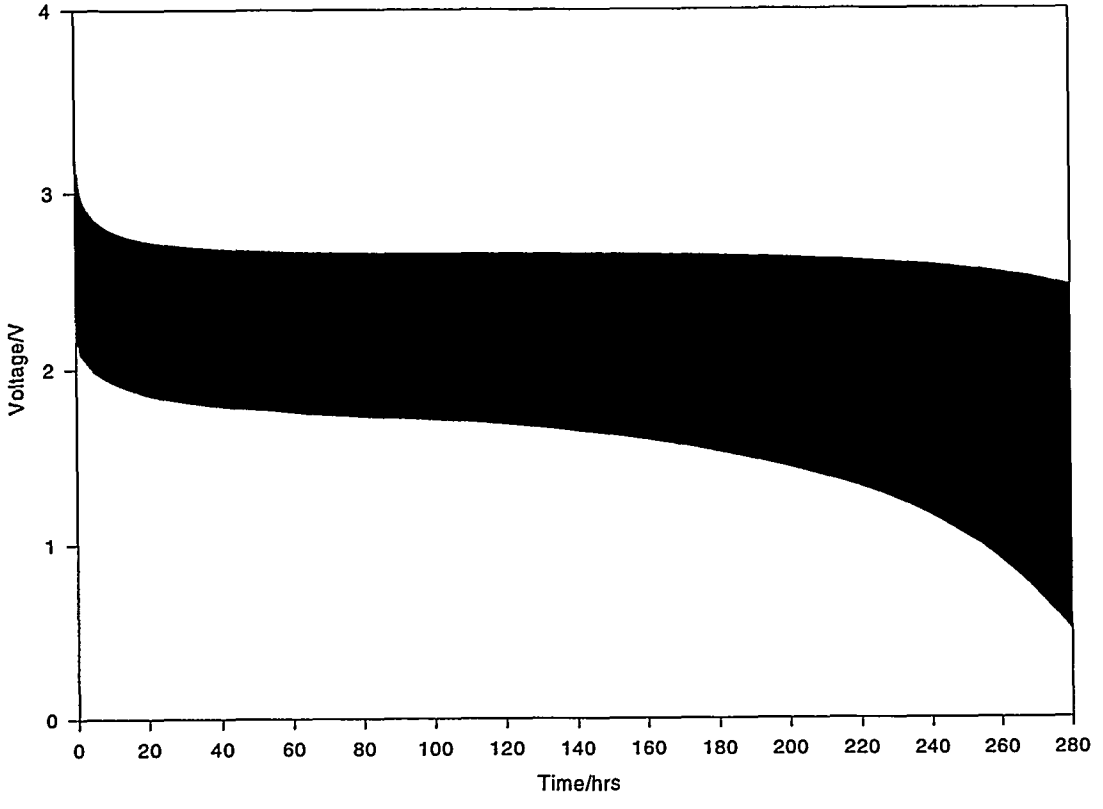

Figure 6-18. Pulse discharge behavior of Silberkraft M20TT cell at –40°C after being aged for three weeks at 50°C.

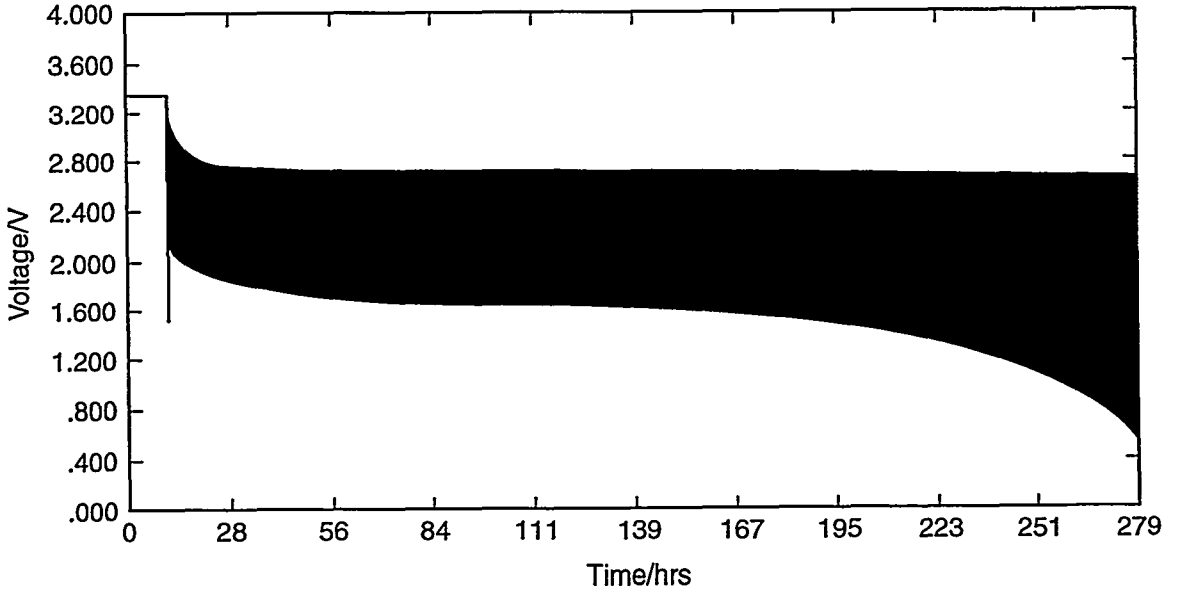

Figure 6-19. Pulse discharge behavior of Silberkraft M20 cell at –40°C after being aged for three weeks at 50°C.

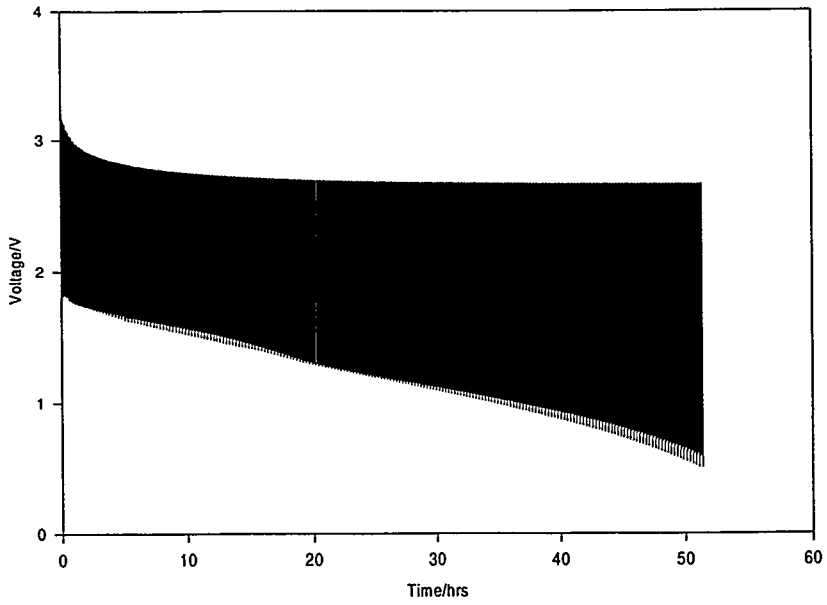

Figure 6-20. Pulse discharge behavior of Ultralife U3360H at –40°C after being aged for three weeks at 50°C.

Examination of the initial pulse behavior of these cells indicated a possible voltage delay phenomenon. Figures 6-21 through 6-23 show the behavior of these cells to the first pulse and the first few pulses making up the pulse train. As can be seen, there is a significant initial voltage drop; however, in less than two seconds the cell reaches a stable response for the remainder of this pulse as well as for subsequent pulses. These data clearly illustrate that the small voltage delay allows the cell to perform within acceptable parameters for this voltage profile.

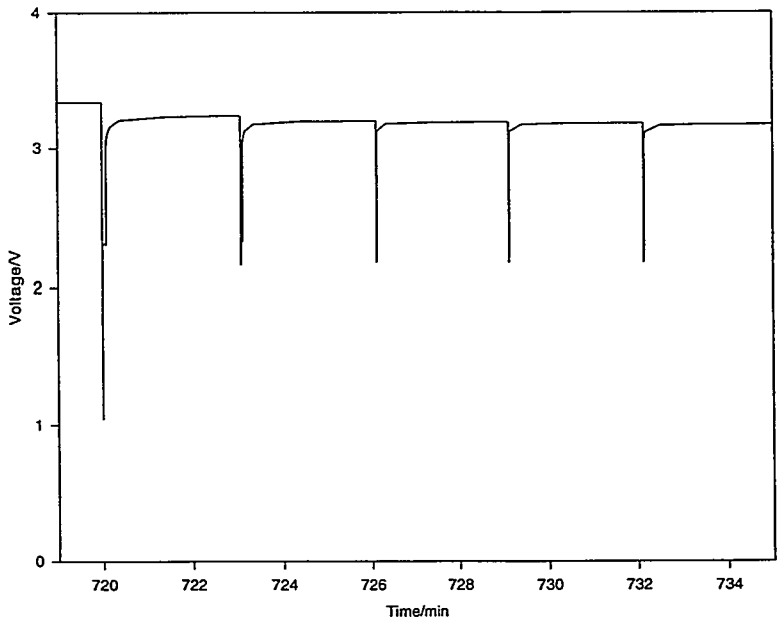

Figure 6-21. Initial pulse discharge behavior of the Silberkraft M20TT cell at –40°C after being aged for three weeks at 50°C. The first pulse is a 5-A, 5-sec pulse followed by four pulses in the pulse train.

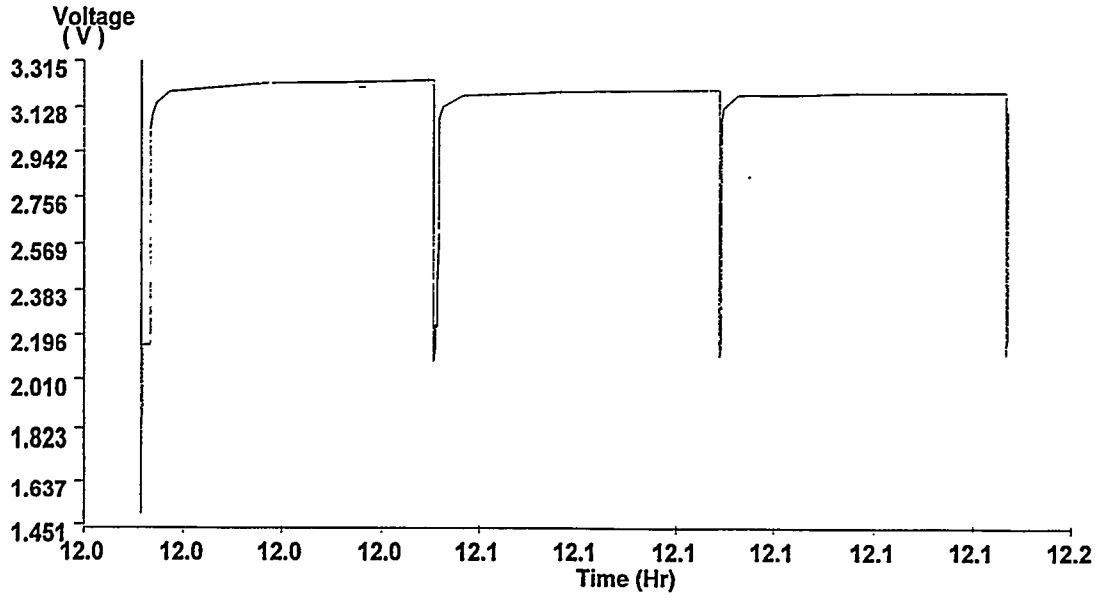

Figure 6-22. **Initial pulse discharge behavior of Silberkraft M20 cell at –40°C after being aged for three weeks at 50°C. The first pulse is a 5-A, 5-sec pulse followed by four pulses in the pulse train.**

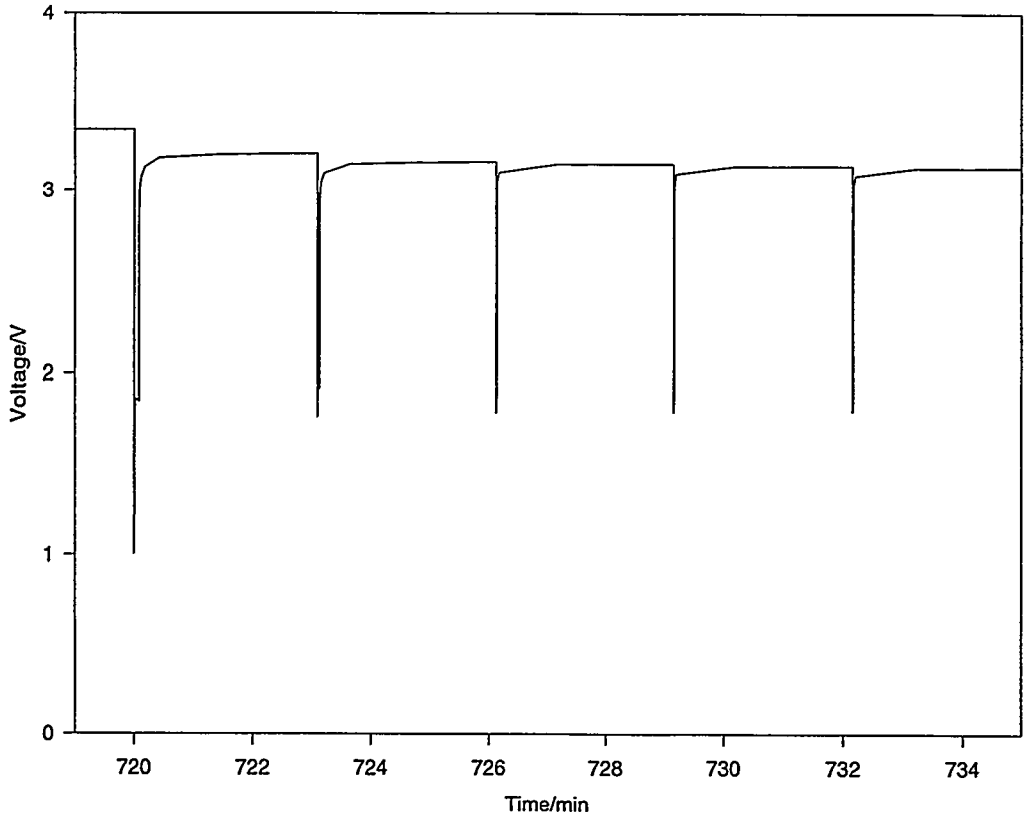

Figure 6-23. **Initial pulse discharge behavior of the Ultralife U3360H cell at –40°C after being aged for three weeks at 50°C. The first pulse is a 5-A, 5-sec pulse followed by four pulses in the pulse train.**

The behavior was also studied in cells that had been aged for 8 weeks at 50°C, and the performance is shown in Figures 6-24 through 6-26. The environmental chamber failed during the collection of these data. At this point, the temperature of the chamber increased to ambient conditions and the discharge continued. When this occurred, the voltage on the cell increased and the voltage drop during the pulse decreased because of a decrease in the effective equivalent series resistance of the cell. This condition occurred over a weekend near the end of discharge of the cell, and when the temperature of the environmental chamber was again lowered to –40°C, the voltage drop during the pulse fell below the end condition of the test. This accounts for the behavior seen in the figures about 2/3 of the way into the discharge in the case of the Silberkraft cells. However, until this point it should be noticed that the discharge behavior is similar to that observed for the cells that had been aged for only three weeks, again indicating that aging under these conditions has very little effect on cell performance.

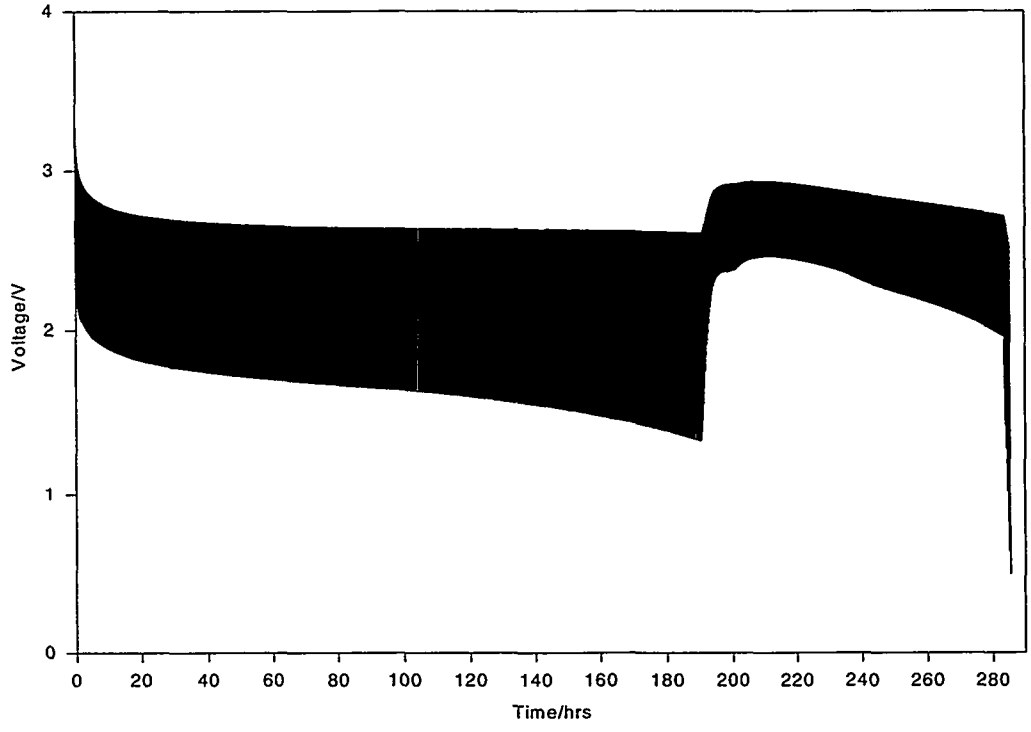

Figure 6-24. Pulse discharge behavior of the Silberkraft M20TT cell at –40°C after being aged for eight weeks at 50°C. The voltage increase at about 190 hours corresponds to a failure of the environmental chamber leading to a rise in the cell temperature to ambient (over a weekend). The chamber was reactivated at about 279 hours.

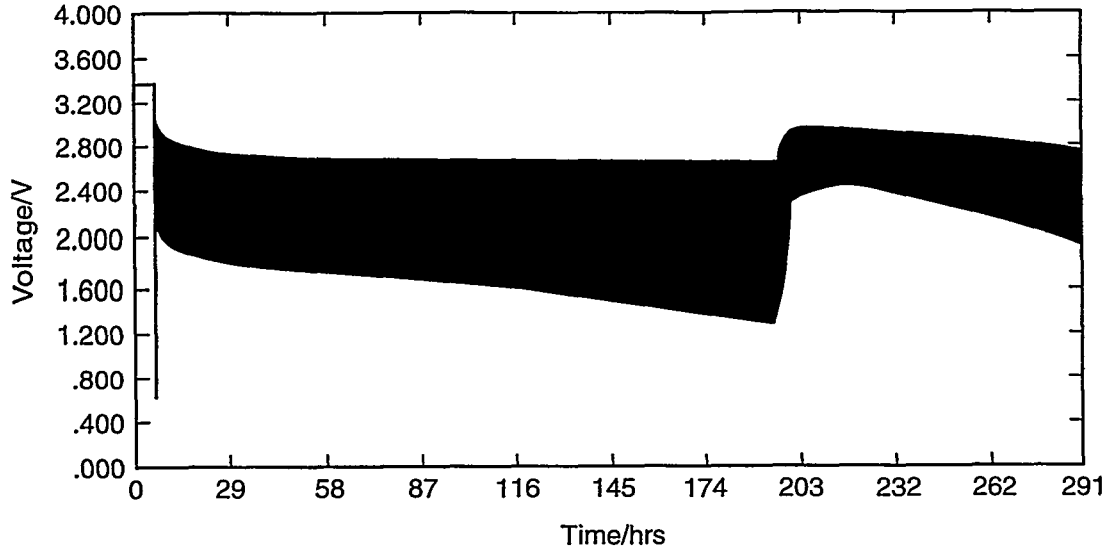

Figure 6-25. Pulse discharge behavior of the Silberkraft M20 cell at –40°C after being aged for eight weeks at 50°C. The voltage increase at about 190 hours corresponds to a failure of the environmental chamber leading to a rise in the cell temperature to ambient (over a weekend). The chamber was reactivated at about 279 hours.

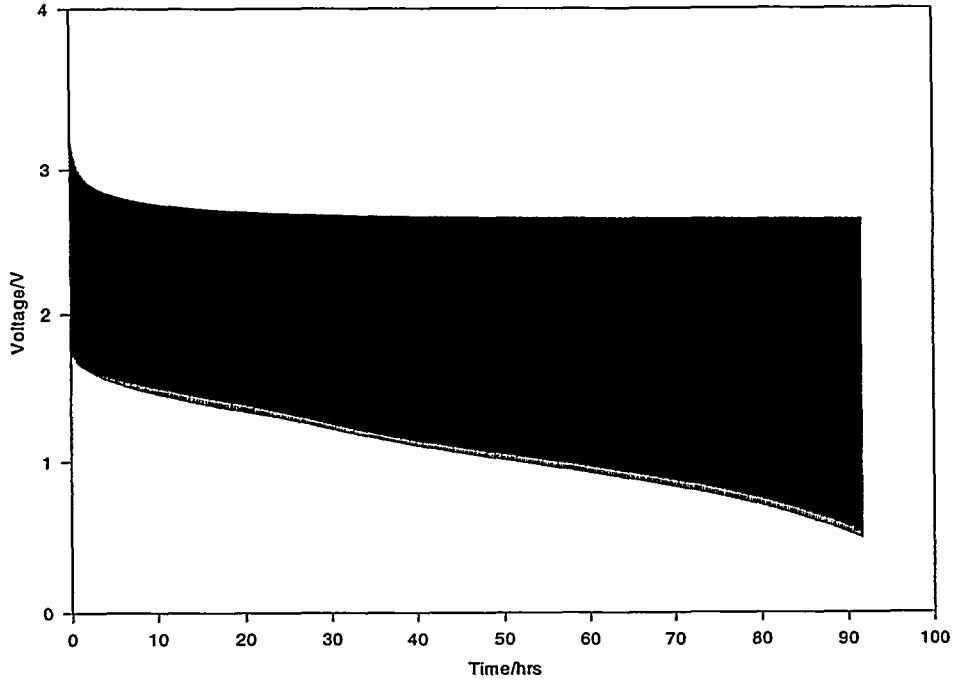

Figure 6-26. Pulse discharge behavior of Ultralife U3360H at –40°C after being aged for eight weeks at 50°C.

The initial pulse behavior of the cells aged for eight weeks can also be examined in closer detail by expanding the scale used in plotting the preceding three graphs. This is done in Figure 6-27 through

The initial pulse behavior of the cells aged for eight weeks can also be examined in closer detail by expanding the scale used in plotting the preceding three graphs. This is done in Figure 6-27 through 6-29, and again the behavior of these cells is similar to what was observed in the case of three-week aging. Although there is an initial voltage drop, it is observed only during the first two seconds of the first pulse applied to the cells. Thereafter, the behavior is relatively stable.

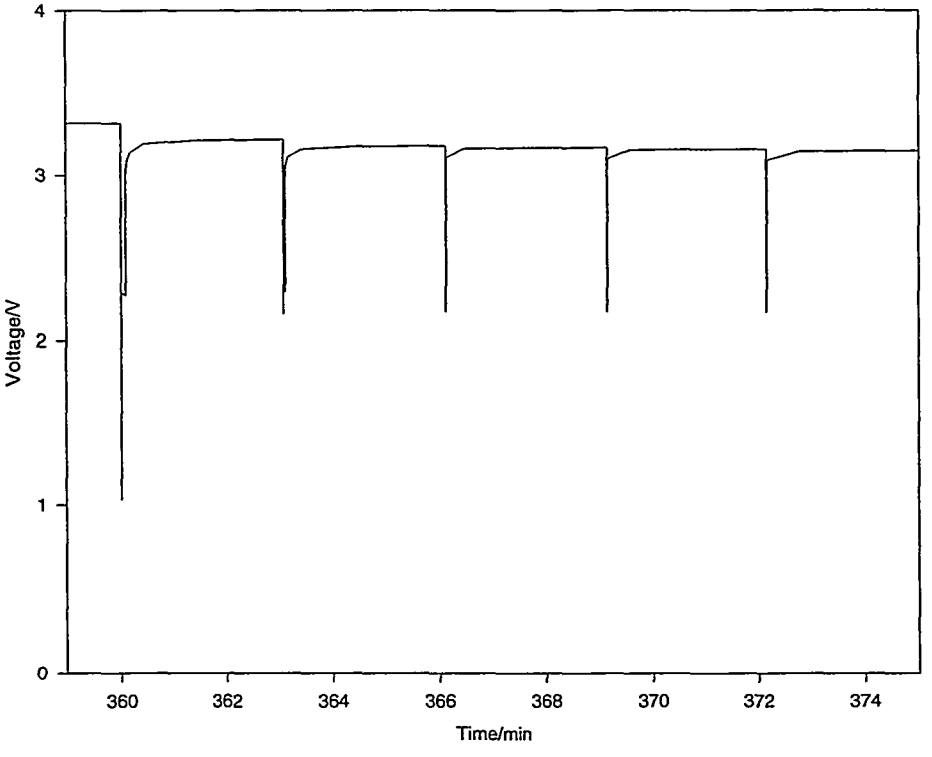

Figure 6-27. Initial pulse discharge behavior of the Silberkraft M20TT cell at –40°C after being aged for eight weeks at 50°C. The first pulse is a 5-A, 5-sec pulse followed by four pulses in the pulse train.

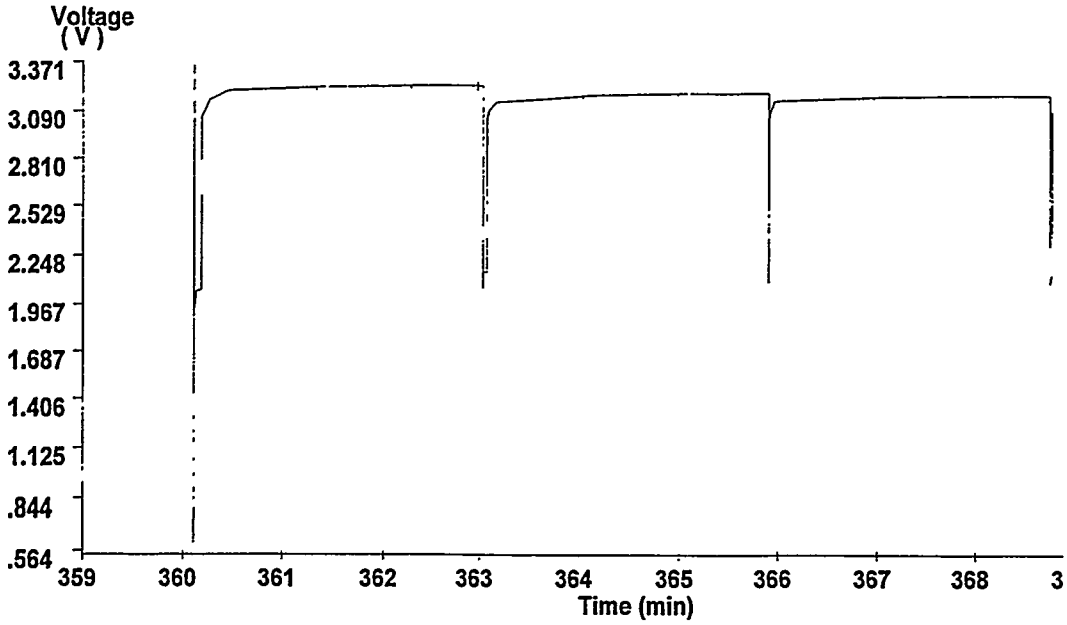

Figure 6-28. Initial pulse discharge behavior of the Silberkraft M20 cell at –40°C after being aged for eight weeks at 50°C. The first pulse is a 5-A, 5-sec pulse followed by four pulses in the pulse train.

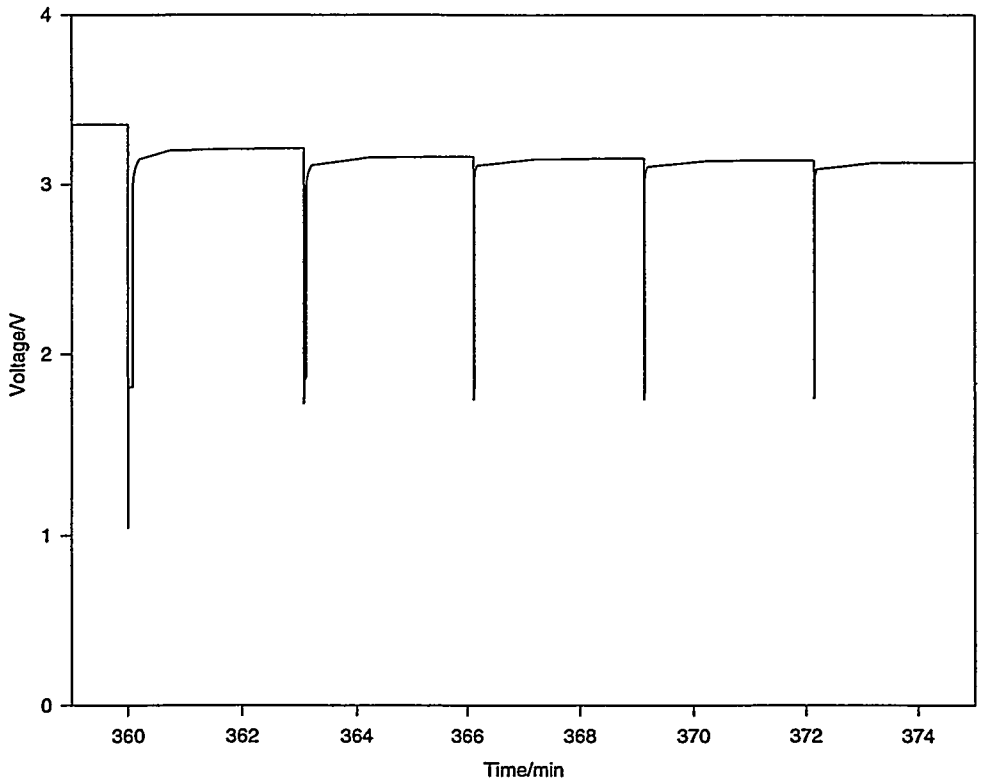

Figure 6-29. Initial pulse discharge behavior of the Ultralife U3360H cell at –40°C after being aged for eight weeks at 50°C. The first pulse is a 5-A, 5-sec pulse followed by four pulses in the pulse train.

6.4 Conclusion

As seen, the lithium/manganese dioxide cells do not exhibit voltage delay, at least in the conventional sense of the term. Although they exhibit a large initial voltage drop when first used at low temperature after aging, the voltage returns to a stable level soon after use. The initial voltage drop is seen only once during the initial pulse, and as shown by the 2/3A cell data, the capacity loss on storage at high temperatures for prolonged time periods is minor and only becomes noticeable when the cell is operated at low temperature. This is consistent with the guarantees made by the various vendors of the consumer cells for a six- to eight-year shelf life with little or no capacity loss. Clearly, further work is warranted if the cells are to be used in applications where there is a low-voltage cut off.

7. Performance Engineering

David Ingersoll, Jill L. Langendorf, Lorie E. Davis, Theodore T. Borek III, and Mark A. Rodriguez

7.1 Introduction

Chemical and engineering characteristics of a cell necessarily define its overall performance. For example, the species used for both positive and negative electrodes generally defines the thermodynamics of the cell, and hence the cell voltage. The reaction kinetics and the transport characteristics of the species present (engineering and chemical characteristics) influence the rate capability (current) of the cell. Therefore, knowledge of individual cell characteristics combined with performance characteristics of the cells promotes a fundamental understanding of the cell behavior. Toward this end, we initiated an effort to determine some of the engineering characteristics of the different cells, and these results are described in the chapter.

7.2 Gross Physical Features

The gross physical characteristics (nominal dimensions and average weights) of the different cell varieties are summarized in Table 7-1. The dimensions reported are the outside dimensions of the cell housing itself including the pin, if any. The Silberkraft D cells have plastic spacers at one end of the cell that bring the overall cell dimensions to a standard D-cell size. The Ultralife cells does this with metallic spacers. In both cases, the spacer is found on the end where the burst disc is located, and presumably ensures a space sufficient for cell venting in the event that the cells are in a close-packed arrangement.

At least two things are apparent upon examination of the mass of the various cells. First, there is a relatively small degree of variation in the mass of the cells provided by different vendors within any given size group. This is because, for a given overall cell size and performance demand, there is an optimum amount of active material that can be made to fit inside the can. This is not surprising because the various vendors use basically the same materials: manganese dioxide, lithium, etc., and they all use a steel cell housing. Second, the variability in the cell mass for any one size from any one vendor, as reflected by the standard deviation, is small. Because of the small variability in weight, one would expect a similarly small variability in the overall performance because it is a direct reflection of the amount of material in the cell. This small variability in performance characteristics of the cells has, in fact, been observed and was discussed in previous chapters. These issues directly impact the question of cell reliability and provide some insight into the quality control at the production line.

7.3 Gross Internal Features

The internal features profoundly influence the performance characteristics of a cell. Some of these engineering features include spiral-wrap versus bobbin configuration, electrode area, and method of attachment of the electrode to the cell can. Both destructive and nondestructive methods for examining these internal features were employed. The nondestructive method examination method was x-ray radiography. Three views of each cell were taken: (1) the downward view on the long axis of the cell, (2) the side view of the cell, and (3) the side view of the cell after a 90° rotation around the long axis from view 2. The magnification used in preparing the radiographs was 1:1, which allows the internal

Table 7-1. Physical Characteristics of Lithium/Manganese Dioxide Cells–Summary Information

Cell Type and Source	Height (cm)	Diameter (cm)	Cell Mass		
			Average (g)	Std. Dev.	n
2/3 A Cells					
Duracell	3.422	1.643	16.721	0.182	15
Eveready	3.377	1.619	16.394	0.101	15
Kodak	3.434	1.652	16.31	0.103	15
Panasonic Black	3.414	1.647	16.054	0.122	15
Panasonic White	3.456	1.641	16.326	-	1
Sanyo	3.419	1.648	15.423	0.176	14
Sony	3.479	1.651	16.433	0.049	15
Ultralife	3.386	1.643	16.871	0.0834	15
Varta	3.4	1.634	16.834	0.185	15
C Cells					
Silberkraft M52	5.078	2.574	55.951	1.092	15
Silberkraft M52TT	5.065	2.608	56.314	0.51	15
Ultralife	6.03	2.55	56.432	0.461	15
5/4 C Cells					
Silberkraft M56TT	6.047	2.602	67.843	0.91	15
Ultralife	5.946	2.554	68.47	0.295	15
D Cells					
Blue Star	5.739	3.33	-	-	-
Silberkraft M20	5.247	3.38	111.077	0.775	15
Silberkraft M20TT	5.239	3.4	115.017	0.838	15
Ultralife	5.509	3.321	116.8735	1.168	15
Double D Cells					
Silberkraft M25	12.394	4.167	350.923	2.131	15

dimensions to be determined simply by measuring the features in the radiograph and by comparison to a known dimension, which in this case is the exterior dimension of the cell can. The destructive method of analysis involved dissection of the cell, typically after its discharge.

Based on the radiographs, the 2/3A cells fall into either of two general categories depending on the method of attachment of the positive electrode grid to the cell top. For Ultralife, Varta, and Duracell, attachment of the positive electrode grid is accomplished through the use of a mechanical compression type of attachment. A small portion of the positive electrode grid along the long edge of the electrode is not coated with oxide. When the electrodes are rolled and placed into the can, this exposed metal grid is

at the top of the can. When the can top is placed onto the cell, the metal grid contacts the cell top, thus providing electrical connection to the cell top. Figure 7-1 shows the radiographs and the final configuration for these three cell types. (The scale of the original radiographs is 1:1. In these figures, dimensions can be determined by using the physical dimensions of the cells and by referring to the dimensions in the radiographs.)

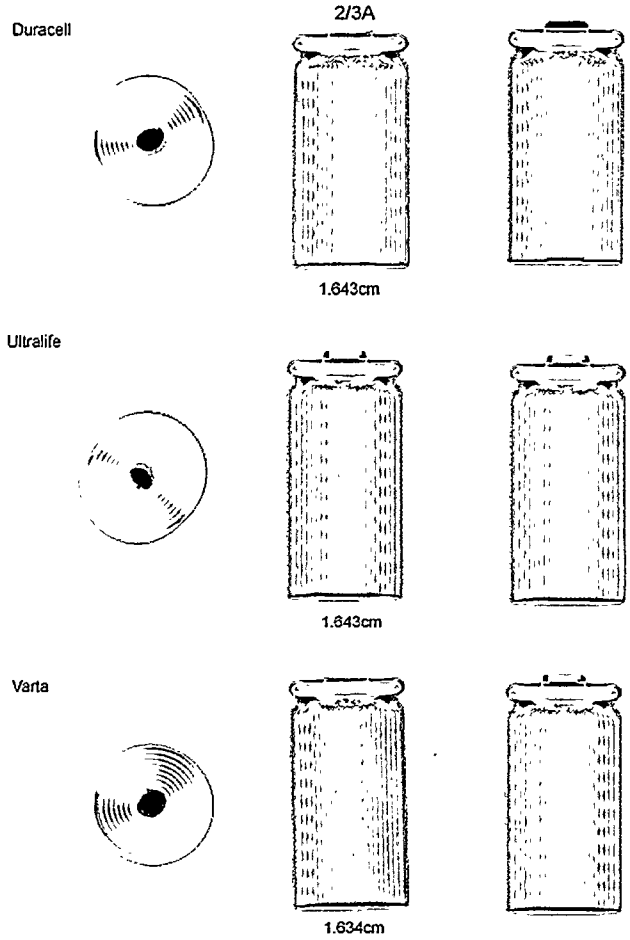

Figure 7-1. Radiographs of Duracell, Ultralife, and Varta 2/3A cells.

For the remaining cells, attachment to the metal grid is accomplished by welding a metal tab between the electrode grid and the cell top. This is apparent in some of the radiographs of the remaining 2/3A cells, which are shown in Figures 7-2 and 7-3.

The different attachments of the electrode to the can might explain some of the behavior observed for the 2/3A cells, which has been previously described. At room temperature, the Duracell cell exhibits performance characteristics superior to those of many of the other cells. However, at reduced temperature, the performance of the Duracell product is inferior to that of some of these same cells partly because the equivalent series resistance of this cell becomes significantly larger than the other cells. Several factors contribute to this variable resistance as a function of temperature, such as the reaction kinetics; however, the magnitude of these effects is expected to be generally the same for each of the cell types with the main difference being the cell connection. As the cell temperature changes, the metal grid is expected to expand and contract, thus changing the contact resistance at the grid/can interface and hence a variable equivalent series resistance. This is expected to become most noticeable at lower temperatures, when the grid contraction is expected to be the greatest. In the case of the other cells

having welded tabs, the grid undergoes similar expansion and contraction; however, because the grid and can are welded, the expansion and contraction are not expected to lead to much change, if any, in the resistance of the internal cell connections.

It is notable that the cells are all quite similar, essentially having the same number of wraps and central cavity dimension. Given this, the overall electrode surface area, which will significantly influence performance, is relatively constant from one cell to the next. On this basis alone, the cells are expected to behave similarly.

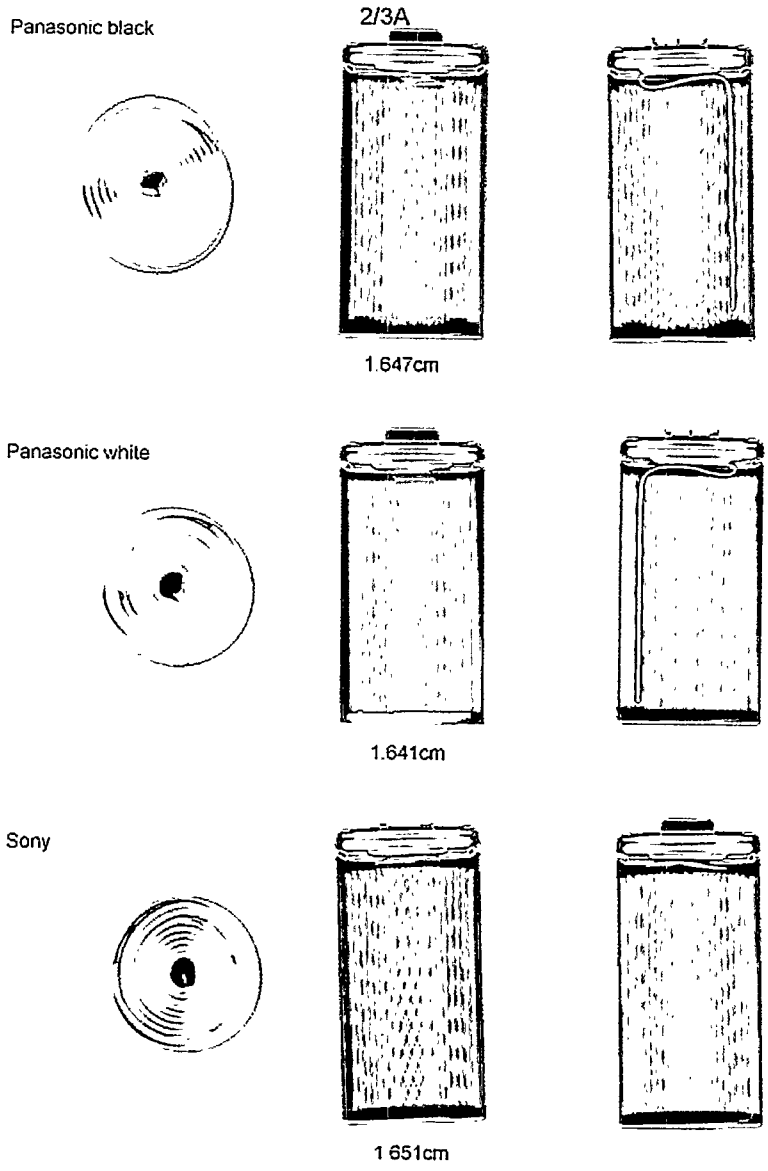

Figure 7-2. Radiographs of the Panasonic (both black and white versions) and Sony 2/3A cells.

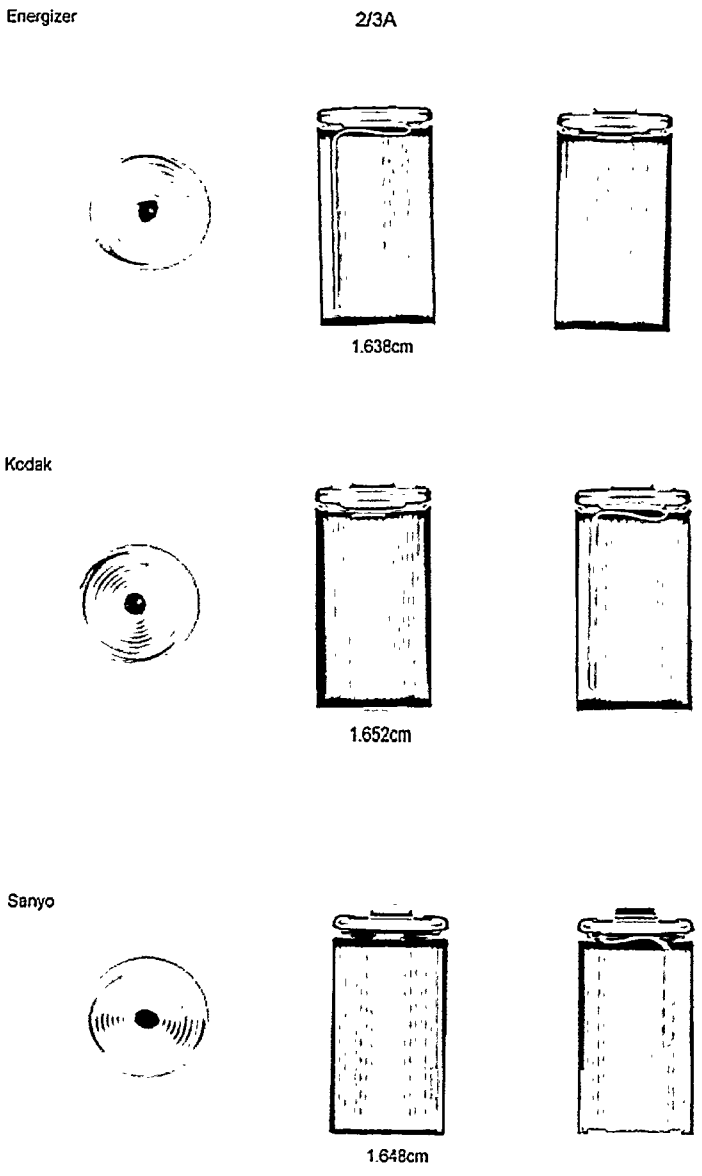

Figure 7-3. Radiographs of the Energizer, Kodak, and Sanyo 2/3A cells.

The radiographs for the D cells are shown in Figure 7-4. As for the 2/3A cells, the internal characteristics of these cells are very similar to one another even though they are from different vendors. One of the interesting features of these cells compared to the 2/3A cells is the relative thickness of the electrodes. As can be seen on comparison, the D-cell electrodes are thicker than the 2/3A cells by a factor of about three. Based on this, the 2/3A cells would be expected to exhibit superior normalized rate capability than the D cells.

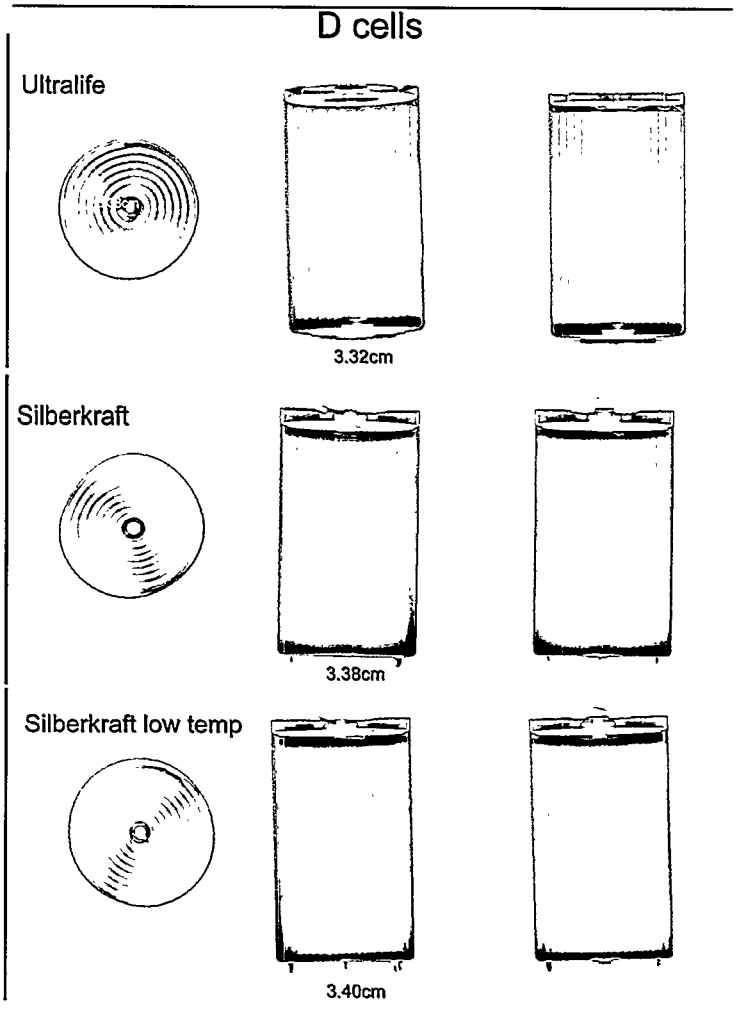

Figure 7-4. Radiographs of Ultralife and Silberkraft D cells.

The cells were also dissected and examined, and photographs of the D-cell components are shown in Figure 7-5. As can be seen, while the internal characteristics of both Silberkraft cells are basically the same, there is a significant difference between the details of these and the Ultralife cells. The differences are manifest in the number and types of separators used as well as the type of current collectors. The Silberkraft cells use a single 1-mil porous polymer separator, but the Ultralife cells have a fibrous mat against the oxide in addition to a porous polymer separator. In addition, a copper foil approximately one-half the width of the lithium metal is used as a current collector in the Ultralife cell, but the Silberkraft cells use a foil that is the full width of the lithium metal and that has holes in the center.

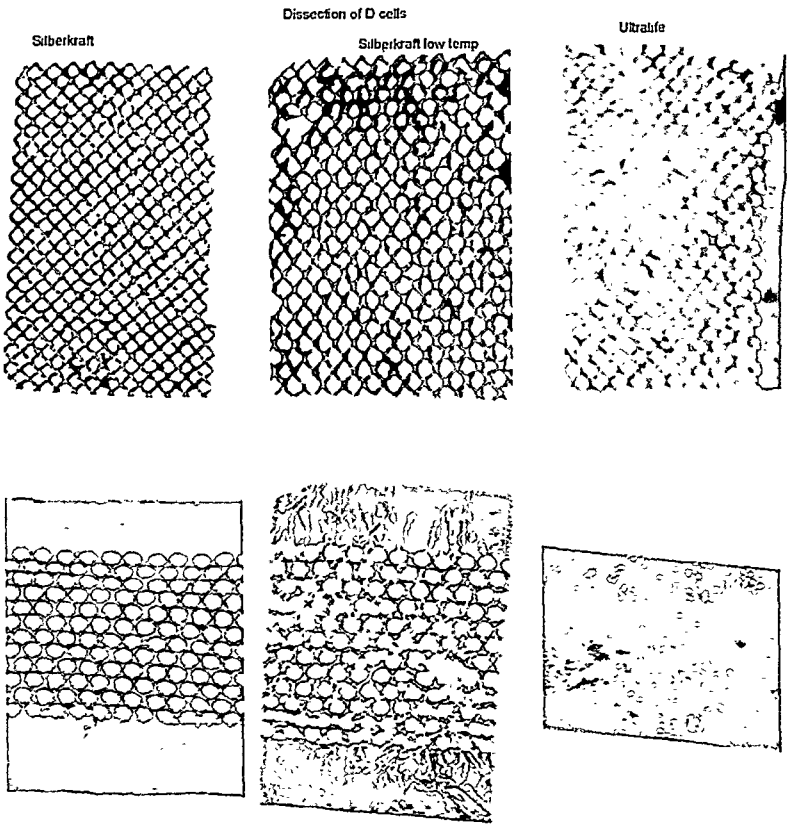

Figure 7-5. Images of some of the Ultralife and Silberkraft D-cell elements. Only the fibrous separator found in the Ultralife cell is shown.

7.4 Supporting Electrolyte System

7.4.1 Introduction

The supporting electrolyte solution significantly affects how the cells perform under a variety of conditions. For this reason, we began a study aimed at elucidation of the species present. As a first step, we extracted data contained on the material data safety sheets (MSDS) that were obtained from the vendors, and these data are summarized in Table 7-2. As shown, a variety of solvents are used in the cells.

Table 7-2. MSDS Solvent Information

Cell Type and Vendor	Solvent					
	Propylene Carbonate	1,2-Dimethoxyethane	Tetrahydrofuran	1,3-Dioxolane	Ethylene Carbonate	Butylene Carbonate
2/3A cells						
Duracell	0.25 g	1.2 g	-	-	0.25 g	-
Kodak	1-5%/w	1-5%/w	-	-	1-5%/w	1-5%/w
Sanyo Cylindrical (crimp) type	-	+	-	-	+	+
Varta	7.2%/w	5.1%/w	-	-	-	-
Eveready	0-8%/w	0-6%/w	-	0-8%/w	-	-
Rayovac	2-6%	-	-	-	-	-
Ultralife	Not Available					
C Cells						
Silberkraft M52	+	+	+	-	-	-
D Cells						
Silberkraft M20	+	+	+	-	-	-
Ultralife U3360H	+	+	+	-	-	-

\+ Identified on the MSDS but amounts not given.
\- Not identified on the MSDS as being present.
Note: The MSDS s not available for Sony, Panasonic, or Silberkraft M20TT.

As an example, the MSDS for the Eveready 2/3A cell states that 1,2-dimethoxyethane, 1,3-dioxolane, and propylene carbonate (Figure 7-6) are present in this battery at levels of 0 to 6% by weight for 1,2-dimethoxyethane, and 0 to 8% by weight for the other organic species. However, because the MSDS provides only general information regarding the makeup of the solution in the cell, we developed a method for characterizing the cells and have performed an initial analysis of one of the cells, in this case a fully charged Eveready 2/3A cell.

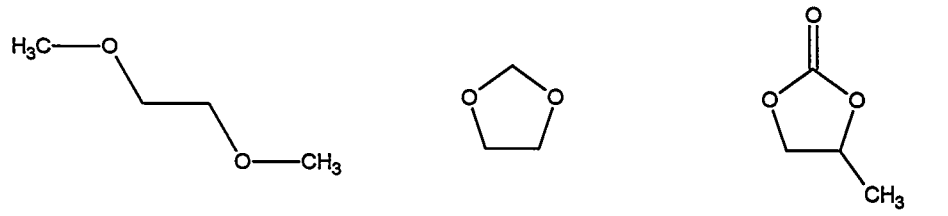

1,2-dimethoxyethane 1,3-dioxolane Propylene carbonate

Figure 7-6. Structure of solvent species identified by the MSDS as being present in the Eveready 2/3A cell.

The internal cell atmosphere was sampled using the fixture shown in Figure 7-7. The fixture was assembled without the cell, evacuated, and back-filled with helium. It was then leak-tested at vacuum and at elevated pressure. After satisfactorily passing these leak checks, the fixture atmosphere was examined by gas chromatography/mass spectrometry (GC/MS) to determine the organic background. No organics were observed. The fixture with the cell was then evacuated, the gas-tight valve closed, and the puncture bit was driven through the cell casing. The bit was withdrawn from the casing allowing the cell atmosphere to fill the fixture. Gas samples were obtained by connecting the fixture by VCR fittings to the analytical equipment.

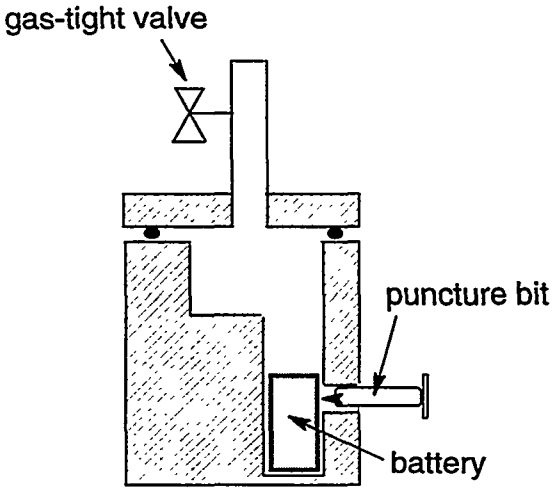

Figure 7-7. Cell puncturing/gas sampling fixture.

7.4.2 Inorganic Gas Analysis

The cell atmosphere was analyzed by gas chromatography to determine the concentrations of inorganic gases using the method shown in Table 7-3.

Table 7-3. Summary of Analytical Conditions for Analysis of Inorganic Gas Analysis

INSTRUMENTATION: Hewlett-Packard 5890 Series II gas chromatograph Detection – thermal conductivity				
GC Column: 5A mole sieve packed column, 6ft × 1/8" Hayesep DB packed column, 6ft × 1/18"				
Gas Sample Loop Volume:	250 µL	Valve Temp:	105°C	
Temperatures	Oven: Isothermal, 80°C for 2.6 min		Injector 150°C	TCD 120°C
Carrier Gas	Helium at 30 mL/min constant flow for 5A mole sieve 45 mL/min constant flow for Hayesep DB			

Standards used were: 1% H_2, CH_4, CO, N_2, O_2, Ar, and CO_2 in helium. The data are reduced on an Excel spreadsheet. The results are summarized in Table 7-4. A separate hydrogen (H_2) analysis was also performed and was found to be present at a relative concentration of 0.2%.

Table 7-4. Summary of Inorganic Gases Found in the Eveready EL123A Cell

Compound	Relative Concentration
O_2/Ar	41.29%
N_2	3.73%
CO	1.09%
CH_4	<0.1%
CO_2	<0.1%

7.4.3 Organic Gas Analysis

Organic gas analysis was performed using the conditions summarized in Table 7-5.

Table 7-5. Analysis Conditions for Organic Gas Analysis

INSTRUMENTATION: Hewlett-Packard 5890 Series II gas chromatograph, flame ionization detection "Full Volatile Organic Carbon" method			
GC Column: DB-1 60 m × 0.53 mm × 1.5 µm df			
Gas Sample Loop Volume: 250 µL	Valve Temp: 195°C		
Temperatures	Oven: 35°C for 7 min, 20°C/min to 225°C, *225°C for 2 min*	Injector 250°C	FID 250°C
Carrier Gas	Helium at 6 mL/min		

The standards used in the organic analysis were: 10 and 100 ppm methane, ethane, propane, n-butane, n-pentane in N2; 1000 ppm ethylene, propylene, 1-butene, and 1-pentene in helium. (The amount of 1 butene in this standard is suspect; it is used for retention time matching only.) A 56-component ozone precursor standard and neat methanol and dimethyl ether samples were analyzed for retention time matching. The data were reduced on an Excel spreadsheet and the results are shown in Table 7-6. The major organic species present is propylene.

Table 7-6. Summary of Organic Gases Found

Compound	Relative Concentration
Methane	3862.2
Ethane	58.5
Propane	<10
n-Butane	44.6
n-Pentane	<10
Ethylene	594.8
Propylene	125113.4 or 12.5%
1-Butene	<100
1-Pentene	<100
1-Hexene	<100

An organic species detected but not quantified was dimethoxyethane. An example of a gas chromatogram for the cell atmosphere is shown in Figure 7-8.

GC/MS using electron mode was also performed on the sample in order to more fully characterize the species present. The conditions used for some of these analyses are shown in Table 7-7.

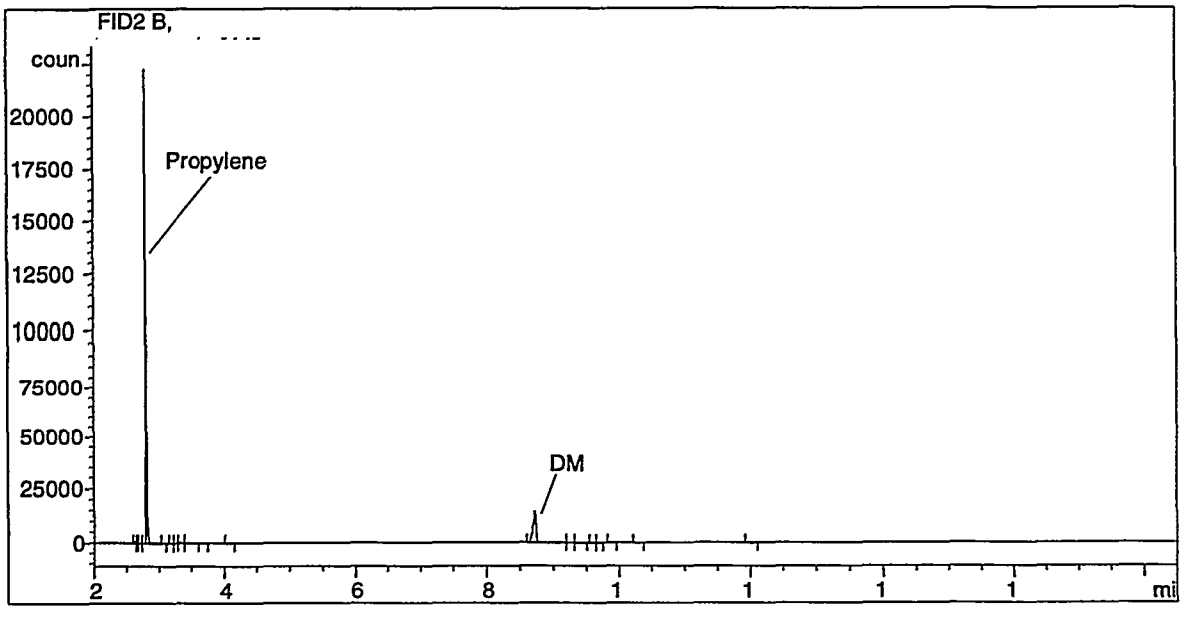

Figure 7-8. GC/Flame Ionization Detectors (FID) of Cell Atmosphere.

Table 7-7. Gas Chromatography/Mass Spectrometry Analytical Conditions

INSTRUMENTATION: Entech Cryofocusing Inlet System/Finnigan Magnum GC/MS

Entech Method: "Default.mpt"

GC Column: J&W DB-624, 60m x 0.25mm, 1.4µm film

GC Parameters: Method Name: "ozo1"

Oven Init.	1st oven Ramp	1st hold	2nd Oven Ramp	Final Hold	Injector
35°C for 10 min	7°C/min	200°C for 5 min	20°C/min	250°C for 3 min	110°C

Carrier Gas: Helium at 19.5 psi, ~1.3 mL/min

MS Parameters: scan mode–full scan; mass range–33 to 380, manifold temp–220°C; transfer line temp–250°C; filament delay–1.0 min; mass defect–100mmu/100 amu; scan–1.0 sec/scan

A 1-mL gas aliquot was used for the analysis, and it greatly overwhelmed the GC/MS. The saturated total ion chromatogram (TIC) is shown in Figure 7-9. The small peak at 7:12 in this chromatogram is n-butane. The other peaks in this system were too saturated to determine the mass fragmentation pattern. The system was then run repeatedly to reduce the amount of sample present to produce unsaturated mass spectra. The reduced-sample total ion count chromatogram is shown in Figure 7-10. The mass spectrum of the species at 20:20 is consistent with dimethoxyethane and is shown in Figure 7-11.

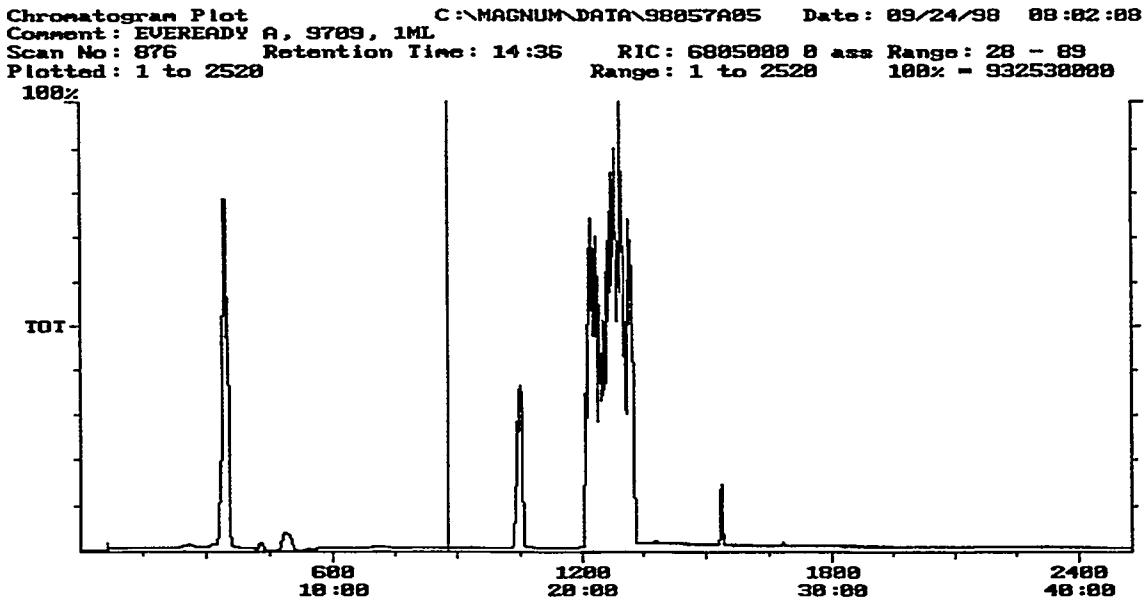

Figure 7-9. Saturated GC/MS TIC of cell atmosphere.

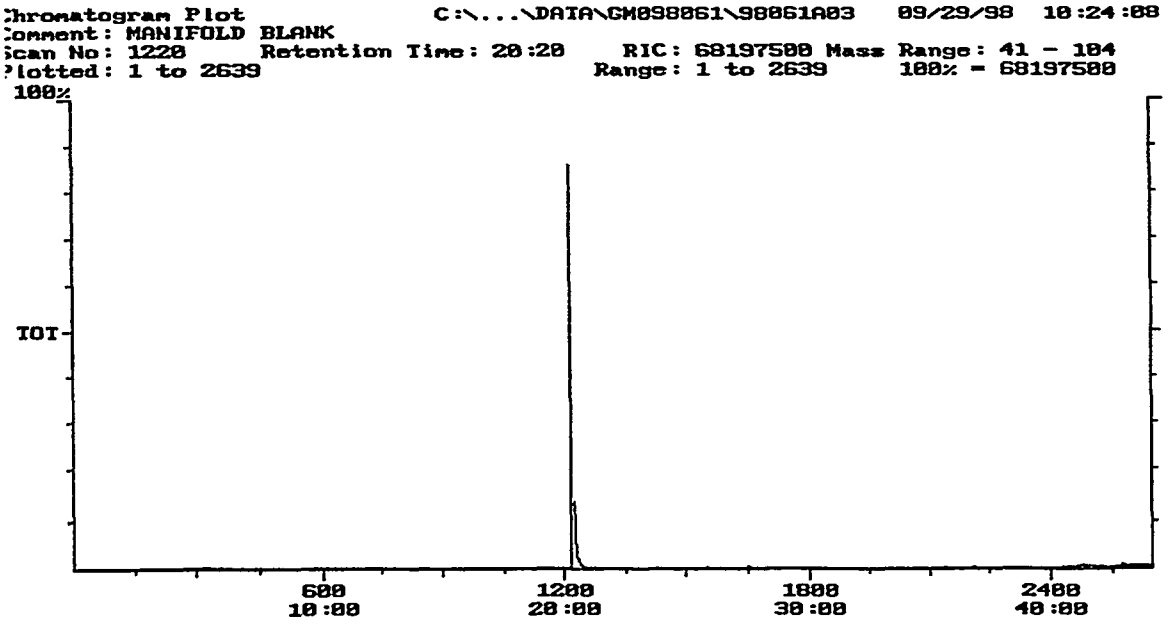

Figure 7-10. Reduced-count GC/MS TIC of cell atmosphere.

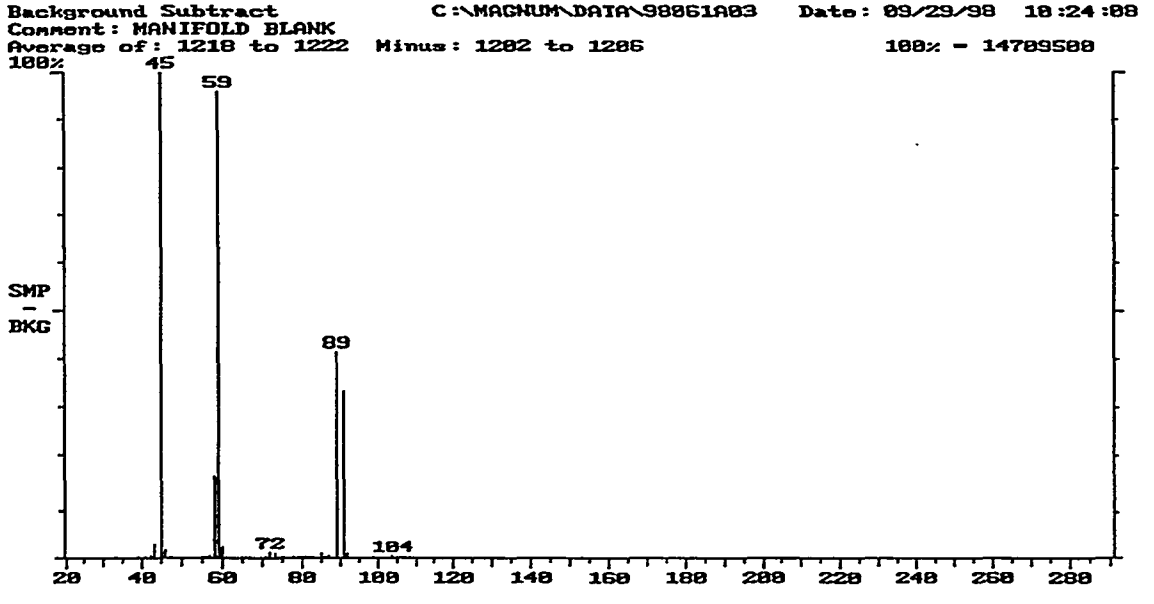

Figure 7-11. Background-subtracted mass spectrum of species at 20:20 consistent with DME.

7.4.4 Conclusion

These data clearly show that the MSDS is a good starting point for information regarding the identity of species present in a cell; however, based on the analytical results, it is evident that a number of other species can also be expected to exist in these cells. This is not particularly surprising because it is generally well recognized that these solvents will react with lithium metal. Nevertheless, full and complete characterization of the cells would provide useful information for understanding performance characteristics.

7.5 Manganese Dioxide Characteristics

7.5.1 Introduction

Because the type of manganese dioxide used will significantly impact cell performance, the dioxide was characterized in two ways. In the first method, the gross morphological characteristics were examined using scanning electron microscopy (SEM). In the second method, the material was analyzed using x-ray diffraction (XRD), both before and after discharge.

7.5.2 X-ray Diffraction

The contents from two different types of 2/3A cells were analyzed, namely Sanyo and Duracell. In addition, the analysis was performed on a fresh, fully charged cell and a discharged cell. The samples for analysis were obtained by first freezing the cells in liquid nitrogen and then opening the cells in a controlled environment. The electrode stack was unrolled and portions of the oxide were removed. The electrode was then rinsed multiple times, first with acetone and then with methanol in order to remove residual solvent and salt. The electrode was then dried under vacuum at elevated temperature before analysis.

Based on the diffraction results, the crystallite size is estimated to be approximately 130 Å in the Sanyo materials and 100 Å in the Duracell. In general, the diffraction data reveals similar behavior for both cells with respect to expansion of the manganese dioxide lattice upon discharge. This is reflected in the shift in the diffraction peaks to lower values of 2-theta values upon discharge, as seen in Figures 7-12 and 7-13. Note that there is a fairly broad peak at about 28 degrees in both patterns that may shift in the Sanyo cell to about 18 degrees upon discharge but seems to disappear in the Duracell material.

Based on the diffraction pattern, it appears that the Duracell cell contains crystalline carbon (graphite) as opposed to an amorphous carbon material, which is apparently used in the Sanyo cell. An unambiguous phase identification (ID) of the materials was not made. Some peaks in the diffraction patterns did match a MnO_2 but not all of them, and it looks like all the peaks in this phase shift so are probably all part of the expanding lattice. In the respective figures, this is indicated by arrows. Also, based on the diffraction pattern, the current collector appears to be stainless steel.

7.5.3 Scanning Electron Microscopy

The gross morphological features of the oxides obtained from discharged Silberkraft and Ultralife D cells and charged Duracell 2/3A cells were examined using SEM. The cells were opened in a controlled environment, and samples of the oxide removed. The samples were thoroughly rinsed, first with acetone and then with methanol, in order to remove residual solvent and salt. The samples were then dried in a vacuum oven at elevated temperature. Photomicrographs of these images are shown in Figures 7-14 through 7-19. These photo micrograms show that there are morphological differences between Ultralife and Silberkraft cells.

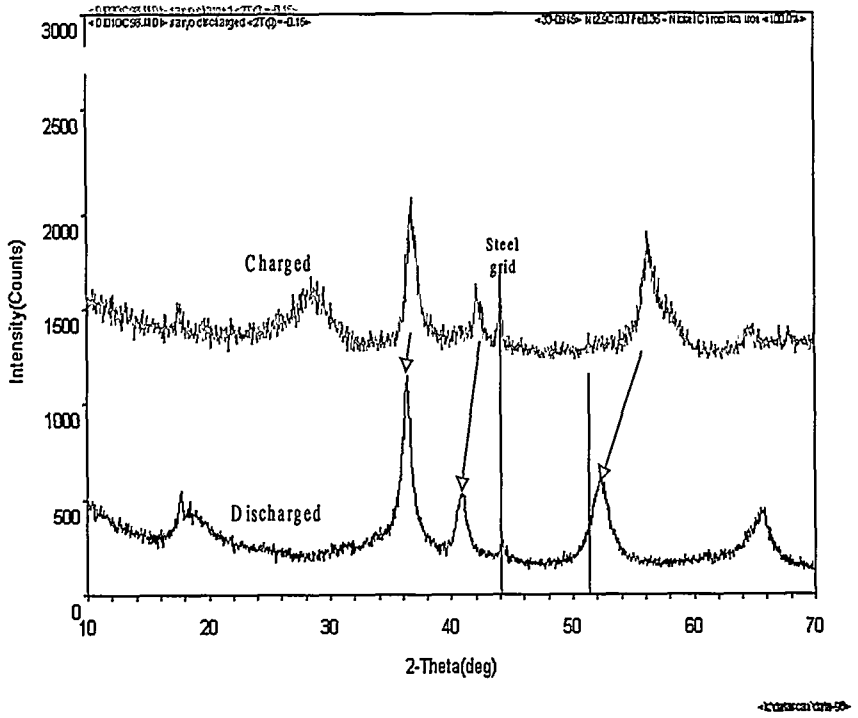

Figure 7-12. **X-ray diffraction pattern of manganese dioxide obtained from the Sanyo cell both before and after discharge. XRD shows shifting to lower 2θ (expanding lattice) when the cell is discharged. Estimated crystallite size based on 42° 2θ peak is ~130Å.**

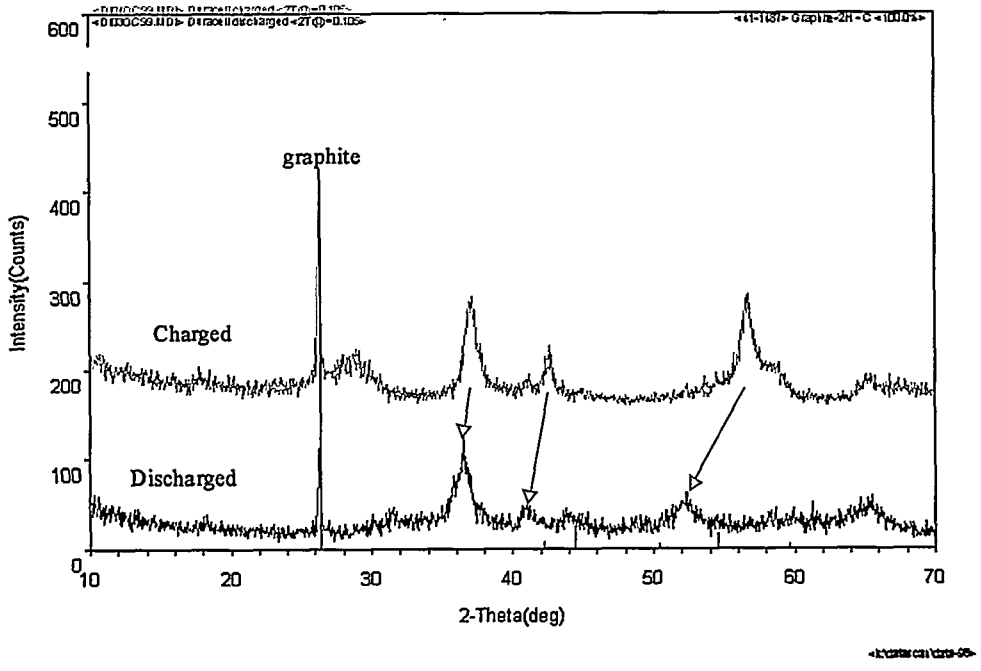

Figure 7-13. **X-ray diffraction pattern of manganese dioxide obtained from the Duracell cell both before and after discharge. XRD shows shifting to lower 2θ (expanding lattice) when the cell is discharged. Estimated crystallite size based on 37° 2θ peak ~100 Å.**

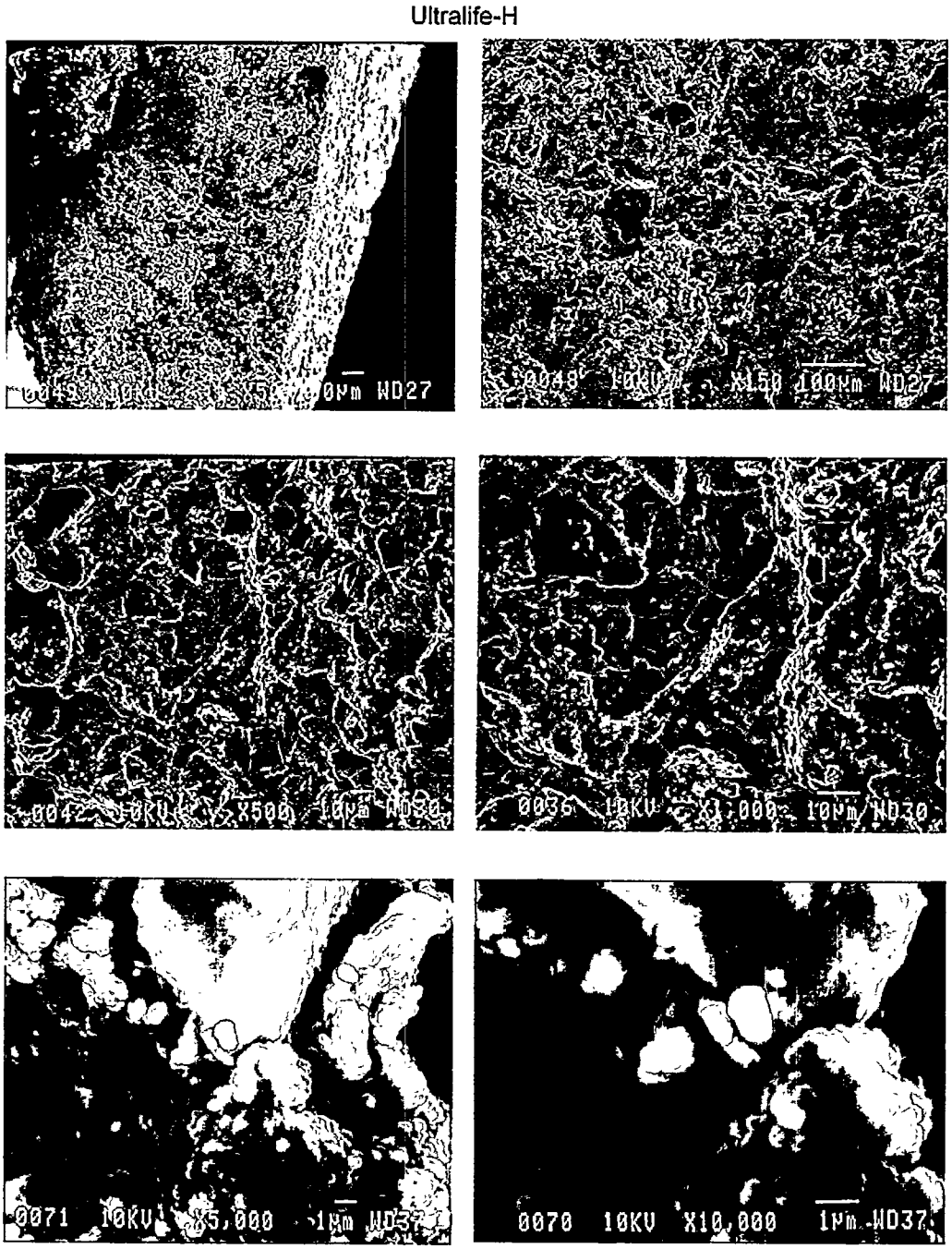

Figure 7-14. Scanning electron photomicrographs of oxide recovered from a discharged Ultralife D cell, type 3360H.

Ultralife-VH

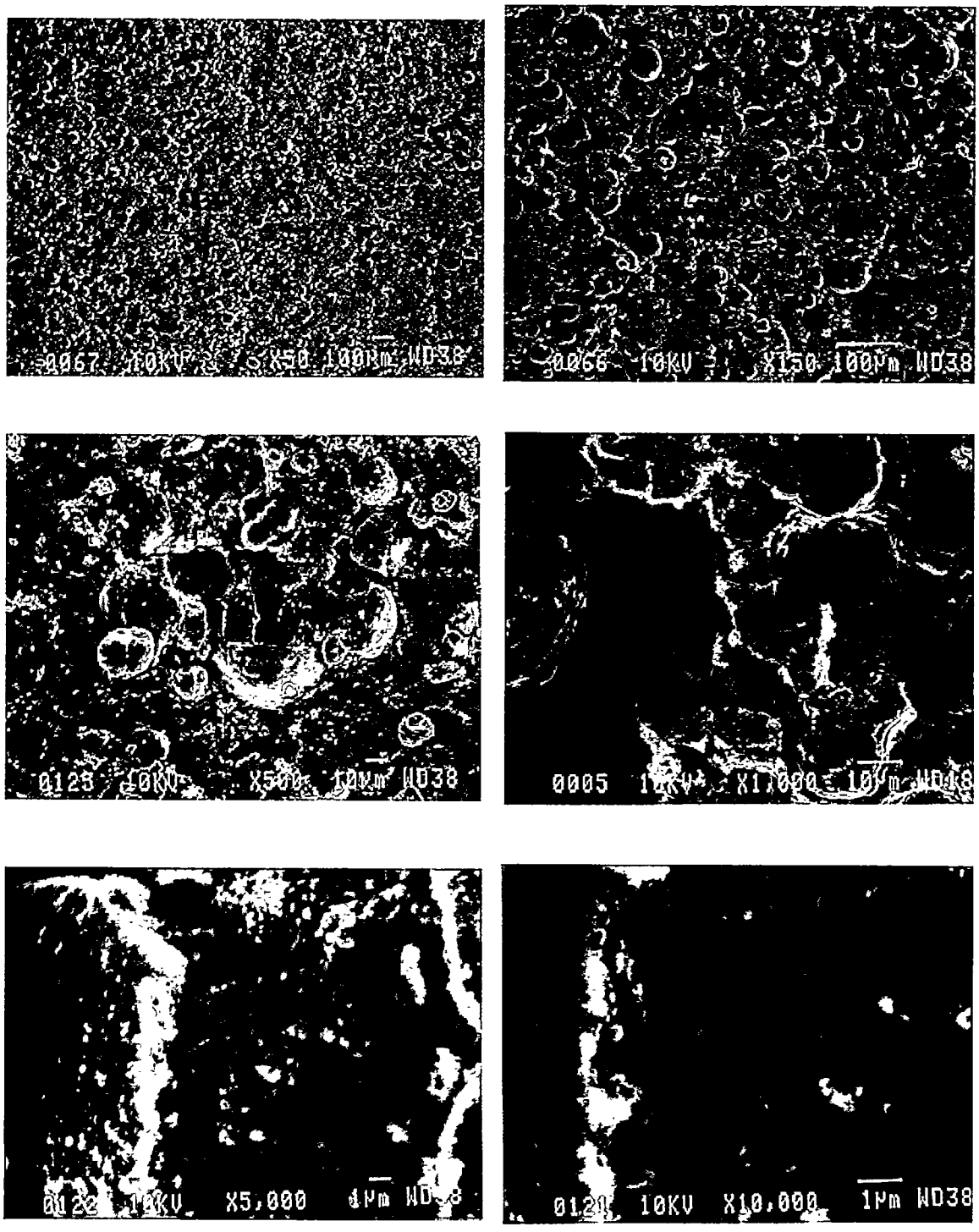

Figure 7-15. Scanning electron photomicrographs of oxide recovered from a discharged Ultralife D cell, type 3360VH.

Silberkraft

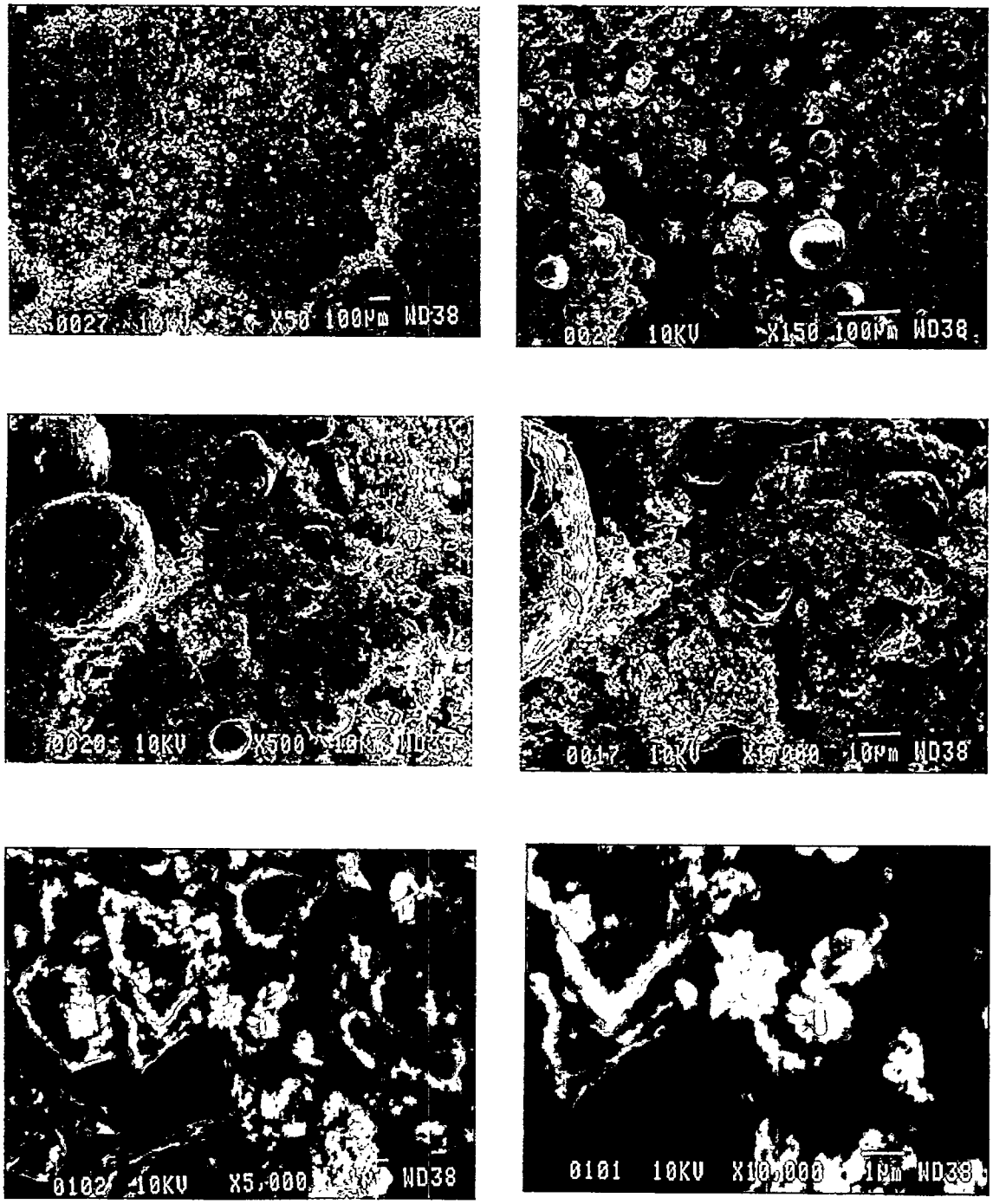

Figure 7-16. Scanning electron photomicrographs of oxide recovered from a discharged Silberkraft D cell, type M20.

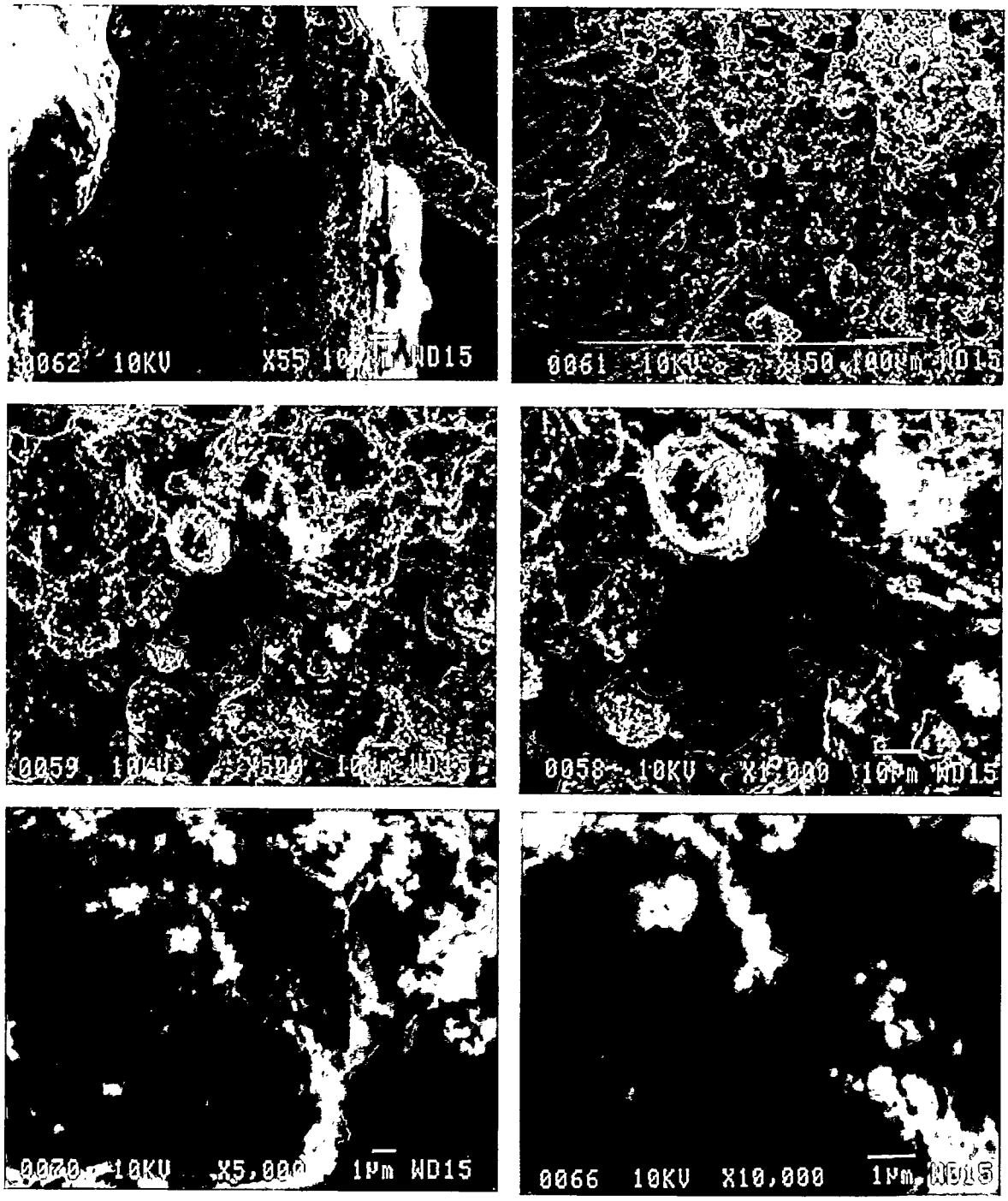

Figure 7-17. **Scanning electron photomicrographs of oxide recovered from a discharged Silberkraft D cell, type M20TT.**

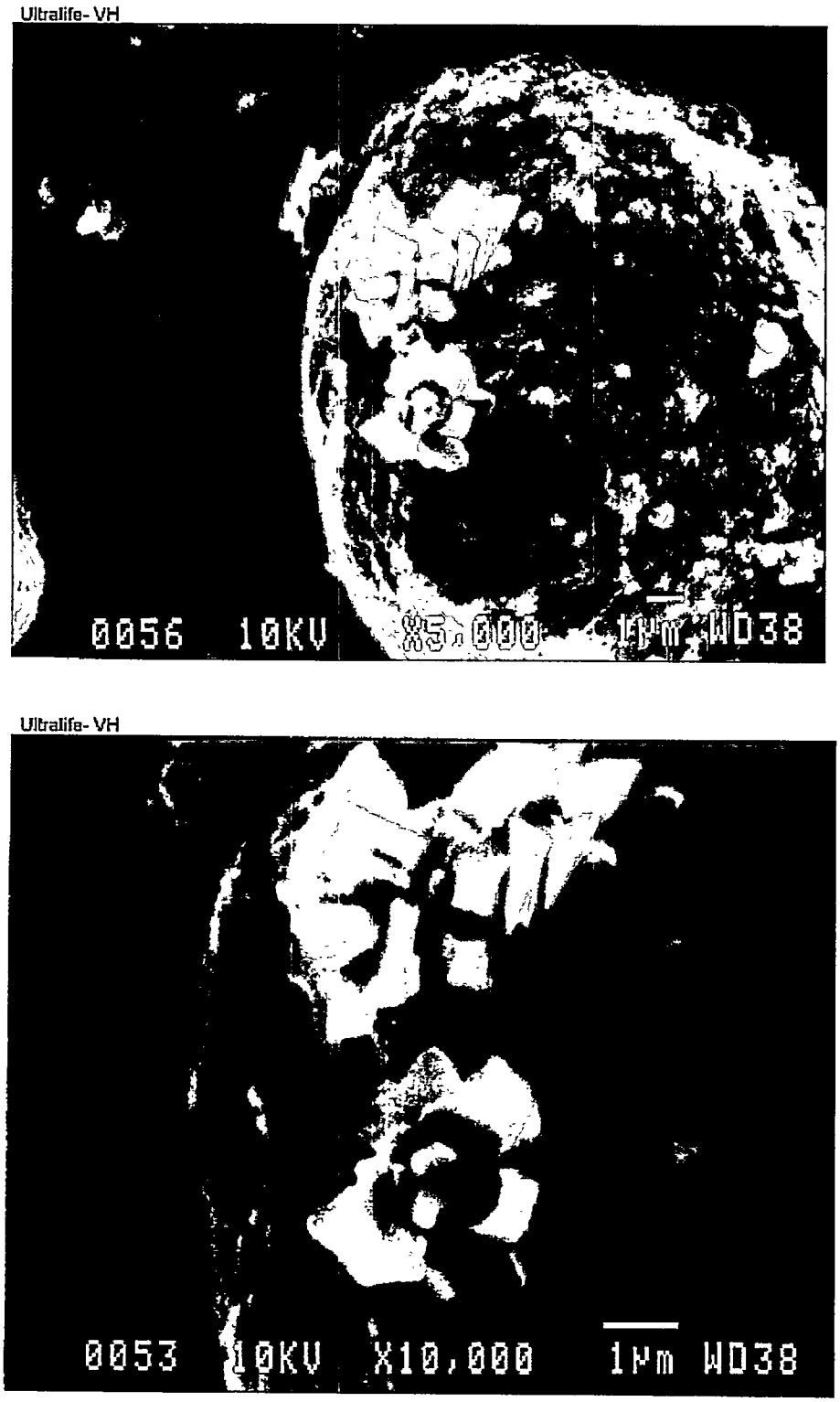

Figure 7-18. **Scanning electron photomicrographs of oxide recovered from a discharged Ultralife D cell, type 3360VH showing unique features observed in this cell.**

2/3 A charged

Sanyo

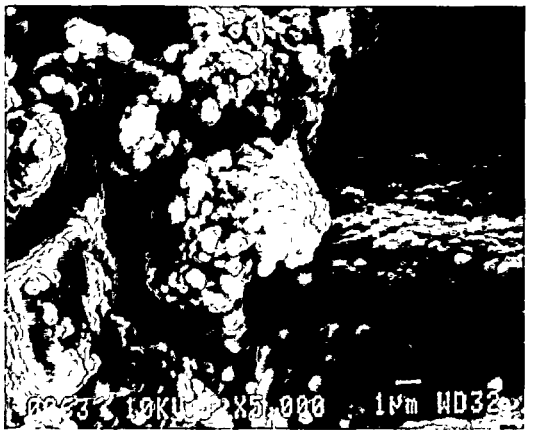

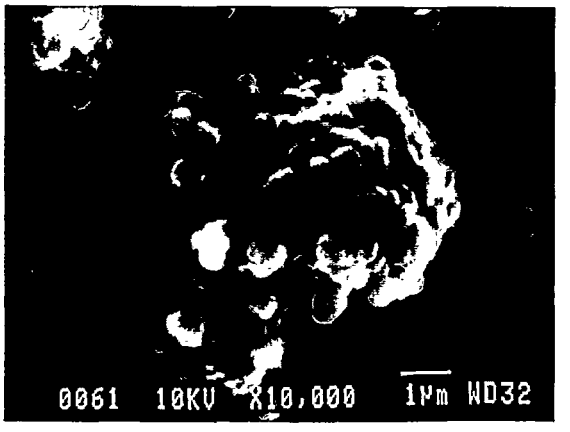

Duracell

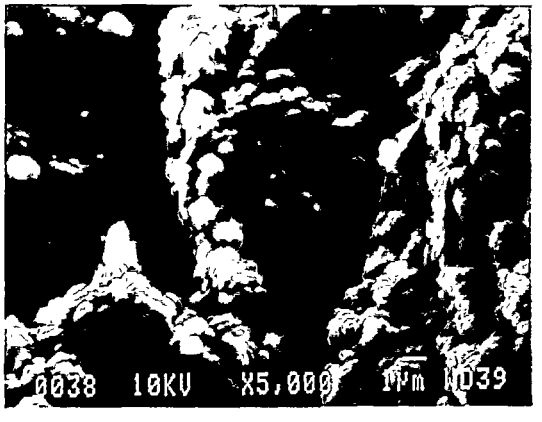

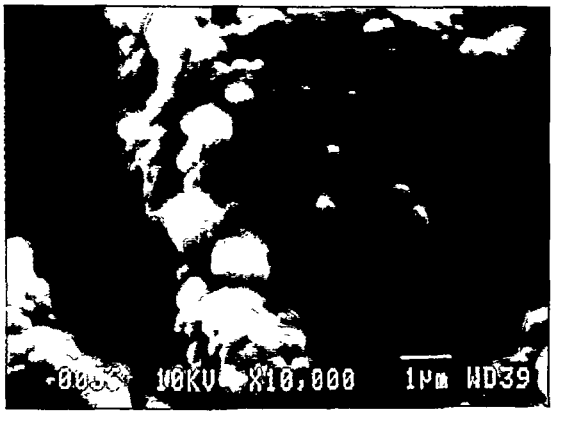

Figure 7-19. Scanning electron photomicrographs of oxide recovered from charged Duracell and Sanyo 2/3A cells.

7.6 Conclusion

As shown, the characterizations provided useful information regarding reliability and performance. It is also clear that these characterization techniques provide valuable information regarding the nature of the species, which make up the active materials in the cells. Based on the limited amount of work performed, it is evident that there are differences in the materials used in these cells. These differences could account for at least some of the performance differences observed in each of the cell types. It is also clear that in order to make unambiguous statements about the cell structural-activity and the relationships, these engineering studies should be completed for all of the cells.

Intentionally Left Blank

8. Testing and Test Protocols

David Ingersoll and Jill L. Langendorf

8.1 Constant Load, Constant Current, Resistive Test Protocols

Much of the data presented in this document were collected using a Maccor Battery Tester, which operates by continuously measuring and controlling the current to the cell to maintain the desired level of the test parameter. For a constant current charge or discharge (a relatively straightforward process) the tester maintains the requisite current at the desired level. For a constant load discharge, the tester measures both the current and voltage and then performs a calculation using Ohm's law to determine the applied load. The current is then adjusted, and the process repeated until the load, as determined by using Ohm's law, achieves the desired level. Similarly, in a constant voltage charge or discharge, the tester maintains the desired voltage level by adjusting the applied current.

Although this approach to battery and cell testing is standard throughout the industry, there is a dissenting view that performance in the application cannot be inferred from these data if the application requires resistive rather than current loads. It is also felt that the preferred approach to testing batteries is to discharge the battery through a purely resistive load, that is, a resistor, or under the actual use profile. Granted, the preferred approach would be to test the cells under the intended application profile; unfortunately, this is not always possible because of resource constraints. Nevertheless, the need for an understanding of the performance remains. The question remains then: how can this dissenting view be reconciled with the limitations of the currently available test hardware and the need to provide performance information?

As a first step in evaluating this view, consider the cell chemistry being evaluated within the context of what is being measured and controlled. For example, it is well recognized that lithium/thionyl chloride cells, the equivalent series resistance of the cell increases significantly during the course of discharge, generally by orders of magnitude. Furthermore, depending on the age of the cell, how it was stored, the test conditions employed, and myriad other factors and combinations of factors, lithium/thionyl chloride cells can exhibit variable cell impedance that can reach values on the order of kΩ or MΩ. Because the battery is in the circuit, its equivalent series resistance must be included as a part of the overall load, over and above that required for the application. Consequently, irrespective of the application requirements, it is clear that the circuit load will be variable and can also be considerable during the discharge of the lithium/thionyl chloride battery. If this is not recognized, quantified, and considered during cell and data evaluation, or *a priori* during the initial design of the test (if this is possible), the interpretation of the results can be misleading.

For lithium/manganese dioxide cells, the equivalent series resistance of the cell changes only slightly if at all during the discharge. Although the equivalent series resistance of the cell can be higher at the start of the discharge because of the formation of a film on the surface of the negative electrode (superficially similar to the lithium/thionyl chloride case), its magnitude is relatively small because of the limited extent of growth of the layer itself. Furthermore, although the equivalent series resistance of the cell is a function of other factors, such as temperature and discharge rates, the equivalent series resistance is relatively well behaved for this chemistry. Therefore, if the equivalent series resistance of the lithium manganese dioxide cell has been adequately characterized and if there is an understanding of the chemical and electrochemical processes, the test method, and the parameter changes, the results can be

reasonably interpreted, and assumptions can be made regarding expected battery behavior in the application. Another possibility is to run the appropriate comparative tests to elucidate how the various approaches affect the results. Both issues are addressed in this chapter.

For these studies, both 2/3A and D cells were used. For the 2/3A cells, a series circuit configuration consisting of a switch, two 2 Ω (nominal) resistors, and a single 2/3A Duracell cell were used. The terminal battery voltage and the voltage across one of the resistors were monitored as the switch was opened and closed periodically to simulate a pulse load. The resistor was thereby used as a current viewing resistor from which the circuit current could then be determined. In the case of the D-cell circuit, the 2 Ω resistors were replaced by resistors having nominal values of 0.281 Ω. For the 2/3A and D cell circuits, the current passing during switch closure was approximately 650 mA and 5 A, respectively. In both cases the switch was repetitively cycled for 17-sec open (circuit off) followed by 3-sec closed (circuit on), simulating a pulsed load condition for the cell.

The voltage profile across the 2/3A cell during discharge is shown in Figure 8-1. The details of the pulse are obscured by the scale used in the plot in combination with the duty cycle of the pulse. Also, a solid envelope is not observed because the data sampling rate. Nevertheless, the cell voltage during both the on and off states of the circuit corresponding to the loaded and resting cell is easily seen. As expected, the cell voltage decreases with time during the discharge, and this can be monitored throughout the discharge.

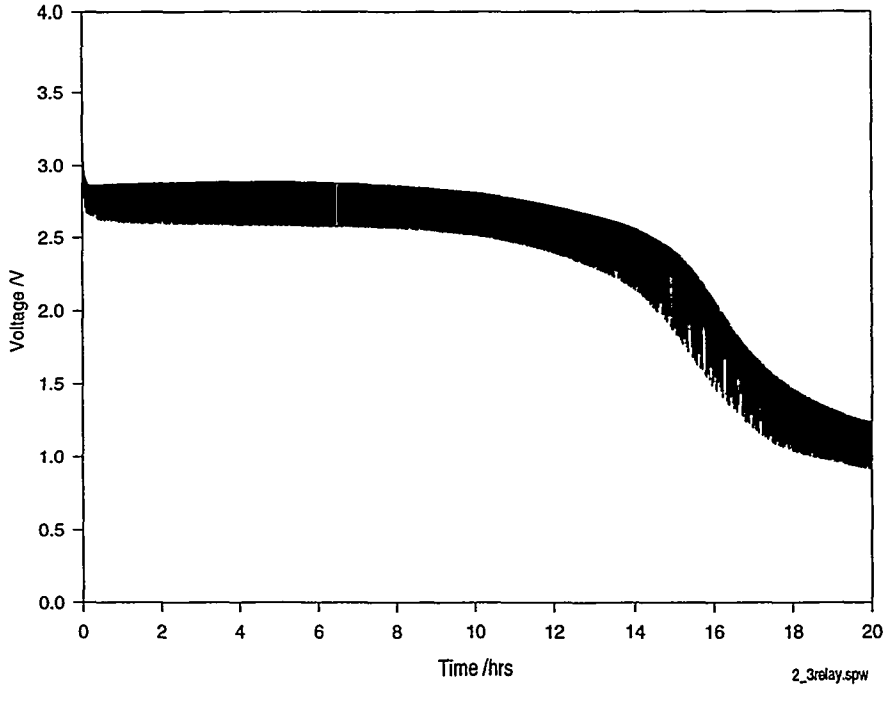

Figure 8-1. Cell voltage of a Duracell 2/3A cell when repetitively pulsed through a 4.115 Ω load resistor for 3 sec followed by standing at open circuit for 17 sec. The discharge was performed at room temperature using a relay.

A similar test profile was run on a fresh 2/3A cell using a constant load profile controlled completely by the battery tester. In this case, Ohm's law and the battery voltage are used to control the magnitude of the current applied to the cell. For this test, a load of 4.115 Ω was the set value. This value is equivalent to the sum of the resistance of the two resistors used in the earlier circuit. (The equivalent series resistance of the cell itself, which is approximately 0.5 Ω, was not included in the 4.115 Ω value. This fact will become important later in understanding the data.) The data shown in Figure 8-2, which is plotted on the same scale as that used for Figure 8-1, shows the battery voltage observed in this case. In comparing these two data sets, it can be seen that they essentially overlay one another.

Figures 8-3 and 8-4 show the current flowing through the circuit during discharge using both the relay circuit and the battery tester constant resistance procedures. Cursory examination of these data show that the current flowing through the circuit is relatively stable during the initial portion of the discharge and is about 620 mA. Later in the discharge, the current decreases significantly. This is because the cell voltage decreases as a result of consumption of the active materials in the battery. During this consumption process, the cell voltage drops as dictated by Nernst's equation and the current must necessarily decrease to maintain the constant load.

Close examination and comparison of the data contained in these two plots reveals a slight difference in the current flowing through the two circuits because when the relay circuit is used, the equivalent series resistance of the cell itself was not included in the applied load. Consequently, the load applied in these two tests is different, and this difference is equal to the value of the equivalent series resistance of the 2/3A cell itself. The total circuit resistance of the tester-controlled circuit is fixed at 4.115 Ω, but for circuit, the total circuit resistance is given by the sum of 4.115 Ω (the fixed resistors) plus the resistance contributed by the cell (~0.5 Ω).

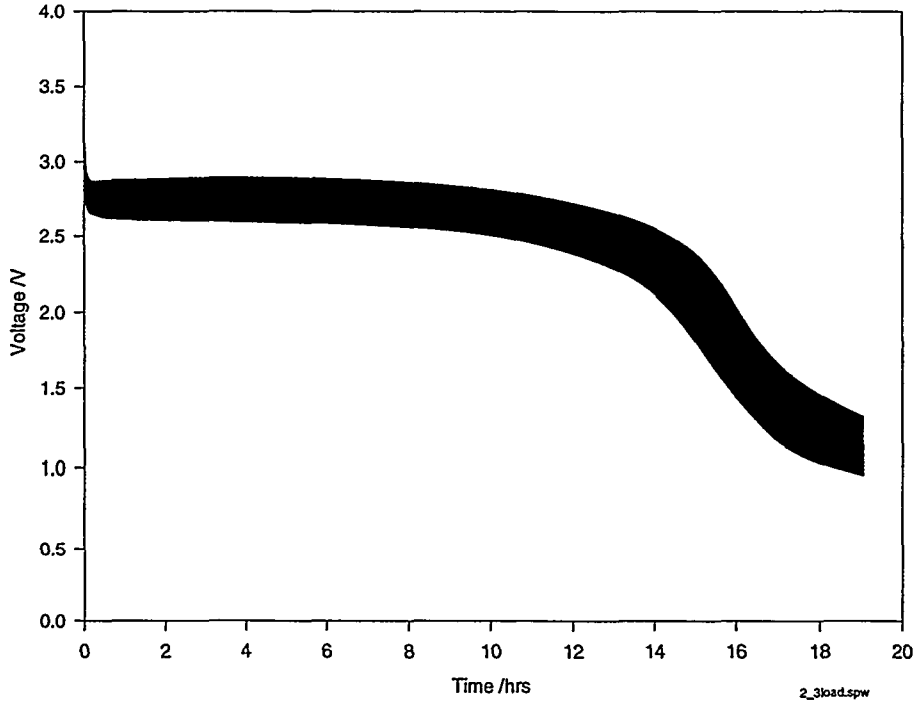

Figure 8-2. Cell voltage of a Duracell 2/3A cell under pulsed load discharge controlled by the battery tester employing Ohm's law. The load values were 4.115 Ω for 3 sec followed by an open circuit stand for 17 sec. The discharge was performed at room temperature.

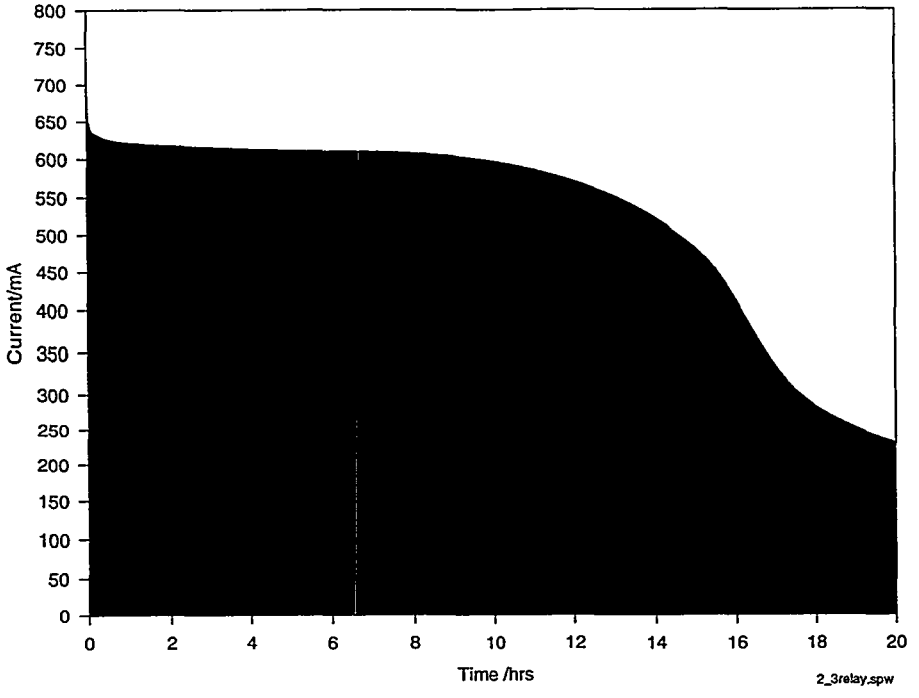

Figure 8-3. **Cell current of the Duracell 2/3A cell shown in Figure 8-1 when repetitively pulsed through a 4.115 Ω load resistor for 3 sec followed by standing at open circuit for 17 sec. The discharge was performed at room temperature using a relay.**

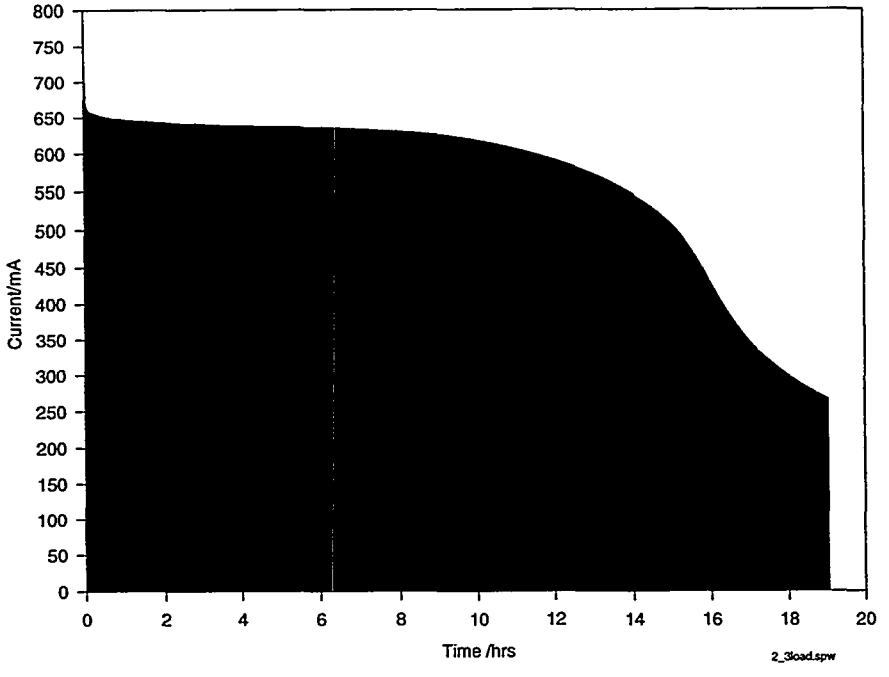

Figure 8-4. **Cell current of the Duracell 2/3A cell shown in Figure 8-2 under pulsed load discharge controlled by the battery tester employing Ohm's law. The load values were 4.115 Ω for 3 sec followed by an open circuit stand for 17 sec. The discharge was performed at room temperature.**

Finally, we also discharged the cell under conditions of constant current using a 620 mA pulse, which is comparable in magnitude to that flowing through the circuits just described during the initial portion of the discharge. These data provide a basis of comparison between the other two types of discharge protocols. The terminal voltage of the cell during the course of the discharge is shown in Figure 8-5. In this case, the tester will attempt to draw the requisite current from the cell regardless of anything else that happens to the cell or circuit. Upon comparison with the previous data shown, it is evident that the cell behavior under this test protocol is similar to that seen previously, especially during the early portion of the discharge when the cell voltage is relatively constant and Ohm's law can be satisfied by maintaining a relatively constant current. At the end of discharge, a larger discrepancy between the results is observed, which is easily understandable because in the case of the constant current test, the circuitry will continue to draw the requisite current, regardless of what happens in the circuit. In contrast, for a constant load or purely resistive load, the current will decrease to satisfy Ohm's law. Consequently, in the constant current case, the cell voltage is expected to decrease more rapidly during the later stages of discharge compared to the constant load and resistive load profiles. This is readily seen by comparing the data shown in Figures 8-1, 8-3, and 8-5. Therefore, the constant current test protocol provides the harshest set of conditions under which to test the cell.

As mentioned, similar data were collected using a Silberkraft D cell, and these data are shown in Figures 8-6 through 8-10. Again there is close comparison between these data, and the differences observed are easily understood in terms of the test protocol used and what is occurring in the cell. The value of the resistance used in the pulsed load profile controlled by the tester is set to 0.563 Ω. This value is equal to the fixed resistor used in the relay circuit. Therefore, the total resistance in the relay circuit is higher by an amount equal to the value of the resistance of the cell (approximately 0.5 Ω). Consequently, the currents flowing through the relay should be somewhat smaller, the voltage drops less, and the run time somewhat longer than for the circuit controlled entirely by the battery tester at the smaller load. All these features are observed experimentally, as seen in the figures.

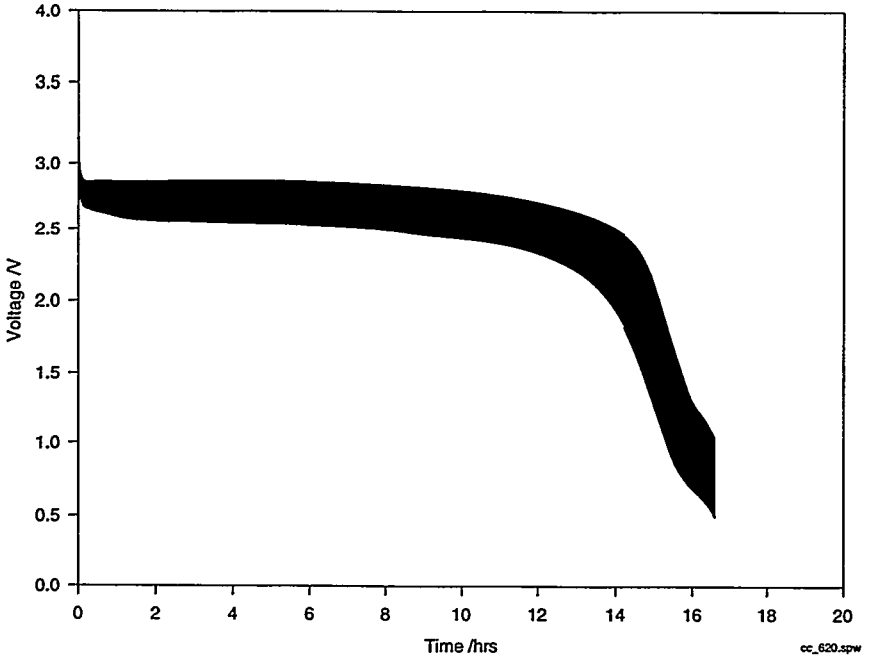

Figure 8-5. Terminal voltage of 2/3A Duracell cell under pulsed current discharge controlled by the battery tester. The pulse profile consisted of 3 sec at 620 mA followed by 17 sec at open circuit. The discharge was performed at room temperature.

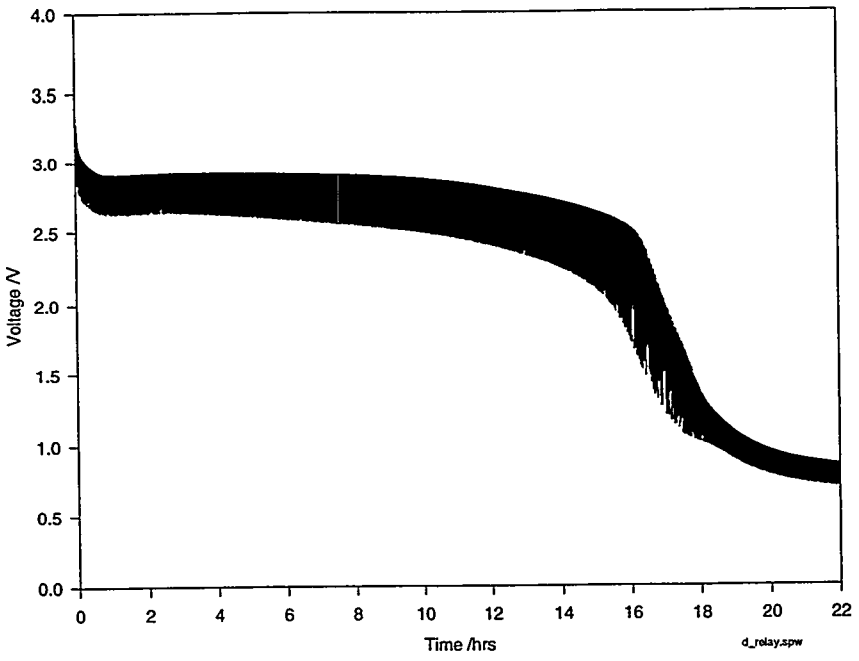

Figure 8-6. **Cell voltage of a Silberkraft D cell under pulsed load through a 0.563 Ω resistor using a relay. The pulse profile consisted of 3 sec under load followed by 17 sec at open circuit. The discharge was performed at room temperature.**

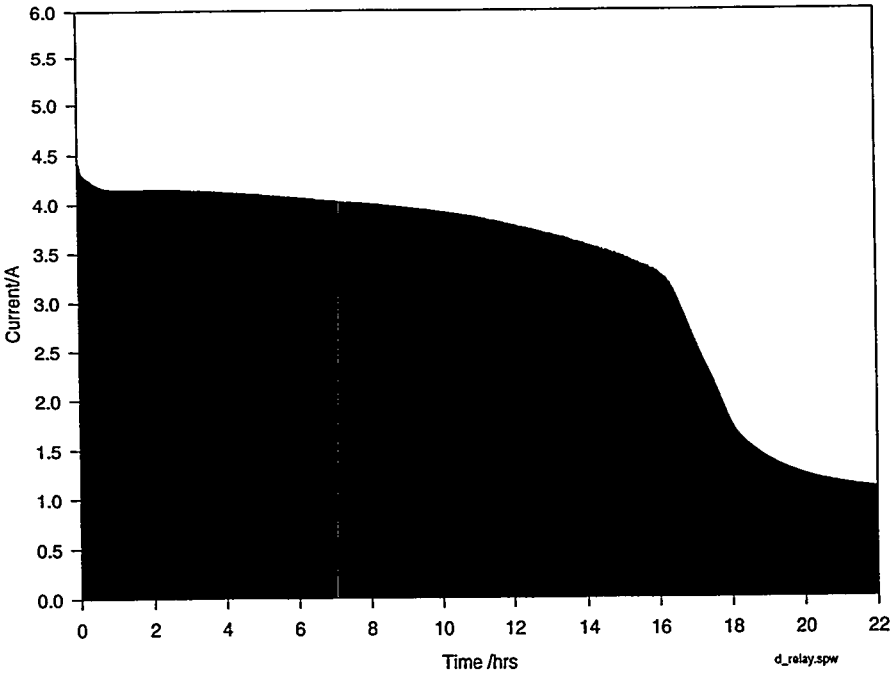

Figure 8-7. **Cell current of the Silberkraft D cell shown in Figure 8-6 pulsed load through a 0.563 Ω resistor using a relay. The pulse profile consisted of 3 sec under load followed by 17 sec at open circuit. The discharge was performed at room temperature.**

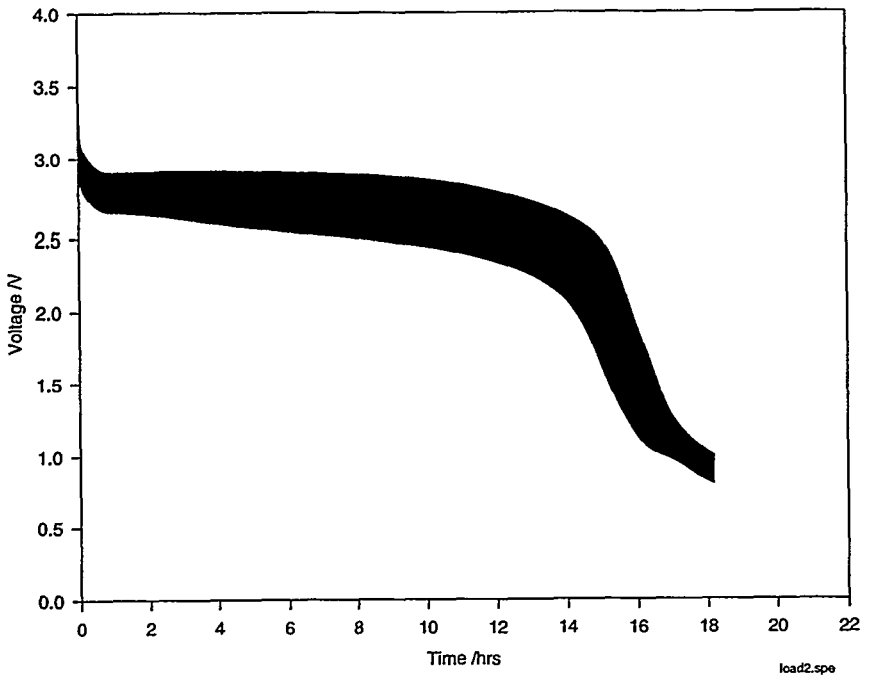

Figure 8-8. **Cell voltage of a Silberkraft D cell under pulsed load controlled by the battery tester employing Ohm's law. The pulse profile consisted of 3 sec at 0.563 Ω followed by 17 sec at open circuit. The discharge was performed at room temperature.**

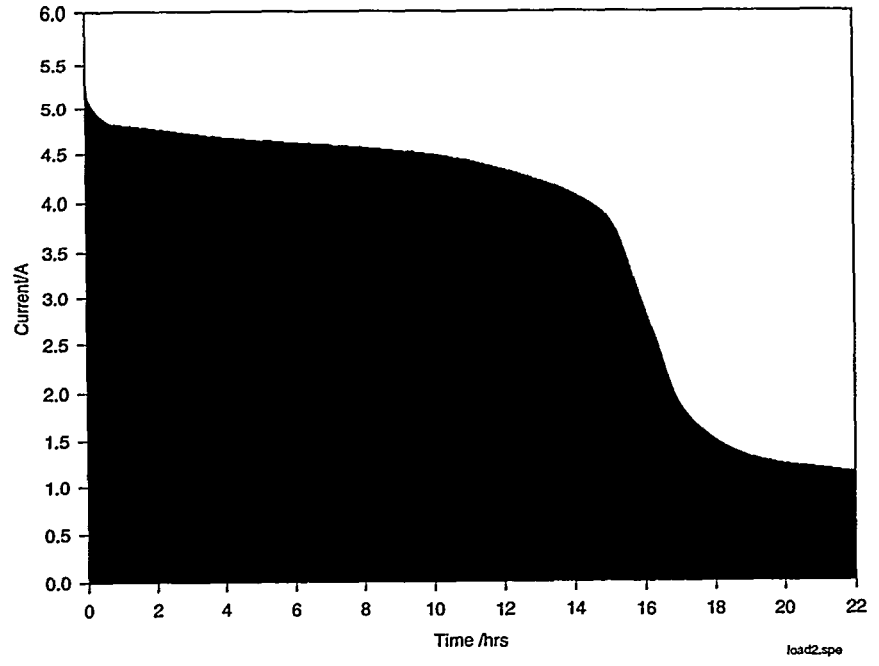

Figure 8-9. **Cell current of the Silberkraft D cell shown in Figure 8-8 under pulsed load controlled by the battery tester employing Ohm's law. The pulse profile consisted of 3 sec at 0.563 Ω followed by 17 sec at open circuit. The discharge was performed at room temperature.**

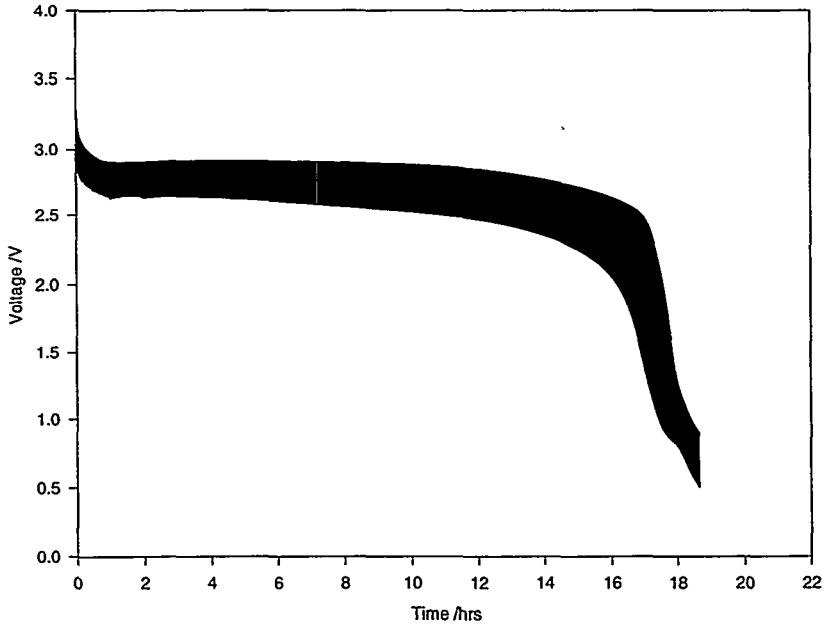

Figure 8-10. Cell voltage of the Silberkraft D cell under pulsed current load controlled by the battery tester. The pulse profile consisted of 3 sec at 4 A followed by 17 sec at open circuit. The discharge was performed at room temperature.

8.2 Testing and Test Hardware Limitations

Much of the battery test equipment used for this activity is limited to relatively small voltages and/or currents. Consequently, it is not possible to use this equipment as it was originally designed, that is to evaluate larger cells and batteries, such as 10 D cells in a series configuration under 5 A pulse trains. Furthermore, it is not possible to use this equipment to evaluate the cells under conditions of a truly resistive load, as described in the previous section. Nevertheless, the need exists to test cells and batteries in these other configurations. The limitations of the battery tester to testing these other conditions can be overcome by relays and by using the tester to control the relay as well as to monitor the voltages across the cell and the load resistor, something that the tester is aptly suited to do. This approach was used for collecting the data described in the previous section, and the circuit used is shown in Figure 8-11. The relays used for this scheme must be suitably sized. That is, the requirements for operation of the relay coil must be within the tester capabilities, and the current and power rating of the relay switches must be capable of passing the expected current and power of the battery. For our systems, this typically means 6-V DC operation of the coil and load carrying capability in excess of 5 A at 40 V. Other considerations of the relay include equivalent series resistance of the switch, rise and fall times of the switch, cycle life, etc.

The adequacy of this approach was demonstrated in the previous section, which showed data collected under conditions of pulsed load. One of the limitations of this approach is the relative sampling rates of the voltage monitoring. This is most noticeable under conditions of high pulse rate, as was previously mentioned with regard to Figure 8-1, when the pulse train for every pulse was not entirely captured. This highlights the fact that the test protocol employed must be within the specifications of the battery tester particularly with respect to sampling frequency.

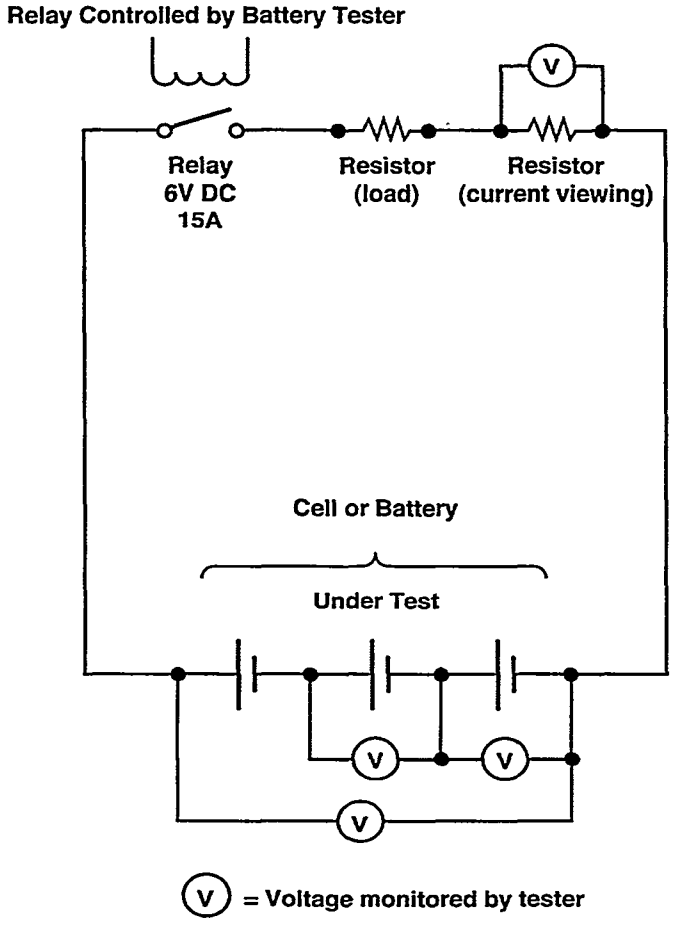

Figure 8-11. Schematic diagram of relay circuit that can be employed to overcome the battery tester hardware limitations in order to test larger batteries and variable loads.

This page intentionally left blank

9. Reliability Considerations

David Ingersoll and Thomas L. Paez

9.1 Introduction

In any application, particularly high-value systems like satellites or tactical nuclear weapons, the ability to assess system reliability is essential for predicting the potential for mission success. This need is especially critical for the power supply because it is used to operate virtually all other subsystems. Hence, the power supply can drive the overall system reliability. The converse is also true; that is, the reliability estimate of the overall system can be used to drive the battery subsystem design. (Consider, for example, the use of multiple redundant parallel strings of batteries to increase the overall system reliability.) The ability to make reliability assessments as early as possible in the design cycle is important to achieving overall mission success.

For primary (nonrechargeable) batteries, the ability to arrive at estimates of the statistical parameters, such as the mean, variance, standard deviation, etc., is complicated by the fact that the measurement process is destructive and sampling with replacement will not be done. That is, an assumption is made that the sample population is truly representative. The assessment of statistical parameter estimates is further complicated by the fact that one cannot say *a priori* that a given battery chemistry, or any of the critical battery response parameters (such as the nominal discharge voltage, capacity, equivalent series resistance, rate capability, etc.) of that chemistry, is normally distributed (Gaussian distribution). A final complication to arriving at reliability estimates is that the statistical parameters of a battery system are often a function of the conditions under which the measurements are made, such as temperature, and these conditions vary randomly during battery use. This necessarily implies that the overall system reliability depends on the probability that the system and hence the battery will be expected to operate over a specified range of environments. These issues, and examples of battery behavior as well as the approach that is taken to address these issues, are discussed in this section.

9.2 Special Builds Versus Commercial Off-The-Shelf Batteries

One approach that addresses some of these issues is to design the cell to the application and then to control subsequent cell builds by specification of the cell design parameters and building to those parameters. For most nuclear weapon system applications, the typical total number of cells built is relatively small, on the order of thousands of cells at the most. Because of the small number, every cell is typically hand built. From the standpoint of a large battery manufacturer, these small numbers of cells and the need to hand build the cells imply that the battery is still in the early development stages or pre-production and that the cell, cell chemistry, design parameters, assembly parameters, etc., have not been optimized.

At least from the standpoint of reliability estimates, the use of hand-built ambient lithium cells suffers from at least two distinct disadvantages compared to commercial-off-the-shelf (COTS) cells. First, even slight, minor modifications to cell components can have a significant effect on cell performance, and hence the statistical parameters of a build. This would not seem to be a problem in the hand-built cells because each cell is built to a controlled set of design and engineering parameters; however, for batteries, some of those parameters can significantly affect performance if they are not controlled, or are only loosely controlled. For example, the compression on a cell stack can significantly affect the cell performance by affecting the overall electronic conductivity. In many hand-built cells, the compression

applied to the electrode stack can significantly affect the cell performance by affecting the overall electronic conductivity. Also, in many hand-built cells, the compression applied to the electrode stack when it is rolled is not measured or carefully controlled. The only considerations given to this process are that (1) the electrode stack must fit into the can when complete, and (2) the electrode stack must not short out during the rolling process or when inserted into the can. This can lead to a significant variation in electrode compression, especially between assemblers. Hence the cell-to-cell variability can be significant.

In addition, because the battery performance and statistical parameters change depending on the conditions under which the measurements are made (as will be shown), the statistical parameters must be determined over the conditions under which the battery will be used. While it is possible to map out the space for a given battery build, this process requires evaluating a sufficient number of batteries under a given set of conditions spanning the space, presenting some practical problems of both expense and time. (Alternatives to mapping the entire space exist and will be discussed in a later section.)

In contrast, using COTS cells that employ a mature technology that is finding widespread use in the consumer market necessarily means that all of the cells are mass produced. This, combined with the fact that these are lithium-based chemistries, that is, they employ highly reactive and energetic materials, generally implies that the assembly process must be well controlled. Although this does not eliminate the need to determine the statistical parameter space of the cell performance, it does imply that the cell-to-cell variation, as well as lot-to-lot variation will be low, and this was seen in both the 2/3A and D cells (Chapters 2 and 5). Consequently, it may be possible to perform an initial mapping of the entire space, followed by mappings of only a portion of the space on subsequent builds. Based on the smaller mappings, a full mapping could then be performed if warranted. This could lead to significant savings in resources.

One of the primary disadvantages of using COTS cells is that the end user has no control over how the cell is built. Furthermore, the end user has very little control if any over the manufacturer to produce or continue producing cells. These issues present problems of their own regarding product availability and reliability. The reliability problem is tractable—an appropriate sampling protocol can be developed to give lot acceptance. The issue of product availability can be addressed by qualifying product from more than a single vendor. Nevertheless, the issues remain.

Another interesting issue that is not addressed here but should at least be mentioned, is security. The Department of Energy (DOE) does not yet possess battery production capability. Instead the DOE relies on contracts placed with specialty battery manufacturers such as Eagle Picher for production of weapon system batteries. Because some of these production companies are foreign-owned (for example, Eagle Picher has recently been acquired by a Dutch company), the security question regarding specialty-built batteries must now be addressed, as in the case of the COTS cells.

9.3 Statistical Variability Issues

Batteries are expected to operate over a wide range of conditions (e.g., temperature and load), only some of which are under direct control. In addition, the processes occurring in the cell are such that the resultant battery will exhibit optimum performance for a given set of conditions. Furthermore, the design engineer has some flexibility in the cell design to optimize the battery for operation under a nominal set of conditions. At least for the most part, the nominal conditions generally selected consist of those encountered most frequently, although they could be the worst-case conditions expected to be encountered. Under normal conditions, one can expect relatively small variations in cell performance.

An example of this relatively small variation in cell performance was described previously and is also shown in Figures 9-1 and 9-2, which show the discharge curves of multiple cells from two separate vendors collected under relatively benign conditions of room temperature and a constant current of 10 mA. Superimposed over these data are the average discharge voltages (indicated by the asterisk) of the cells at select time intervals that were determined from the data using an artificial neural network (ANN), as well as the 3-sigma value of the data at these times. (The ANN was trained using each of the discharge curves. Since ANNs are good at data interpolation, this computationally intensive tool is effective for providing the requisite values from the independent data sets.)

As shown, during the initial part of the discharge, the voltage profiles of the curve closely overlay one another, and there appears to be very little spread in the data. Intuitively, one might expect that this situation will be entirely different under conditions away from the nominal. Closer examination and consideration of these data bear out these expectations. Figure 9-2 shows the discharge curve of 18 replicate 2/3A Sanyo cells discharged at room temperature, and it is apparent that the cell-to-cell variation increases significantly, as measured by the 3-sigma value, at end of charge under room temperature conditions. Similar behavior is shown by the Duracell cells shown in Figure 9-1.

What constitutes nominal conditions for cell and battery performance? Some might argue that this discussion is purely one of semantics, and in some sense it is. However, we have elected to take a more pragmatic engineering view and define nominal conditions as those near the center of the performance envelope. Any set of conditions experienced by the cell or battery away from these conditions are not nominal. That is, those conditions for which the battery has been designed and which do not unduly stress the battery can be considered nominal. This view has significance for cell and battery operation, because significant differences in cell-to-cell behavior occur at the extremes or away from the nominal.

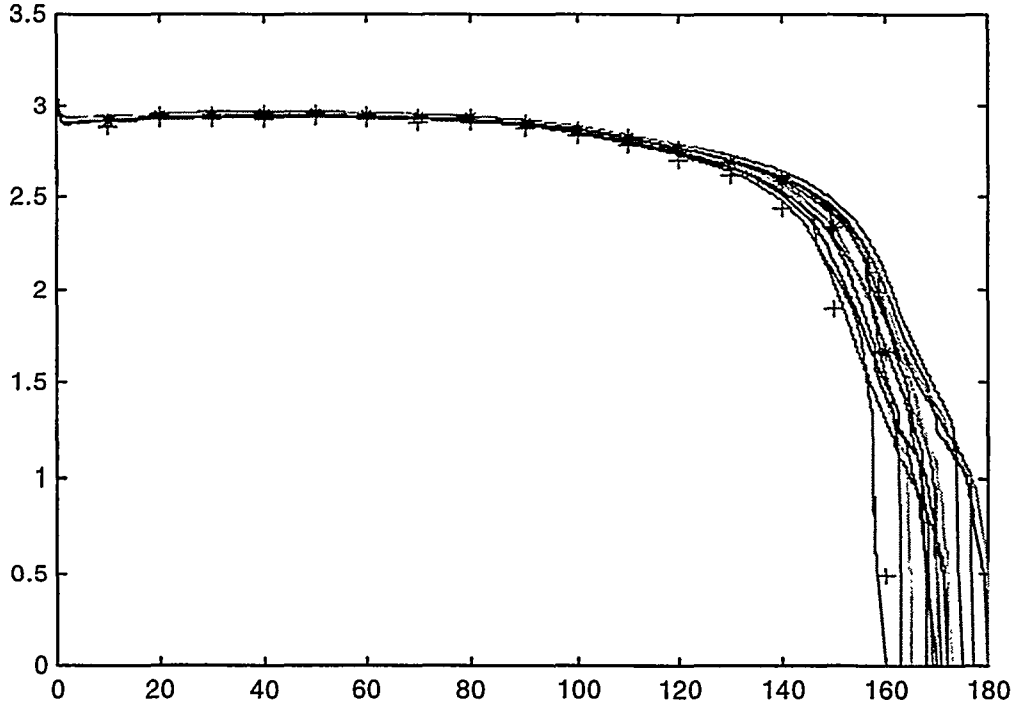

Figure 9-1. Room temperature discharge curves of 15 replicate Duracell 2/3A cells discharged at 10 mA constant current. Mean (*) and 3σ (+) values are also shown at periodic intervals along the discharge curve.

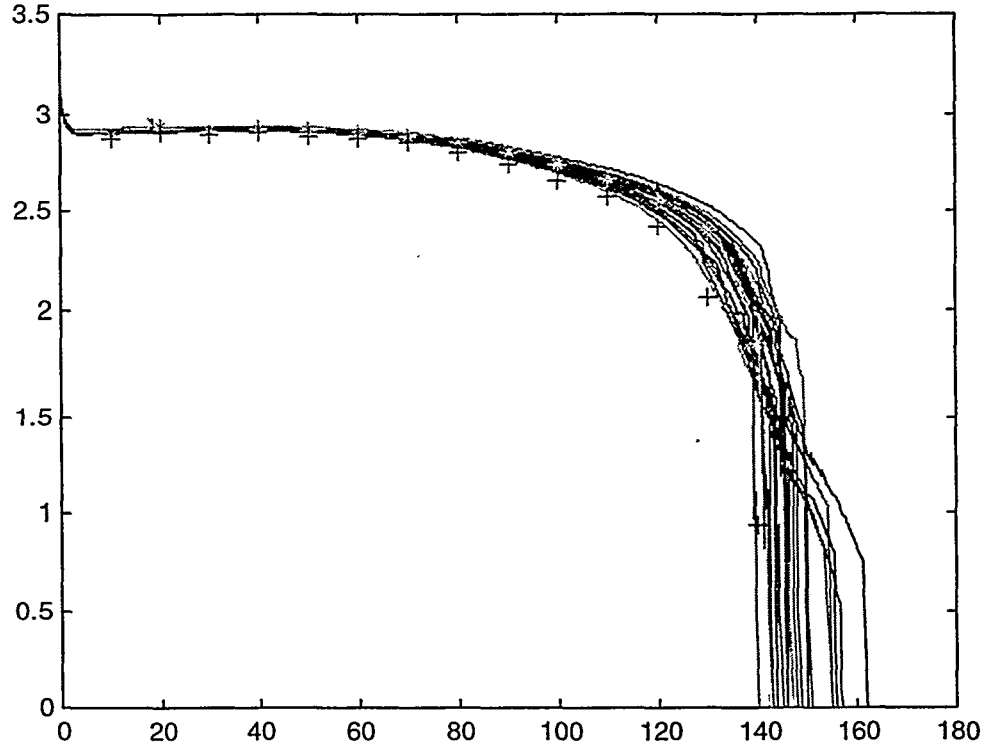

Figure 9-2. Room temperature discharge curves of 24 replicate Sanyo 2/3A cells discharged at 10 mA constant current. Mean (*) and 3σ (+) values are also shown at periodic intervals along the discharge curve.

With this definition in mind, the exact set of conditions making up the nominal set is highly dependent on the cell and battery being used because they can be designed to operate under a specific set of conditions. Nevertheless, some general parameters can be defined for those conditions, and the data shown in Figures 9-1 and 9-2 illustrate one set. During the initial portion of the discharge curve at room temperature and relatively low rates, most cells operate near their optimum. In this case then, nominal conditions refer to the initial 80% of cell operation, and the last 20% of operation constitute operation near the edge of the performance envelope.

Another characteristic of cell behavior at the extremes of their performance envelope is highlighted by the data in Figure 9-3, which shows the kernal density estimator of the probability density function for the capacity delivered by the Sanyo 2/3A cells at room temperature at the end of discharge, that is, the capacity delivered from the cell when the cell voltage drops to 2 V for the cells shown in Figure 9-2. Casual inspection of this curve might indicate that the data are normally distributed; however, overlying this curve is a plot showing a theoretical probability density function of an ideal Gaussian distribution having the sample mean and variance. As shown, the kernel density estimator, which reflects the distribution in the underlying population, is not symmetrical and is skewed to lower values. Furthermore, because the Gaussian probability density function is by definition symmetric about the mean, and because the finite cell size places a physical limitation on the upper limit of useful capacity that can be obtained from an individual cell of given dimensions and cells are often built to maximize this amount, the cells are non-Gaussian by their very nature.

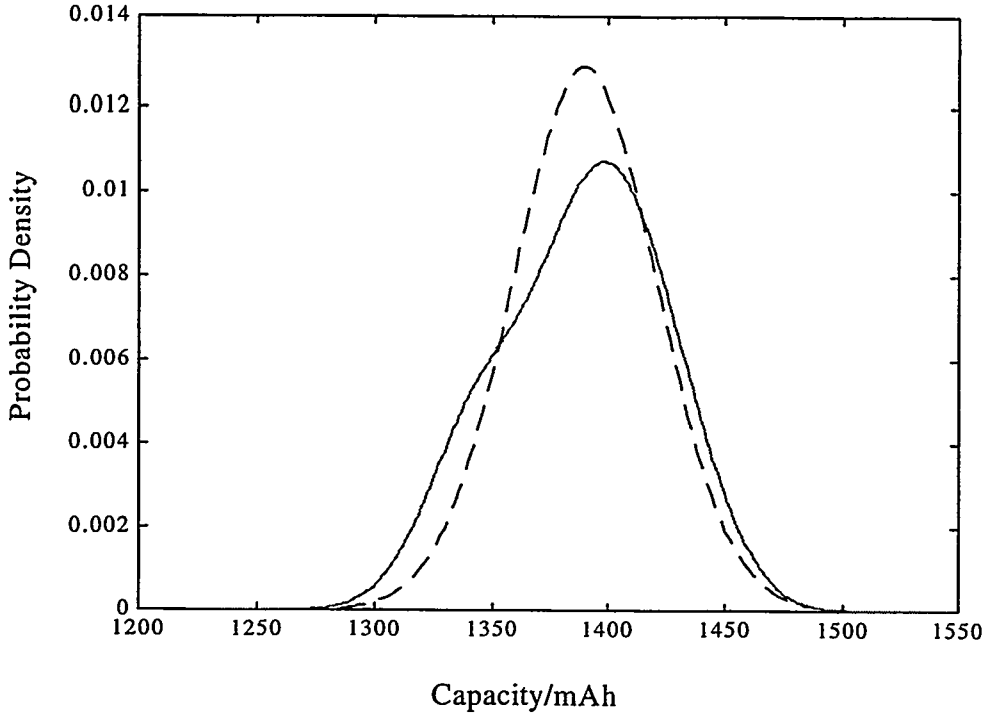

Figure 9-3. Kernal density estimator of the probability density for the capacity obtained at 2 V for 24 replicate Sanyo 2/3A cells (——) discharged at room temperature and the probability density for the theoretical normal distribution curve (-----) having a mean and standard deviation of the replicate data.

Although the definition and its use are arguable, from a purely pragmatic standpoint it is clear that a significant change in the statistical parameters is associated with voltage as a function of depth of discharge. The dynamics of the statistical parameters are further highlighted upon closer consideration of those conditions or sets of conditions for batteries that constitute the nominal, and this leads us to identify room temperature, new cells, low discharge rates, low depth of discharge, etc., as being nominal. Any other conditions that have substantial probability of being encountered, including low operating temperatures, end of discharge conditions, very high rates, etc., are defined as not being nominal, and their statistical characteristics are different than those observed under nominal conditions.

Figures 9-4 and 9-5 show the discharge curves of replicate Sanyo 2/3A cells at temperature extremes of –20°C and –40°C, temperature regimes known to limit, at least to some extent, the ability of the cell to perform. The data clearly show that a significant increase in the cell-to-cell variability and hence the statistical parameters are associated with the discharge at –20°C, not only at the end of discharge but over a wider range. At –40°C, near the operational limit of this chemistry, the variation decreases and will vanish altogether when the temperature reaches a level where none of the cells perform.

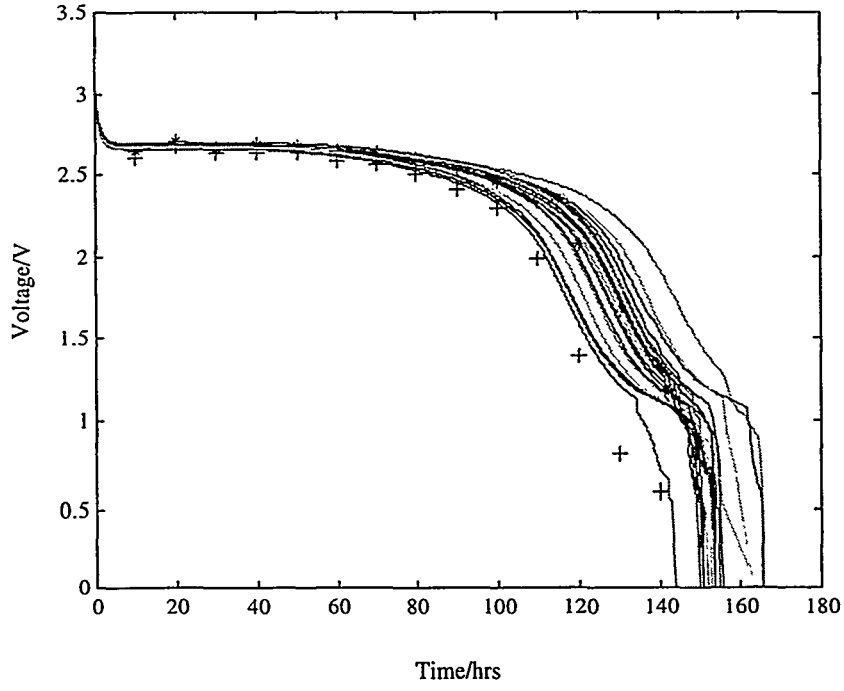

Figure 9-4. **Discharge curves of 19 replicate Sanyo 2/3A cells discharged at 10 mA constant current and –20°C. Mean (*) and 3σ (+) values are also shown at periodic intervals along the discharge curve.**

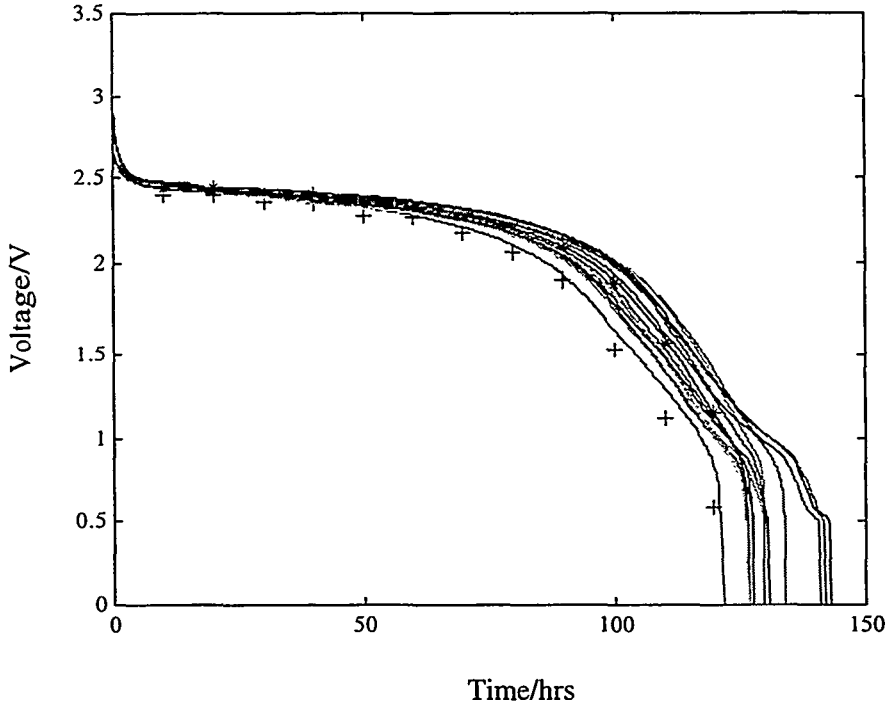

Figure 9-5. **Discharge curves of 15 replicate Sanyo 2/3A cells discharged at 10 mA constant current and –40°C. Mean (*) and 3σ (+) values are also shown at periodic intervals along the discharge curve.**

Another interesting exercise is to create the kernal density estimator of the probability densities of the data for the capacity obtained at end of discharge, at the three temperatures, and to overlay the probability density function of the theoretical normal distribution curves. In this case end of discharge refers to the capacity obtained from the cell when the cell voltage reaches 2 V, 1.75 V, and 1.5 V for room temperature, –20°C, and –40°C, respectively. (For this exercise, the end-of-discharge condition has been somewhat arbitrarily defined. The end-of-discharge criteria will affect the statistical measures, and this is evident on inspection of the discharge curves and noting the distribution in the data as a function of time or voltage.) This has been done, and these are shown in Figure 9-6. Examination of the data for the other data sets reveal that they are clearly non-Gaussian and that the mean and deviation are a function of temperature.

This type of behavior is not confined to 2/3A cells; it can be found in all of the cell sizes examined, as well as in virtually every battery chemistry, presumably as a result of the confluence of all of the processes occurring in the cells. Further, it is interesting to note that the measures of cell behaviors in these situations are non-Gaussian and therefore random variables associated with these behaviors are not normally distributed.

How the cell-to-cell variation in behavior and the non-normality of measures of behavior affect reliability estimates is deceptively simple. First, based on the criteria used to assess cell failure—and development and selection of these criteria are neither straightforward nor trivial, as will be seen—statistical behavior must be developed as functions of the conditions to be encountered. That is, battery behavior must be specified in a conditional probability framework, with these data mapping the statistical space from present to future states. With this mapping, a reliability estimate of the cell can be obtained that is based on the probability of failure within the space of the battery states and accounting for the probability of the cell encountering specific conditions.

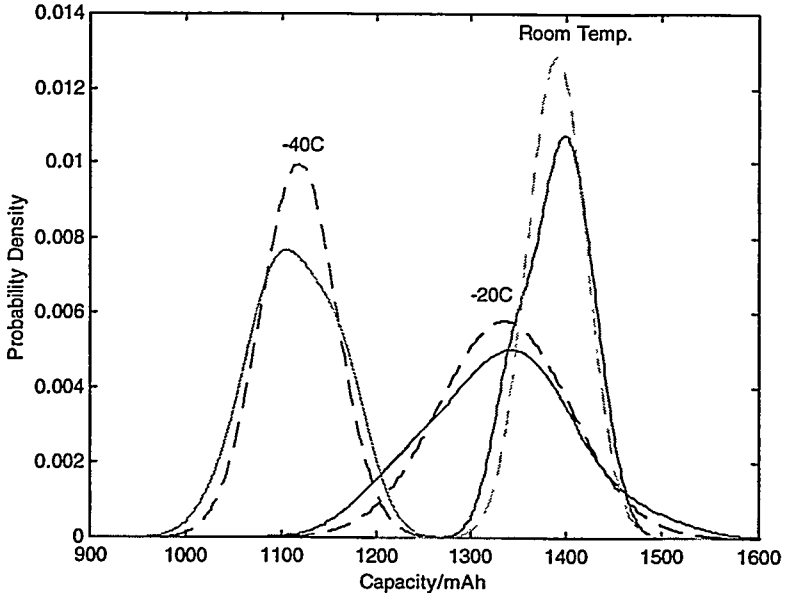

Figure 9-6. Comparison of kernal density estimator of the probability density for the capacity obtained for replicate Sanyo 2/3A cells (——) and the probability density function for the theoretical normal distribution curve (-----) having a mean and standard deviation of the replicate data at –40°C, –20°C and room temperature at cutoff voltages of 1.5 V, 1.75 V, and 2 V, respectively.

For example, the probability of cell failure in the system at –40°C is functionally related to both the probability of cell failure at –40°C and the probability of the system with the batteries in it being found at –40°C. In the event that other conditions can significantly influence the statistical space of the cell, such as high current pulses, they can also be factored into the reliability estimate as a probability that the cell will be called on to deliver the high-current pulses under those conditions. These examples of lower temperatures and higher current pulses are given primarily to illustrate realistic use conditions that are known to affect cell performance and hence reliability estimates, and yet which are otherwise known or well characterized. That is, the problem is tractable and soluble.

A separate but related issue is the question of the characterization of the statistical parameters themselves, which has been only briefly touched on. From a historical standpoint, a normal or Gaussian distribution is typically assumed. Acceptance of this assumption necessarily implies something about the distribution of elements within the performance space, especially their distribution at the tails, which is an important area of the distribution curve at least with respect to system failure. Rather than accept this assumption, we explored other options for obtaining the statistical parameters that make no assumptions regarding the distribution or the nature of the distribution.

The approach used to characterize these parameters is called the Bootstrap approach, which was first described in 1979 and is tied to the Jackknife method, first published in the 1950s. Development of the Bootstrap method was motivated by the need to assess the accuracy of statistics for random variables assumed to have been sampled from processes with unknown probability distributions in the realistic situation of limited data. As with other sampling techniques, the Bootstrap approach has three major advantages: (1) the underlying data need not come from a Gaussian source; (2) the sampling distributions of interest need not be Gaussian or Gaussian-related; and (3) approximation of the joint sampling distribution of multiple statistics is easy.

At least two other options exist for generation of the statistical parameters used to make reliability estimates. One of these approaches is to make predictions based on worst case conditions, that is, perform a series of measurements under the worst case conditions expected to be experienced for that battery use those numbers to calculate statistical parameters and perform the reliability analysis. This is a reasonable approach and has distinct advantages, including the psychological comfort of having a single number or set of numbers to rely on; however, this belies the true nature of the problem. Furthermore, the worst case conditions depend on the cell chemistry and design employed. Hence, without insight into how the system will perform or where and how it will be used, it is necessary to conduct a number of studies under different sets of conditions in order to attempt to make that determination. The other approach is to make the assumption that the behavior and measures of the behavior are Gaussian, as has been previously discussed.

Alternatively, by collecting this series of data, and by then collecting a minimum amount of additional data under well defined conditions over the entire space, it should be possible to map the entire statistical parameter space of the cell using an artificial neural network. We are currently in the process of collecting the requisite data to support both activities.

Another nontrivial issue that must be considered is how to judge failure; this cannot be done separate from the application. For example, is it considered a battery failure when the cell voltage drops below a certain level, fails to deliver a certain capacity, fails to function at low temperature, or exhibits combinations of these and/or other criteria? In addition, is there some characteristic of a new cell that can be measured that is nondestructive to the cell and is a reliable predictor of the future performance? These issues, as well as others, are being considered and addressed.

9.4 Reliability Calculations

The evaluation of battery system reliability can be cast as a first passage problem for a nonstationary random process. A solution can be formulated because the battery response process can be expressed as a first order Markovian random process whose transition probabilities can be approximated based on battery response realizations measured during laboratory experiments. The analysis may be described as a first passage-type problem because failure will often be reckoned by the first passage of the battery voltage below a specific cutoff value while the capacity drawn from the battery is lower than a pre-established quantity. The solution of such a problem depends on the analyst's ability to evaluate the probability that a random process passes outside a predefined region within a certain range of values of the parameter (independent variable) of the random process (e.g., time, or battery capacity). Many approximate solutions for first passage probabilities exist, and one involves the description of the underlying random process as a Markov process. The battery response random process is indeed a Markov random process because its behavior at any particular time can be described in terms of a finite number of measures of the battery state at a time immediately preceding the present.

A Markov random process is characterized by its probability distribution of initial states, and its transition probabilities. The transition probabilities of a Markov random process describe the chance that a particular state will be realized at an independent variable value Δt units in the future, given that the current state is specified. Such transition probabilities can be estimated for a battery when laboratory data are available using classical rules for probability estimation. Confidence bounds on initial and transition probability estimates can be developed using the Bootstrap approach.

Though the relations of cell reliability to battery reliability, and battery reliability to series system, parallel system, and series/parallel system reliability have not been considered, it can be analyzed using basic or advanced methods. System reliability can be evaluated based on fundamental principles when (2) the reliability of each component is known, (1) system components act in a statistically independent manner, and (3) the topology of the system is specified.

The estimation of system reliability is, however, more complicated when the topology of a system is complex and the components do not act in an independent manner. Nevertheless, when the joint probabilistic behavior of the components in a system is known, the probability distribution of measures of system behavior can be approximated using such techniques as first- and second-order reliability methods and the advanced mean value method. The combination of Markov techniques with these tools may assist the analysis of complex systems.

9.5 Conclusions

Significant variability exists in cell data that are not normally distributed. Furthermore, not only is the cell behavior affected by the environmental conditions, the statistical estimators of this behavior are also affected or perhaps reflect that dependence. Statistical techniques, other than those relying on standard Gaussian distributions, have been developed and are available. In addition, the requisite computational hardware that makes use of the these techniques feasible is now available in the form of desktop computers and workstations. The confluence of these factors has led us to consider the variable nature of battery behavior and its effect on system reliability, and to investigate new tools for making reliability assessments and parameter characterizations.

This page intentionally left blank

10. Safety Characteristics

Julie A. Banner, David Ingersoll, Chris C. Crafts and Nancy H. Clark

10.1 Introduction

The safety characteristics of both cells and batteries must be considered should the stored energy be released in an uncontrolled, perhaps even catastrophic, fashion. The behavior of cells and batteries must be evaluated under credible abuse scenarios to ensure personnel and hardware safety under these abuse conditions. Engineering controls should be able to be incorporated into the battery pack to ensure safe operation. We began an initial evaluation of the behavior of cells and batteries both alone as well as in combination with engineering controls to abuse conditions. The results of these initial studies are described here.

10.2 Silberkraft D-Cell Testing

This section summarizes the results of the initial cell and battery level safety testing performed on the Silberkraft lithium/manganese dioxide cells. The cell-level testing described in Section 10.2.1 was performed by C. Crafts. The battery level testing described in Section 10.2.2. was performed by the Battery Technology Group of the Electrochemistry Branch, Carderock Division, Naval Surface Warfare Center (NSWC). In this latter case, all of the testing was conducted in accordance with the guidelines set forth in the Navy Technical Manual S9310-SAF-AQ-010, which describes the testing requirements for lithium batteries used in Navy applications. Although these batteries are not necessarily intended for use by the Navy, the testing guidelines provide a good basis for comparison to other fielded batteries.

10.2.1 Single-Cell Testing – D Cells

The Silberkraft D cells vent when the cell-case temperature reaches a value of between 140°C and 150°C, regardless of how this heating occurs, that is, whether the heat is a result of a short circuit condition or whether it is supplied by an external heat source. In this venting, a significant amount of electrolyte is expelled from the cell. This venting has very little, if any, effect on the state of charge. For example, the venting of a discharged cell by shorting appeared similar to the shorting of a fresh cell. The electrolyte loss during short-circuit venting is so great that the resulting cell can support little current. The time to venting is about seven minutes under short-circuit conditions. Only once did the vented electrolyte ignite, and this was probably partially caused by confinement of the vented vapor stream. Our testing was done in an unconfined area, permitting cell venting into the open. Under these conditions, there is probably some evaporative cooling of the hot vapor.

The short-circuit current capability of the cell was monitored by placing a 0.05 Ω current-viewing resistor in the circuit during evaluation. It was found that the short-circuit current of the Ultralife cells was significantly smaller than those observed for the M20 Silberkraft cell, 20 A versus 27 A respectively.

D cells with a shunt diode are protected once the bias potential across the parallel cell/diode pair reaches about –0.440 V. Some cell heating is found prior to reaching this voltage, and not surprisingly, the degree of heating is greater as the current through the test circuit is increased.

10.2.2 Battery-Level Testing

Two versions of the Friwo-Silberkraft D cells (models M20 and M20TT) were supplied to NSWC for testing. The M20 cells were manufactured using a standard electrolyte mixture, whereas the M20TT cells employed a modified electrolyte to provide improved low-temperature performance. Battery packs consisted of thirteen cells spot-welded in a series configuration. The cells were configured into a battery assembly using double-sided tape and adhesive glass tape to wrap the cells into a cluster. Figure 10-1 shows the typical assembly. The cells are clustered into a triangular shape with two stacks of four cells and one stack of five cells. The cluster of cells was insulated in Fiberfrax to simulate worst-case adiabatic conditions. During each test, cell or battery voltage and current (where applicable), as well as cell case temperatures were monitored and recorded. Cells and batteries were tested in the vertical position at ambient temperature with the vents facing up. At least one type-K thermocouple (Omega chromel/alumel) was affixed to each cell case (13 per battery) using adhesive glass tape. The position of the thermocouples was documented and consistently maintained for all cells and batteries. Ambient air temperature in the test chamber was monitored and recorded.

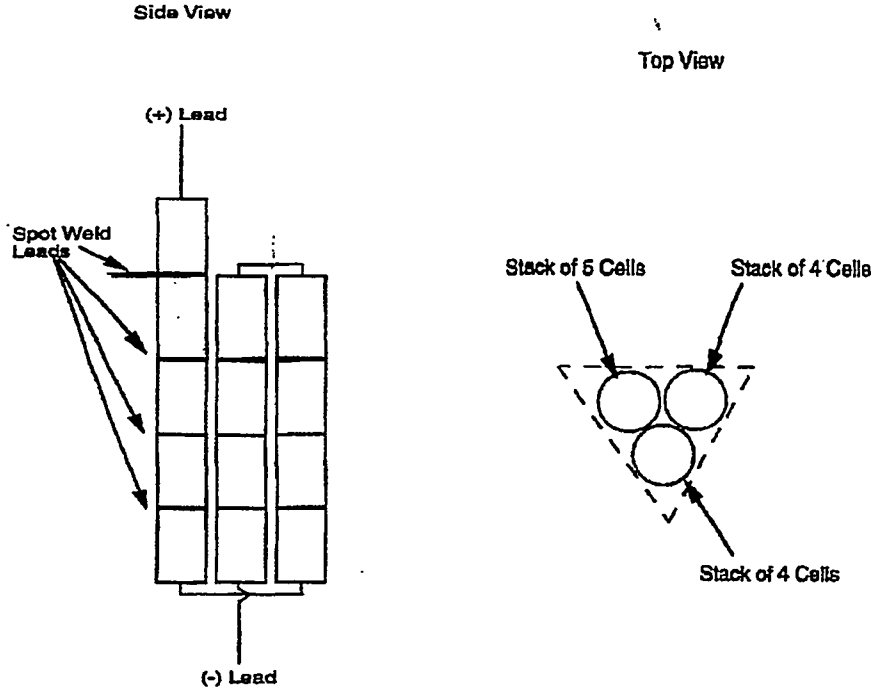

Figure 10-1. Battery pack schematic.

10.2.2.1 Incoming Inspection

The cells were assigned NSWC serial numbers for tracking purposes. The NSWC serial number of each cell was clearly marked on the outside of the cell case in permanent ink. Each cell was visually inspected for defects, such as corrosion, abnormal shape or coloration, abnormal temperature, electrolyte leakage, or any other visible anomaly.

The weight of each cell and battery pack was measured to the nearest 0.1 gram using a calibrated bench scale. The open-circuit voltage of each cell and battery pack was measured using a calibrated multi-meter. The closed-circuit voltage test for each cell consisted of recording the cell voltage for 30 seconds at open circuit, followed by 60 seconds with that cell subjected to a 60 Ω load (approximately 55 mA at

3.3 V), followed by 60 seconds at open circuit. The closed-circuit voltage test for each battery pack consisted of recording the battery voltage for 30 seconds at open circuit, followed by 60 seconds with that battery pack subjected to a 780 Ω load (approximately 55 mA at 42.9 V), followed by 60 seconds at open circuit. The alternating current resistance (ACR) of each cell and battery pack was measured with a Hewlett Packard Model 4328A, 1000 Hz milliohmeter. All data from the incoming inspection test series were recorded on incoming inspection data sheets.

No cells were identified as having anomalous incoming inspection values. However, one M20TT cell was inadvertently shorted while the OCV was being measured. The vent operated immediately, ejecting a small amount of electrolyte from the cell. No flame was observed during this venting. The short was removed immediately after the venting, halting any further chemical reaction. It was also noted during the assembly of the battery packs that the positive tabs were prone to breaking off from the cells.

10.2.2.2 Thermal-Abuse Test

This test was conducted on one M20 cell. The cell was instrumented with two K-type thermocouples and a single layer of flexible heating tape to provide maximum control and reliability for heating. It was then wrapped in one layer of Fiberfrax insulation. The cell was heated at a rate of ~7°C/minute until the heating source was damaged and could no longer function. This test indicates the response to an absolute worse-case condition and is not considered a probabilistic abuse scenario.

Approximately 23 minutes after heating was initiated, the cell vented benignly, releasing a small amount of smoke. The voltage dipped slightly in response to this event. The approximate temperature on the outside of the cell case was between 175°C and 195°C. Seven minutes later, while continuing the heat, the cell voltage dropped rapidly to 0 V and smoke began to issue from the vent opening. The thermocouples recorded temperatures between 200°C and 220°C at this time. Thirty seconds later, again with continued heating, a torch-like flame began to exit through the vent opening, lasting about six seconds. External heating of the cell was halted at this time. The cell-case temperature rapidly increased to almost 550°C as a result of the lithium burning. The event was over within two minutes.

10.2.2.3 Short-Circuit Test

This test was conducted twice: once on a battery built from M20 cells and a second time on a battery built from M20TT cells. A short-circuit of less than 0.02 ohms was applied to the battery between the positive and negative battery pack terminals by means of a relay-controlled circuit.

M20 Battery. Upon energizing the relay to close the circuit, the battery generated a peak current of 67 A. Over the next two minutes, the current slowly decreased to around 27 A, then began to rise again. During this time, the battery pack was smoking and the temperature was slowly rising. Approximately two minutes into the test, the current began to drop off and two audible vents were identified. Eight seconds later, a cell vented, accompanied by fire. Six minutes later, after the flames had gone out and reignited multiple times in response to audible ventings, a very loud report issued from the battery pack, and the battery was engulfed in flame.

M20TT Battery. The results of this test were similar in magnitude to those described above. The most significant difference was that the violent reactions consumed the battery much more quickly.

10.2.2.4 High-Rate Discharge into Voltage Reversal Test

Two versions of the high-rate discharge into voltage reversal test were conducted: a constant-current version and a pulsed version. For the constant-current version a battery built from M20 cells was discharged at ambient temperature using an electronic load set in the constant-current mode at 2.5 A. The discharge was continued into voltage reversal using a DC power supply. The maximum output voltage of the power supply was limited to 43 V, the nominal OCV of the battery pack at the start of the test. The battery discharged at 2.5 A to below 25 V in approximately 4.5 hours. By this point in the discharge, the temperatures of the cells had increased to as high as 145°C. At this time, a single cell vented accompanied by smoke and opened the series string. Approximately four minutes later, a cell vented audibly and a burst of flame was observed. Shortly thereafter, several more cells vented with a loud report, and flames and gases were expelled from multiple areas in a torch-like fashion.

In the pulsed version of the high-rate discharge into voltage reversal test, a battery built from M20 cells was discharged at ambient temperature. The test set-up used an electronic load, a timer, and a relay set-up to apply a repeated load profile consisting of a 5 A pulse for 3 seconds followed by a rest at open circuit for 17 seconds. The discharge was continued into voltage reversal using a DC power supply. The maximum output voltage of the power supply was limited to 43 V, the nominal OCV of the battery pack at the start of the test. This limit was raised as necessary to overcome iR losses in the circuit and maintain the peak pulse current of 5 A, but was never increased above 30 V. This battery discharged in the pulse regime for 14 hours before reaching 25 V. As the battery voltage dropped due to individual cells being depleted, it became necessary to increase the voltage of the power supply to force the battery to support 5 A during each pulse. A maximum temperature of 124°C was recorded just before the current dropped out, 17.5 hours into the test. At this time, the battery voltage during the 5 A pulses was approximately –20 V. Nine minutes after the current dropped to 0 A, the battery vented and released smoke. Twenty seconds later, a series of cell ventings accompanied by torch-like gas ejections occurred.

10.2.2.5 Conclusions and Recommendations

The results from these tests indicate that the D cells from Friwo-Silberkraft (models M20 and M20TT) are sensitive to short circuit and voltage reversal conditions. The high occurrence of fire in conjunction with cell venting indicates that the vent mechanisms do not open until the electrolyte materials are very close to their flash points. The vent does not shut down or prohibit the ability of the cells to continue to function (i.e., to carry current and voltage). Safety devices, improving the overall safety character of these cells, include shutdown separators and bypass diodes. If a shutdown separator were successfully incorporated into the cells, the response to short circuit could be greatly improved. In some systems these devices have been employed such that the cells never get hotter than 90°C on a dead short, and they do not vent. Bypass diodes should be incorporated into a battery design to limit the exposure of the cells to voltage reversal conditions. Thermal management of the battery pack to draw any heat generated during discharge away from the battery, and to eliminate temperature increases from other sources within the system is also a key element to maintaining the safety of a battery comprised of these cells.

10.3 Bypass Diodes

Early evaluation of BlueStar cells with fusible separators offered hope that mitigation of violent cell failure under short circuit or reversal conditions could be avoided. However, the lack of supply of cells having a fusible separator prevents implementation of this option. Hence, the use of bypass diodes for the series string of D cells was evaluated. These diodes are placed in parallel with each cell in the series string and are reverse-biased by the adjacent cell voltage. In the event that the cell voltage drops below

zero due to its being driven into reversal, the diode will be forward-biased and conduct current around the cell. Schottky rectifier-type diodes are the best choice for this application because they will begin to conduct at a low forward voltage drop of about 75 mV. This configuration raises a concern with the reliability of the diode and determining what the most probable failure mode is. In fact, bypass diodes would not be considered useful safety devices if their reliability were lower than the cells or if their mode of failure were short circuit. However, diode reliability is typically high, and reliability values as high as 0.9999+ are found. The most probable diode failure mode is open circuit. Another consideration in diode selection is the leakage current through the diode. Leakage current will place a parasitic load on the cell and could remove considerable amounts of capacity if too high. The first candidates evaluated in this selection process have leakage currents of less than 100 nA, which is acceptable for this application.

Testing of Silberkraft M20TT cells consisted of discharging a cell using a load of 8 Ω to close to end of discharge. The test cell was then placed into a string with 11 fresh Li/SO_2 cells and the discharge was continued while monitoring the Li/MnO_2 cell and diode during the reversal. The test parameters monitored were string voltage, total string current, test cell voltage, diode current, and the test cell temperature. Figure 10-2 shows a plot of the diode current and cell voltage versus discharge time. The diode current was measured by monitoring the voltage across a 0.005 Ω current viewing resistor in series with the diode. The diode does not shunt appreciable current until the reverse bias on the test cell is 0.4 V. As time goes on the portion of current passing through the diode increases to about 490 mA, but the potential across the diode is relatively stable at 0.4 V. The total circuit current was about 800 mA, as shown in Figure 10-3, which shows the total string voltage and current as a function discharge time. Comparing the currents in the circuit reveals that approximately 310 mA is still being forced through the cell. Nevertheless, no appreciable cell heating occurs, as can be seen in Figure 10-4, which shows that the test cell skin temperature did not exceed 35°C and diminished at longer times.

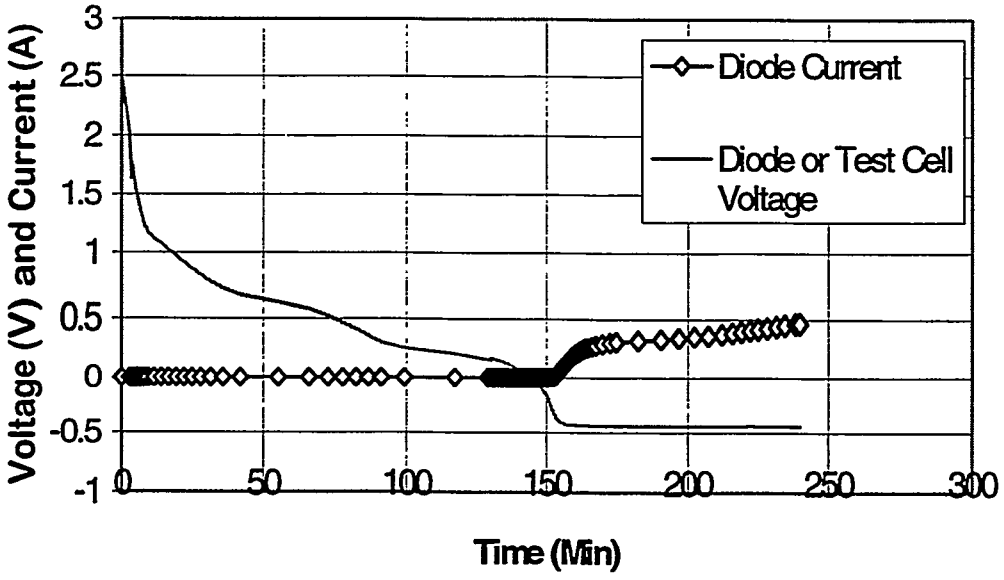

Figure 10-2. Silberkraft M20TT cell voltage reversal and diode current.

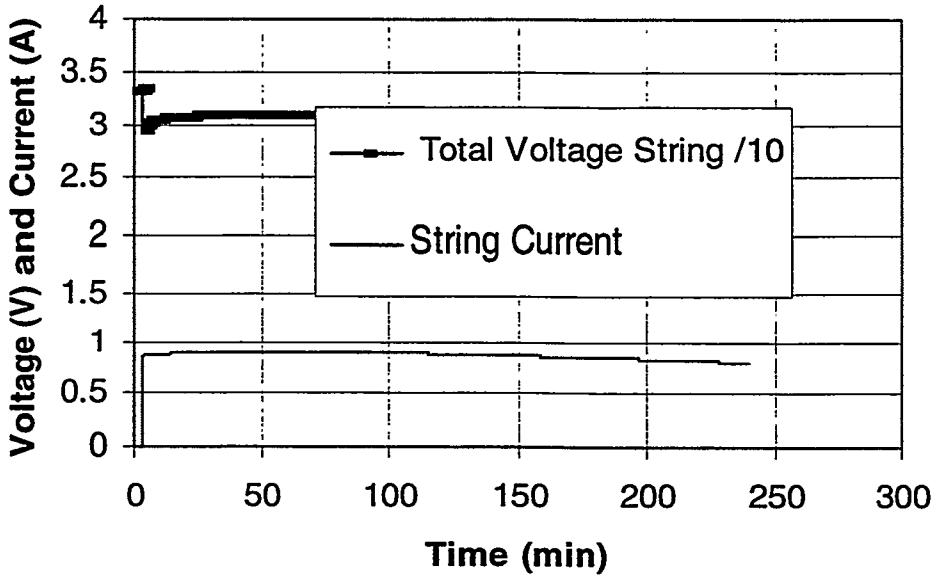

Figure 10-3. Total string voltage and current for all Li/SO_2 cells in series with one Li/MnO_2 cell.

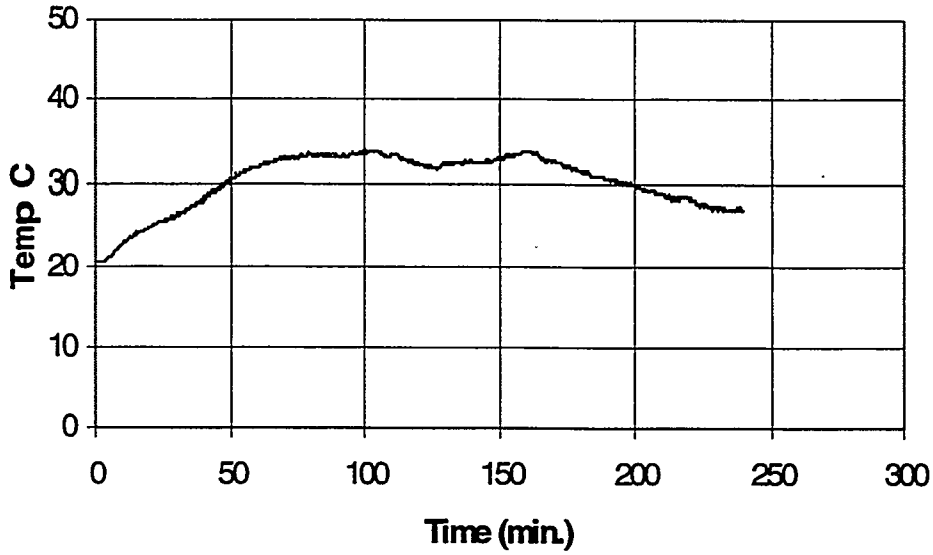

Figure 10-4. Skin temperature of Silberkraft M20TT cell during discharge and reversal with a bypass diode.

10.4 Positive Temperature Coefficient Switches

Positive temperature coefficient (PTC) switches are composed of carbon-filled plastic, which allows for good electronic conduction at room temperature. Heating of the material results in its expansion, which in turn leads to a decrease in the particle-to-particle contact of the carbon filler. This results in an increase of the resistance of the device, ultimately leading to an open-circuit condition. As such, these devices provide a means for thermal protection of the circuit. When engineered into a cell, they provide a safety mechanism for thermally activated events resulting from passage of current, such as short circuit.

Because they are thermally activated switches, any process that leads to an increase in the cell temperature will activate the switch. Provided that the cell is not internally shorted, the opening of the PTC switch should prevent a thermal runaway event in the cell. Furthermore, provided the cells and PTC are appropriately matched, the switch may even prevent irreversible damage to the cell.

The consumer 2/3A cells are engineered with PTC switches, and we have evaluated the performance characteristics of some of these. These evaluations were performed on both individual cells as well as on battery configurations under short-circuit conditions. In the individual cell case, the PTC was evaluated by attaching a thermocouple to the cell body and then placing the cell into a programmable oven. A constant current load of 0.1 A is then placed on the cell and the temperature of the oven slowly increased. During the cell heating, the cell temperature and the cell voltage are continuously monitored. As seen in Figure 10-5, the voltage increases slightly during the initial heating of the cell. When the cell temperature reaches about 115°C, the PTC activates and an additional resistance of about 10 Ω is added to the circuit, leading to a drop in the operating voltage. If the cell is then allowed to cool, the PTC resets and the cell continues to operate normally, as shown.

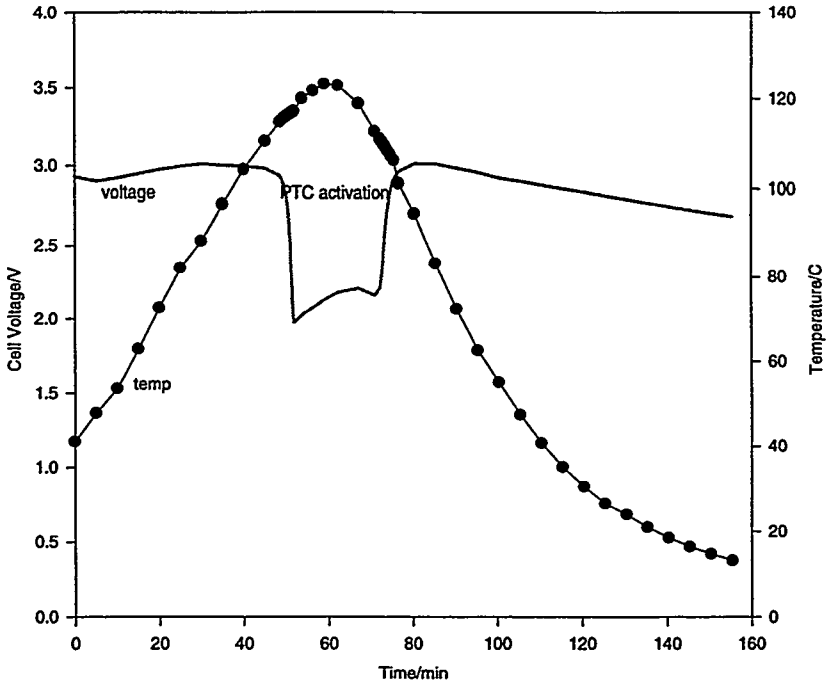

Figure 10-5. Voltage profile of a 2/3A Varta cell showing the reversible behavior of the PTC. The cell is under a constant-current load of 0.1 A as the temperature of the cell is slowly increased and then decreased.

If, on the other hand, heating of the cell continues, the cell will vent when the temperature reaches about 140°C. An immediate decrease in the cell temperature occurs as a result of evaporative cooling, and the cell is unable to support a load. (Recall that these cells are not welded. They are in fact sealed through the use of a crimp seal and gasket.) This behavior is shown in Figure 10-6. At least two types of cell behavior have been observed after allowing the cell to cool. In one case the cell is internally shorted, and hence will serve as a hard-wired connection in the case of a battery configuration and will not, by itself, support a load. In the other case the cell exhibits a normal open circuit voltage i.e., a stable battery voltage is observed. However, when a load is applied it cannot support the load and the voltage immediately drops.

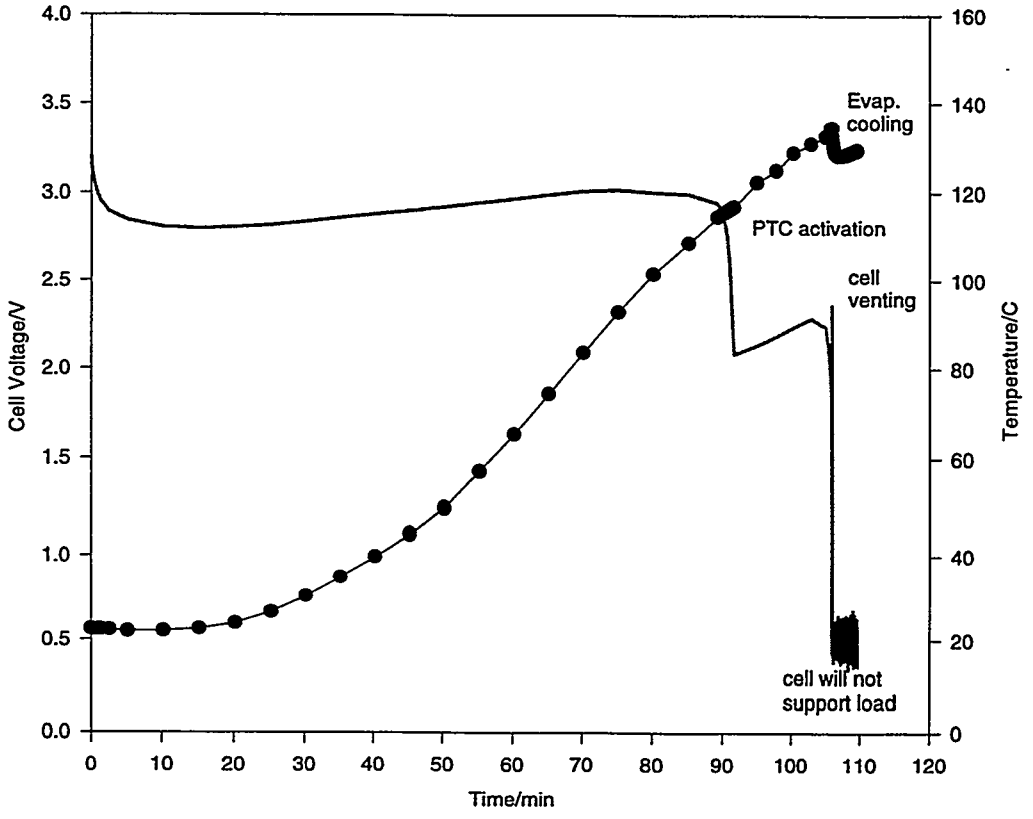

Figure 10-6. Voltage profile of a 2/3A Varta cell showing the irreversible venting of the cell upon heating. The cell is under a constant-current load of 0.1 A while heating of the cell occurs.

The short-circuit behavior of the 2/3A cells with PTCs was also evaluated in a battery configuration. In this case, two configurations were evaluated, one consisting of two parallel strings of six cells connected in series (a 2X6 configuration) and one consisting of two parallel strings of 11 cells in series (a 2X11 configuration). A current viewing resistor was placed in series with the battery stack and a relay was used to complete the circuit. A schematic diagram of the circuit is used for the battery configuration shown in Figure 10-7 for the 2X6 configuration. Both the current and voltage were monitored during short circuit.

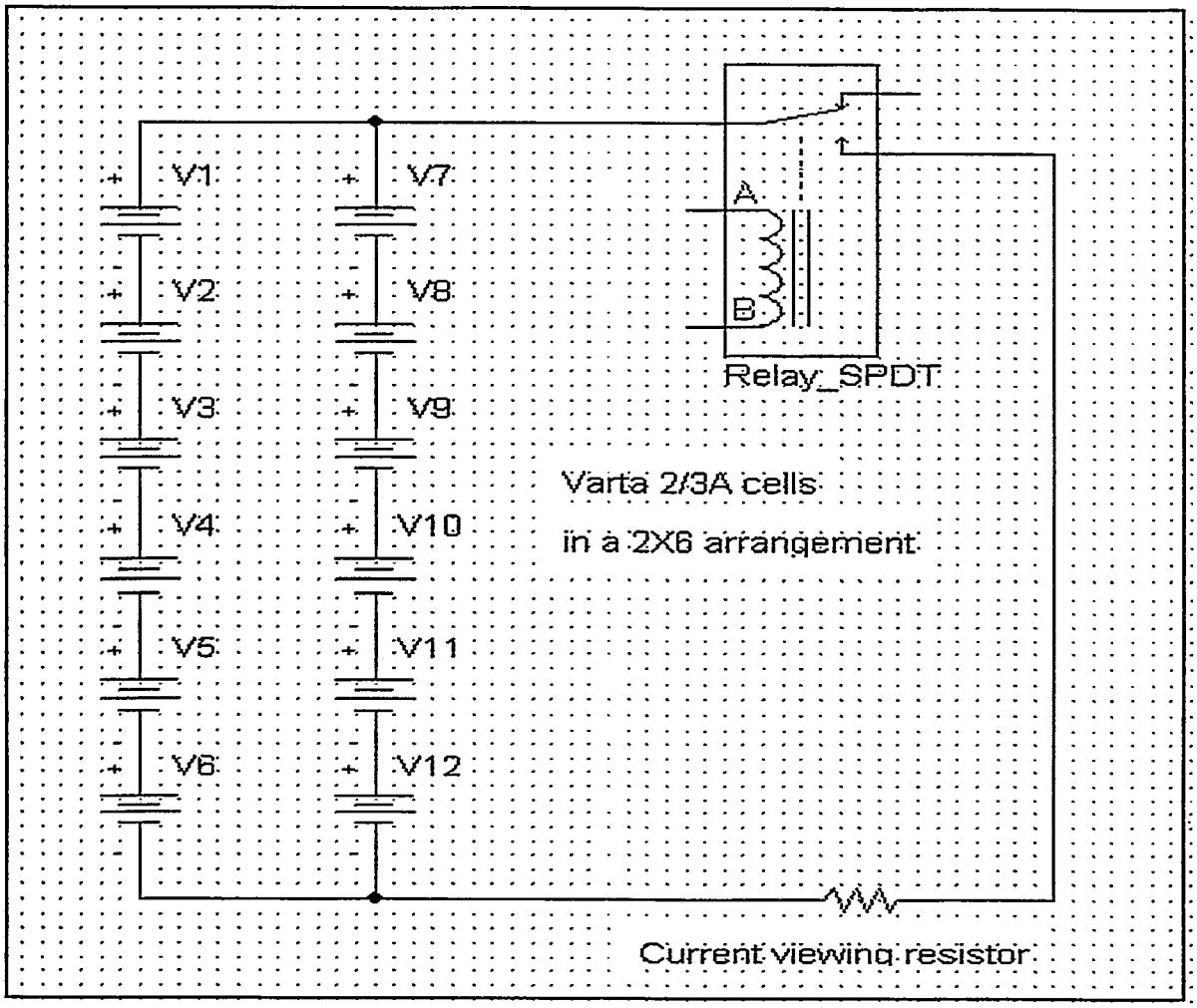

Figure 10-7. Schematic diagram of the circuit used for short circuit characterization of the PTC using Varta 2/3A cells in a 2X6 arrangement.

Figure 10-8 shows the short circuit response for a battery composed of Varta 2/3A cells. As seen, peak currents in excess of 30 A are initially observed, which slowly decay over the next 10 seconds to a relatively constant level of about 14 A. This level is maintained for another 10 seconds, at which time the current is seen to abruptly decrease by about one half. Shortly thereafter, the current is seen to decrease again to about 1 A. The reason for this behavior is easily understood in view of the tests just described. The initial sharp decrease in the current results from one or more PTC switch opening and cell venting(s) in one of the two parallel legs. When this occurs, the contribution of current from this leg of the circuit stops. Shortly thereafter another PTC switch activates and the cell vents in the other leg of the circuit opens, thereby interrupting the current flow from this portion of the circuit.

During this process, the temperature of the cells was monitored, and the maximum temperature observed on the outside of the cell was 50°C. After they cooled, the cells were examined, and one cell in each of the parallel strings was found to have expelled some solvent. There was no violent venting of any of the cells in any of the strings.

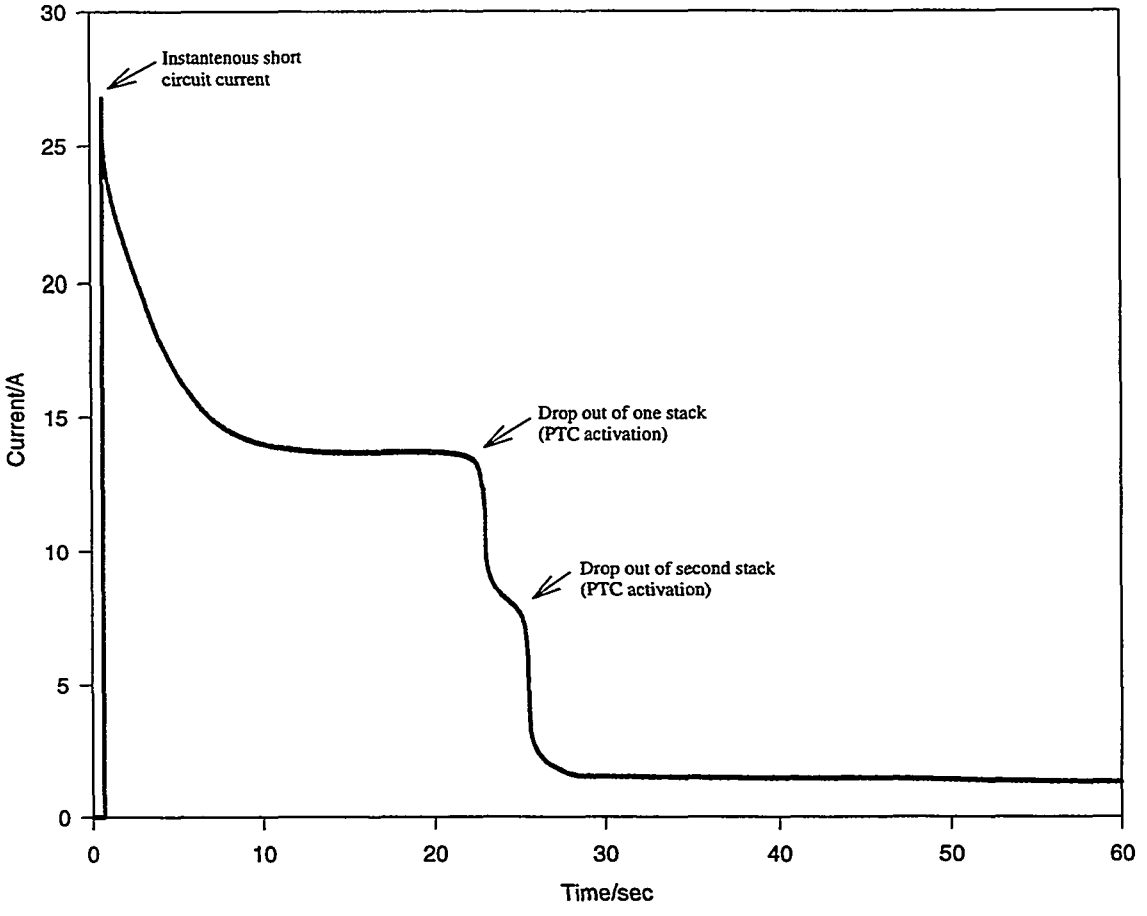

Figure 10-8. Short-circuit behavior of Varta battery consisting of two parallel strings of six Varta 2/3A cells connected in series.

The short-circuit behavior of the cells from two different vendors was also evaluated in a 2X11 configuration, and the behavior observed is similar to that just described except that the currents are correspondingly higher. This behavior is shown in Figures 10-9 and 10-10 for the Varta and Sanyo cells, respectively. One of the Sanyo battery stacks continued to operate at relatively high currents for the entire duration of the test, indicating that the cells did not get hot enough to vent.

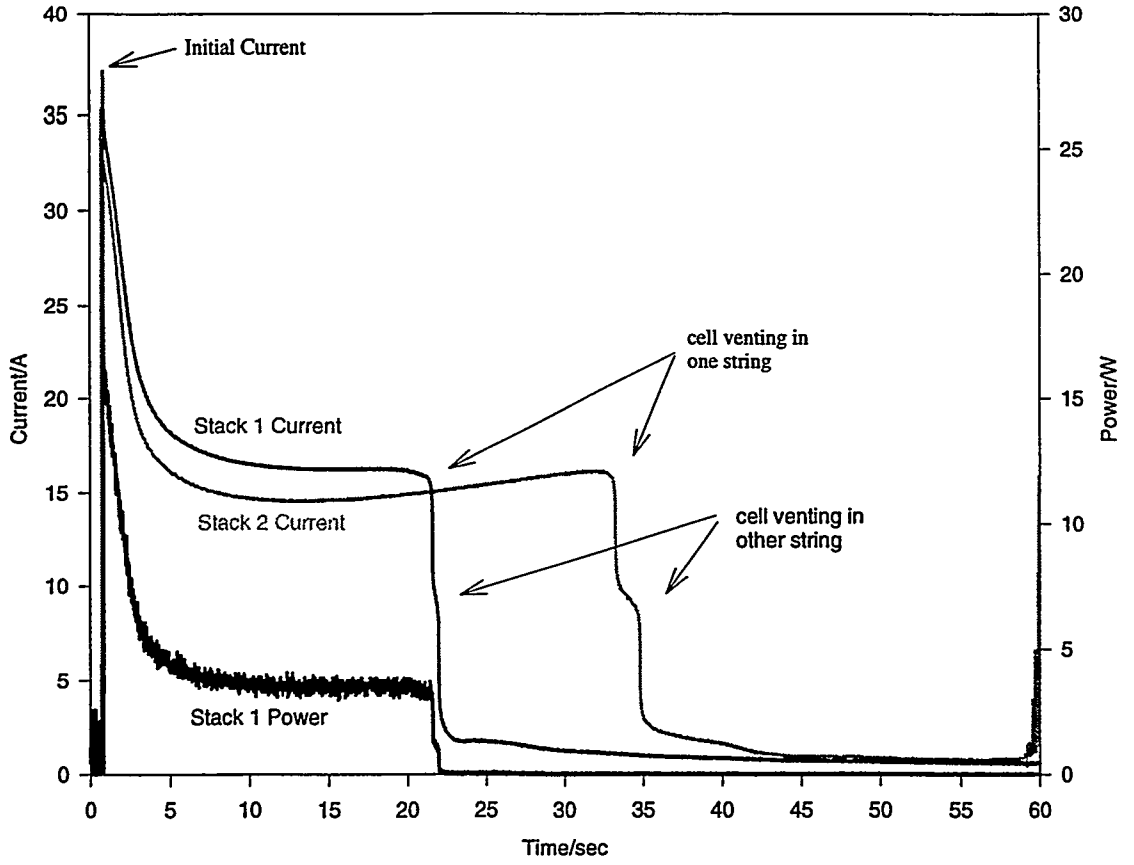

Figure 10-9. Short-circuit behavior of two different 2X11 battery stacks made up of Varta 2/3A cells.

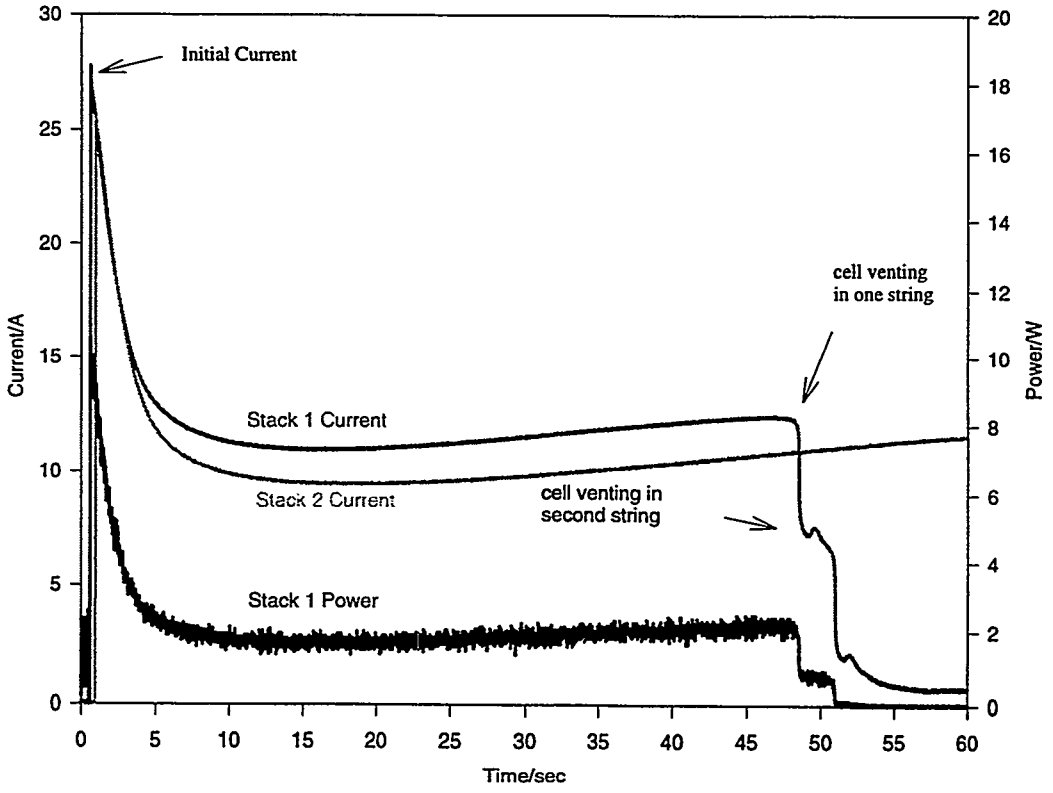

Figure 10-10. Short-circuit behavior of two different 2X11 battery stacks made up of Sanyo 2/3A cells.

10.5 Conclusions and Recommendations

The results from these tests indicate that the D cells from Friwo-Silberkraft (models M20 and M20TT) are sensitive to short circuit and voltage reversal conditions. The high occurrence of fire in conjunction with cell ventings indicates that the vent mechanisms do not open until the electrolyte materials and low vapors are very close to their flash points. The vent does not shut down or prohibit the ability of the cells to continue to function (i.e., to carry current and voltage). Devices improving the overall safety of these cells include shutdown separators and bypass diodes. If a shutdown separator were successfully incorporated into the cells, the response to short circuit could be greatly improved. In some systems, these devices have been employed such that the cells never get hotter than 90°C on a dead short, and they do not vent. Bypass diodes should be incorporated into a battery design to limit the exposure of the cells to voltage reversal conditions. Thermal management of the battery pack is a key safety element to draw any heat generated during discharge away from the battery, and to eliminate temperature increases from other sources within the system.

The 2/3A cells tested with a PTC show that they perform as expected. The temperature of the case increases and, in some cases, the cell itself is shorted so it cannot be used again. No major safety problems occurred.

11. Modeling

David Ingersoll and James F. Stamps

11.1 Introduction

PSpice is a computer-aided design tool used by electrical engineers for designing and modeling electronic circuits. This software package has ideal power supplies that can be called out as parts and placed in the circuit during the design process—ideal in the sense that they are able to deliver any load required by the circuit. Within this framework, it is possible to develop optimized circuit designs when these power supply models (for example, the electric grid) are available. However, when they are not available (for example, when a battery is used), the final circuit design will most likely not be the optimum solution.

Batteries are not ideal power sources and exhibit several characteristics that could severely limit the final system design. For example, it is known that the capacity of a battery is a function of the current, with higher capacities generally being delivered at lower rates. Other functional relationships of batteries that must be considered include the dependence of capacity on temperature, cell design, chemistry, cell history, etc.; the dependence of cell voltage on temperature, load, chemistry, cell design, etc.; the dependence of effective series resistance of the cell on state of charge, cell design, load, temperature, etc.; and the interaction of these factors. Because of these myriad factors and the possibilities available to the design engineer (for example, circuit design and battery options during the design process), it is conceivable that the circuit can be tailored (1) to function within the constraints of the battery limitations or (2) to optimize the battery selection based on the circuit characteristics. The ability to design the system within the constraints of the power-supply characteristics depends on the availability of PSpice models for the power-source options. Within the past year, a program to fulfill this objective began, and development began of PSpice models for power sources that can be used during the circuit design process and that can emulate the battery performance. The objective for this activity was to be able to simulate the battery performance within at least 30% of its actual performance. As will be shown, we have far exceeded our initial goals.

11.2 PSpice Battery Model Framework

A basic framework for a PSpice battery model was developed, and a PSpice schematic is shown in Figure 11-1 illustrating the basic model elements. To develop a model for a particular battery, critical cell parameters for each of these circuit elements for that battery system must be available and placed into the PSpice model framework. Although several approaches can be used to populate the model, the primary approach used involves first measuring critical cell parameters for the cell of interest. These cell data are used to generate tables, functional relationships, etc., which are then placed into the PSpice framework.

11.3 Model Examples and Validation

Using this approach, initial PSpice models of most of the 2/3A lithium/manganese dioxide cells as well as the Ultralife D cell and the low-rate lithium/thionyl chloride ($Li/SOCl_2$) cell have been developed. Examples of the performance of these models are discussed below.

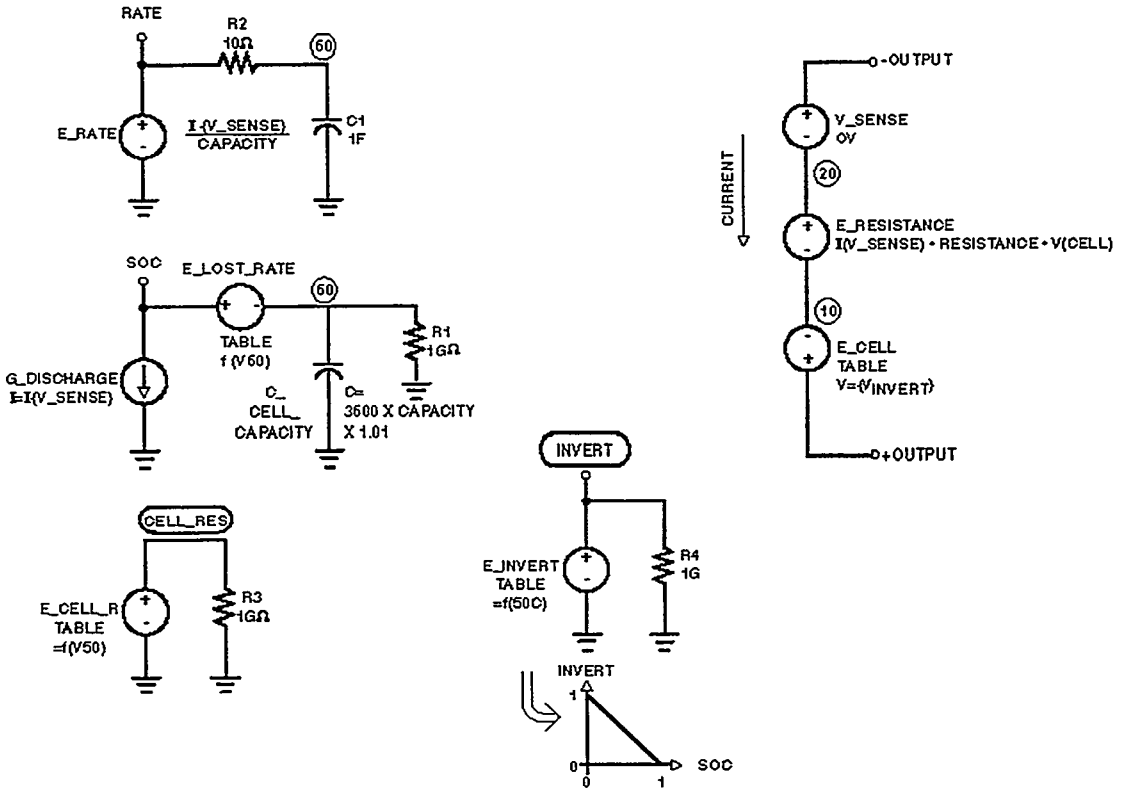

Figure 11-1. Schematic representations of PSpice battery model framework.

Figure 11-2 shows a comparison between the actual and predicted performance behavior of the discharge of a low-rate lithium/thionyl chloride cell upon a low-duty-cycle pulse discharge. In this case, the pulse train consists of switching the applied load between 250 Ω and 50 Ω. As shown, the predicted performance very closely simulates the actual performance, except at the end of discharge and at the very beginning. The discrepancy at the beginning and end of discharge can be readily ascribed to a change in the equivalent series resistance of the cell during the course of discharge, which is not captured in this preliminary model. This explanation has some basis in fact because it is generally recognized that at the beginning of discharge, a passive film on the negative electrode results in an initially high equivalent series resistance, and at the end of discharge deposition of lithium chloride at both electrodes also leads to an increased equivalent series resistance. In the preliminary model, the cell resistance is held constant over the entire state of discharge. Modifications to the model to address this shortcoming have been made, as discussed below.

The preliminary model was improved by incorporating a look-up table for the equivalent series resistance of the cell as a function of state of charge. An example of the predictive capability of this improved low-rate lithium/thionyl chloride model to a pulsed load is shown in the figures below. Figure 11-3 shows the actual behavior of the low-rate lithium/thionyl chloride cell to a more complex pulse load. Note that the voltage drop of the cell upon application of the pulsed load increases noticeably during the course of discharge and becomes very pronounced at about 90% depth-of-discharge. The preliminary model and improved model predictions are shown in Figures 11-4 and 11-5, respectively. As shown, the actual and simulated curves of the improved model are comparable, especially at that point in the discharge curve when the equivalent series resistance of the cell begins to increase significantly. As shown in Figure 11-6, if an expanded scale is used, differences in the simulated and experimental curves are better seen.

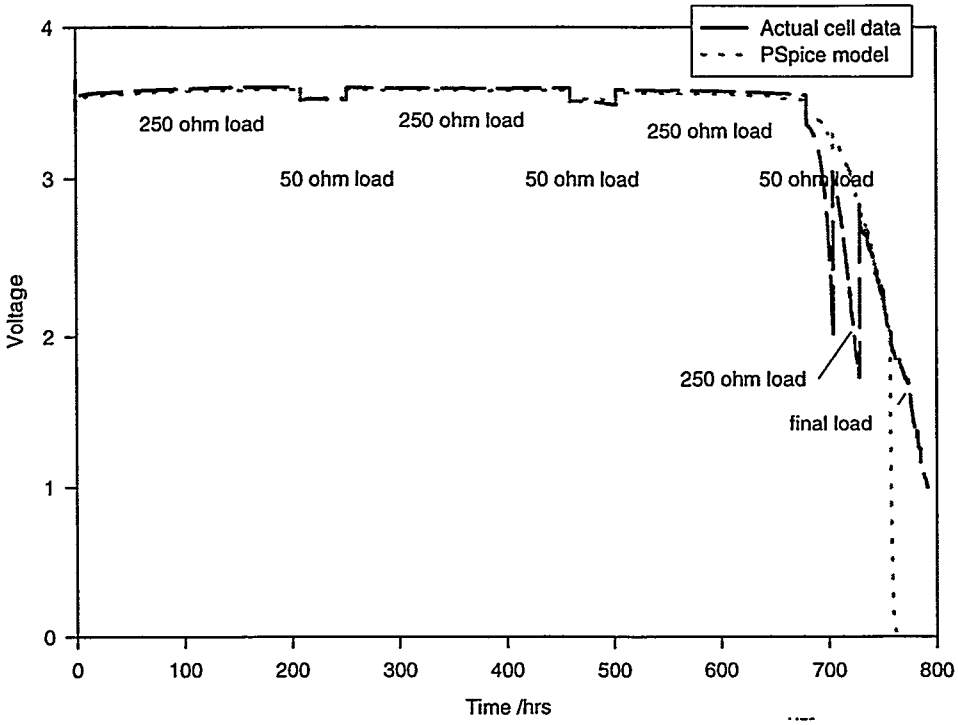

Figure 11-2. Pulse discharge behavior of SNL lithium/thionyl chloride low-rate cell at room temperature.

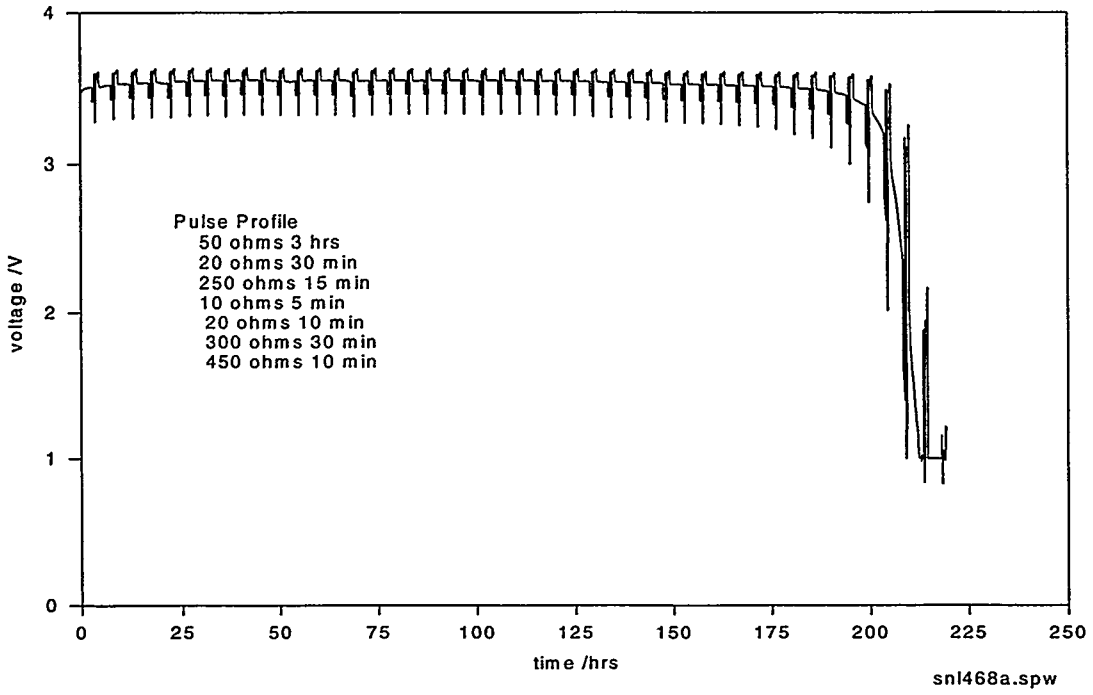

Figure 11-3. Behavior of a lithium/thionyl chloride low-rate cell to a pulsed discharge at room temperature.

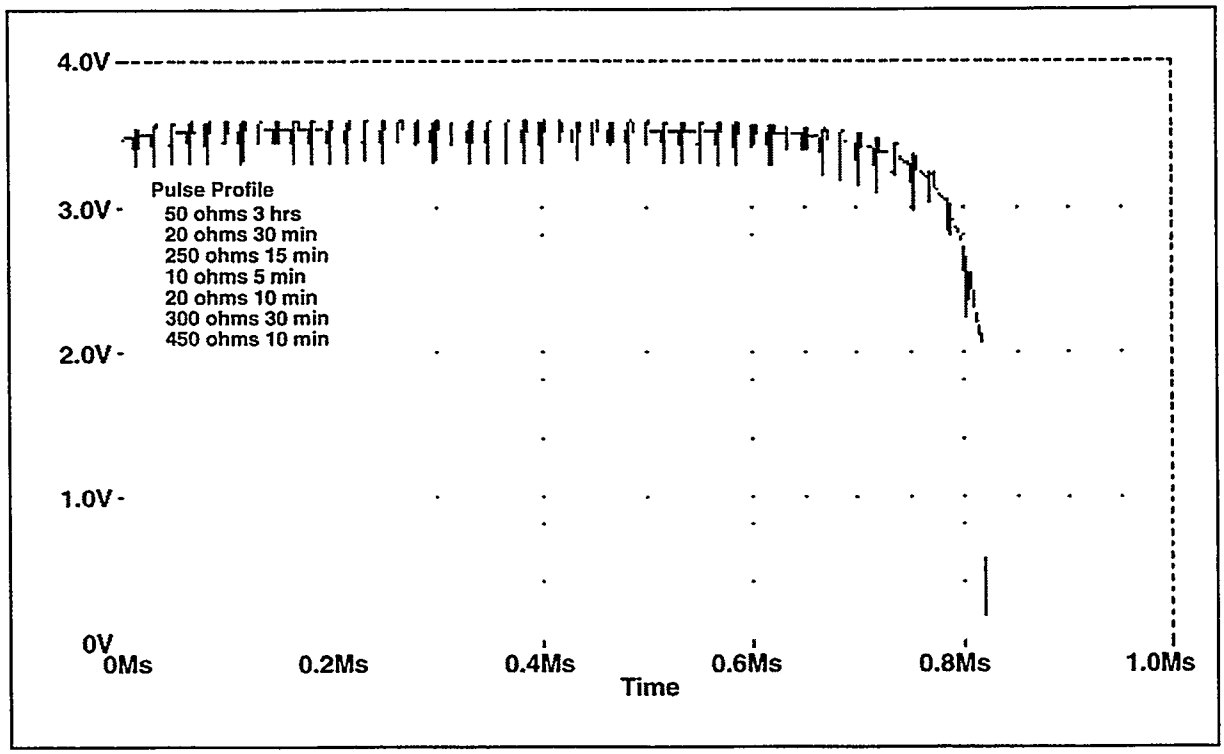

Figure 11-4. Predictions of the preliminary lithium/thionyl chloride low-rate cell model to a pulsed discharge at room temperature.

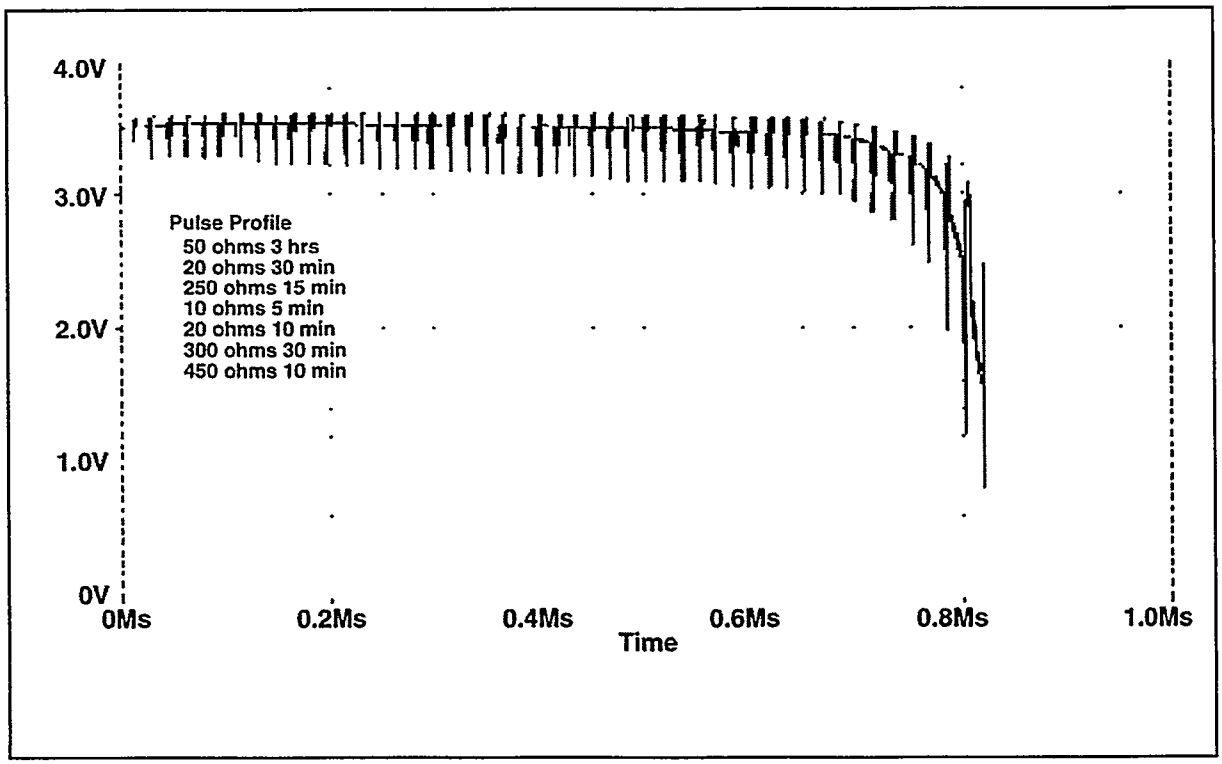

Figure 11-5. Predictions of the improved lithium/thionyl chloride low-rate cell model to a pulsed discharge at room temperature.

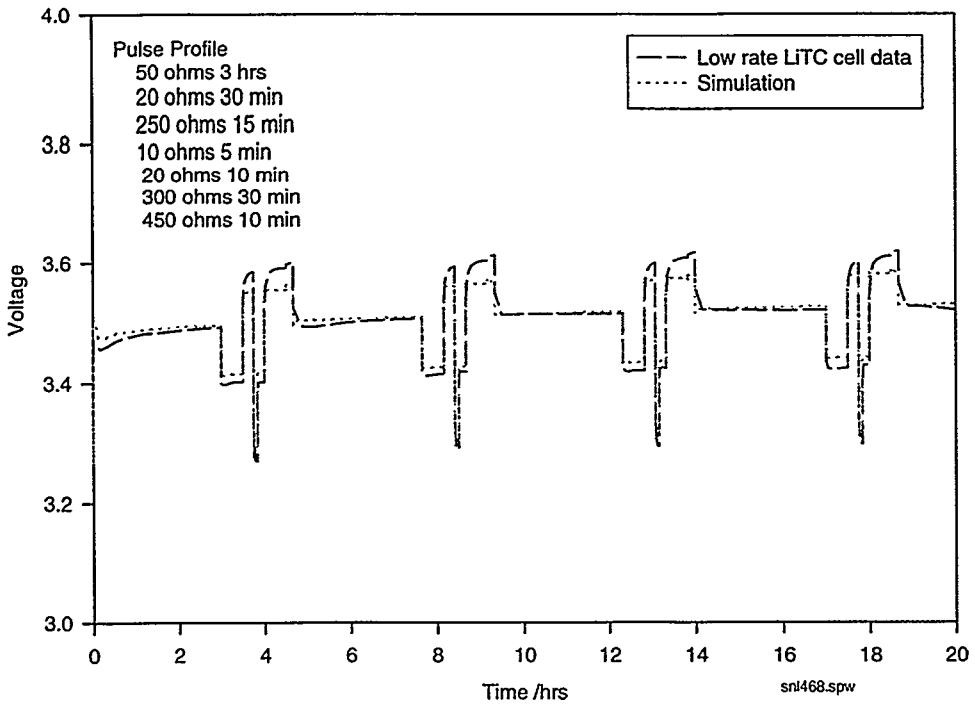

Figure 11-6. Comparison of the improved model and actual behavior of a low-rate lithium/thionyl chloride cell to a pulsed discharge at room temperature.

Finally, an example of one of the Li/MnO_2 models is shown. In the case of this chemistry, while the cell equivalent series resistance does increase at the end of discharge, the amount of change is relatively small. Consequently, the model employing the fixed equivalent series resistance can give a relatively good approximation of the actual behavior of the battery. This is illustrated in Figures 11-7 and 11-8, which show the predicted behavior of Varta and Sanyo 2/3A cells to a pulsed load. As expected, the model predicts different behavior for the two cells, and this is observed experimentally. The apparent discontinuities at the end of the discharge in the case of the Varta cell arises from the discontinuity in the look-up table used in the model. This abnormal behavior demonstrates the utility of using multiple replicate discharge curves to obtain average values and use of these average values in developing the model. Furthermore, these model predictions demonstrate that the model can predict battery performance under high pulse rate conditions. However, it should be noted that at even faster pulse rates, on the order of milliseconds in duration, the model may not accurately simulate the battery behavior and so should be used in a strictly qualitative fashion.

Besides the model's shortcomings outlined above, another issue that must be addressed is that the current models are not temperature tracking, that is, the temperature characteristics of the batteries are not explicitly included in the model. To overcome this limitation, at least for the immediate future, developing separate models for different temperature regimes seems to be the most expedient approach. However, modification of the original PSpice model framework to include temperature tracking capability is being considered. The data being collected to develop these individual models would then also be incorporated into the temperature tracking versions.

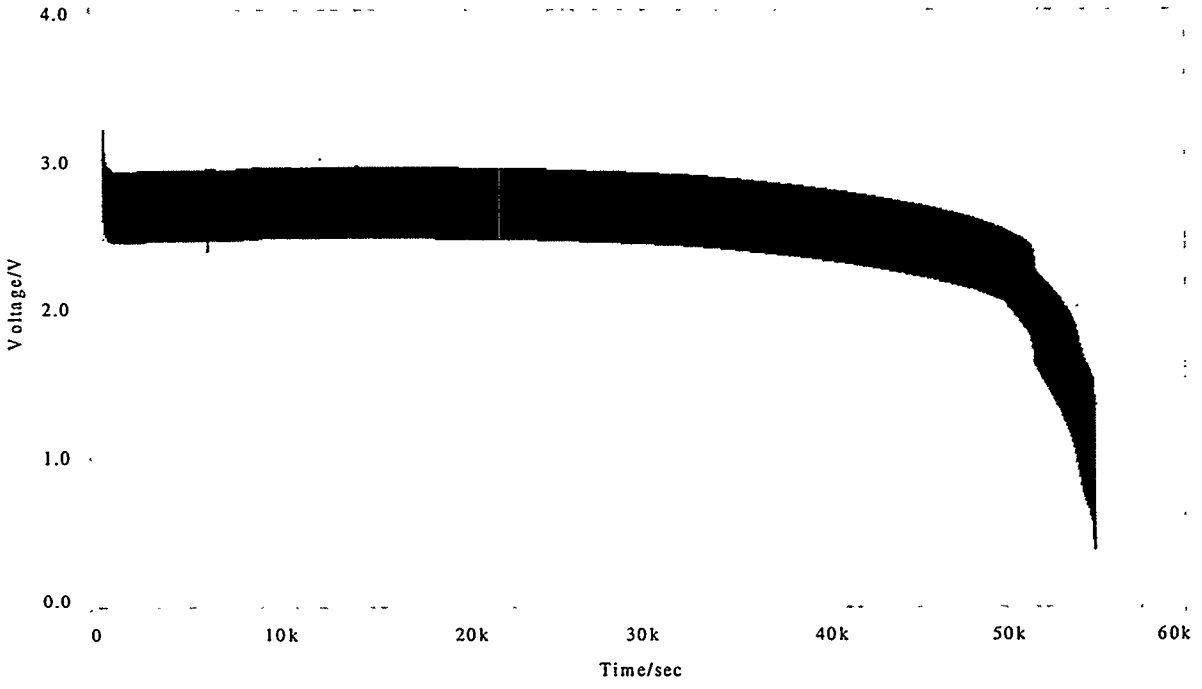

Figure 11-7. Example of model predictions of a Varta 2/3A cell under a pulse discharge of 3 sec at 714 mA followed by 17 sec at open circuit.

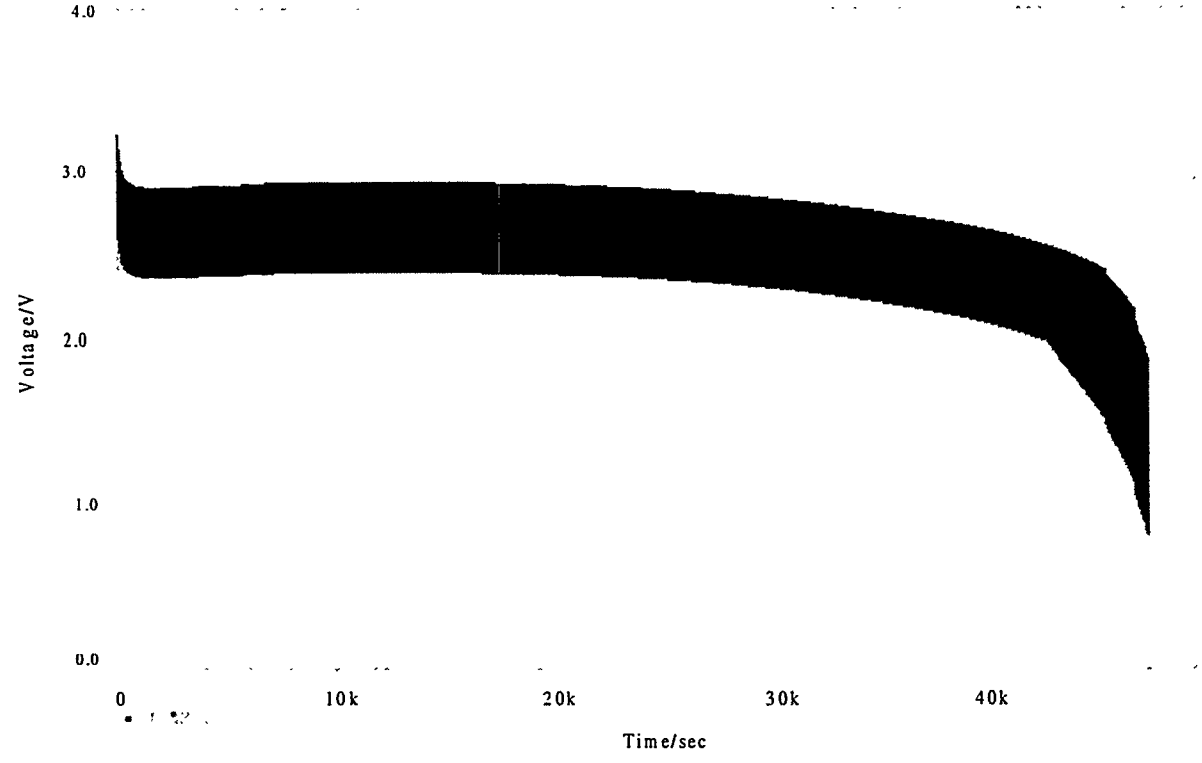

Figure 11-8. Example of model predictions of a Sanyo 2/3A cell under a pulse discharge of 3 sec at 714 mA followed by 17 sec at open circuit.

12. Summary and Conclusions

Nancy H. Clark

12.1 Summary of Evaluated Cells

The results of the characterization of Li/MnO_2 COTS individual cells and packs of cells in both series and parallel configurations has been reported in the previous sections. Table 12-1 shows all of the cells that were characterized by the respective suppliers.

Table 12-1. Li/MnO_2 Cells Studied

Vendor	2/3A	C	5/4C	D
Sanyo	+			
Sony	+			
Panasonic	+			
Varta	+			
Kodak	+			
Duracell	+			
Eveready	+			
Ultralife	+	+	+	
Ultralife-HR				+
Bluestar				+
Silberkraft		+	+	+
Silberkraft-HR		+	+	+

12.2 Cell Performance

Most of the measurements were performed on a Maccor tester with constant and pulse current loads. Some tests were performed using resistive loads. The type of load had little impact on the results; consequently the conclusions in this section are based on the current load data.

The capacity of all of the cells from each supplier was measured, and in some cases, multiple measurements were made on cells from particular suppliers. It was found that if the measurement were made at room temperature and at a low rate (<C/50), the nominal voltage was ~2.9 V. The measured capacities and the calculated energy and specific densities are summarized below.

Table 12-2. Summary of Room Temperature Data as a Function of Cell Size

Size	Capacity(Ah)	Gravimetric Energy Density (kW/KG)	Volumetric Energy Density (kW/L)
2/3A	1.2-1.6	200-270	500-630
C	5.1-5.7	225	470-495
5/4C	7.1	294	654
D	9.6-11	240-280	515-614

The capacity was also measured at higher rates and at various temperatures. For example, as the rate increased to 2C, the nominal voltage decreased to 2 V, and the total available capacity decreased by half. The decrease in temperature also decreased the capacity and the voltage. For example in D cells, the voltage decreased to ~2.5 V, and the capacity decreased by 20% at –40°C for the standard type of cells. In the versions designed for high rate and low temperature the voltage drop was the same, but the loss in capacity was less than 10%. However, if any of the cells that were tested at low temperature, were warmed to room temperature the remaining capacity that was not removed at low temperature became available.

In cases where multiple cells of a given size from the same supplier were measured and standard deviations were calculated, the standard deviations were less than 4% except at low temperatures for devices not designed for use under these conditions. In the worst cases such as Silberkraft M20 D cells a bimodal distribution of capacity was found at –55°C, with one mode being 0.35 Ah and the other being 5.8 Ah. Using data from 2/3A cells, initial results show it is possible to model these variations using a combination of Bootstrap and artificial intelligence techniques. However, more work is necessary to evaluate the results for a given cell.

The results from operating these cells in various pulse profiles showed essentially the same patterns as in the capacity measurements. Low temperature and higher currents result in lower measured capacities. The new factor in pulsed environments was the rest period between pulses. It was found that particularly at low temperatures, if the rest period is on the order of minutes, the capacity removed at low temperatures is essentially the same as at room temperature—with the rest period only lasting several seconds, the measured capacity is 25% to 75% less.

PSpice models that were developed using characteristics of some of the batteries are quite good for room temperature pulse data.

Pulse data were also used to measure performance in old (aged) and cold cells. Data were collected on both 2/3A cells, which were aged for about two years and D cells, which were aged for at least 60 days. The results showed that at most, cells require 2 sec of current pulse to perform like new cells. This is in contrast to other chemistries that may require 2- to 3- to 5-sec pulses in order to perform as they did when they were new.

Tests were also performed to see how a cell behaved in short circuit and reversal modes. D cells and battery packs of D cells vented under both conditions. In one case, the venting in a single cell resulted in the ignition of the solvent. Ignition of the solvent occurred in all battery pack tests. If bypass diodes are used, this problem can be avoided. These results indicate that packs using D cells require additional safety features. Similar tests were performed on 2/3A cells; cell case temperatures increased and, after

cool-down, some cells were shorted and unusable. This indicates that the PTC fuse is sufficient in this size range and additional safety features may not be necessary.

12.3 Intrinsic Characteristics

The gross physical characteristics are essentially the same for cells of a given size independent of the manufacturer or of the fact that there is little variability, which indicates manufacturing processes are effective at eliminating this variability. The gross internal features, however, show more variations between suppliers. In the 2/3 A cells, the major variations are in how the connections are made to the electrodes. In the D cells, cell construction is different from supplier to supplier. Electrode systems use a variety of solvents. Other specific components also vary. The microscopic characterization of Li/MnO_2 cells was done by using X-ray diffraction and SEM, which showed variability from supplier to supplier. The data acquired on selected samples using all of these techniques show the potential to use them to predict performance.

12.4 Summary

Our evaluations led us to make the following statements about the performance of the Li/MnO_2 cells:

- Li/MnO_2 cells have predictable energy and power densities.
- The variability within a given lot of cells is low and may be predictable as long as performance requirements are not at the extremes.
- Approximately 2 sec are required to achieve the desired voltage at low temperature extremes with aged cells.
- Performance can be successfully modeled using PSpice.
- Performance degrades under extreme temperature conditions, but lost performance can be recovered after return to nominal conditions.
- Performance for a particular environment can be engineered into the cell, but performance in one environment is sometimes achieved by sacrificing performance in another environment.
- Larger (C, 5/4C, and D) Li/MnO_2 cells require additional safety devices to protect cells in reversal or short circuit mode.
- The loaded voltage is a function of temperature and load.
- The shape of the curve of the voltage change and the time to a preset voltage can vary from cell to cell particularly at the performance extremes.
- MnO_2 cells will perform safely in a variety of applications over a broad range of temperatures if fuse and diodes are a part of the design.

This page intentionally left blank

Cumulative Listing of Tests Performed on Li/MnO_2 Cells and Batteries

Jill L. Langendorf and Lorie E. Davis

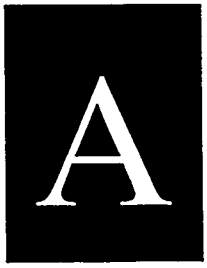

Appendix A
Cumulative Listing of Tests Performed on Li/MnO_2 Cells and Batteries

This appendix is a compilation of the tests that have been performed to date on all cells and cell configurations employing Li/MnO_2 chemistries. The data presented in the earlier chapters are select presentation of some of the data making up this database. These data are available in digital format and all will be published in a separate stand alone document with the original data files intact.

Table A-1

Ultralife C-cell:	**U2550VH-T2-UF**			
Filename	**Current**	**End Cond.**	**Temperature**	**Date**
Constant Current Tests:				
U255D50	50 Ma	0.5 V	RT	11/06/97
U255D500	500 mA	0.5 V	RT	11/06/97
U255D103	1 A	0.5 V	RT	11/06/97
U255D203	2 A	0.5 V	RT	11/06/97
CM40D50	50 mA	0.5 V	–40°C	11/10/97
CM40D50A	50 mA	0.5 V	cont @ RT	
CM40D500	500 mA	0.5 V	–40°C	11/12/97
CM40D500A	500 mA	0.5 V	cont @ RT	
CM40D103	1 A	0.5 V	–40°C	11/12/97
CM40D1A	1 A	0.5 V	cont @ RT	
CM40D203	2 A	0.5 V	–40°C	11/11/97
CM40D2A	2 A	0.5 V	cont @ RT	
	50 mA	0.5 V	–20°C	
	500 mA	0.5 V	–20°C	
	1 A	0.5 V	–20°C	
	2 A	0.5 V	–20°C	
UC70D50	50 mA	0.5 V	70°C	11/12/97
UC70D500	500 mA	0.5 V	70°C	11/12/97
UC70D103	1 A	0.5 V	70°C	11/18/97
UC70D203	2 A	0.5 V	70°C	1/14/98
Pulse Discharge	Pulse Profile:	3 seconds 3 A		sample every .02 V or ::0.5
		27 seconds off		sample every .02 V or ::2
		end when pulse voltage <0.5 V		
CPLSM40		3 A	–40°C	11/10/97
CPLSM40A			–40°C	
CPLSM40B			cont @ RT	
CPLSM20			–20°C	11/13/97
CPLSM20A			cont @ RT	
			0°C	
CPLSRT		3 A	RT	11/10/97
CPLSRTA			RT	
UCPLS70			70°C	1/14/98
Resistive Load Tests:				
UCDRM30	2 Ω	2.0 V	–30	2/17/98

Table A-2

Low Temp Silberkraft D Cells M20 TT - Variability Studies				
PULSE DISCHARGE				
Pulse Profile:	3 sec at 5.0 A			
	17 sec off	sample every .02 V or ::0.5		
	end when pulse voltage <0.5 V	sample every .02 V or ::0.5		
Filename			Temp.	Date
DTT40P1 , A			-40°C	2/2/98
DTT40P2 , A			-40°C	2/2/98
DTT40P3			-40°C	2/3/98
DTT40P4			-40°C	2/3/98
DTT40P7			-40°C	
DTT40P8			-40°C	
DTT40P9			-40°C	
DTT40P10			-40°C	
DTT40P11			-40°C	
DTT40P12			-40°C	
DTT40P13			-40°C	
DTT40P14			-40°C	
DTT40P15			-40°C	
DTT40P16			-40°C	
DTT40P17			-40°C	
DTTM20P1			-20°C	2/26/98
DTTRTP1			RT	2/24/98
			70°C	
DW STYLE PULSING:				
DTTDWP5	5 A	0.5V	-40°C	2/12/98
Pulse Profile:	3 sec at 4.0 A			
	17 sec off	sample every .02 V or ::0.5		
	end when pulse voltage <0.5 V	sample every .02 V or ::0.5		
DTT40P5			-40°C	2/5/98
DTT40P5A			RT	
DTT40P6			-40°C	2/5/98
DTT40P6A			RT	
Pulse Profile:	3 sec at 3.0 A	sample every .02V or ::0.5		
	17 sec off	sample every .02V or ::0.5		
	end when pulse voltage <0.5 V			
DTT40P31			-40°C	2/6/98
DTT4P31A			RT	
DTT40P32			-40°C	2/6/98
DTT4P32A			RT	
INTERIM TESTING : following skdp403,skdp404				
DTT40CC3	CC 40mA	0.5 V end	cont @ -40°C	
DTTDWP3	DW type pulse	0.5 V end	cont @ -40°C	
DTTRTCC3	CC 50mA	0.5 V end	RT	
DTT40CC4	CC 40mA	0.5 V end	cont @ -40°C	

DTTDWP4	DW type pulse	0.5 V end	cont @ –40°C	
DTTRTCC4	CC 50mA	0.5 V end	RT	
FOUR IN SERIES:				
4DTTM40			–40°C	2/9/98
4DTTM40A			cont @ RT	
Separated Cells (from above series):				
DTTM4A1			cont @ RT	
DTTM4A2			cont @ RT	
DTTM4A3			cont @ RT	
DTTM4A4			cont @ RT	
Constant Current 50mA Discharge to 0.5V				
Variability Studies				
DTTCC40A	50 mA	0.5 V	–40°C	2/16/98
DTTCC40B	50 mA	0.5 V	–40°C	2/16/98
DTTCC40C	50 mA	0.5 V	–40°C	2/16/98
DTTCC40D	50 mA	0.5 V	–40°C	2/16/98
DTTCC40E	50 mA	0.5 V	–40°C	2/16/98
DTTCC40F	50 mA	0.5 V	–40°C	2/16/98
DTTCC40G	50 mA	0.5 V	–40°C	2/16/98
DTTCC40H	50 mA	0.5 V	–40°C	2/16/98
	50 mA	0.5 V	–40°C	
	50 mA	0.5 V	–40°C	
	50 mA	0.5 V	–40°C	
	50 mA	0.5 V	–40°C	
	50 mA	0.5 V	–40°C	
	50 mA	0.5 V	–40°C	
	50 mA	0.5 V	–40°C	
DTTCC55A	50 mA	0.5 V	–55°C	1/6/98
DTT55RTA	50 mA	0.5 V	RT	
DTTCC55B	50 mA	0.5 V	–55°C	1/6/98
DTT55RTB	50 mA	0.5 V	RT	
DTTCC55C	50 mA	0.5 V	–55°C	1/6/98
DTT55RTC	50 mA	0.5 V	RT	
DTTCC55D	50 mA	0.5 V	–55°C	1/6/98
DTT55RTD	50 mA	0.5 V	RT	
DTTCC55E	50 mA	0.5 V	–55°C	1/6/98
DTT55RTE	50 mA	0.5 V	RT	
DTTCC55F	50 mA	0.5 V	–55°C	1/6/98
DTT55RTF	50 mA	0.5 V	RT	
DTTCC55G	50 mA	0.5 V	–55°C	1/6/98
DTT55RTG	50 mA	0.5 V	RT	
DTTCC55H	50 mA	0.5 V	–55°C	1/6/98
DTT55RTH	50 mA	0.5 V	RT	
	50 mA	0.5 V	–55°C	
	50 mA	0.5 V	–55°C	
	50 mA	0.5 V	–55°C	
	50 mA	0.5 V	–55°C	
	50 mA	0.5 V	–55°C	
	50 mA	0.5 V	–55°C	
DTTCC30A	50 mA	0.5 V	–30°C	1/6/98
DTTCC30B	50 mA	0.5 V	–30°C	1/6/98

DTTCC30C	50 mA	0.5 V	–30°C	1/6/98
DTTCC30D	50 mA	0.5 V	–30°C	1/6/98
DTTCC30E	50 mA	0.5 V	–30°C	1/6/98
DTTCC30F	50 mA	0.5 V	–30°C	1/6/98
	50 mA	0.5 V	–30°C	
	50 mA	0.5 V	–30°C	
	50 mA	0.5 V	–30°C	
	50 mA	0.5 V	–30°C	
	50 mA	0.5 V	–30°C	
	50 mA	0.5 V	–30°C	
	50 mA	0.5 V	–30°C	
	50 mA	0.5 V	–30°C	
	50 mA	0.5 V	–30°C	
	50 mA	0.5 V	–20°C	
DTTCCRT	50 mA	0.5 V	RT	2/9/98
DTTCCRTA	50 mA	0.5 V	RT	2/11/98
DTTCCRTB	50 mA	0.5 V	RT	2/11/98
DTTCCRTC	50 mA	0.5 V	RT	2/11/98
DTTCCRTD	50 mA	0.5 V	RT	2/11/98
DTTCCRTE	50 mA	0.5 V	RT	2/11/98
DTTCCRTF	50 mA	0.5 V	RT	2/11/98
DTTCCRTG	50 mA	0.5 V	RT	2/11/98
DTTCCRTH	50 mA	0.5 V	RT	2/11/98
	50 mA	0.5 V	RT	
	50 mA	0.5 V	RT	
	50 mA	0.5 V	RT	
	50 mA	0.5 V	RT	
	50 mA	0.5 V	RT	
	50 mA	0.5 V	RT	

Table A-3

SILBERKRAFT D-cell	Fresh Cell	Type M 20		
Constant Current Tests				
Filename	Current	End Cond.	Temperature	Date
SKDD50RT	50 mA	0.5 V	RT	1/9/98
SKDM40	50 mA	0.5 V	m40°C	1/6/98
SKDM40A	continuation RT	0.5 V	RT	
SKDM20	50 mA	0.5 V	m20°C	1/28/98
SKD5070	50 mA	0.5 V	70°C	1/13/98
SKDDM55	30 mA	0.5 V	m55°C	1/30/98
SKDDM55A	continuation RT	0.5 V	RT	2/2/98
SKDDM55B	continuation RT	0.5 V	RT	2/5/98
PULSE DISCHARGE				
Pulse Profile:	3 sec at 5.0 A	sample every .02 V or ::0.5		
	17 sec off	sample every .02 V or ::2		
	end when pulse voltage <0.5 V			
SKDPLM40			m40°C	1/6/98
SKDPLM4A	continuation RT		RT	
SKDPLM20			m20°C	1/14/98
SKDPLM2A	continuation RT		RT	
SKDPLSZ			0°C	1/28/98
SKDPLSZA	continuation RT		RT	
SKDPLSRT			RT	1/6/98
			70°C	
SKDPM55			m55°C	1/30/98
	continuation RT			
FOUR IN SERIES:				
4SKDM40			m40°C	1/16/98
4SKDM40A	continuation RT		RT	
4SKDM20			m20°C	1/14/98
4SKDM20A	continuation RT		RT	
4SKDRT			RT	1/14/98
Pulse Profile:	3 sec at 4.0 A	sample every .02 V or ::0.5		
	17 sec off	sample every .02 V or ::2		
	end when pulse voltage <0.5 V			
SKDP4M40			m40°C	1/16/98
SKDP4M4A	continuation RT		RT	
SKDP4RT			RT	1/20/98

Table A-4

Ultralife 5/4 C-cell				
U2560VH-T2-UF				
Filename	Current	End Cond.	Temperature	Date
constant current				
U256D50	50 mA	0.5 V	room temp	
U256D500	500 mA	0.5 V	room temp	
U256D103	1 A	0.5 V	room temp	
U256D203	2 A	0.5 V	room temp	
54M40D50	50 mA	0.5 V	–40°C	
54M4AD50	50mA	0.5 V	–40°C	
54M40D12	500 mA	0.5 V	–40°C	
54M4AD12	500mA	0.5 V	–40°C	
54M4OD1	1 A	0.5 V	–40°C	
54M4OD1A	2 A	0.5 V	–40°C	
54M40D2	2 A	0.5 V	–40°C	
54M40D2A	3 A	0.5 V	–40°C	
	50 mA	0.5 V	–20°C	
	500 mA	0.5 V	–20°C	
	1 A	0.5 V	–20°C	
	2 A	0.5 V	–20°C	
5470D50	50 mA	0.5 V	70°C	11/12/97
5470D500	500 mA	0.5 V	70°C	
5470D103	1 A	0.5 V	70°C	
	2 A	0.5 V	70°C	
Pulse Discharge				
Pulse Profile:				
	3 sec 3 A		sample every .02 V or ::0.5	
	27 sec off		sample every .02 V or ::2	
	end when pulse voltage <0.5 V			
54PLSM40			–40°C	
54PLSM4A			–40°C	
54PLSM4B			–40°C	
54PLSM20			–20°C	11/13/97
54PLSM2A			–20°C	
			0°C	
54PLSRT			room temp.	
			70°C	

Table A-5

2/3 A - SEVEN IN PARALLEL					
Pulse Discharge:					
Filename	Manufacturer	Configuration	Temperature	Date	Maccor
Pulse Profile:	3 sec 5A	sample every .02 V or ::0.5			
	17 sec off	sample every .02 V or ::2			
	end when pulse voltage <0.5 V				
SA7PLM40	Sanyo	parallel – seven	–40°C	11/11/97	8(6)
SA7PLM4A	Sanyo	parallel - seven	cont. @ RT		
SA7PLM20	Sanyo	parallel - seven	–20°C	11/14/97	8(3)
SA7PLM2A	Sanyo	parallel - seven	cont. @ RT		8(7)
	Sanyo	parallel - seven	0°C		
SAPLSRT	Sanyo	parallel - seven	room temp.	11/11/97	8(7)
	Sanyo	parallel - seven	70°C		
SO7PLM40	Sony	parallel - seven	–40°C	11/11/97	8(3)
SO7PLM4A	Sony	parallel - seven	cont. @ RT		
SO7PLM20	Sony	parallel - seven	–20°C	11/14/97	8(2)
SO7PLM2A	Sony	parallel - seven	cont. @ RT		8(1)
	Sony	parallel - seven	0°C		
SOPLSRT	Sony	parallel - seven	room temp.	11/11/97	8(1)
	Sony	parallel - seven	70°C		
V7PLM40	Varta	parallel - seven	–40°C	11/12/97	8(2)
V7PLM40A	Varta	parallel - seven	cont. @ RT		8(1)
V7PLM20	Varta	parallel - seven	–20°C	11/13/97	8(3)
V7PLM20A	Varta	parallel - seven	cont. @ RT		8(7)
	Varta	parallel - seven	0°C		
	Varta	parallel - seven	room temp.		
	Varta	parallel - seven	70°C		
U7PLM40	Ultralife	parallel - seven	–40°C	11/12/97	8(3)
U7PLM40A	Ultralife	parallel - seven	cont. @ RT		8(7)
U7PLM20	Ultralife	parallel - seven	–20°C	11/13/97	8(2)
U7PLM20A	Ultralife	parallel - seven	cont. @ RT		8(1)
	Ultralife	parallel - seven	0°C		
U7PLSRT	Ultralife	parallel - seven	room temp.	1/20/98	8(7)
	Ultralife	parallel – seven	70°C		

Table A-6

Pulse Discharge using Bluestar D			
Pulse Profile:	3 sec 5 A	sample every .02 V or ::0.5	
	17 sec off	sample every .02 V or ::2	
	end when pulse voltage <0.5 V		
Filename	Temperature	Date	Maccor
BSDPM40	–40°C	11/12/97	8(6)
BSDPM4A	cont. RT		8(4)
BSDPM20	–20°C	11/15/98	8(2)
BSDPM2A	cont. RT		8(1)
	0°C		
BSDPLRT	room temp.	12/12/97	8(4)
	70°C		
FOUR IN SERIES			
4BSDPRT	RT	12/16/97	8(1)
4BSDPM40	–40°C	01/20/98	8(2)
4BSDPM4A	cont. RT	01/21/98	8(8)
Constant Current Tests:	50 mA to 0.5 V		
Filename	Temperature	Date	Maccor
BSD50M40	–40°C	12/9/97	8(6)
BSD50M4A	cont. RT		8(7)
BSD50RT	RT	1/16/98	64(42)
Pulse Discharge using Ultralife D			
Pulse Profile:	3 sec 5 A	sample every .02 V or ::0.5	
	17 sec off	sample every .02 V or ::2	
	end when pulse voltage <0.5 V		
Filename	Temperature	Date	Maccor
UDPLSM40	–40°C	11/12/97	8(5)
UDPLSM4A	cont. RT		8(8)
UDPLSM20	–20°C	11/15/97	8(3)
UDPLSM2A	cont. RT		8(7)
	RT		
Constant Current Tests:	50 mA to 0.5 V		
Filename	Temperature	Date	Maccor
	–40°C		
	cont. RT		
	RT		
Eagle Pitcher EPDRT	RT	1/5/98	64(33)

Table A-7

Pulse Discharge Single 2/3A Cells				
Fresh Cells				
Filename	Manufacturer	Temperature	Date	Maccor
Pulse Profile:	3 sec 714 mA	sample every .02 V or ::0.5		
	17 sec off	sample every .02 V or ::2		
	end when pulse voltage <0.5 V			
VCRPM40	Varta	–40°C	11/05/97	64(59)
	Varta	–20°C		
	Varta	0°C		
VCRD714	Varta	room temp.	11/03/97	64(21)
VPLS60	Varta	60°C	11/05/97	64(22)
SOPLSM40	Sony	–40°C	11/11/97	64(9)
SOPLSM4A	Sony	cont. at RT		64(45)
	Sony	–20°C		
	Sony	0°C		
SOPLSRT	Sony	room temp.	11/10/97	64(47)
SOPLS60	Sony	60°C	11/11/97	64(23)
SAPLSM40	Sanyo	–40°C	11/11/97	64(10)
SAPLSM4A	Sanyo	cont. at RT		64(46)
	Sanyo	–20°C		
	Sanyo	0°C		
SAPLSRT	Sanyo	room temp.	11/10/97	64(48)
SAPLS60	Sanyo	60°C	11/11/97	64(24)
Constant Current Discharge Tests				
Single 2/3 A Cells				
SO23D10	Sony	RT	11/12/97	64(2)
U23D10	Ultralife	RT	11/12/97	64(3)

Table A-8

Constant Current 10 mA Discharge to 0.5 V			
Tests within lot #			
Filename	Lot #	Manufacturer	Temperature
SO10RT1	7636	Sony	RT
SO10RT2	7636	Sony	RT
SO10RT3	7636	Sony	RT
SO10RT4	7636	Sony	RT
SO10RT5	7636	Sony	RT
SO10RT6	7636	Sony	RT
SO10RT7	7636	Sony	RT
SO10RT8	7636	Sony	RT
SO10RT9	7636	Sony	RT
SO10RT10	7636	Sony	RT
SO10RT11	7636	Sony	RT
SO10RT12	7636	Sony	RT
SO10RT13	7636	Sony	RT
SO10RT14	7636	Sony	RT
SO10RT15	7636	Sony	RT

Table A-9

Constant Current 10 mA Discharge to 0.5 V				
Tests within lot #				
Filename	Lot #	Manufacturer	Temperature	Date
DL10RT1	713013	Duracell	RT	1/13/98
DL10RT2	713013	Duracell	RT	1/13/98
DL10RT3	713013	Duracell	RT	1/13/98
DL10RT4	713013	Duracell	RT	1/13/98
DL10RT5	713013	Duracell	RT	1/13/98
DL10RT6	713013	Duracell	RT	1/13/98
DL10RT7	713013	Duracell	RT	1/13/98
DL10RT8	713013	Duracell	RT	1/13/98
DL10RT9	713013	Duracell	RT	1/13/98
DL10RT10	713013	Duracell	RT	1/13/98
DL10RT11	713013	Duracell	RT	1/13/98
DL10RT12	713013	Duracell	RT	1/14/98
DL10RT13	713013	Duracell	RT	1/20/98
DL10RT14	713013	Duracell	RT	1/20/98
DL10RT15	713013	Duracell	RT	1/20/98
DL10M20A	713013	Duracell	–20°C	1/28/98
DL10M20B	713013	Duracell	–20°C	1/28/98
DL10M20C	713013	Duracell	–20°C	1/28/98
DL10M20D	713013	Duracell	–20°C	1/28/98
DL10M20E	713013	Duracell	–20°C	1/28/98
DL10M20F	713013	Duracell	–20°C	1/28/98
DL10M20G	713013	Duracell	–20°C	1/28/98
DL10M20H	713013	Duracell	–20°C	1/28/98
DL10M20I	713013	Duracell	–20°C	1/28/98
DL10M20J	713013	Duracell	–20°C	1/28/98

Table A-10

Pulse Discharge Single 2/3A Cells			
Aged Cells			
Filename	Manufacturer / Lot #	Temperature	Date
Pulse Profile:	5 sec 714 mA sample every .02 V or :: 0.2		
	17 sec off	sample every .04 V or ::2	
	3 sec 714 mA	sample every .03 V or ::0.6	
	17 sec off	sample every .04 V or ::2	
	end when pulse voltage <0.5 V		
DAGEM40A	Duracell / 5J30X	m40°C	11/18/97
DAGEM40B	Duracell / 5J30X	m40°C	11/18/97
DAGEM40C	Duracell / 5127X	m40°C	11/18/97
DAGEM40D	Duracell / 5127X	m40°C	11/18/97
SAGEM40A	Sanyo	m40°C	11/18/97
SAGEM40B	Sanyo	m40°C	11/18/97
SAGEM40C	Sanyo	m40°C	11/18/97
SAGEM40D	Sanyo	m40 C	11/18/97
GOVERNMENT CELLS			
Fresh Cells			
Filename	Manufacturer / Lot #	Temperature	Date
Pulse Profile:	17 sec off	sample every .02 V or ::2	
	3 sec 714 mA	sample every .02 V or ::0.5	
	end when pulse voltage <0.5 V		
G024PM40		m40°C	12/15/97
G024PM4A		cont. at RT	
G049PM40		m40°C	12/15/97
G049PM4A		cont. at RT	
G021PRT		RT	12/16/97
G059PRT		RT	12/16/97
Constant Current Discharge Tests:			
G036D10	10 mA / 0.5V end	RT	12/15/97
G050D10	10 mA / 0.5V end	RT	12/15/97

Table A-11

Silberkraft D Cells M20 - Variability Studies				
PULSE DISCHARGE				
Pulse Profile:	3 sec at 5.0 A	sample every .02 V or ::0.5		
	17 sec off	sample every .02 V or ::0.5		
	end when pulse voltage <0.5 V			
Filename			Temp.	Date
SKDP401, A			-40°C	2/2/98
SKDP402, A			-40°C	2/2/98
SKDP403			-40°C	2/3/98
SKDP404			-40°C	2/3/98
SKDP407			-40°C	
SKDP408			-40°C	
SKDP409			-40°C	
SKDP410			-40°C	
SKDP411			-40°C	
SKDP412			-40°C	
SKDP413			-40°C	
SKDP414			-40°C	
SKDP415			-40°C	
SKDP416			-40°C	
SKDP417			-40°C	
DW STYLE PULSING:				
SKDDWP5	5 A	0.5 V	-40°C	2/12/98
Pulse Profile:	3 sec at 4.0 A	sample every .02 V or ::0.5		
	17 sec off	sample every .02 V or ::0.5		
	end when pulse voltage <0.5 V			
SKDP405			-40°C	2/5/98
SKDP405A			RT	
SKDP406			-40°C	2/5/98
SKDP406A			RT	
Pulse Profile:	3 sec at 3.0 A	sample every .02 V or ::0.5		
	17 sec off	sample every .02 V or ::0.5		
	end when pulse voltage <0.5 V			
SKD40P31			-40°C	2/6/98
SKD4P31A			cont at RT	2/11/98
SKD40P32			-40°C	2/6/98
SKD4P32A			cont at RT	2/11/98
Filename			Temp.	Date
INTERIM TESTING : following skdp403,skdp404				

SKDD403	CC 40 mA	0.5 V end	cont @ –40	
SKDW403	DW type pulse	0.5 V end	cont @ –40	
SKDDRT3	CC 50 mA	0.5 V end	RT	
SKDD404	CC 40 mA	0.5 V end	cont @ –40	
SKDW404	DW type pulse	0.5 V end	cont @ –40	
SKDDRT4	CC 50 mA	0.5 V end	RT	
Constant Current 50 mA Discharge to 0.5 V				
Variability Studies				
Filename	Current	End Cond.	Temp.	Date
SKDCC40A	50 mA	0.5 V	–40°C	1/6/98
SKD40RTA	50 mA	0.5 V	cont @ rt	
SKDCC40B	50 mA	0.5 V	–40°C	1/6/98
SKD40RTB	50 mA	0.5 V	cont @ rt	
SKDCC40C	50 mA	0.5 V	–40°C	1/6/98
SKD40RTC	50 mA	0.5 V	cont @ rt	
SKDCC40D	50 mA	0.5 V	–40°C	1/6/98
SKD40RTD	50 mA	0.5 V	cont @ rt	
SKDCC40E	50 mA	0.5 V	–40°C	1/6/98
SKD40RTE	50 mA	0.5 V	cont @ rt	
SKDCC40F	50 mA	0.5 V	–40°C	1/6/98
SKD40RTF	50 mA	0.5 V	cont @ rt	
SKDCC40G	50 mA	0.5 V	–40°C	1/6/98
SKD40RTG	50 mA	0.5 V	cont @ rt	
SKDCC40H	50 mA	0.5 V	–40°C	1/6/98
SKD40RTH	50 mA	0.5 V	cont @ rt	
	50 mA	0.5 V	–40°C	
	50 mA	0.5 V	–40°C	
	50 mA	0.5 V	–40°C	
	50 mA	0.5 V	–40°C	
	50 mA	0.5 V	–40°C	
	50 mA	0.5 V	–40°C	
	50 mA	0.5 V	–40°C	
SKDCC55A	50 mA	0.5 V	–55°C	1/6/98
SKD55RTA	50 mA	0.5 V	cont @ RT	
SKDCC55B	50 mA	0.5 V	–55°C	1/6/98
SKD55RTB	50 mA	0.5 V	cont @ RT	
Filename	Current	End Cond.	Temp.	Date
SKDCC55C	50 mA	0.5 V	–55°C	1/6/98
SKD55RTC	50 mA	0.5 V	cont @ RT	
SKDCC55D	50 mA	0.5 V	–55°C	1/6/98
SKD55RTD	50 mA	0.5 V	cont @ RT	
SKDCC55E	50 mA	0.5 V	–55°C	1/6/98
SKD55RTE	50 mA	0.5 V	cont @ RT	
SKDCC55F	50 mA	0.5 V	–55°C	1/6/98

SKD55RTF	50 mA	0.5 V	cont @ RT	
SKDCC55G	50 mA	0.5 V	–55°C	1/6/98
SKD55RTG	50 mA	0.5 V	cont @ RT	
SKDCC55H	50 mA	0.5 V	–55°C	1/6/98
SKD55RTH	50 mA	0.5 V	cont @ RT	
	50 mA	0.5 V	–55°C	
	50 mA	0.5 V	–55°C	
	50 mA	0.5 V	–55°C	
	50 mA	0.5 V	–55°C	
	50 mA	0.5 V	–55°C	
	50 mA	0.5 V	–55°C	
	50 mA	0.5 V	–55°C	
SKDCC30A	50 mA	0.5 V	–30°C	1/6/98
SKDCC30B	50 mA	0.5 V	–30°C	1/6/98
SKDCC30C	50 mA	0.5 V	–30°C	1/6/98
SKDCC30D	50 mA	0.5 V	–30°C	1/6/98
SKDCC30E	50 mA	0.5 V	–30°C	1/6/98
SKDCC30F	50 mA	0.5 V	–30°C	1/6/98
	50 mA	0.5 V	–30°C	
	50 mA	0.5 V	–30°C	
	50 mA	0.5 V	–30°C	
	50 mA	0.5 V	–30°C	
	50 mA	0.5 V	–30°C	
	50 mA	0.5 V	–30°C	
	50 mA	0.5 V	–30°C	
	50 mA	0.5 V	–30°C	
	50 mA	0.5 V	–30°C	
SKDCCRTA	50 mA	0.5 V	RT	2/11/98
SKDCCRTB	50 mA	0.5 V	RT	2/11/98
SKDCCRTC	50 mA	0.5 V	RT	2/11/98
Filename	Current	End Cond.	Temp.	Date
SKDCCRTD	50 mA	0.5 V	RT	2/11/98
SKDCCRTE	50 mA	0.5 V	RT	2/11/98
SKDCCRTF	50 mA	0.5 V	RT	2/11/98
SKDCCRTG	50 mA	0.5 V	RT	2/11/98
SKDCCRTH	50 mA	0.5 V	RT	2/11/98
	50 mA	0.5 V	RT	
	50 mA	0.5 V	RT	
	50 mA	0.5 V	RT	
	50 mA	0.5 V	RT	
	50 mA	0.5 V	RT	
	50 mA	0.5 V	RT	
	50 mA	0.5 V	RT	

Table A-12

Constant Current 10mA Discharge to 0.5 V					
Tests within lot #					
2/3 A Cells					
Filename	Lot #	Manufacturer	Temperature	Date	Maccor
SA10M20A	AI	SANYO	–20°C	12/9/97	64/31
SA10M20B	AL	SANYO	–20°C	12/9/97	64/32
SA10M20C	AL	SANYO	–20°C	12/9/97	64/40
SA10M20D	AL	SANYO	–20°C	12/9/97	64/41
SA10M20E	AI	SANYO	–20°C	12/9/97	64/42
SA10M20F	AI	SANYO	–20°C	12/9/97	64/43
SA10M20G	AL	SANYO	–20°C	12/9/97	64/44
SA10M20H	AI	SANYO	–20°C	12/9/97	64/51
SA10M20I	AL	SANYO	–20°C	12/9/97	64/52
SA10M20J	AL	SANYO	–20°C	12/16/97	64/31
SA10M20K	AL	SANYO	–20°C	12/16/97	64/32
SA10M20L	AL	SANYO	–20°C	12/16/97	64/40
SA10M20M	AL	SANYO	–20°C	12/16/97	64/41
SA10M20N	AL	SANYO	–20°C	12/16/97	64/42
SA10M20O	AL	SANYO	–20°C	12/16/97	64/43
SA10M20P	AL	SANYO	–20°C	12/16/97	64/44
SA10M20Q	AL	SANYO	–20°C	12/16/97	64/51
SA10M20R	AL	SANYO	–20°C	12/16/97	64/52
SA10M20S	AL	SANYO	–20°C	1/28/98	64(44)
SAD10RT1	AI	SANYO	RT	12/11/97	64/1
SAD10RT2	AI	SANYO	RT	12/11/97	64/7
SAD10RT3	AI	SANYO	RT	12/11/97	64/33
SAD10RT4	AI	SANYO	RT	12/11/97	64/34
SAD10RT5	AI	SANYO	RT	12/11/97	64/35
SAD10RT6	AI	SANYO	RT	12/11/97	64/36
SAD10RT7	AL	SANYO	RT	12/11/97	64/37
SAD10RT8	AI	SANYO	RT	12/11/97	64/38
SAD10RT9	AI	SANYO	RT	12/11/97	64/39
SA10RT10	AI	SANYO	RT	12/15/97	64/2
SA10RT11	AL	SANYO	RT	12/16/97	32/1
SA10RT12	AL	SANYO	RT	12/16/97	32/4
Constant Current 10mA Discharge to 0.5 V					
Tests within lot #					
2/3 A Cells					
Filename	Lot #	Manufacturer	Temperature	Date	Maccor
SA10RT13	AL	SANYO	RT	12/16/97	32/5
SA10RT14	AL	SANYO	RT	12/16/97	32/6
SA10RT15	AL	SANYO	RT	12/16/97	32/7
SA10RT16	AL	SANYO	RT	12/16/97	32/8
SA10RT17	AL	SANYO	RT	12/16/97	32/15
SA10RT18	AL	SANYO	RT	12/16/97	32/16
SA10RT19	AL	SANYO	RT	12/16/97	32/17

SA10RT20	AL	SANYO	RT	12/16/97	32/18
SA10RT21	AL	SANYO	RT	12/17/97	64/3
SA10RT22	AL	SANYO	RT	12/17/97	64/33
SA10RT23	AL	SANYO	RT	12/17/97	64/35
SA10RT24	AL	SANYO	RT	1/9/98	32/4
SA10M40A	AL	SANYO	–40°C	1/13/98	64/52
SA10M40B	AL	SANYO	–40°C	1/13/98	64/44
SA10M40C	AL	SANYO	–40°C	1/13/98	64/41
SA10M40D	AL	SANYO	–40°C	1/13/98	64/31
SA10M40E	AL	SANYO	–40°C	1/13/98	64/32
SA10M40F	AL	SANYO	–40°C	1/13/98	64/40
SA10M40G	AL	SANYO	–40°C	1/13/98	64/43
SA10M40H	AL	SANYO	–40°C	1/13/98	64/51
SA10M40I	AL	SANYO	–40°C	1/13/98	64/39
SA10M40J	AL	SANYO	–40°C	1/20/98	64(31)
SA10M40K	AL	SANYO	–40°C	1/20/98	64(32)
SA10M40L	AL	SANYO	–40°C	1/20/98	64(40)
SA10M40M	AL	SANYO	–40°C	1/20/98	64(44)
SA10M40N	AL	SANYO	–40°C	1/20/98	64(51)
SA10M40O	AL	SANYO	–40°C	1/20/98	64(52)

Table A-13

SILBERKRAFT C-CELL				
Fresh Cell				
Type M 52				
Filename	Current	End Cond.	Temperature	Date
SKCD50RT	50 mA	0.5 V	RT	1/6/98
SKCD500	500 mA	0.5 V	RT	1/6/98
SKCD103	1.0 A	0.5 V	RT	1/6/98
SKCD203	2.0 A	0.5 V	RT	1/6/98
SKCM40	50 mA	0.5 V	m40°C	1/6/98
SKCM40A	50 mA	0.5 V	cont. @ RT	
SKC50040	500 mA	0.5 V	m40°C	1/20/98
SKC5004A	500 mA	0.5 V	cont. @ RT	
SKC10340	1.0 A	0.5 V	m40°C	1/20/98
SKC1034A	1.0 A	0.5 V	cont. @ RT	
SKC20340	2.0 A	0.5 V	m40°C	1/20/98
SKC2034A	2.0 A	0.5 V	cont. @ RT	
	50 mA	0.5 V	m20°C	
	500 mA	0.5 V	m20°C	
	1.0 A	0.5 V	m20°C	
	2.0 A	0.5 V	m20°C	
SKCD5070	50 mA	0.5 V	70°C	1/13/98
SKC50070	500 mA	0.5 V	70°C	1/13/98
SKC10370	1.0 A	0.5 V	70°C	1/13/98
SKC20370	2.0 A	0.5 V	70°C	1/13/98
PULSE DISCHARGE				
Pulse Profile:	3 sec. 2 A	sample every .02 V or ::0.5		
	27 sec off	sample every .02 V or ::2		
	end when pulse voltage <0.5 V			
SKPLSM40			m40°C	1/6/98
SKPLSM4A				
SKCPM20			m20°C	
SKCPM20A				
			0°C	
SKPLSRT			RT	1/6/98
SKPLS70			70°C	1/13/98
Pulse Profile:	3 sec. 3 A	sample every .02 V or ::0.5		
	27 sec off	sample every .02 V or ::2		
	end when pulse voltage <0.5 V			
SKCPM40			m40°C	1/6/98
SKCPM40A			cont. @ RT	
SKCP3M20			m20°C	1/15/98
SKCP3M2A			cont. @ RT	

SKCP3Z			0°C	1/28/98
SKCP3ZA			cont. @ RT	
SKCP3RT			RT	1/21/98
			70°C	
Resistive Load Tests:				
SKCDRM30	2 Ω	2.0 V	–30°C	2/17/98

Table A-14

Constant Current 10mA Discharge to 0.5V				
Tests within lot #				
Filename	Lot #	Manufacturer	Temp.	Date
SO10RT1	7636	Sony	RT	1/13/98
SO10RT2	7636	Sony	RT	1/13/98
SO10RT3	7636	Sony	RT	1/13/98
SO10RT4	7636	Sony	RT	1/13/98
SO10RT5	7636	Sony	RT	1/13/98
SO10RT6	7636	Sony	RT	1/13/98
SO10RT7	7636	Sony	RT	1/13/98
SO10RT8	7636	Sony	RT	1/13/98
SO10RT9	7636	Sony	RT	1/13/98
SO10RT10	7636	Sony	RT	1/13/98
SO10RT11	7636	Sony	RT	1/13/98
SO10RT12	7636	Sony	RT	1/13/98
SO10RT13	7636	Sony	RT	1/13/98
SO10RT14	7636	Sony	RT	1/13/98
SO10RT15	7636	Sony	RT	1/13/98

Table A-15

Constant Current 10mA Discharge to 0.5V				
Tests within lot #				
Filename	Lot #	Manufacturer	Temp.	Date
DL10RT1	713013	Duracell	RT	1/13/98
DL10RT2	713013	Duracell	RT	1/13/98
DL10RT3	713013	Duracell	RT	1/13/98
DL10RT4	713013	Duracell	RT	1/13/98
DL10RT5	713013	Duracell	RT	1/13/98
DL10RT6	713013	Duracell	RT	1/13/98
DL10RT7	713013	Duracell	RT	1/13/98
DL10RT8	713013	Duracell	RT	1/13/98
DL10RT9	713013	Duracell	RT	1/13/98
DL10RT10	713013	Duracell	RT	1/13/98
DL10RT11	713013	Duracell	RT	1/13/98
DL10RT12	713013	Duracell	RT	1/14/98
DL10RT13	713013	Duracell	RT	1/20/98
DL10RT14	713013	Duracell	RT	1/20/98
DL10RT15	713013	Duracell	RT	1/20/98
DL10M20A	713013	Duracell	–20	1/28/98
DL10M20B	713013	Duracell	–20	1/28/98
DL10M20C	713013	Duracell	–20	1/28/98
DL10M20D	713013	Duracell	–20	1/28/98
DL10M20E	713013	Duracell	–20	1/28/98
DL10M20F	713013	Duracell	–20	1/28/98
DL10M20G	713013	Duracell	–20	1/28/98
DL10M20H	713013	Duracell	–20	1/28/98
DL10M20I	713013	Duracell	–20	1/28/98
DL10M20J	713013	Duracell	–20	1/28/98

Table A-16

DW TEST PROTOCOL			
D CELLS			
Pulse Amplitude:			
Filename	Amps	Temp	Date
BS040M40	4.5	-40°C	12/16/97
BS40M40A	3.75	-40°C	12/16/97
BS40M40B	3	-40°C	12/16/97
BSDWM20	4.5	-20°C	12/24/97
BSDWM20A	3.75	-20°C	12/24/97
BSDWM20B	3	-20°C	12/24/97
BSDWZ	4.5	0°C	1/28/98
BSDWZA	3.75	0°C	1/28/98
BSDWZB	3	0°C	1/28/98
SKDWM40	4.5	-40°C	1/19/98
SKDWM40A	3.75	-40°C	1/19/98
SKDWM40B	3	-40°C	1/19/98
SKDWM20	4.5	-20°C	1/27/98
SKDWM20A	3.75	-20°C	1/27/98
SKDWM20B	3	-20°C	1/27/98
SKDWZ	4.5	0°C	1/28/98
SKDWZA	3.75	0°C	1/28/98
SKDWZB	3	0°C	1/28/98
ULD		-40°C	
		-40°C	
		-40°C	
		-20°C	
		-20°C	
		-20°C	
		0°C	
		0°C	
		0°C	
Pulse Load:			
Filename	Ohms	Temp	Date
B40RLM40	1.02	-40°C	12/22/97
B40RLM4A	0.77	-40°C	12/22/97
B40RLM4B	0.58	-40°C	12/22/97
BSRLM20	1.02	-20°C	1/5/98
BSRLM20A	0.77	-20°C	1/5/98
BSRLM20B	0.58	-20°C	1/5/98
BSRLZ	1.02	0°C	1/28/98
BSRLZA	0.77	0°C	1/28/98
BSRLZB	0.58	0°C	1/28/98
SKRLM40	1.02	-40°C	1/19/98
SKRLM40A	0.77	-40°C	1/19/98
SKRLM40B	0.58	-40°C	1/19/98
SKRLM20	1.02	-20°C	1/27/98

SKRLM20A	0.77	–20°C	1/27/98
SKRLM20B	0.58	–20°C	1/27/98
SKRLZ	1.02	0°C	1/28/98
SKRLZA	0.77	0°C	1/28/98
SKRLZB	0.58	0°C	1/28/98
Pulse Load:			
Filename	Ohms	Temp	Date
ULD	1.02	–40°C	
	0.77	–40°C	
	0.58	–40°C	
	1.02	–20°C	
	0.77	–20°C	
	0.58	–20°C	
	1.02	0°C	
	0.77	0°C	
	0.58	0°C	

DISTRIBUTION LIST

Julie Banner
Naval Surface Warfare Center
Carderock Division
Electrochemistry Branch Code 683
9500 MacArthur Blvd.
West Bethesda, MD 20817-5700

Tyler X. Mahy
U.S. Government
Central Intelligence Agency
130 Duvall Lane Apt. T-1
Gaithersburg, MD 20877

Kathy Steele
U.S. Government
111 Falls Avenue
Falls Church, VA 22046

George Methlie
Central Intelligence Agency
2120 Naraua Ct.
Falls Church, VA 22043

Joseph Stockel
National Reconnaisance Office
14675 Lee Rd.
Chantilly, VA 20151

Jeff Harris
SANDERS, A Lockheed Martin Co.
4394 Eaton Place
Alexandria, VA 22310

Dan Peterson
Tactical Defense Systems
Lockheed Martin
P.O. Box 64525
MS U2 X26
St. Paul, MN 55164-0525

Kenneth E. Beene
Tactical Defense Systems
Lockheed Martin
P.O. Box 64525
MS U2 X26
St. Paul, MN 55164-0525

01500/MS0953	W. E. Alzheimer
01521/MS0613	D. H. Doughty (2)
01521/MS0613	C. C. Crafts
01521/MS0613	L. E. Davis
01521/MS0613	D. Ingersoll
01521/MS0613	J. L. Langendorf
01522/MS0614	D. E. Mitchell
01522/MS0614	D. B. Hardy
01522/MS0614	D. E. Weigand
01523/MS0614	R. W. Bickes, Jr.
01525/MS0613	P. C. Butler
01525/MS0613	N. H. Clark (20)
01822/MS0343	T. T. Borek, III
01822/MS1405	M. A. Rodriguez
02121/MS0487	J. D. Clark
02121/MS0487	T. A. Denman
02125/MS0519	D. J. Gelet
02167/MS0481	J. M. Montoya
02167/MS0481	M. A. Rosenthal
02167/MS0481	D. L. Thomas
02168/MS0481	J. L. McClellan
05825/MS0764	J. L. Schoeneman
08115/MS9106	R. E. Oetken
09119/MS0557	T. L. Paez
04916/MS0899	Technical Library (2)
00111/MS0619	Review & Approval For DOE/OSTI (1)
08940-2/MS9018	Central Technical Files